Understanding the role of Caspr2 in the developing cerebellum

D.Phil. thesis



by **Liam Argent**

Final submission date: Hilary term 2019
Supervisors: Professors Esther Becker and Elena Seiradake
Department: Physiology, Anatomy and Genetics
College: Green Templeton College

"The best way to scare a Tory is to read"
- IDLES, 2017, Mother

Abstract

Despite receiving renewed attention due to the revelation it is involved in higher cognitive functions, we still know little about how the cerebellum develops and operates. Studies suggest Contactin-associated protein-like 2 (Caspr2), a member of the Neurexin superfamily, has a cerebellar function. However, the cellular and molecular bases for this remain unknown.

An initial assessment of the spatio-temporal expression pattern of Caspr2, using immunohistochemistry and biochemical fractionation, suggested that Caspr2 is expressed at specific synapses in the developing cerebellum. Little is known about the function of Caspr2 at synapses and so the Caspr2 domain exposed to the synaptic cleft, the Caspr2 extra-cellular domain (ECD), was focused on. The addition of recombinant Caspr2 ECD to organotypic cerebellar slice cultures prepared from *Cntnap2*$^{-/-}$ mice rescued a dendritic morphology defect observed in untreated cultures, suggesting Caspr2 affects cellular morphology during cerebellar development. To understand the molecular basis for this effect, a pull down assay was used to identify the synaptic binding partners of Caspr2. Unexpectedly, mass spectrometry analysis of this experiment revealed that the Ca^{2+} channel Inositol 3,4,5-trisphosphate receptor type I (IP_3R1) is a cognate partner of Caspr2 at synapses in the developing cerebellum. Further biochemical assays revealed both that the Caspr2-IP_3R1 interaction underlies the regulation of cellular morphology by Caspr2 and that Caspr2 may modulate cytoplasmic Ca^{2+} levels. Combined with data from co-immunoprecipitation assays suggesting that Caspr2 interacts with the IP_3R1 pore-forming domain, these data are consistent with Caspr2 acting via IP_3R1 to regulate cellular morphology during cerebellar development, most likely by directly affecting the IP_3R1 pore region environment.

Together, these experiments therefore reveal novel cellular and molecular roles for Caspr2 in the developing cerebellum. As well as improving our understanding of the nervous system, knowledge such as this will likely be increasingly clinically relevant, given the previously overlooked links between the cerebellum and cognition.

Acknowledgements

Thanks go first of all to my main supervisors, Prof. Esther Becker and Prof. Elena Seiradake, without whom this project would not have been possible. In addition, I am grateful for Prof. Radu Aricescu's supervision during the initial stages of the project. I am also particularly indebted to Friederike Winter, who never hesitated to help me during my first few months. The director of the OxION programme, Prof. Stephen Tucker and my college tutor, Prof. Ken Reid, deserve my gratitude as well, for the excellent advice they have shared with me over the course of my D.Phil.
Many aspects of this project required collaborating with others and I am grateful to all of those who were kind enough to spare me their time and effort. Mimi *Austin Powers* Prickett, Maria Carrasquero Ordaz, Prof. Helen Christian and Prof. Holger Kramer all made significant contributions and I owe each of them a great deal. Profs. Pawel Swietach and Maike Glitsch also offered me invaluable technical advice and I thank both of them for that.
Finally and most importantly, thank you to my friends and family for your love, support and encouragment throughout. And thankyou Ali, my favourite person, both for your love and for your incredible patience.

Table of contents

Title page i

Abstract iii

Acknowledgements iv

Table of contents v

List of figures viii

List of tables x

List of abbreviations xi

1 Introduction 1

1.1 Anatomy and function of the cerebellum 1
1.2 Cerebellar development 10
1.3 Caspr2-related pathologies suggest a role for Caspr2 in the cerebellum 16
1.4 Caspr2: a Neurexin superfamily protein 20
1.5 Currently available Caspr2 expression data 29
1.6 Aims 31

2 Methods 33

2.1 Animals 33
2.2 Molecular biology 35
2.3 Cell biology 41
2.4 Biochemistry 47
2.5 Data analysis and statistics 55

3 Caspr2 affects Purkinje cell dendritic morphology 60
3.1 Introduction . . . 60
3.2 Caspr2 expression in the developing cerebellum . . . 63
3.3 Cloning, expression and purification of recombinant Caspr2 ECD . . . 69
3.4 Caspr2 affects Purkinje cell dendritic morphology . . . 73
3.5 Discussion . . . 75

4 Identification of synaptic Caspr2-interacting proteins 82
4.1 Introduction . . . 82
4.2 Pull-down experiments identify IP_3R1 as a potential synaptic binding partner of Caspr2 in the cerebellum . . . 84
4.3 Validation of the Caspr2-IP_3R1 interaction . . . 87
4.4 Identification of key binding domains . . . 93
4.5 Examining the possibility that Caspr2 interacts directly with IP_3R1 . . . 96
4.6 IP_3R1 and Caspr2 can interact in the synaptic cleft . . . 99
4.7 Discussion . . . 101

5 Functional consequences of the Caspr2-IP_3R1 interaction 109
5.1 Introduction . . . 109
5.2 Caspr2 inhibits IP_3R1-induced morphology changes . . . 111
5.3 Caspr2 does not affect IP_3R1 localisation . . . 116
5.4 Caspr2 regulates Erk phosphorylation . . . 118
5.5 Discussion . . . 123

6 General discussion 129
6.1 The Caspr2-IP_3R1 interaction . . . 131
6.2 A clue from the clinic: the multiple, distinct phenotypes caused by Caspr2 dysfunction . . . 137
6.3 Caspr2 in the peripheral nervous system (PNS): developmental diaschisis and Autsim spectrum disorder (ASD) . . . 140
6.4 A potential distinct function for the second, smaller Caspr2 isoform . . . 141
6.5 Conclusions . . . 143

7 References 145

Appendix A: Alignment of Caspr-family primary protein sequences a

Appendix B: LC-MS/MS data **i**

List of figures

1.1 Cerebellar anatomy 1: anatomical position 1
1.2 Cerebellar anatomy 2: foliation pattern 2
1.3 Cerebellar anatomy 3: cytoarchitecture 3
1.4 The circuitry of the the cerebellum 4
1.5 Purkinje cell differentiation 15
1.6 Caspr2 affects cerebellar-specific behaviours 17
1.7 The Neurexin superfamily of proteins 21
1.8 Homology modelling of the human Caspr2 domain annotated as a fibrinogen C-terminal domain-like domain in the Uniprot database . . 23
1.9 Caspr2 is expressed in the cerebellum, throughout post-natal development 31

3.1 Caspr2 expression in the developing cerebellum: immunohistochemistry 64
3.2 Caspr2 expression in the developing cerebellum: biochemical fractionation 66
3.3 Caspr2 is an integral cell membrane protein 69
3.4 The Caspr2 ECD expression construct 71
3.5 Recombinant Caspr2 ECD can be biotinylated *in vivo* 72
3.6 Large-scale purification of recombinant Caspr2 ECD. 72
3.7 Caspr2 affects Purkinje cell dendritic morphology. 75

4.1 Pull-down experiments identify IP_3R1 as a potential synaptic binding partner of Caspr2 in the cerebellum 86
4.2 Caspr2 and IP_3R1 interact *in vitro* 88
4.3 Caspr2 and IP_3R1 co-occur in the deep molecular layer of the developing cerebellum 90
4.4 Caspr2 and IP_3R1 co-localise in the developing cerebellum 92
4.5 Key Caspr2 domains mediate the Caspr2-IP_3R1 interaction 94

4.6 The IP_3R1 LL3 domain mediates the Caspr2-IP_3R1 interaction 96
4.7 IP_3R1 can be purified from rat cerebella 97
4.8 Co-IP of recombinant IP_3R1 and Caspr2 98
4.9 IP_3R1 and Caspr2 can interact in the synaptic cleft 100

5.1 Expression of Caspr2 inhibits cellular extensions induced by the expression of IP_3R1 113
5.2 The Caspr2 juxta-membrane region (JXM) domain is required for the inhibition of IP_3R1-induced morphology changes by Caspr2 114
5.3 The absence of Caspr2 does not affect gross IP_3R1 staining patterns. . 117
5.4 The absence of Caspr2 does not perturb the expression of IP_3R1 at synapses 118
5.5 Erk phosphorylation is reduced in *Cntnap2*$^{-/-}$ mice 120
5.6 Erk phosphorylation is not affected by Caspr2 over-expression in HEK293FT cells 121
5.7 Caspr2 boosts post-IP_3R1 agonist treatment Erk phosphorylation, in HEK293FT cells 122

A.1 Alignment of Caspr-family primary protein sequences . . . . . b

List of tables

2.1 Primers for PCR cloning 37
2.2 PCR conditions for Caspr2 ECD expression construct cloning 37
2.3 PCR conditions for Caspr2 JXM domain expression construct cloning 37
2.4 PCR conditions for Δ LL3 IP_3R1 expression construct cloning 38
2.5 Genotyping primers 40
2.6 Genotyping PCR conditions 40
2.7 HPLC gradient method used for LC-MS / MS analysis 54
2.8 Antibodies used for immunofluorescence microscopy 58
2.9 Antibodies used for electron microscopy 58
2.10 Antibodies used for Western blotting 59
2.11 Antibodies used for immunoprecipitations 59

B.1 Pull-down experiment LC-MS/MS data: bait = mock . . . . . j
B.2 Pull-down experiment LC-MS/MS data: bait = Caspr2 ECD . . . . . q

List of abbreviations

ASD Autsim spectrum disorder

Caspr2 Contactin-associated protein-like 2

CCAS cerebellar cognitive affective syndrome

CCH Carbachol

CDFE Cortical dysplasia focal epilepsy

CNS central nervous system

co-IP co-immunoprecipitation

DMEM Dulbecco's modified Eagle's medium

E embryonic day

ECD extra-cellular domain

EGF epidermal growth factor-like

ER endoplasmic reticulum

Erk Extracellular signal-related kinases 1/2

FCS foetal calf serum

ICD intra-cellular domain

IMAC immobilised metal affinity chromatography

IP_3 inositol 3,4,5-trisphosphate

IP_3R1 Inositol 3,4,5-trisphosphate receptor type I

JXM juxta-membrane region

JXP juxta-paranode

LL3 third lumenal loop

NEAA non-essential amino acids

P post-natal day

PBS phosphate-buffered saline

PDZ PSD-95/Disc large 1/Zonula occludens 1

PEI Polyethylenimine

Pen-Strep Penicillin-Streptomycin

PErk phospho-Extracellular signal-related kinases 1/2

PIP_2 Phosphatidylinositol 4,5-bisphosphate

PKC Protein kinase C

PLC Phospholipase C

PNS peripheral nervous system

RT room temperature

RTK Receptor tyrosine kinase

SAXS small angle x-ray scattering

SCA15 Spinocerebellar ataxia 15

SDS-PAGE sodium dodecyl sulfate-polyacrylamide gel electrophoresis

1 Introduction

1.1 Anatomy and function of the cerebellum

Anatomy

In humans, the cerebellum lies at the extreme caudal end of the rostral-caudal axis, underneath the tentorium cerebelli. It occupies most of the posterior cranial fossa, which also contains the brainstem. Similar to humans, the murine cerebellum is also found in an extreme posterior position. However, rather than being ventral, as the human cerebellum is, the mouse cerebellum is dorsal. (Figure 1.1).

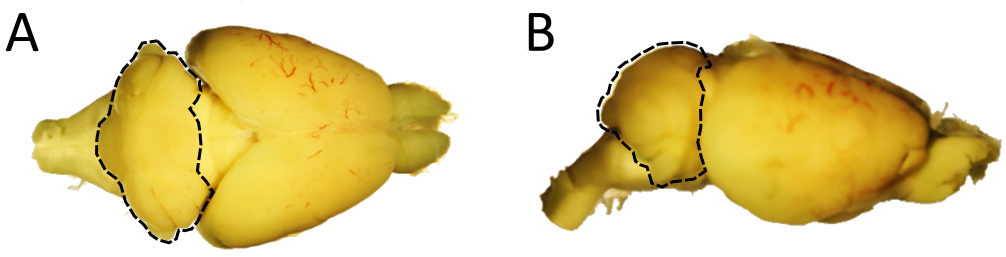


Figure 1.1: Cerebellar anatomy 1: anatomical position. An adult, murine brain, fixed in 2% paraformaldehyde and 0.25% gluteraldehyde. Dashed line, outline of the cerebellum, images are magnified 1.7X. **A)** Dorsal view. **B)** Lateral view. Adapted from[170].

The cerebellum is connected to the rest of the brain via three pairs of peduncles that facilitate communication between itself and the brainstem. The superior peduncle

is continuous with the midbrain, the inferior peduncle joins with the medulla peduncle and the middle peduncle connects to the pons.

The cerebellum spans the entire lateral axis of the brain and has two hemispheres connected by the medial vermis. Each hemisphere hosts one of each of the paired peduncles. The hemispheres themselves are split into anterior and posterior lobes by the primary fissure, which runs along the lateral axis. In mammals, other, less prominent fissures further divide the vermis and hemispheres into ten smaller lobules[81; 82] (Figure 1.2). These fissures also run along the lateral axis, whilst being distributed roughly radially with respect to the deep cerebellum. This creates lobules that are separated in the saggital plane.

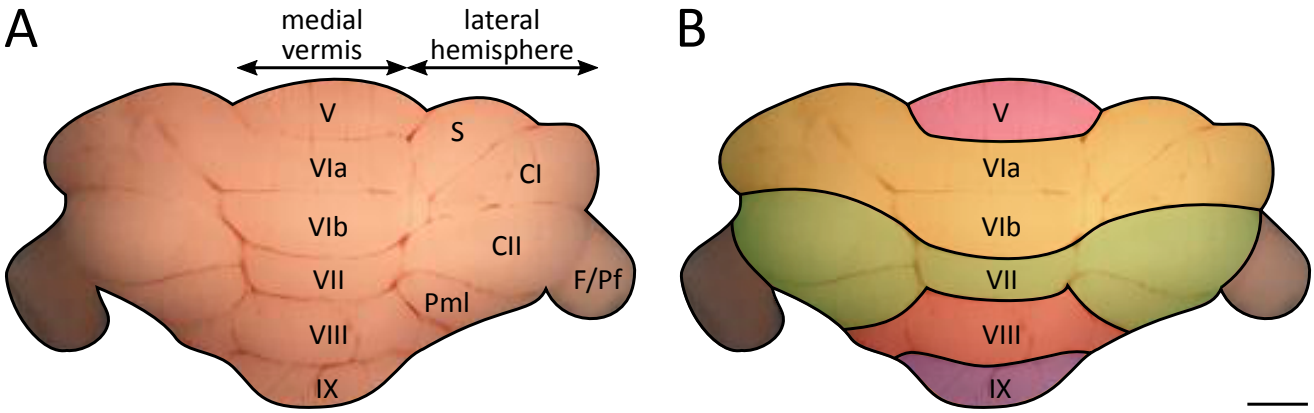


Figure 1.2: Cerebellar anatomy 2: foliation pattern. A) Posterodorsal view of an unfixed, adult, murine cerebellum. Visible lobules are indicated. Roman numerals denote vermis lobules. S, simplex lobule, CI, Crus I, CII, Crus II, Pml, Paramedian lobule F / Pf, floculus / parafloculus. **B)** As A), but with lobules that span the cerebellum across the lateral axis highlighted. Scale bar = 300µm. Adapted from [165].

The distribution of cells in the cerebellum is strikingly uniform, with the same cellular layers present throughout the entire structure. Moving from superficial to deep, the adult cerebellum is comprised of the molecular, Purkinje and granule cell layers, white matter and the 4 pairs of deep cerebellar nuclei (dentate, emboliform, globose / interposed and fastigial) (Figure 1.3, deep cerebellar nuclei not shown). Most neuronal somata are localised to the densely populated granule cell layer. Neuronal

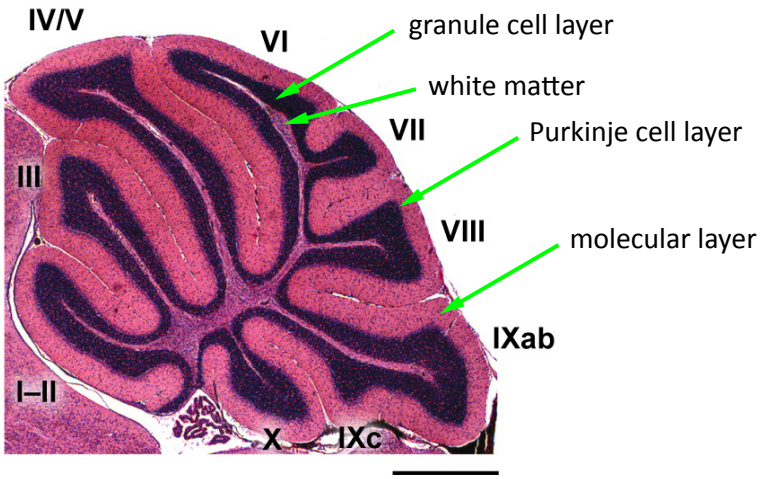


Figure 1.3: Cerebellar anatomy 3: cytoarchitecture. A mid-saggital section of an adult, murine cerebellum stained with crysel violet to highlight somata. Scale bar = 750µm. Adapted from[133].

cell bodies are also found in the deep cerebellar nuclei and in the single-cell thick Purkinje cell layer. The white matter is mostly comprised of myelinated Purkinje cell axons, whilst the molecular layer contains only a few interneuron somata but many neurites. These are mainly parallel fibres that make synaptic contacts with Purkinje cell dendrites.

Neuronal circuitry

The uniform cytoarchitecture of the cerebellum leads to similarly uniform circuitry (Figure 1.4), which is relatively simple compared to the circuitry found in other brain areas. Each of the different cellular layers of the cerebellum has its own distinct population of neuronal somata and neurites that together form a single circuit.

The three most superficial layers of the cerebellum, the granule cell, Purkinje cell and molecular layers, compose the cerebellar cortex. The deepest of these, the granule cell layer, contains the cell bodies of granule cells and Golgi cells as well as granule cell dendrite, Golgi cell axon and mossy fibre terminii.

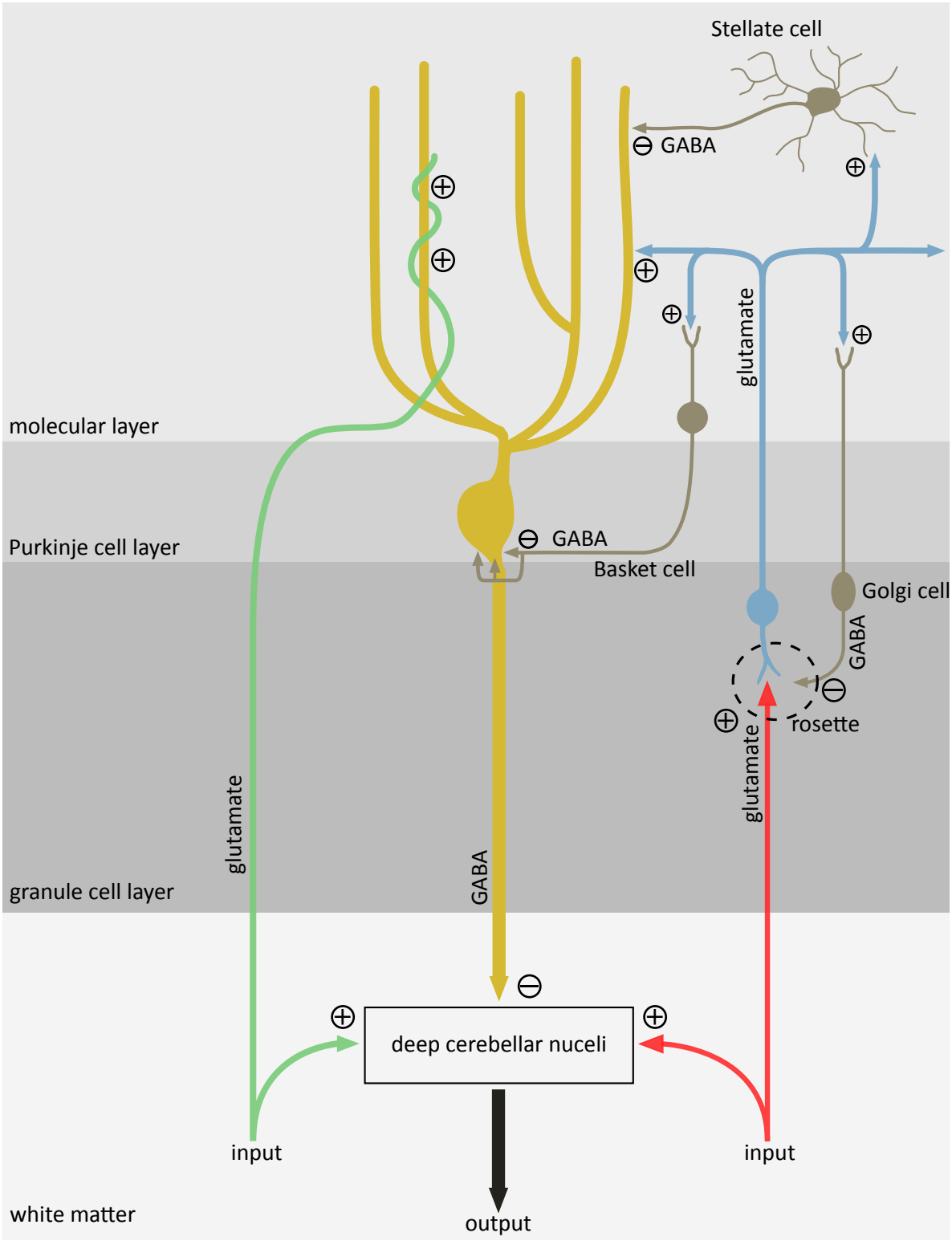


Figure 1.4: The circuitry of the cerebellum. Schematic of the neuronal circuit found in the adult cerebellum. Purkinje cell, gold, granule cell, light blue, climbing fibre, fern green, mossy fibre, red, interneurons (individually labelled), grey, +, excitiatory synapse, -, inhibitory synapse.

Adapted from a scalable vector graphic originally created by Marcel Wiesweg, distributed under a CC-BY 2.5 license, wikimedia accession code 1359241.

Mossy fibres are a collection of axons that project from various central nervous system (CNS) areas, including both other brain regions and the spinal cord. Alongside climbing fibres (discussed below), they carry input information into the cerebellum. Golgi cell axons and mossy fibres synapse simultaneously with granule cell dendrites. Each excitatory mossy fibre often contacts multiple granule cell dendrites in close proximity to each other and these synapses are then all also contacted by a single Golgi cell axon. Together, this cluster of synapses forms a rosette-like structure known as a glomerulus. Golgi cells are inhibitory interneurons that carry feedback directly from granule cell axons. Thus the glomerulus structure acts not just to propagate incoming information but also to transform that information into a regular temporal pattern.

The axons of granule cells reach up, through the Purkinje cell layer, into the molecular layer. Here, they bifurcate and then travel parallel to the lateral axis of the cerebellum, where they synapse with both Purkinje and interneuron dendrites (these synapses are all excitatory). After bifurcation, the resulting two axons travel in opposite directions. For this reason, and because they travel parallel to the lateral axis, granule cell axons are known as parallel fibres. Also present in the granule cell layer, but not illustrated in Figure 1.4, are the somata of Lugaro (classical and globular) and unipolar brush cells. The cell bodies of classical Lugaro cells are found in the most superficial part of the granular cell layer, just under the Purkinje cell layer. These cells extend two pairs of dendrites, one pair from each pole of the cell body, just underneath the Purkinje cell layer in the coronal plane. The two dendrites that form each pair do not diverge greatly along the lateral axis and so the dendrites of classical Lugaro cells cover a rectangular area, the long axis of which is the anteroposterior axis. They are innervated by Purkinje cell axon collaterals and basket cells, as well as by extra-cerebellar serotonergic input (inhibitory). The cell bodies of

globular Lugaro cells are found slightly deeper in the granular layer. In contrast to classical Lugaro cells, the dendrites of globular Lugaro cells extend up into the molecular layer, where they are innervated by granule cell axons and classical Lugaro cells. The axons of both types of Lugaro cell will form inhibitory synapses with any interneuron cell type that has available dendrites in the molecular layer.

Unipolar brush cells effectively add another transformation to the computation that takes place at the glomerulus. The brush-like dendrites of unipolar brush cells receive simultaneous input from mossy fibres and Golgi cell axons, just as granule cell dendrites do. This information is then passed to granule cells via excitatory unipolar brush cell axon-granule cell dendrite synapses. These synapses are located outside of the glomerulus and there is therefore no direct input from Golgi cells.

Superficial to the granule cell layer lies the Purkinje cell layer. Purkinje cells facilitate the only route by which information can be output from the cerebellum and thus they act to integrate signals from the cerebellar circuitry. The dendrites of these cells grow up into the molecular layer and then form extensive, two-dimensional arbours that are transverse to the lateral axis. Distal Purkinje cell dendrites are contacted by parallel fibres, which are arranged perpendicular to the Purkinje dendritic arbour. Proximal Purkinje cell dendrites, on the other hand, are contacted by climbing fibres. Climbing fibres are the one other source of excitatory input to the cerebellum, alongside mossy fibres. They originate in the inferior olive nucleus in the brainstem and like the parallel fibres of granule cells, use glutamate to excite Purkinje cells. Outgoing signals are transmitted through the Purkinje cell axon, which passes through both the granule cell layer and the white matter, to the deep cerebellar nuclei. From there, this integrated signal is sent to other brain areas and the spinal cord, as well as back to the cerebellum.

The most superficial layer of the cerebellar cortex, and the cerebellum, is the mo-

lecular layer. Although mostly comprised of neurites, the cell bodies of basket cells and stellate cells (both GABAergic neurons) do localise here. They receive excitatory input from parallel fibres and provide inhibitory input to Purkinje cells. Stellate axons synapse with Purkinje cell dendrites, whilst the axons of basket cells wrap around the Purkinje cell somata and axon initial segment. This forms the basket-like structure, known as the pinceau, from which these neurons take their name.

Glial cells

Immediately underneath the cerebellar cortex lies the white matter, so called because the Purkinje cell axons that pass through it are myelinated by oligodendrocytes. These fibres are the only ones in the cerebellum to be myelinated and so cerebellar oligodendrocytes are found almost exclusively in the white matter. In addition to this, the cerebellum also hosts several subtypes of astrocytes. Bergman glia are one such subtype and are unique to the cerebellum. These cells extend long radial processes from the Purkinje cell layer, where their somata reside, up into the molecular layer. During development, granule cells migrate along these fibres to move deeper into the cerebellum and into the granule cell layer. In adulthood, Bergman glia modulate a variety of processes, including synaptic plasticity.

Function

Ever since Sir Charles Sherrington described the cerebellum as the ”head ganglion of the proprioceptive system”, most research into cerebellar function has focused on its role in the fine tuning of motor function, in motor learning and in control of vestibular function[46]. This idea was reinforced by the results of Sir Gordon Holmes seminal analysis of disorders precipitated by cerebellar lesions. He found that soldiers who had suffered cerebellar injury during WWI developed ataxia and

adiadochokinesia, the inability to rapidily alternate between directly opposed muscular movements [60; 60].

The theory which most comprehensively explains how motor signals are fine-tuned by the cerebellum, the adaptive filter theory, was originally postulated by Fujita in 1982[50], who built on previous work done by Masao Ito [68]. In brief, the circuitry of the cerebellum is constructed to facilitate the comparison of an intended movement and the actual movement executed. Cerebellar output is then adjusted based on any errors detected to produce smooth movements[74]. This computation is made possible by the cortex-pons-cerebellum-thalamus-cortex loop. A copy of all motor commands sent from the motor cortex are relayed to cerebellar Purkinje cells via the climbing fibres of the inferior olive. Sensory information resulting from the actual movement performed is also transmitted to the cerebellum via mossy fibres. This signal is passed via granule cells to Purkinje cells, where it is compared to the signal sent directly from motor cortex. The resulting error signal is then relayed back to the motor cortex and the movement is fine-tuned[69; 166]. Dysfunction of the cerebellum therefore leads to uncoordinated movements and disequilibrium, as this fine-tuning is impaired.

Over time, plasticity mechanisms include this error signal in the computation performed at parallel fibre-Purkinje cell synapses. This plasticity underlies motor learning in the cerebellum[54; 68].

More recently, evidence has emerged that implicates the cerebellum in higher order brain functions, as well as the control of motor activity. The first such indication came from observations of patients who had suffered cerebellar lesions. It was noticed that in some cases, motor function was not significantly affected, but instead executive function, language and affective processing were all impaired. The term cerebellar cognitive affective syndrome (CCAS) was coined to describe the non-

motor phenotype displayed by these patients[125]. The results of many studies have since supported the idea that the cerebellum has a role in cognitive and affective processes[142]. In particular, cerebellar injury at birth has been associated with cognitive defects, in addition to possible motor deficits, in later life[2; 25]. Viral tracing experiments provided early evidence of a physical link between the cerebellum and non-motor brain areas. The herpes simplex virus was injected in to the dorsolateral prefrontal cortex, a neo-cortical area strongly associated with spatial working memory, of several *Cebus apella* monkeys and labelled cells were subsequently found in a distinct area of the cerebellar dentate nucleus[95]. More recent fMRI imaging studies have revealed that each region of the human cerebellum maps topographically to a cognate region of the neocortex[26]. Together, these studies confirm that the communication between the cerebellum and the neocortex necessary for the cerebellum to influence non-motor output does occur.

Interestingly, the uniform architecture of the cerebellum suggests the same computation is performed in each cerebellar lobule, regardless of what neocortical region any particular lobule is associated with. This prompted Schmahmann to suggest that the cerebellum could well fine tune cognition and affective responses, in exactly the same manner as it does motor processes. If this is the case, then CCAS could be described as a dysmetria of thought[124]. Indeed, the lesion of anterior lobules is associated with motor deficits, whilst lesion of posterior lobules is associated with language and executive function deficits[138], consistent with different regions of the cerebellum all performing the same calculation, but processing data from different cortical areas. Further, it has recently been found that cerebellar granule cells also encode the expectation of reward[160]. This suggests not only that granule cells can carry cognitive information, but that the cerebellum may also inform decision making as well as fine tuning the execution of tasks.

Because the higher order roles of the cerebellum, such as those affected in autism, have only recently been recognised, there remains much to be discovered in this area. There is therefore now a real need to understand cerebellar function, not only in order to build a complete picture of CNS function, but also because this information may be clinically relevant. The role of the cerebellum in many different diseases may have been overlooked because it was previously assumed the cerebellum operated solely to control motor processes.

1.2 Cerebellar development

Cerebellar development is protracted relative to other brain regions. In humans, it starts before, and finishes after, development of the neo-cortex, beginning at roughly 4 weeks post conception and ending at around 7 post-natal months. During the last trimester, celllular proliferation increases dramatically, resulting in a 5-fold increase in volume and a 30-fold increase in surface area. This expansion drives the formation of the primary and posterior fissures that divide the cerebellum, through the anterior-posterior axis, into the anterior, posterior and flocculo-nodular lobes. These prominent fissures are present at birth, but the cerebellum is then further divided into ten lobules postnatally as the granule cell population continues to proliferate and migrate inwards. These ten lobules are numbered I-X, along the anterior-posterior axis (Figure 1.2). Adult foliation patterns are present after 2 post-natal months.

Cerebellar development in rodents begins at embryonic day (E)8-9 and ends around post-natal day (P)30. Relative to the human cerebellum, the murine cerebellum is under-developed at birth. The murine cerebellum does not reach a developmental

stage equivalent to the newly born human cerebellum until P10[21].

Origin, proliferation and migration of local cerebellar cells

All cells local to the cerebellum arise from two proliferative zones. The precursors of all of cerebellar glutamatergic neurons are born in the rhombic lip, the most dorsal tip of the rhombencephalon. GABAergic neurons, on the other hand, arise from the ventricular neuroepithelium that lines the 4th ventricle, which is ventral of the rhombic lip. The ventricular neuroepithelium is also known as the ventricular zone. The progenitors of different cell types are born in distinct waves. In mice, the first group of neuronal precursors to leave the rhombic lip migrate to the nuclear transition zone at E10-12. The nuclear transition zone is a cluster of glutamatergic and GABAergic neuron progenitors that will eventually form the deep cerebellar nuclei. The second wave of cells to leave the rhombic lip are the precursors of granule cells. They form a transient layer on the surface of the cerebellum, known as the external granule cell layer, and proliferate there until early postnatal development. After differentiation, post-mitotic granule cells migrate along the axons of Bergmann glia. These axons are arranged radially and so provide a route for granule cells to travel down from the external granule cell layer into the internal granule cell layer. This migration is complete, and the external granule cell layer eliminated, by P20 in mice. Finally, between E14 and E19, the progenitors of unipolar brush cells arise from the rhombic lip. They then migrate through the developing white matter until they reach the internal granule cell layer[41].

Similar to the rhombic lip, the first cells to arise from ventricular zone do so at E10-12 are also destined for the nuclear transition zone. The second wave of cells to leave, at E11-13, are the precursors of Purkinje cells[85]. Initially, these cells migrate along radial glia and form multi-layered clusters, which are interspersed with the clusters

of cells that comprise the nuclear transition zone. At around P4, these clusters thin out to produce the single-layer of cells that defines the mature Purkinje cell layer. Following the proliferation of Purkinje cell progenitors, interneuron precursors are born in a temporal pattern that is inversely proportional to the magnitude of the depth vector at which their somata settle. For example, the precursors of the most superficial cerebellar interneurons, stellate cells, are born last. The radial orientation-birth date relationship also holds true for different subtypes of interneuron within the individual cellular layers of the cerebellar cortex. Basket cells, which are born earlier than stellate cells, come to rest deeper in the molecular layer than later born stellate cells[86].

Input fibre pathfinding

Input information is delivered to the cerebellum by climbing fibres and mossy fibres. Climbing fibres originate in the inferior olive nucleus in the brainstem, whereas mossy fibres originate in a variety of brain nuclei, as well as in the spinal cord.

Climbing fibres first contact Purkinje cells around birth and form multiple synaptic contacts with the somata of Purkinje cells. Starting at around P10, multiple climbing fibres compete to the climb the developing Purkinje cell dendritic arbour, by following the ascending collaterals of basket axons[135]. Fibres are eliminated until only one remains and mono-innervation is usually complete by P14[163]. The remaining single climbing fibre will then form multiple synapses with the proximal dendrites of the Purkinje cell arbour.

Mossy fibres arrive in the granule cell layer before the granule cell somata have descended through the molecular layer. Unable to form contacts with granule cells, the newly arrived mossy fibres instead form transient synapses with developing Purkinje cells. As granule neurons begin to arrive, the mossy fibres switch from Purkinje

cells to granule cells, with the first functional mossy fibre-granule neuron synapses established by P10[28]. The glomeruli are also formed during this period, with an excessive number of synaptic junctions initially established and then pruned away. This pruning is not complete until P45.

Development of the cerebellar circuitry

As they migrate along the axons of Bergmann glia, granule cells leave behind thin, bifurcating process. These extend along the long axis of the folia, largely in the coronal plane, and will eventually become parallel fibres. Parallel fibre-Purkinje cell synapses form as soon as the Purkinje cell arbour reaches the developing molecular layer, at around P10. Purkinje cell-granule synapse formation is complete after 1 post-natal month. Initially, these synapses form in the deeper parts of the molecular layer. However, from P15 onwards they are eliminated from proximal Purkinje cell dendrites and replaced by the "winning" climbing fibre[63]. Of note, a shared Ca^{2+} signalling pathway underlies both the elimination of parallel fibres and climbing fibres. The activtation of mGluR1, a metatrobic glutamate receptor expressed in the Purkinje cell dendrite synaptolemma, leads to the subsequent activation of the Ca^{2+} ion channel IP_3R1. The resulting increase in cytoplasmic Ca^{2+} levels is essential for climbing fibre and parallel fibre elimination[63; 64]. As well as being important for the correct formation of synpases involving Purkinje cell dendrites, Ca^{2+} also plays a crucial role in the development of Purkinje cell dendritic morphology. IP_3R1 is encoded by *Itpr1*. Purkinje cells, taken from *ITPR1*$^{-/-}$ mice at P1-2 and cultured for 14 days *in vitro*, were found to develop primary dendrites that were thinner and less branched than those taken from *ITPR1*$^{+/+}$ animals[59]. Thus, Ca^{2+} appears to play a dual role in the developing cerebellum, controlling both dendritic and synaptic properties. However, it may be that the apparent affects of Ca^{2+} signalling on dend-

ritic morphology are a donwstream consequence of Ca^{2+} signalling at synapses. The synaptrophic hypothesis, first proposed in 1989, postulates that dendritic outgrowth is driven by synaptic activity[157]. This could be the case during Purkinje cell development, with post-synaptic Ca^{2+} signalling in Purkinje cell dendritic spines affecting the development of the Purkinje cell dendritic arbour.

Similar to mossy fibres, golgi cells also arrive in the granule cell layer at birth, before granule cells, their intended synaptic partners. Unlike mossy fibres however, these cells do not form transient synapses in the interlude and only make connections with granule cells once they arrive. As mentioned above, the glomeruli in which they participate take several weeks to mature. The dendrites of Golgi cells also take several weeks to develop fully.

Initial synapses between basket cells and Purkinje cell dendrites are formed around birth[135], but activity-dependent maturation of these synapses continues for around a month[6; 159]. It is not until after P14 that the basket-like pinceau, a cluster of synapses around the Purkinje cell axon initial segment, are formed. Stellate cells, by contrast, synapse with more distal Purkinje cell dendrites.

Purkinje cell differentiation

Adult Purkinje cells are one of the most structurally complex neuronal cell types in the human body. As might be expected, given this complexity, the differentiation of Purkinje neurons involves many stages (Figure 1.5).

In rodents, Purkinje cell differentiation begins around two weeks after conception. At E14.5, Calbindin, a Ca^{2+}-binding protein and a marker of Purkinje neuron differentiation, can be detected in the majority of Purkinje cells. Axonal growth begins almost immediately afterwards and by E18 these neurites are extended most of the way to their targets in the deep cerebellar nuclei. Dendritic growth is limited un-

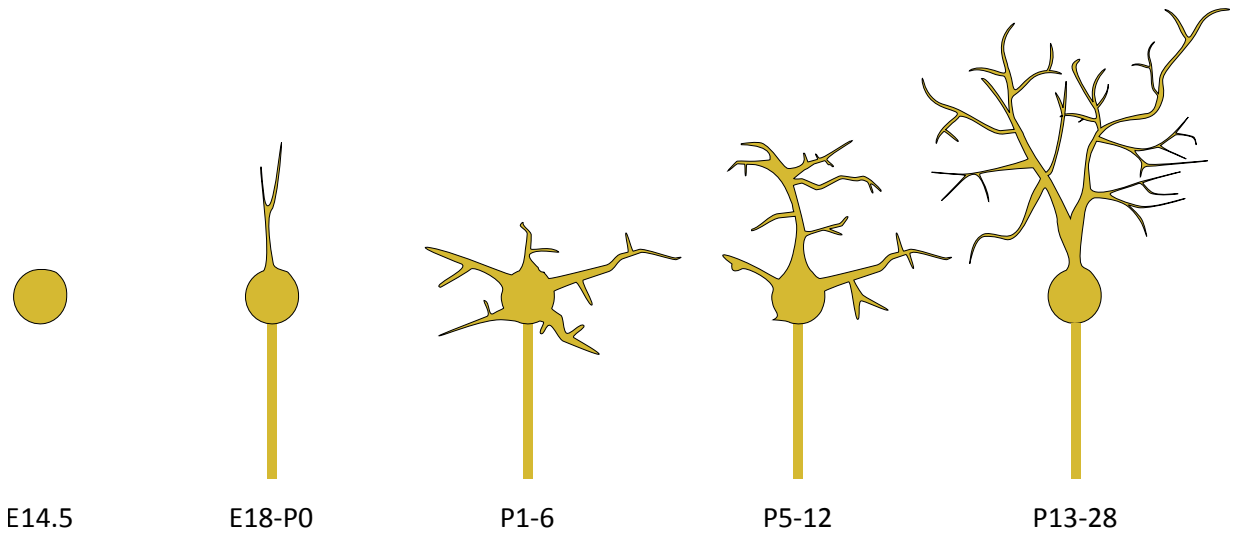


Figure 1.5: Purkinje cell differentiation. Illustration of the morphology of Purkinje cells at different stages of differentiation. Dendrites and somata are outlined in black. Axons are represented by perfectly vertical bars with no outline. Based on the morphologies reported in [75].

til around birth. By P0, Purkinje cells have entered the fusiform stage. Although they are still grouped in clusters along the mediolateral axis, fusiform Purkinje cells become polarised and extend a single, unbranched dendrite from a site directly opposite the axon hillock. This dendrite may grow parallel or perpendicular to the pial surface. The polarisation present in the fusiform stage is then temporarily lost as, from P1-6, Purkinje neurons pass through the stellate stage. During this stage, multiple transient dendrites are extended, growing from any part of the soma. Extensive dendritic reorganisation also occurs, although dendritic outgrowth is minimal. Apical-basal polarity is re-established as early as P6 as some of these transient dendrites begin to be pruned away and (in most cases) a single primary dendrite emerges from the apical cone. This particular dendrite thickens and arbourises rapidly. Dendritic branching, outgrowth and pruning all continue until around P28, at which point only the single primary dendrite extended from the apical membrane after the stellate stage remains.

In some cases, multiple primary dendrites are retained into adulthood[23].

1.3 Caspr2-related pathologies suggest a role for Caspr2 in the cerebellum

Recent advances demonstrating its importance in higher-order cognitive functions have fuelled renewed interest in the cerebellum, but there is still much to learn about how the cerebellum develops and operates at the cellular and molecular levels. There are a variety of strategies a researcher can adopt to address questions such as these. One of those is to identify proteins that cause phenotypes specific to the tissue in question when dysfunctional and then to study those proteins in detail.

A growing body of evidence suggests that the type 1 transmembrane protein Caspr2 has a role in the cerebellum. Auto-antibodies against Caspr2 have been found in the sera of patients diagnosed with autoimmune cerebellar ataxia[15]. In addition, unpublished work from the Becker lab shows that *Cntnap2*$^{-/-}$ mice (*Cntnap2* encodes Caspr2) have a cerebellar-associated motor phenotype (Figure 1.6) as well as a previously described ASD-like phenotype (discussed below). Eyeblink conditioning deficits, a phenotype specific to cerebellar dysfunction, has also been observed in these mice[77]. Of note, no gross morphology changes in the cerebella of these mice were found, suggesting that either fine morphology or function is affected when Caspr2 is absent. Interestingly, only the longer of the two *Cntnap2* isoforms is knocked out in these mice. The shorter isoform, which is lacking most of the N-terminal end of the ECD present in the longer isoform, is still expressed (Figure 1.7). This suggests a critical role for the ECD of Caspr2 in the ASD-like and cerebellar-associated endophenotypes observed. Structural magnetic resonance imaging and diffusion tensor imaging has also revealed that *CNTNAP2* polymorphisms are associated with reduced cerebellar grey matter volume in humans[147]. A similar MRI study using mice reported an association between the homozygous deletion of *Cnt-*

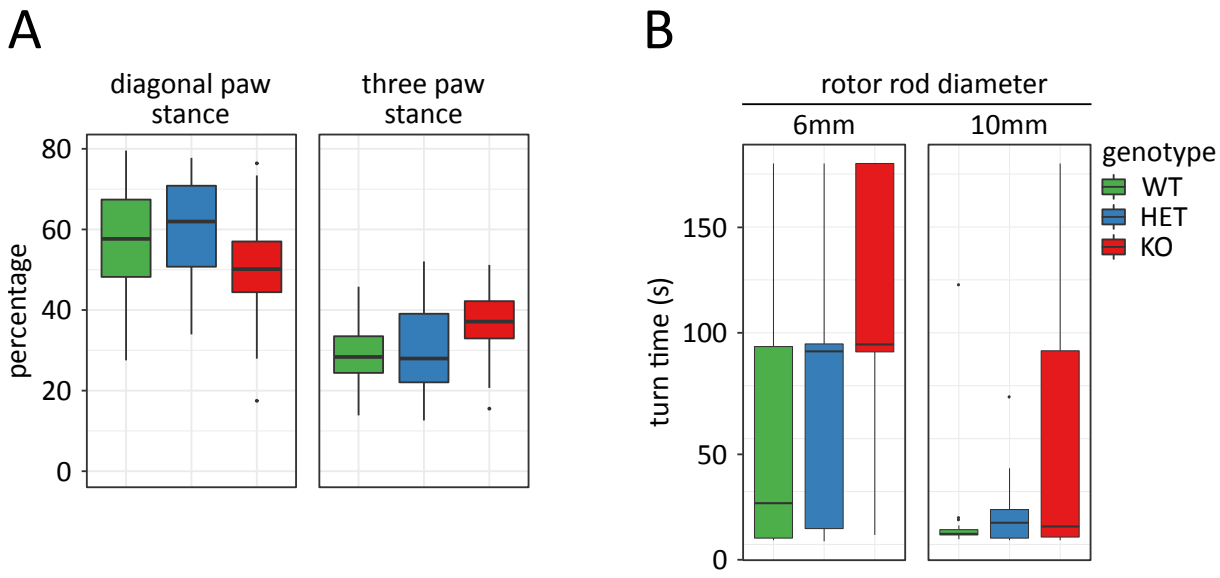


Figure 1.6: Caspr2 affects cerebellum-specific behaviours. **A)** When walking, *Cntnap2*$^{-/-}$ mice spend more time supporting themselves on three paws than *Cntnap2*$^{+/+}$ and *Cntnap2*$^{+/-}$ littermates. $p < 0.0001$ for time spent in the diagonal paw stance and $p < 0.00001$ for time spent in the three paw stance, main effect of genotype in a three-way (age*sex*genotype) mixed model ANOVA. The time points assessed were 5-6 weeks, 3 months and 5-6 months. n = 3 uninterrupted runs along a CatWalk XT walkway per animal per time point. Data for five animals (1∗WT, 3∗HET and 1∗KO) was excluded from the 3 post-natal months CatWalk dataset due to an accidental change in recording parameters. **B)** *Cntnap2*$^{-/-}$ mice take longer to turn around whilst navigating a static rod than *Cntnap2*$^{+/+}$ and *Cntnap2*$^{+/-}$ littermates. n = 2 trials per animal per rod diameter, $p < 0.05$, main effect of genotype in a three-way (sex*rod-type*genotype) mixed model ANOVA. For both A) and B), N = 8 female, 9 male *Cntnap2*$^{-/-}$ mice, 10 female, 10 male *Cntnap2*$^{+/-}$ mice and 10 female, 11 male *Cntnap2*$^{-/-}$ mice. Error bars represent mean, interquartile range and interquartile range∗1.5.

These experiments were conceived, executed and analysed by Friederike Winter (Becker lab, University of Oxford).

nap2 and a larger cerebellum[40].

For Caspr2 to have a cerebellar function, it of course must be expressed in the cerebellum. The first paper to report the identification of Caspr2 did indeed find it to be expressed here[110]. Taken all together, this evidence strongly suggests that Caspr2 has an important role in the cerebellum. However, the molecular and cellular bases for this are unknown and warrant investigation.

The cerebellum and ASD

One of the most commonly diagnosed mental health conditions, ASD is a developmental disease characterised by three core endophenotypes: impaired social interactions and communication, restrictive and repetitive behaviour, and language deficits[4; 162]. Recent clinical studies have implicated cerebellar pathology in ASD[1; 13; 25; 37; 87; 117]. Most notably, cerebellar injury around birth increases the risk of an individual developing ASD more than 30-fold[87]. Further, recent work has revealed that the degree of reduction of cerebellar grey matter volume in ASD individuals predicts the severity of the observed phenotype[37].

Experiments using mutant mouse models have also linked the cerebellum with ASD. Mutations in either of the *Tsc1* or *Tsc2* genes causes Tuberous Sclerosis, a condition commonly co-morbid with ASD. Specifically deleting *Tsc1* in Purkinje cells has been found to induce an ASD-like phenotype in mice[150]. Stimulation of Purkinje cells that harboured the *Tsc1* deletion was subsequently shown to ameliorate the social impairments displayed by these mice, further demonstrating that the cerebellum, and specifically Purkinje neurons, can act as a locus for ASD pathology[137]. Removing the synaptic protein Shank2 from murine Purkinje neurons also induces an ASD-like phenotype[106].

Caspr2 and ASD

ASD is highly heritable[10], however ASD individuals have very heterogeneous genotypes (over 1000 genes have been associated with the disorder thus far[62]) and present with a broad spectrum of resulting endophenotypes; confounding this problem, only a handful of ASD-associated mutations result in fully penetrant disease.

One of these fully-penetrant mutations is the homozygous deletion of the *CNTNAP2* gene. Individuals lacking the *CNTNAP2* gene develop a syndromic form of ASD

called Cortical dysplasia focal epilepsy (CDFE)[118; 140]. This aetiology-phenotype relationship is maintained in mice. *Cntnap2*$^{-/-}$ mice have been found to display endophenotypes similar to the three core autism behaviours seen in human patients. In the three-chamber social interaction test, *Cntnap2*$^{-/-}$ mice spent less time interacting with other mice than *Cntnap2*$^{+/+}$ did, consistent with *Cntnap2*$^{-/-}$ mice having a social impairment. In addition, adult *Cntnap2*$^{-/-}$ mice were less capable of adapting to the Morris water maze reversal paradigm, whilst *Cntnap2*$^{-/-}$ pups were found to emit far fewer ultrasonic vocalisations, suggesting that *Cntnap2*$^{-/-}$ mice also have restrictive behaviours and language / communication deficits[105]. Treatment with risperidone was able to alleviate the repetitive behaviour, but not social interaction deficits, an effect that is also seen in human patients with ASDs. Importantly, as ASD is a developmental disorder, it must be the case that Caspr2 has an important function during development.

Given that Capsr2 dysfunction causes both cerebellar-associated and ASD phenotypes, it is possible that impaired Caspr2 function, specifically in the cerebellum, underlies CDFE. Further evidence linking Caspr2 to ASD comes from a study that found Caspr2 to be expressed at synapses in the rat brain[11]. Recent work has suggested that synapses play a key role in ASD pathology, with synaptic pathophysiology found to be common in syndromic and nonsyndromic rodent models of autism[12]. *Pten*[146], *Mecp2*[99] and *Fmr1*[78] knockout mice all display a synaptic phenotype, in conjunction with ASD-like behaviours. In addition, mutations in *SHANK3*[39] and *NRXN1*[173] (two genes that code for proteins with functions at the synapse) are also associated with ASD in humans. This raises the intriguing possibility that Caspr2, expressed at synapses in the cerebellum, could be related to autism.

1.4 Caspr2: a Neurexin superfamily protein

Caspr2 is a member of the Neurexin superfamily of proteins, which contains the classical Neurexins and the Caspr-family members. Members of this group are all type 1 transmembrane proteins and are expressed in the nervous system. They function as cell adhesion molecules and have important roles in the development of the nervous system. The classical Neurexins are very well characterised and so, given their similarity to Caspr-family proteins, can provide important clues as to the role of Caspr2.

Genes

There are a total of three genes that code for classical Neurexin proteins, named *NRXN*1-3. Each of these genes has two promoters[154; 155; 156], the second of which is located far downstream of the first. The presence of this alternative promoter site leads to the transcription of a long and a short variant transcript of each *NRXN* gene. These 6 mRNAs are then all subject to extensive alternative splicing, producing potentially 1000s of classical Neurexin variants[153]. This splicing can radically alter the function of classical Neurexins translated from the same immature mRNA[152].

Classical Neurexins translated from the long variant transcripts of *NRXN* genes are known as α-Neurexins, whilst those translated from short variant transcripts are known as β-Neurexins (Figure 1.7).

5 distinct genes, termed *CNTNAP*1-5, encode the Caspr protein family in humans. In mice, two duplication events have produced three paralogues of the murine *Cntnap5* gene and so there are 8 murine *Cntnap* genes in total, *Cntnap*1-4 and *Cntnap*5-1, -2 and -3[104; 110; 136]. No alternative splicing of the *Cntnap2* genes has been noted. However, similar to the classical Neurexins, *Cntnap2* does have a second, down-

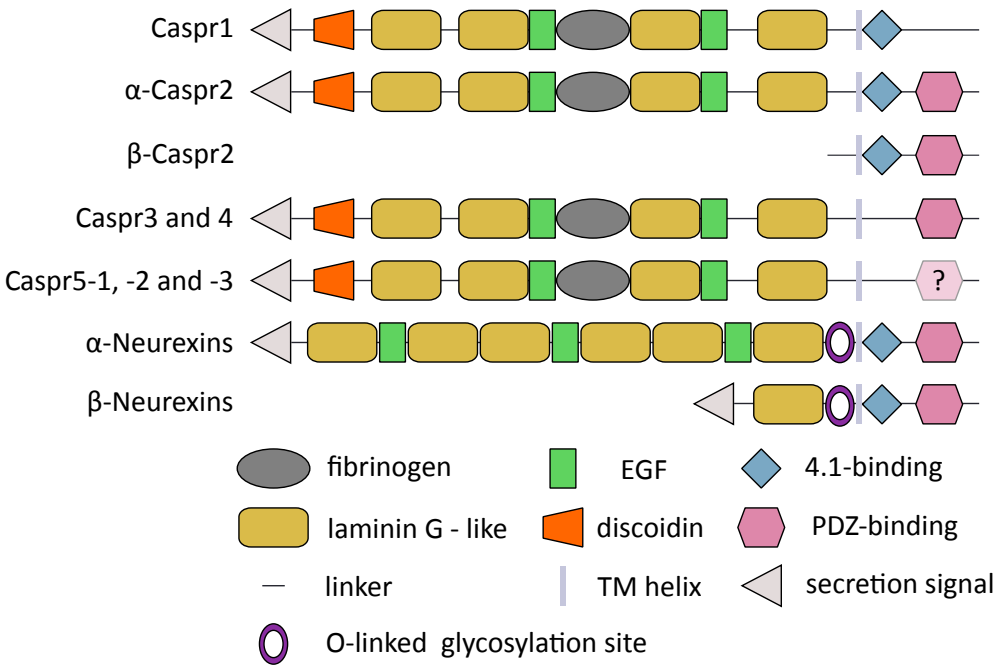


Figure 1.7: The Neurexin superfamily of proteins. Domain architectures of the different Neurexin superfamily proteins found in mice. Domain localisation information was taken from Uniprot in the first instance. Where Uniprot entries were incomplete, data was taken from the relevant primary sources described in the text. Note that no studies have yet confirmed the presence of any of the possible Caspr5 isotypes *in vivo*, and so the domain architecture presented here for these proteins is based on theoretical translations only. Proteins are not drawn to scale. Note that the long and short isoforms of Caspr2 are termed α-Caspr2 and β-Caspr2 only to encourage comparison with the α- and β-Neurexins. This nomenclature is not in use in the literature.

stream promoter[171]. Transcription initiated from this second promoter produces a transcript encoding an additional, smaller Caspr2 isoform[29]. Aside from this, each of the *Cntnap* and *CNTNAP* genes is thought to encode a single Caspr-family protein.

Domain architecture

See Figure 1.7 for an illustration of the domain architectures of the individual members of the Neurexin superfamily. See appendix A for a comparison of Caspr-family primary protein sequences.

One of the reasons the classical Neurexins are grouped with Caspr-family proteins in the Neurexin superfamily is that they share closely related domain architectures.

In fact, the *Drosophila melanogaster* orthologue of Caspr2, Neurexin-IV, was originally proposed to be an orthologue of α-Neurexin1[14].

The ECDs of all of the longer isoforms of Neurexin superfamily proteins contain both Laminin G-like and epidermal growth factor-like (EGF) domains. α-Neurexin ECDs are almost entirely comprised of a repeating Laminin G-like-EGF-Laminin G-like domain pattern[38; 155] and, whilst there are fewer Laminin-G like and EGF domains in the ECDs of long-isoform Caspr-family proteins, those that are present are arranged in the same pattern as in the α-Neurexins[104].

Despite this similarity, there are some major differences between the classical Neurexins and the Caspr-family proteins. Most notably, the ECDs of long-isoform Caspr-family proteins contain discoidin and fibrinogen-like domains. Neither of these are present in the classical Neurexins. The Caspr-family fibrinogen-like domain is located in a comparable position to the fourth α-Neurexin Laminin-G like domain, whilst the discoidin domain is found at the N-terminus of mature Caspr-family proteins. Thus, the domain architecture of long-isoform Caspr-family proteins can be considered to be a duplicate of the domain architecture of the α-Neurexins, save that the first α-Neurexin Laminin-G like and EGF domains are replaced by a discoidin domain in Caspr proteins and the fourth α-Neurexin Laminin-G like domain is exchanged for a fibrinogen-like domain.

Interestingly, although 207 residues are annotated as a fibrinogen-like domain in the Uniprot entry for *Homo sapiens* Caspr2, these domains are actually only around 45 residues long. To investigate this discrepancy, predictions of the structure of the region annotated as a fibrinogen-like domain were generated using the homology modelling tool Phyre^2 (Figure 1.8).

Whilst this search did return a model based on the fibrinogen C-terminal domain-like domain (PDB accession code 1JC9), this model only aligned to residues 596 to

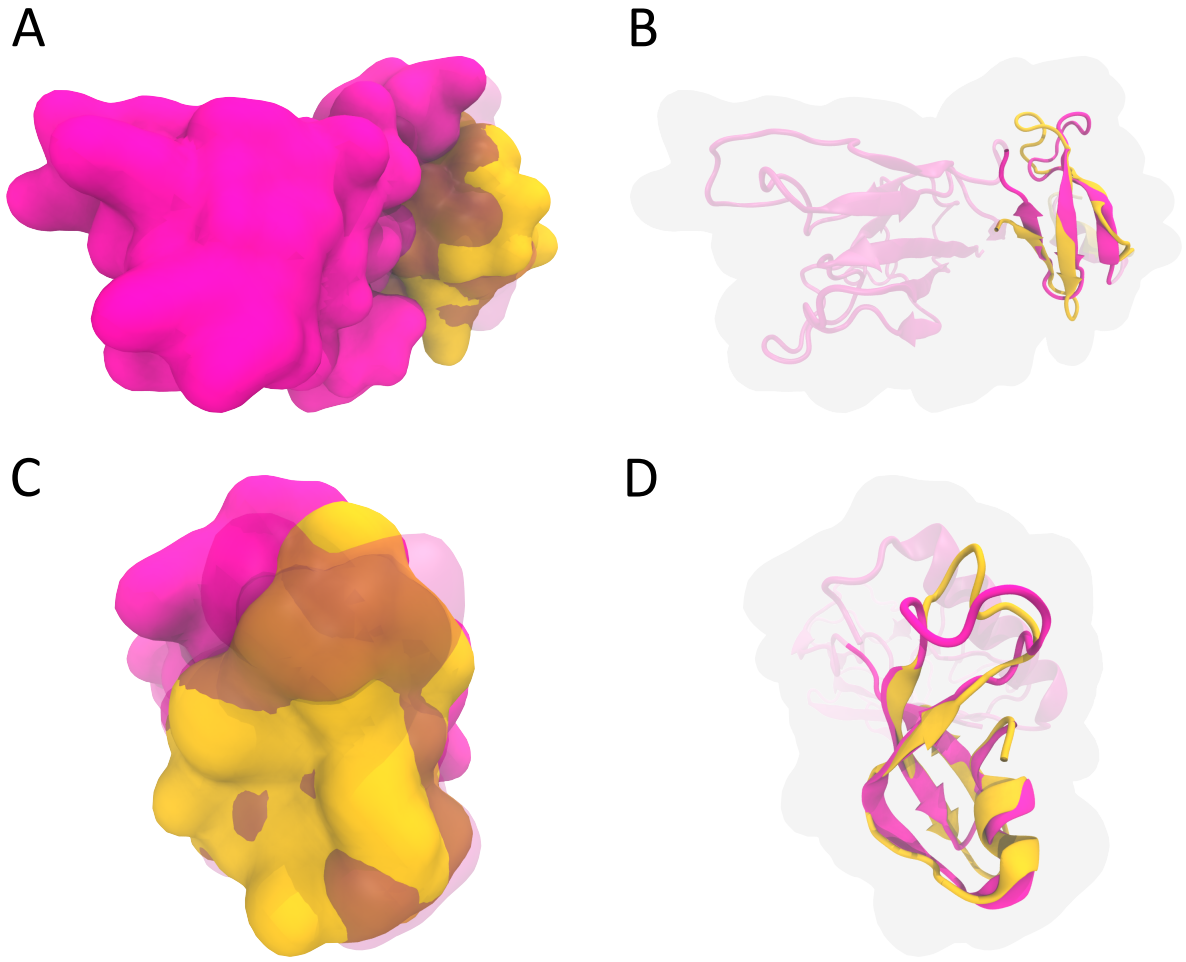


Figure 1.8: Homology modelling of the human Caspr2 domain annotated as a fibrinogen C-terminal domain-like domain in the Uniprot database. Residues 592 to 798 of the primary sequence of uniprot entry Q9UHC6 (Human Caspr2) are annotated as a fibrinogen C-terminal domain-like domain. This stretch of primary sequence was submitted to the Phyre[2] homology modelling server, with the search mode set to normal. The highest scoring model, based on Collagen α1(III) (PDB accession code 6FZV), and the model based on the fibrinogen C-terminal domain-like domain (PDB accession code 1JC9) were then superimposed. Superimposition was guided by primary sequence and was also carried out using Phyre[2]. Images were rendered in the Visual Molecular Dynamics program. Model based on fibrinogen, orange, model based on Collagen, magenta, maximum intensity projections for the volumetric Gaussian density maps of both models were combined and then flattened to give the grey areas. **A)** Density maps, side view. **B)** Secondary structures, side view. Residues 660-680 (present in the Collagen-based model only) have been removed for clarity. **C)** Density maps, end view. **D)** Secondary structures, end view.

641 of the human Caspr2 protein, amounting to 22% coverage of the domain labelled as a fibrinogen C-terminal domain-like domain on Uniprot. The highest-scoring

model, based on Collagen (PDB accession code 6FZV), aligned with residues 597 to 792 of the human Caspr2 primary sequence. This amounted to 95% coverage of the domain labelled as a fibrinogen C-terminal domain-like domain on Uniprot. Together, these observations reveal that although this stretch of primary sequence probably folds into a single globular shape, this structure is likely not solely comprised of a fibrinogen-like fold. Thus, it is likely that the labelling of this stretch of sequence as a fibrinogen-like domain is, at best, an incomplete annotation and that the true identity of this domain is unknown. Given that this is one of only two domains found in the Caspr-family proteins and not in the classical Neurexins, it may well represent a key structure that dichotomises the functions of the two groups. Describing the structure of this domain would be a worthwhile goal for a future structural biology project.

All members of the Neurexin superfamily have a short intracellular tail, which may contain either or both of a juxta-membrane protein 4.1-binding site and a C-terminal PSD-95/Disc large 1/Zonula occludens 1 (PDZ)-binding domain. All of the classical Neurexins have both protein 4.1-binding[88; 91; 155] and PDZ-binding sequences[97; 131; 155]. Caspr1 and Caspr2 both have protein 4.1-binding sites[91; 104; 110], but of these two only Caspr2 has a PDZ-binding domain[17; 110]. In contrast, Caspr3 and 4 have PDZ-binding sequences only[136]. Little is known about the human Caspr5 protein or any of the three murine Caspr5 paralogues. In fact, Caspr5 proteins are yet to be detected *in vivo*. *Cntnap5* mRNA has been detected however[136] and it has been noted, after inspection of theoretical translations, that Caspr5-1,-2 and -3 likely do not have 4.1B binding domains[149]. It is not clear if these proteins have a cytoplasmic PDZ- binding domain. The (predicted) extreme C-termini of Caspr5-1,-2 and -3 are somewhat homologous to the other Neurexin superfamily proteins and so it is possible that they also bind PDZ domains. However, the (theoretical)

C-terminal sequences of the Caspr5 proteins are distinct enough from those of the other Neurexins to raise doubts. PDZ-binding sequences are C-terminal and only 4-5 residues in length. Comparing the five residues at the extreme C-termini of the murine Caspr proteins, all members of the Caspr family have a strictly conserved Glu at position 2 (where position 5 is the final, C-terminal residue-see appendix A). Caspr1, the only Caspr-family member known not to have a PDZ-binding domain, does not have residues in positions 3, 4 and 5. Instead, the conserved Glu at position 2 is the terminal residue for this protein. All of the Caspr5 paralogues have residues in these positions, consistent with the presence of a PDZ-binding domain. Further, the residues in positions 4 ad 5 are conserved between the Caspr5 paralogues and the *Drosophila melanogaster* Caspr2 orthologue NrxIV, which does have a PDZ-binding domain. However, Caspr5-3 has a glutamine residue at position 1 and an aspartic acid at position 3, which are dissimilar to the residues found at these positions in the other Caspr-family proteins. For Caspr5-1 and -2, position 1 is taken up by an arginine, which is similar to the lysine at this position in the Caspr2 primary sequence. The tyrosine at position 3 matches the one found in Caspr4. Thus Caspr5-1 and -2 are more likely to have a PDZ-binding domain than Caspr5-3, although it is possible that all three of the murine Caspr5 paralogues do so.

Function

Broadly speaking, Neurexin superfamily proteins are cell adhesion proteins. Thus far, classical Neurexins have been found to mediate communication between pairs of neuronal cells[155]. Caspr family proteins, on the other hand, have been found to link glia to glia and glia to neurons[104; 123].

The canonical binding partners of the classical Neurexins are the Neuroligins, another family of Type 1 transmembrane proteins expressed in the nervous system.

The classical Neurexins are pre-synaptic, whilst Neuroligins are post-synaptic and so by interacting they facilitate trans-synaptic communication[22; 35]. The huge variety of potential classical Neurexin splice isoforms combined with the 20 possible isoforms of Neuroligin creates a computational code that specifies synaptic properties[128; 143]. As an example, the classical Neurexins are necessary for correct calcium current amplitudes at synapses formed by cultured murine hippocampal neurons[98]. Missler et al suggest that by interacting both with transmembrane adhesion proteins found in the synaptolemma of apposed post-synaptic membranes, and with cytoplasmic, pre-synaptic PDZ domain-containing proteins, the classical Neruexins may localise the synapse-specific regulation of Ca^{2+} channels to synaptic sites[98]. The authors point out that CASK[57] and Mints[19], and the synaptic vesicle protein synaptotagmin[107], are all known to interact with the cytoplasmic domain of the classical Neurexins and may also modulate Ca^{2+} channels[9; 93].
Neurexins are also involved in synapse formation and maturation, but are apparently not essential for synaptogenesis[114; 152].
Interestingly, although classical Neurexins are localised exclusively to synapses, they also regulate dendrite growth. Experiments in the embryonic *Xenopus laevis* optic tectum have demonstrated that Neurexin-Neuroligin complexes are required for post-synaptic maturation, which in turn is necessary for activity-driven dendritic growth. This synaptotrophic dendritic arbourisation is crucial for the correct development of neuronal circuits[30]. The classical Neurexins have an extensive functional proteome and interact with many proteins other than the Neuroligins[143]. It was recently discovered, for example, that Neurexin-1β communicates with Gluδ2 channels via the Cerebellin-1 protein, which is secreted into the synaptic cleft at parallel fibre-Purkinje cell synapses[152]. The tripartite Neurexin-1α, Cerebellin-1, Gluδ2 complex is required for synapse formation at this synapse, suggesting that Neurex-

ins may influence synaptotrophic dendritic growth by modulating post-synaptic ion channel activity and not just by effecting synapse maturation. In addition, it is worth noting that GluRδ2 is specifically expressed by Purkinje cells and the majority of Cerebellin-1 is expressed by granule cells. Thus, the regulation of parallel fibre-Purkinje cell synaptogenesis by this Neurexin-1α, Cerebellin-1, Gluδ2 complex represents a good example of how the variety of the Neurexin superfamily proteome facilitates the encoding of synapse specificity[152].

Caspr1 and 2 both link neurons to myelinating glia[18; 112; 148], and this link is required both for timely myelination during development[129] and for the correct localisation of K^+ channels at the juxta-paranode (JXP)[18; 24; 55; 123]. By definition, the glia-neuron communication mediated by Caspr1 and 2 involves the ECDs of Caspr1 and 2.

Similar to the classical Neurexins, Caspr-family proteins interact with a variety of intracellular binding partners via their 4.1-binding and PDZ-binding domains[29; 121; 136]. For example, Caspr4 interacts with CASK, via the CASK PDZ-domain, in much the same way as the classical Neurexins do[136].

In summary, the classical Neurexins and the Caspr-family proteins play important roles in development. The fact that both protein families have similar domain architectures suggests that they perform similar functions. Each of the long isoforms of the classical Neurexins and Caspr-family proteins have long, extracellular adhesion domains that are used for facilitating communication between neighbouring cells. They also both localise intracellular machinery to sites of intercellular communication, using 4.1- and PDZ- binding domains. Differences in the interaction proteomes of the different Neurexin superfamily members adjust both the types of cell bound by each family member, as well as the downstream effects of any interaction. Although the general mechanism by which the Neurexin superfamily proteins

function can be thought of as similar, this means that the classical Neurexins and the Caspr-family proteins may potentially have quite divergent functions. For example, as only the classical Neurexins are extensively alternatively spliced, it is unlikely that the Caspr-family of proteins specifies synapse types via the same mechanism.
Interestingly though, Caspr2 is expressed at synapses[11] and has been shown to affect synapse numbers in dissociated hippocampal neuron cultures, as well dendritic morphology[5]. This suggests that although Caspr2 may not be involved in synapse specification like the classical Neurexins, it may still have an important synaptic role. More detailed accounts of the known functions of Caspr2 are provided in the introduction sections of chapters 3 and 5.

Links between Neurexin-superfamily proteins and disease

Of the Neurexin superfamily proteins, it is not just Caspr2 that has been associated with disease. In addition to the homozygous deletion of *CNTNAP2* causing CDFE[140], a syndromic form of autism, various mutations in *NRXN1* have also been linked to ASD[76; 145; 167; 169]. Mutations in Neuroligin3 and 4 have been linked to the condition as well[70], providing further evidence that the dysfunction of Neurexin-containing complexes leads to autism.
The classical Neurexins are specifically synaptic and Caspr2 has also been found to be expressed at synapses[11; 155]. Given this, and the fact that the dysfunction of either Caspr2 or Neurexin-1 results in autism, it seems likely that Caspr2 has an important role at the synapse. Perhaps unsurprisingly, given the important role the Neurexin superfamily proteins play in the development of the CNS and the huge variety of α-Neurexins that exist, mutations in these proteins have also been linked to other brain disorders. For example, *NRXN1* deletions have been associated with schizophrenia[161]. Other Caspr-family proteins have also been implicated in

disease. Most recently, Caspr1 was found to be a host receptor for *Escherichia coli* invasions that cause meningitis[172]. It should also be noted that the dysfunction of Caspr2 has been associated with conditions that are not linked to the cerebellum. Autoantibodies directed against Caspr2 have been found to induce a pain phenotype, as well as autoimmune encephalitis and neuromyotonia[34; 67; 80]. Interestingly, in some clinical cases these autoantibodies had previously been found to target the voltage-gated K^+ channel complex, although it was not known exactly which component of the complex represented the antigen. Irani et al suggest that the binding of autoantibodies to Caspr2 moieties involved in the complex could be sufficient to impair K^+ channel function. Further, they hypothesise that this may represent the aetiology of the myotonia presented by some patients who have autoantibodies against Caspr2 circulating in their sera[67].

1.5 Currently available Caspr2 expression data

CNTNAP2 was initially detected in human tissue[110]. Northern blotting revealed high levels of *CNTNAP2* expression in the nervous system and low levels in the ovaries and testis. *CNTNAP2* transcripts were not detected in any other tissue. Analysis of individual brain regions revealed expression in multiple areas, including the medulla, the amygdala, the hippocampus and the cerebellum. In the same paper, the Caspr2 protein was then identified in rats by immunoblotting. It was found in both the PNS, in the sciatic nerve, and the brain, in similar locations to where the transcripts were found in humans. The authors reported that Caspr2 is first expressed in rat brain at E15, with expression then increasing throughout development[110]. A similar whole brain temporal expression pattern has also been observed in mice[105]. Specialised sites that facilitate saltatory transduction are spaced regularly along the

long axis of myelinated axons. These sites are called the nodes of Ranvier and they are essential for the efficient propagation of action potentials. Nodes of Ranvier are defined by clusters of Na^+ channels and an absence of myelination, which together facilitate depolarisation. On either side of the Node of Ranvier are the paranode and JXP regions. The JXP is more distal from the Node of Ranvier than then the paranode, such that the modularity of a myelinated axon structure is defined by repetitions of an internode-JXP-paranode-node of Ranvier-paranode-JXP-internode pattern. Whilst Na^+ channels are found at the nodes of Ranvier, K^+ channels are clustered at the JXP, where they help to maintain the resting membrane potential. Immunohistochemistry revealed Caspr2 localises to the juxtaparanode in the myelinated fibres of the optic nerve and cerebellar Purkinje cells in rats[110].

In addition to being present at the JXP, Caspr2 also localises to the dendrites of rat cortical neurons[110], the axon initial segment of human pyramidal neurons (temporal lobe)[65], the somata of dorsal root ganglion cells[34] and rat brain synapses[11]. It has also been found at presynaptic sites in cultures of rat hippocampal neurons[109]. Previous work done in the Becker lab has shown that Caspr2 is expressed in the murine cerebellum, throughout post-natal development (Figure 1.9). Interestingly, qPCR data indicates that *Cntnap2* is expressed from P4, but protein expression is only upregulated at around P14, when parallel and climbing fibres are forming synapses with the Purkinje cell dendritic arbour. This is consistent with Caspr2 having a role at these synapses, with post-transcriptional regulation of expression inhibiting translation of Caspr2 until they begin to form.

A more detailed account of the information currently available about the expres-

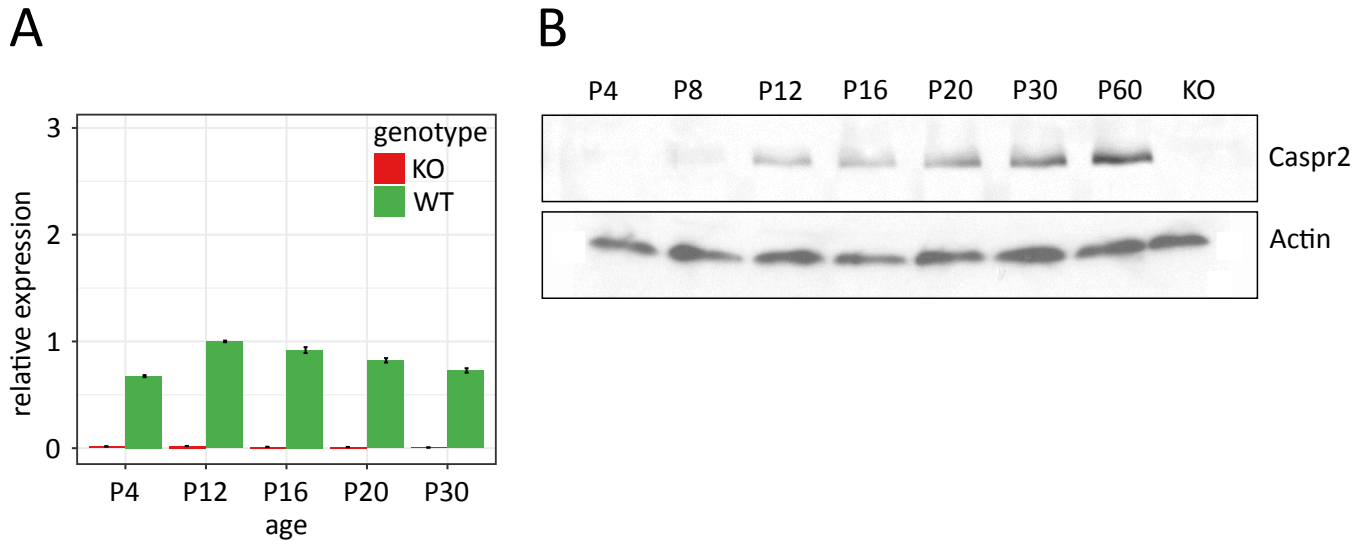


Figure 1.9: Caspr2 is expressed in the cerebellum, throughout post-natal development. A) *Cntnap2* transcript levels in the murine cerebellum, over time, as assessed by qPCR. N = 1 animal for each time point, n = 3 RT-qPCR replicates. Error bars represent mean values ± SEM. **B)** Temporal expression of Caspr2 expression levels in the murine cerebellum, as assessed by Western blotting. N = 1 animal per time point.

These experiments were conceived, executed and analysed by Friederike Winter (Becker lab, University of Oxford).

sion of Caspr2 in the cerebellum is provided in the introduction section of chapter 3.

.

1.6 Aims

Despite all of the evidence that implicates *CNTNAP2* and Caspr2 in cerebellar function, the functional role of *CNTNAP2* in the developing cerebellum remains unknown. Moreover, nothing is known about the molecular basis of the role of Caspr2 at the synapse or how, if at all, this is related to Caspr2-related pathologies.

The aim of this thesis was therefore to describe the function of Caspr2 at synapses in the developing cerebellum, in order to better understand the role of *CNTNAP2* in the developing cerebellum and by extension how its dysfunction might be involved

in cerebellar pathologies such as autism and ataxia.

The objectives for the programme of work presented in this thesis were as follows:

- Determine the spatial expression pattern of Caspr2 in the developing cerebellum
- Describe the functional effect of Caspr2 on cellular development in the cerebellum
- Identify the synaptic binding partners of Caspr2 in the developing cerebellum
- Determine the functional consequences of any interactions uncovered

Using a combination of histology, biochemistry and molecular biology, each of the above objectives were achieved. Caspr2 was found to regulate Purkinje cell dendritic development and to interact with the Ca^{2+} ion channel IP_3R1 at Purkinje cell synapses in the developing molecular layer of the cerebellum. Further investigation revealed that Caspr2-IP_3R1 communication affects cellular morphology and that Caspr2 may regulate cellular Ca^{2+} levels, possibly by controlling IP_3R1 Ca^{2+} currents.

Together, these results shed light on the mechanism of Caspr2 function in cerebellar development, improving our understanding of this previously overlooked brain region. These data may also provide a platform from which future studies can examine how Caspr2 dysfunction at the synapse leads to the cerebellum-associated phenotypes we observe in the clinic.

2 Methods

Unless otherwise stated, all of the results presented in this thesis are comprised of data taken from a minimum of two identical but independent experiments.

2.1 Animals

Mouse lines

Two distinct strains of mice were used in this study. One strain was homozygous for an engineered mutation: an insertion of the *neomycin* gene into exon 1 of the *Cntnap2* gene [112]. The *neomycin* gene was inserted in the opposite direction of the *Cntnap2* gene, and replaced a section that included the *Cntnap2* start codon. This line has since been back-crossed >10 times on to the C57BL/6J background. Mice homozygous for the neomycin-insertion mutation are referred to as *Cntnap2*$^{-/-}$ mice. They do not express the long isoform of Caspr2, but do express the shorter Caspr2 isoform. It was not discovered that *Cntnap2*$^{-/-}$ mice express this shorter isoform until after work on this project had begun.

The other strain had no copies of this mutant allele and were instead homozygous for the wild-type *Cntnap2* gene. These mice are referred to as *Cntnap2*$^{+/+}$ and they express both isoforms of Caspr2.

Where possible, both strains were obtained by crossing *Cntnap2*$^{+/-}$ mice so that littermates could be compared. In some instances, which are noted, this was not possible and *Cntnap2*$^{+/+}$ animals were instead sourced from a separate C57BL/6J colony.

Rat lines

6 week old Wistar and Spontaneously hypertensive rats were kindly provided by Emma Bardsley (Paterson lab, University of Oxford). As these animals were used only as a source of IP_3R1 protein, tissue from both strains was pooled.

Tissue collection

Where murine tissue was collected, mice were euthanised via exposure to a rising concentration of CO_2 and then decapitated. This technique is one of the approved killing methods defined by Schedule 1 of the Animals (Scientific Procedures) Act.
Where rat tissue was collected, rats were first anaesthetised via exposure to isoflurane and then, after no response to a tail pinch could be detected, euthanised by pentobarbitone overdose (drug was delivered via intraperitoneal injection). Rat euthanasia was performed by Emma Bardsley (Paterson lab, University of Oxford).
Regardless of whether rats or mice were used, the cerebellum was quickly dissected out following euthanasia. Cerebella to be used for immunohistochemistry were submerged in optimum cutting temperate (OCT) compound (Agar scientific) and then frozen on dry ice, before being stored at -80°C until required. Cerebella to be used for slice preparation were submerged in ice cold HHGN (1X HBSS, 2.5mM HEPES, pH7.4, 35mM glucose, 4mM Na^+ bicarbonate) before being processed further. If intended for any other purpose than slice preparation or immunohistochemistry, dissected cerebella were snap frozen in liquid N_2 and stored at -80°C until required.

2.2 Molecular biology

All primers were purchased from Sigma-Aldrich, in desalt form. Restriction enzymes were purchased from NEB. All molecular biology reagents / kits were used as per the manufacturers' instructions.

Agarose gel electrophoresis

To prepare agarose gels, agarose was combined with either TBE (45mM Tris-borate, 1mM EDTA,pH8) or TAE (40mM Tris, 20mM acetic acid, and 1mM EDTA,pH8) buffer and the mixture was heated until the agarose was fully solubilised. The agarose percentage (w/v) used was varied depending on the size of the DNA fragment to be resolved. TAE was used when DNA was to be extracted from the gel after being resolved because boric acid inhibits enzymes used further downstream in the cloning process. TBE was used in all other cases.

Next, the DNA stain SYBR safe (ThermoFisher) was added at a ratio of 1:10,000 (v/v) and the solution was poured and allowed to solidify. The set gel was submerged in running buffer (the buffer used to prepare the gel) and DNA samples, combined with 6X gel loading dye (NEB), were then loaded. An aliquot of pre-stained DNA ladder (NEB) was also loaded. A constant voltage was passed across the gel until the DNA ladder was satisfactorily resolved. An Alpha Imager 3400 (Alpha Innotech) was used to measure levels of UV absorption throughout the gel and thus visualise resolved DNA bands.

Construct design and cloning

The primers used for PCRs during cloning are given in Table 2.1. Restriction sites that were included in order to be subsequently digested and thus to produce sticky

ends are also indicated in Table 2.1. PCR conditions are given in Tables 2.2, 2.3 and 2.4.

The nucleotide base sequence encoding the ECD of mouse Caspr2 (protein residues 28-1262 from Uniprot E9QNF7, base sequence as in Ensembl ENSMUST00000114641.7) was inserted, by PCR cloning, into the pHL-Avitag3 vector[7].

An empty pHL-Avitag construct was created by digesting the pHL-Avitag3 vector with EcoRI and XhoI to remove the MCS, blunting the resulting overhangs and then ligating the linearised backbone to re-form a plasmid.

The LL3 region of a pre-existing IP_3R1 expression construct (primary protein sequence as in GenBank: AAA41357.1, base sequence as in [96]) was deleted to create a ΔLL3 IP_3R1 expression construct (primary protein sequence as in GenBank: AAA41357.1, but with AAs 2451-2555 removed). An initial PCR reaction was used to both delete the sequence encoding the IP_3R1 LL3 region from the pre-existing plasmid, and to insert BsiWI restriction sites at both the 5' and 3' termini of the PCR product. The resulting linearised, Δ LL3 IP_3R1 plasmid was then digested with BsiWI and re-ligated. The original, full-length IP_3R1 expression vector (IP_3R1 in pCB1) was provided by Greg Mignery (Mignery lab, Loyola University).

The JXM Caspr2 (protein residues 592-1257 from Uniprot Q9UHC6, base sequence as in Ensembl ENST00000361727.7) expression construct was generated by using PCR cloning to insert the relevant sequence in to a 3XFLAG-CMV-10 vector (Sigma).

The JXM Caspr2 construct was generated by Imogen Prickett (Becker lab, University of Oxford).

The BirA construct was a kind gift from Verity Jackson (Miller lab, MRC LMB).

Table 2.1: Primers for PCR cloning. Restriction sites are highlighted in **bold**

name	sequence
ECD C2 fw	CATTAG**ACCGGT**GCTCCCTCCACGTTCCAAAAATGTGAT
ECD	CATTAG**CGTACG**TGAGTTTCTGTTGACTCCATTTCTTATAGCTTGG
Δ LL3 fwd	CATTAG**CGTACG**TCCAAAGAGGAGCCTCTGTTTGC
Δ LL3 rev	CATTAG**CGTACG**GTCATCCTTGAAGAACAGGTAGCC
JXM C2 fw	CATTAG**GGTACC**TAACTCTATCTACGAGCCTTCCTG
JXM C2 rv	CATTAG**TCTAGA**GACTCCATTTCTTATAGCTTGG

Table 2.2: PCR conditions for Caspr2 ECD expression construct cloning

reagent	volume	temperature	time	
template DNA (50ng/µ)L	1.0µL	95°C	10′	
forward primer (10µM each)	1.5µL	95°C	30″	|
reverse primer (10µM each)	1.5µL	55°C	30″	| 34 cycles
PCR nucleotides (25mM each)	4.0µL	72°C	8′	|
DMSO (100%)	0µL	72°C	5′	
$MgSO_4$ (50mM)	0µL			
Pyrobest buffer (Takara) (10x)	1µL			
Pyrobest polymerase (Takara) (5EU/µL)	0.2µL			
nuclease-free H_2O (Ambion)	up to 50µL			

Table 2.3: PCR conditions for Caspr2 JXM domain expression construct cloning

reagent	volume	temperature	time	
template DNA (50ng/µ)L	1.0µL	95°C	2′	
forward primer (10µM each)	1.5µL	95°C	30″	|
reverse primer (10µM each)	1.5µL	53°C	30″	| 34 cycles
PCR nucleotides (25mM each)	1.0µL	72°C	2′	|
DMSO (100%)	2.5µL	72°C	10′	
$MgSO_4$ (50mM)	1.0µL			
PfuUltra buffer (10x) (Agilent)	1µL			
PfuUltra polymerase (2.5EU/µL) (Agilent)	1.0µL			
nuclease-free H_2O	up to 50µL			

Table 2.4: PCR conditions for Δ LL3 IP_3R1 expression construct cloning

reagent	volume	temperature	time	
template DNA (50ng/µ)L	1.0µL	92°C	2′	
forward primer (10µM each)	1.5µL	92°C	10″	|
reverse primer (10µM each)	1.5µL	55°C	30″	| 5 cycles
PCR nucleotides (25mM each)	1.0µL	68°C	26′	|
DMSO (100%)	2.5µL	followed by		
$MgSO_4$ (50mM)	1.0µL	92°C	10′	|
PfuUltra buffer (10x)	1µL	60°C	30″	| 30 cycles
PfuUltra polymerase (2.5EU/µL)	1.0µL	68°C	26′	|
nuclease-free H_2O	up to 50µL			

Human (in pCDNA3.1+) and murine (in pCMV6-entry) Caspr2 constructs were obtained from Angela Vincent (Vincent lab, University of Oxford) and Friederike Winter (Becker lab, University of Oxford), respectively. Eric Lancaster (Lancaster lab, University of Pennsylvania) kindly provided the ΔDisc-EGF1 and the ΔFib-Lam4 Caspr2 deletion constructs (both in Prk5)[103].

DNA purification after PCR was achieved using a QIAquick PCR purification kit (QIAGEN), whereas DNA purification after restriction was achieved using a QIAquick gel extraction kit (QIAGEN). A Quick Ligation Kit (NEB) was used to catalyse ligation reactions.

Transformation

50µL of competent cell suspension was first thawed on ice and then mixed with an aliquot of the plasmid DNA to be transformed (1-10ng). The mixture was incubated on ice for 5min, heat shocked at 42°C for 30s and then again incubated on ice for a further 2min. The cells were supplemented with 250µL SOC medium (Invitrogen) and then incubated at 37°C for one hour, whilst being rotated at 240rpm. Transformed bacteria were spread on antibiotic selection plates and left overnight at 37°C

(100µg/mL of either ampicillin or kanamycin was added to LB agar to produce selection plates). Plates on which colonies were observed to have grown were stored at 4°C until required.

Top10 ONESHOT *E.coli* (Life Technologies) were used for plasmid amplification where low amounts of plasmid were available, for example after sub-cloning. Library Efficiency DH5α *E.coli* (Sigma) were used in all other cases.

Plasmid amplification

Individual colonies from plates, or small amounts of glycerol stocks of previously prepared cultures, were picked using a pipette tip and placed in 5ml of Lennox broth containing 100µg/mL of either ampicillin or kanamycin. The cultures were then incubated at 37°C, whilst rotating at 225rpm. If smaller amounts of DNA were required (25-35µg), cells were grown for 16 hours and plasmid DNA was purified from the resulting cultures using a QIAprep miniprep kit (Qiagen). For larger amounts of DNA (500µg-10mg), cells were grown for 8 hours and the resulting cultures were then used to inoculate larger volumes of Lennox Broth. Once confluent, plasmid DNA was then purified from these larger cultures using either a QIAprep maxiprep (for 200mL of confluent culture, Qiagen) or gigaprep kit (for 5L of confluent culture, Qiagen).

Sequencing

The DNA sequences of recombinant plasmids were confirmed by Sanger sequencing (outsourced either to Beckman Coulter Genomics-silver service or to Source-Bioscience) and pairwise alignment with the expected sequence (Emboss needle).

Genotyping

A PCR-based genotyping procedure was used to differentiate between *Cntnap2*$^{-/-}$, *Cntnap2*$^{+/-}$ and *Cntnap2*$^{+/+}$ mice. An earclip was taken from each mouse and then lysed via overnight incubation in lysis buffer (100mM Tris pH8.0, 5mM EDTA pH8.0, 0.2% SDS, 200mM NaCl) containing Proteinase K (Roche) at 55°C. Genomic DNA was precipitated with isopropanol and the samples were then centrifuged at 13,000*g* for 20 minutes, at 4°C. The resulting supernatant was exchanged for ice-cold 70% (v/v) ethanol and the samples were again centrifuged at 13,000*g* for 20 minutes, at 4°C. Following centrifugation, the supernatant was discarded and the pellet was dried at 37°C until the leftover ethanol had completely evaporated. The remaining pellet was resuspended in nuclease-free water and incubated for 10 minutes at 65°C to speed the solubilisation of the precipitated DNA. This solubilised DNA was then

Table 2.5: Genotyping primers

name	sequence
Cntnap2$^{+/+}$ forward	TGCTGCTGCCAGCCCAGGAACTGG
Cntnap2$^{+/+}$ reverse	TCAGAGTTGATACCCGAGCGCC
Cntnap2$^{-/-}$ forward	AGCAGCCGATTGTCTGTTGT
Cntnap2$^{-/-}$ reverse	CTCACCCAATCTCACAAACAAG

Table 2.6: Genotyping PCR conditions

reagent	volume	temperature	time	
10X RedTaq buffer (Sigma)	2.5µL	94°C	4′	
PCR nucleotides, (25mM each)	0.5µL	94°C	30″	|
primers (10µM each)	1µL	60°C	30″	| 34 cycles
RedTaq DNA polymerase	1.2µL	72°C	30″	|
(1EU/µL) (Sigma)		72°C	10′	
nuclease-free H_2O	up to 25µL			

used as template DNA for two separate PCR reactions: one using a set of primers matching a sequence unique to the *Cntnap2*$^{+/+}$ genotype, the other using a set of

primers matching a sequence unique to the *Cntnap2*$^{-/-}$ genotype (see Table 2.5 for primer sequences and Table 2.6 for cycling conditions). The resulting PCR products were run on an agarose gel, with the resulting band pattern describing the genotype of the relevant mouse: a positive signal from the *Cntnap2*$^{+/+}$ PCR indicated the presence of at least one *Cntnap2*$^{+/+}$ *Cntnap2* allele, whilst a positive signal from the *Cntnap2*$^{-/-}$ PCR indicated the presence of at least one *Cntnap2*$^{-/-}$ *Cntnap2* allele.

2.3 Cell biology

Details of all antibodies used with methods described in this section can be found in Tables 2.8, 2.9 and 2.10.

Tissue culture

HEK293FT cells were maintained in 5% CO_2 , at 37°C and in humidified conditions. The volume of Dulbecco's modified Eagle's medium (DMEM) (containing GlutaMax, Gibco) used, and the amount of foetal calf serum (FCS) (GE Healthcare) and Penicillin-Streptomycin (Pen-Strep) (Invitrogen) added as a supplement, were varied as required.

When used to express Caspr2 ECD on a large scale (to produce protein for the dosing of cerebellar slices), HEK293FT cells were cultured in 12 $*$ 2L roller bottles. 200mL medium, with 2% FCS and 0% Pen-Strep, was used to feed the cells in each bottle. At this scale, cells were cultured for 96 hours post-transfection. In all other cases, cells were only cultured for 48 hours post-transfection (see below for details of transfection procedures).

Large-scale HEK293FT cell culture was performed by Maria Carrasquero-Ordaz (Seiradake lab, University of Oxford).

Caspr2 ECD was produced on a much smaller scale for use in pull down studies. For this, HEK293FT cells were grown in 10mL Advanced DMEM (containing GlutaMax, Gibco) supplemented with 2% FCS + 1% Pen-Strep, in 10cm^2 dishes.
For immunocytochemistry experiments, HEK293FT cells were seeded on to poly-lysine coated glass coverslips, situated in 24-well plates, and maintained in 1mL medium, with 10% FCS + 1% Pen-Strep, for 24 hours before being transfected.
For the assessment of cytoplasmic Ca^{2+} levels and for co-immunoprecipitation (co-IP) experiments, HEK293FT cells were cultured in 6-well plates. 3mL medium, with 10% FCS + 1% Pen-Strep, was used to feed each well.
For the preparation of cerebellar slices, dissected cerebella from P9 mice were submerged in HHGN (1X HBSS, 2.5mM HEPES, pH7.4, 35mM glucose, 4mM Na^+ bicarbonate) and the meninges were removed under a dissection microscope. 400µm sagittal slices were cut using a McIlwain tissue chopper (Mickle Laboratory Engineering) and transferred to 0.4µm pore, Millicell cell culture inserts (Millipore), which were placed inside 35mm tissue culture dishes. Culture medium (1X MEM [Gibco], 25mM Hepes, 25% horse serum [Invitrogen], 6.5 mg/ml D-glucose, 2 mM glutamine, and Pen-Strep) was added to the bottom of the dishes such that slices were resting on the air-medium interface. Slices were incubated at 37°C, 5% CO_2 . The medium was changed every 3 days. Dosing was carried out after 1 DIV and then after every change of media. Slices were either dosed with a vehicle treatment (10mM Tris pH 8, 200mM NaCl) or 20µg/mL ECD Caspr2. Slices were cultured for a total of 8 days.

Transfection

To transfect HEK293FT cells in order to express recombinant Caspr2 on a large scale, 5.4mg avitagged Caspr2 ECD expression construct DNA and 0.6mg BirA expression construct DNA were combined together. A one tenth volume of chloroform was then added and the mixture was centrifuged at 16,000*g* for 10mins, at 4°C. The aqueous layer containing the plasmid DNA was removed and added to 600mL serum-free DMEM (supplemented with 1% non-essential amino acids (NEAA) [Gibco] and L-Glutamine). Polyethylenimine (PEI) was also added, at ratio of 2:1 (w/w) (PEI : plasmid DNA), and this transfection cocktail was then incubated for 10mins. During this time the cell media in each roller bottle was exchanged for 200mL DMEM (also supplemented with 1% NEAA and L-Glutamine) containing 2% FCS. Biotin (Sigma) was also added up to a final concentration of 62.5µM. After the allotted 10mins incubation time had passed, 50mL of transfection cocktail was added to each of the 12 roller bottles.

In all other cases, HEK293FT cells were transiently transfected with the appropriate construct(s) using FuGene HD (Roche), as per the manufacturers instructions. Where *in vivo* biotinylation was required, the cell medium was supplemented with biotin up to 40µM.

Immunocytochemistry

Coverslips were washed with 1X phosphate-buffered saline (PBS) and then fixed by immersion in ice-cold acetone for 5 minutes, permeabilised via incubation in 0.4% (v/v) Triton X-100 (Sigma) / 1X PBS for 20 minutes and then blocked using 10% skimmed milk powder, 1% normal goat serum (Sigma), 1X TBST for ICC (150mM NaCl, 10mM Tris, pH8, 0.02% Tween-20 [Bio-rad]). Coverslips were next washed three times with 1X PBS, before being incubated overnight, at 4°C, in antibody car-

rier solution (3% BSA [Fisher Scientific], 0.02% NaN_3, 1X TBST for ICC) containing the appropriate amount of primary antibody. After being washed three times in 1X PBS, coverslips were then incubated in antibody carrier solution containing an alexa dye-conjugated secondary antibody for 2hours, at room temperature (RT). Finally, a further three 1X PBS washes were used to remove the secondary antibody solution, before the coverslips were mounted on to a slide using VECTASHIELD mounting medium containing DAPI (Vector Laboratories). Stained cells were visualised using a TCS SP5II confocal microscope (Leica Microsystems CMS GmbH) and Leica application suite software (Leica).

Immunohistochemistry for confocal microscopy

Where sections were used, 14µm thick, sagittal sections were cut using a cryo-stat, placed on Superfrost slides (VWR International) and stored at -80°C until required. When needed, they were left to defrost at RT for 10 minutes before being fixed. Where slices were used, these were fixed whilst still attached to the inserts on which they had been cultured.

Both slices and sections were fixed in ice-cold acetone for 5 minutes and then rehydrated in PBS, blocked in 10% normal goat serum, 0.3% Triton X-100 in PBS and then incubated with primary antibodies diluted in blocking solution overnight, at 4°C. Following this incubation, slices were washed with blocking solution, incubated with secondary antibodies diluted in blocking solution, washed again with blocking solution and then washed once more with PBS. Secondary antibodies were conjugated to various alexa dyes. The immuno-stained slices were then mounted on to a slide and a coverslip was added (on to both slices and sections) using VECTASHIELD mounting medium containing DAPI. Stained sections and slices were visualised using an Olympus FluoView3000 laser scanning confocal microscope (Olympus) and

the FV3000 software module (Olympus).

Immunohistochemistry for electron microscopy

After overnight fixation in 3% Paraformaldehyde, 0.05% Glutaraldehyde in 0.1M phosphate buffer (4:1, 0.2M Na2PO4 : 0.2M Na2HPO4, diluted to 0.1M), at 4°C, cerebella were washed in 0.1M acetate buffer, pH 6.8 (sodium actetate trihydrate in distilled water) and stained with 2% Uranyl Acetate in acetate buffer. The stained cerebella were then dehydrated by means of an increasing methanol gradient and incubated overnight, at -20°C, with 50/50 (v/v) LR Gold resin (Agar Scientific) / absolute methanol. Following a further 1hour incubation in pure LR Gold resin, cerebella were again incubated overnight at -20°C, this time in 2.5 mg/mL Benzil / LR Gold resin. After embedding in moulds using pure LR Gold, resin polymerisation was catalysed via exposure to UV light for 16-18 hours, at -20°C. 50-80nm thick sections were then cut using a Reichert Ultracut S ultramicrotome (Leica) and mounted on 200-mesh nickel grids (Agar Scientific). Sections were blocked with 10mg/mL chicken egg albumin (Sigma) / PBS, incubated with primary antibodies diluted in blocking buffer, washed with blocking solution again, incubated with gold-conjugated secondary antibodies diluted in blocking solution, washed a third time with blocking solution and then finally washed with distilled water. Sections were counter-stained using Uranyl-less (TAAB Laboratories Equipment) and then examined with a JEOL transmission electron microscope (JEM-1010, JEOL). Images were collected with a Gatan Orius digital camera (Gatan).

Sectioning was performed by Lynne Cox (Christian lab, University of Oxford) and image collection was performed by Helen Christian (Christian lab, University of Oxford).

Whole-cell lysate preparation

Cells were lysed in hypo-osmotic shock buffer (150mM NaCl, 10mM Tris, pH 8) and centrifuged at 16000*g* for 20 minutes, at 4°C. The resulting supernatant (whole-cell lysate) was transferred to a new tube. If cerebella were used, these were homogenised using a Dounce homogeniser during exposure to the hypo-osmotic shock buffer (1mL / 100µg of cerebellum). If HEK293FT cells were used, these cells were subjected to 5 seconds sonication at an amplitude of 5-7µm during exposure to the hypo-osmotic shock buffer (1.2mL / 6-well plate).

Assessment of cytoplasmic Ca^{2+} levels

Where basal cytoplasmic Ca^{2+} levels were assessed, whole-cell lysates prepared from either transfected HEK293FT cells or dissected cerebella were subject to Western blotting. The protocol was identical to this when the effect of Carbachol (CCH) was examined, except that either CCH (up to a final concentration of 10µM) or an equivalent volume of vehicle (1X PBS) was added to the culture medium 5 minutes before whole-cell lysate preparation.

Cell surface biotinylation

Cerebellar slices were pooled in a 35mm dish. After three washes with ice cold physiological solution (PBS with 2mM Ca^{2+} and 1mM Mg^{2+}), slices were incubated in physiological solution with 100µM sulfo-NHS-SS-biotin (Pierce) for 30 minutes, at RT and with gentle agitation. The reaction was quenched using 50mM Tris, pH8 and the slices were then washed twice with physiological solution. RIPA buffer (Thermo Fisher), containing 1X phos-stop and complete protease inhibitors (Roche), combined with 5 seconds sonication at an amplitude of 5-7µm, was used to lyse the

tissue. A Soniprep 150 (MSE) was used for sonication. Cell debris was removed by centrifuging the lysates at 16000*g*, at 4°C, for 10 minutes and then transferring the supernatant to an Eppendorf tube. The supernatant was incubated with equilibrated MyOne Streptavidin-coated Dynabeads (Thermo Fisher), for 1hour, at 4°C, with gentle agitation. The resulting supernatant constituted the non-biotinylated / intracellular fraction. The beads were then washed three times with RIPA buffer, containing 1X phos-stop and complete protease inhibitors. Bound proteins were eluted by adding 3X WBSB and boiling for 5 minutes (cleaving the reducible linker in the sulfo-NHS-SS-biotin and releasing previously biotinylated proteins into solution). The resulting eluent constituted the biotinylated / extracellular fraction. Samples were analysed by Western blot.

2.4 Biochemistry

Details of all antibodies used with methods described in this section can be found in Tables 2.10 and 2.11.
All buffers contained 1X phos-stop and complete protease inhibitors.

Sodium dodecyl sulfate-polyacrylamide gel electrophoresis
Sodium dodecyl sulfate-polyacrylamide gels, either home-made or pre-cast (Bis-Tris, 4-12%, Thermo-Fisher) were first submerged in running buffer. For home-made gels, the running buffer was comprised of 25mM tris-base, pH8.3, 190mM glycine and 0.1% SDS. For pre-cast gels, 1X MOPS running buffer (ThermoFisher), supplemented with 500µL Nu:Page antioxidant (Thermo Fisher), was used. The acrylamide content of the home-made gels was varied as required. Protein samples, already combined with 1X Western blot sample buffer (WBSB, 43.67mM Tris, pH6.8, 7%

(v/v) glycerol, 1.4% (w/v) SDS and 100mM DTT), were then loaded. An aliquot of pre-stained protein ladder (NEB) was also loaded. A temporally-controlled voltage, appropriate to the type of gel used, was passed across the gel until the protein ladder was satisfactorily resolved.

Western blotting

Blotting was achieved by sandwiching a resolved sodium dodecyl sulfate-polyacrylamide gel and a sheet of Protran nitrocellulose paper (GE Healthcare) between filter papers (Whatman), submerging the sandwich in transfer buffer (25mM tris-base, pH8.3, 190mM glycine, 20% [v/v] methanol) and then applying a constant amperage of 250mA, for a period of 1.5hours, across the transfer sandwich. If two gels were transferred concurrently, transfer time was increased to 2hours. Blots were then blocked using 5% (w/v) skim milk powder, 1X TBST for WB (150mM NaCl, 10mM Tris, pH8, 0.1% Tween 20), for 1hour, at RT and with gentle agitation. Blocking buffer was exchanged for Western blot antibody carrier solution (3% BSA in 1X TBST for WB) containing an appropriate primary antibody and the blots were incubated overnight, at 4°C, with gentle agitation. Following three washes with 1X TBST for WB, blots were then incubated in Western blot antibody carrier solution containing the relevant HRP-coupled secondary antibody, for 1.5 hours, at RT and with gentle agitation. Blots were washed three times with 1X TBST for WB and then an additional time with distilled water, before being incubated with enhanced chemiluminescence detection reagent (GE Healthcare) for 1 minute, at RT. An ImageQuant LAS 4000 (GE Healthcare) was used immediately following this incubation to assess chemiluminescence. Images were processed using ImageJ (National Institutes of Health, Bethesda). For all Western blots reported, n = 1 blot per individual sample i.e. no technical repeats of any Western blots were performed.

Coomassie staining

Resolved sodium dodecyl sulfate-polyacrylamide gels were first washed with distilled water, then stained with Imperial Protein Stain (Thermo Fisher) and finally washed again with distilled water. For each step, the gel was submerged and microwaved for 90s and the liquid was then exchanged. An Alpha Imager 3400 was used to image stained gels using white light.

Fractionation

Cerebellar synaptosomes were generated using Syn-PER synaptic protein extraction reagent (Thermo Fisher). A Dounce homogeniser was used to homogenise cerebellar tissue in the presence of 1mL Syn-PER / 100µg cerebellum, on ice. The homogenised tissue was centrifuged at 1200g for 10min, at 4 °C. The resulting supernatant (input fraction) was transferred to a new tube and centrifuged again, but this time at 15000g for 20min, at 4°C. The resulting pellet (synaptosomes) and supernatant (cytosolic fraction) were then used as required.

For the initial assessment of Caspr2 expression at synapses, prepared synaptosomes were lysed using hypo-osmotic shock buffer. Protein concentration was measured by the Bradford method and equal amounts of protein from the cell lysate and synaptic fractions were analysed by Western blotting.

To produce pre- and post-synaptic, synaptic junction protein fractions, synaptosome pellets were resuspended in 500µL 0.1mM $CaCl_2$ and 1500µL of a buffer containing 2% Triton X-100, 40mM Tris, pH6. The synaptosome suspension was then incubated on ice, with gentle agitation, for 30 minutes, before being centrifuged at 40,000g for 30 minutes at 4°C. The resulting supernatant (extra-junctional synaptic fraction) was discarded and the pellet washed twice in 500µL 1% Triton X-100, 20mM Tris,

pH6, before being resuspended in 2000µL 1% Triton X-100, 20mM Tris, pH8, incubated at 4°C for 30 minutes with gentle mixing and then centrifuged at 40,000*g* for 30 minutes, at 4°C. The supernatant (pre-synaptic fraction) was stored at 4°C until needed. The pellet (post-synaptic fraction) was resuspended in 500µL 1% Triton X-100, 20mM Tris, pH8. A 10 X volume of ice cold acetone was added to all fractions, which were then incubated overnight at -20°C. Precipitated proteins were collected by centrifuging the suspensions at 15,000*g* for 30 minutes, at 4°C. 5% SDS was used to solubilise the resulting pellets. Protein concentration was measured by the Bradford method and equal amounts of protein from each fraction were analysed by Western blot.

Co-immunoprecipitation

Where cellular fractions were used as bait pools, it was first necessary to lyse any organelles present to ensure the entire proteome of these fractions was available for binding. Synaptosomes were lysed by exposure to hypo-osmotic shock buffer and synaptic junction fractions were lysed by resuspension in hypo-osmotic shock buffer, combined with sonication for 5 seconds at an amplitude of 5-7µm. Whole cell lysates prepared from transfected HEK293FT cells were used as is. Prepared lysates were then incubated with 1µg of primary antibody (see 2.10) at 4°C, for 2hours, with gentle mixing. Following the initial 2hour incubation, the lysates were incubated with 30µL equilibrated IgG-coated dynabeads (Thermo Fisher) for a further 1hour, again at 4°C. The beads were then washed three times in hypo-osmotic shock buffer, on ice. Bound proteins were eluted by addition of 3X WBSB, followed by boiling for 5 minutes. Analysis of eluted proteins was by Western blot.

For the ”direct” co-IP, where only purified recombinant Caspr2 ECD and purified

IP_3R1 were used, the two proteins and 0.2µg of $\propto$ IP_3R1 antibody (see 2.10) were combined in hypo-osmotic shock buffer. The Caspr2 ECD and IP_3R1 proteins were included at a molar ratio of 1:1. The mixture was incubated with gentle mixing, at 4°C, for 30 minutes and 5µLs of IgG-coated dynabeads were then added. The mixture was incubated for a further 15 minutes, again at 4°C. Washing, elution and analysis were as described above.

Caspr2 ECD purification

For large-scale preps, conditioned cell medium was collected, centrifuged at 7000rpm for 20 mins, at 4°C and filtered through a stericup / steritop vacuum filter (Millipore). Filtered medium was then dialysed against 2L of a diafiltration buffer composed of 20mM Tris, pH 7.6, 1X PBS and 150mM NaCl before being subjected to immobilised metal affinity chromatography (IMAC): after equilibrating a HP HisTrap 5mL (GE Healthcare) column using 4 column volumes of 300mM PBS, the concentrated medium resulting from the diafiltration step was run through, followed by 20 column volumes of 20mM Tris pH8, 300mM NaCl, 40mM imidazole to wash. His-tagged protein was eluted into separate 1.5mL fractions using elution buffer, which contained 20mM Tris, pH8, 300mM NaCl and 500mM imidazole. The amount of protein in each fraction was assayed using Bradford reagent. Further purification was carried out using size exclusion chromatography. A HiLoad 16/600 Superdex 200pg column (GE Healthcare) was equilibrated with 120mL of 10mM Tris pH 8, 200mM NaCl. Protein fractions were then injected, with the equilibration buffer used as a running buffer. Protein purity and yield were assessed by UV spectrometry and by Coomassie staining. Eluent fractions containing recombinant protein were then combined and concentrated by repeated centrifugation, at 4000rpm for 4 minutes per spin, using a 10000 MWCO spin concentrator (Millipore), until the

concentration reached 5mg/mL.

Size exclusion chromatography was performed by Maria Carrasquero-Ordaz (Seiradake lab, University of Oxford)

For small-scale preps, conditioned medium was collected, centrifuged at 1000rpm for 1 minute to pellet any cell debris, filtered through a 0.22µm filter and then buffered using Tris, pH8, up to a final Tris concentration of 10mM. Recombinant protein was then purified using IMAC: after washing 100µL of Nickel Excel beads (GE healthcare) three times in 1mL distilled water and then once in 1mL of Tris, pH8, the beads were incubated overnight at 4°C, with gentle shaking, in separate 10mL aliquots of filtered and conditioned medium. The beads were then washed three times in 1.50mL of 10mM Tris pH8, 10mM imidazole and once in 1mL of 10mM Tris pH 8, 150mM NaCl, 10mM imidazole. Bound protein was then eluted using 0.2mL of 500mM imidazole, 10mM Tris pH 8, 150mM NaCl. For both large-and small-scale preps, Western blotting was used to determine the presence of recombinant protein during initial screening and after purification. Addition of a streptavidin-horseradish peroxidase complex to purified protein aliquots allowed us to quantify biotinylation.

Pull-down assays

Purified, biotinylated Caspr2 ECD protein was incubated with equilibrated MyOne streptavidin-coated dynabeads for 30 minutes, at room temperature and with gentle mixing. As the affinity of the biotin-streptavidin interaction is extremely high, we assumed that by adding an excess of biotinylated protein to the streptavidin-coated beads, the resulting ”beadome” would be comprised of biotinylated Caspr2 ECD

and little else. After 30 minutes, the supernatant was removed and the beads were washed a further three times in 1X PBS, before being stored until needed, at 4°C, in hypo-osmotic shock buffer.

Cerebellar synaptosomes were lysed using hypo-osmotic shock buffer. The resulting lysates were incubated with previously prepared, bait protein-coated dynabeads. Incubation was overnight, at 4°C, with gentle mixing. After incubation, the beads were washed four times in hypo-osmotic shock buffer. Bound protein was then eluted by adding 4X Nu:Page loading buffer (Thermo Fisher), supplemented with DTT up to 100mM, and boiling for 5 minutes. The resulting supernatant was removed and reserved. Bound bait protein was then eluted by addition of 95% formamide + 80mM NaOAc, followed by a further 5 minutes of boiling. Analysis of eluted proteins was done by mass spectrometry and by Western blot.

LC-MS / MS

Protein samples were resolved using SDS-PAGE and then stained using a coomassie dye. Each gel lane was cut into 5 equal pieces. Excised gel fragments were then washed overnight, using a buffer comprised of 50% methanol, 5% acetic acid. After dehydration with acetonitrile, proteins in the gel fragments were reduced and then alkylated with 10mM DTT and 50mM iodoacetamide respectively. Gel pieces were incubated on ice with 20ng/uL Trypsin (sequencing grade, Promega) for ten minutes and any excess trypsin was then removed. After the addition of 50mM ammonium bicarbonate to keep the gel fragments hydrated, the digestion reaction was allowed to continue overnight, at 37°C. Proteins were extracted by sequential incubations with 50mM ammonium bicarbonate, then 50% acetonitrile, 5% formic acid and finally 85% acetonitrile, 5% formic acid. Extraction supernatants were combined and dehydrated using a vacuum centrifuge, before being resuspended in 2% acetonitrile,

0.1% formic acid ready for HPLC injection.

The following steps were outsourced to the OXION core proteomics facility.

An Ultimate 3000 nano-HPLC system (Dionex, Sunnyvale, CA, USA) was used for the liquid chromatography step. In-gel digested material was pushed through a trapping column (Dionex, 300µm i.d., 0.1cm) at a flow rate of 20µL/min to facilitate initial concentration. Separation was achieved using a C18 Pepmap column (Dionex, 75µm i.d., 15cm) and a flow rate of 250nL/min. A two-solvent gradient buffer (see Table 2.7) was used for elution, where solvent A was 98% H2O, 2% acetonitrile, 0.1% formic acid and solvent B was 80% acetonitrile, 20% water, 0.1% formic acid.

Table 2.7: HPLC gradient method used for LC-MS / MS analysis

composition (% solvent B)	run time (min)
2-10	0-3
10-25	3-18
25-50	18-30
50-90	30-30.2

The HPLC system interfaced directly with a 3D high capacity ion trap mass spectrometer (amaZon; Bruker Daltonics). Ion trap target mass was set at 850m/z, compound stability at 100% and smart ICC at 250,000. HyStar software (version 3.2) was used to initiate MS / MS analysis upon detection of a contact closure signal. Helium gas, with a 30%-200% collision energy sweep of amplitude 1.0, was used to produce collision-induced dissociation. Five or fewer precursor ions were selected per cycle with active exclusion (0.5min).

Purification of IP_3R1 from rat cerebella

This method was adapted from [43]. Dissected rat cerebella were homogenised in

50mM Tris, pH 8.3, 1mM EDTA using a Dounce homogeniser. The resulting lysates were centrifuged at 4000g for 15 minutes, at 4°C. The pellet was discarded and the supernatant was again centrifuged at 4000g for 15 minutes at 4°C. The supernatant was then centrifuged at 90000g for 30min, 4°C to produce a microsome pellet. This was dissolved in 2% (w/v) CHAPS in 50mM Tris (pH 7.4), 150mM NaCl, 1mM DTT, 1mM EDTA (buffer A) and centrifuged at 100000g for 1hour to remove any insoluble particles (the resulting pellet was discarded). Solubilised microsomes were then incubated overnight, at 4°C, with gentle mixing, along with 2µg / cerebellum of an $\propto$ IP_3R1 antibody. 60textmuL protein-G coated Dynabeads were added and the mixture was incubated for a further hour, again at 4°C, with gentle mixing. Protein-loaded beads were washed by alternating between buffer A with 1.4% CHAPS and buffer A with 1.4% CHAPS and 500mM NaCl twice over and then washing once with buffer A containing 0.2% CHAPS. IP_3R1 was eluted using buffer A containing 0.4% CHAPS and 0.2mg/mL immunogenic IP_3R1 peptide (Designer Bioscience). Eluted IP_3R1 was concentrated to 1mg/mL in buffer A with 0.4% CHAPS using an Amicon Ultracel-100 centrifugal filter (Sigma). Finally, the protein solution was centrifuged at 16000g for 15 min, the supernatant was transferred to a new Eppendorf tube and sucrose was added up to a final concentration of 5%. The purified protein was aliquoted, snap frozen in liquid N_2 and stored at -80°C. Western blotting was used to confirm the identity of the purified IP_3R1.

2.5 Data analysis and statistics

All processing of images not explicitly explained below was carried out using imageJ. Plots were constructed in QtGrace (freeware) and figures were created in Inkscape (freeware).

Comparison of the number of HEK293FT cells with IP_3R1-induced extensions

The number of cells with and without extensions were counted whilst the experimenter was blind to the transfection conditions each sample was subjected to and then summed in a mega-analysis. An extension was defined as any protrusion that noticeably interrupted the rolling average of the angle of membrane curvature and also measured greater than 10µM. The binom.test function from the R (freeware) Binom package was used to calculate pearson 95% clopper-pearson confidence intervals and Graph Pad Prism (GraphPad Software) was used to perform the chi-square test.

Comparison of the number of Purkinje cells with multiple primary dendrites

Counts of the number of Purkinje cells displaying, and not displaying, multiple primary dendrites were summed for each animal / dose condition and treated as a single Bernoulli experiment. Counting was performed whilst the experimenter was blind to the genotype of each culture and to the dosing regimen each culture was subjected to. The metaprop function from the R meta package was then used to combine both proportions and clopper-pearson confidence intervals in a weighted fashion: for this, a fixed effects, inverse variance method with logit transformation was employed. Graph Pad Prism was used to perform the regular two-way ANOVA and Sidak's post-hoc test.

Assessment of IP_3R1 and Caspr2 co-occurrence in the cerebellum

Using the ImageJ coloc2 plugin, Mander's co-efficients of co-occurrence were calculated for individual images of co-stained cerebella sections. The region selected for analysis was restricted to the deep portion of the molecular layer where fibrous

Caspr2 staining pattern was clearly visible. The Manders's co-efficients reported for each of the individual images were then averaged. Costes significance tests were also performed simultaneously, alongside the co-efficient calculations, using 100 randomisations. A Costes P-value of 1 was reported for all images examined.

Measurement of Erk phosphorylation

Western blot band density was quantified using the imageJ analyse gels function. For each individual protein sample assessed, the density of the band corresponding to phospho-Extracellular signal-related kinases 1/2 (PErk) was normalised to that of the band corresponding to Extracellular signal-related kinases 1/2 (Erk). These normalised PErk values were then used to calculate the required ratios, which were averaged to give mean ratios $\pm$ SEM.

LC-MS/MS data processing

DataAnalysis 4.0 (Bruker Daltonics) was used to produce Mascot compatible files from raw LC-MS/MS data. Mascot (Matrix Science, algorithm version 2.5.1) was used to perform database searches of the Uniprot SwissProt "*Mus musculus*" database (v2018.07.18). Variables were set to: 2+, 3+ and 4+ ions, peptide mass tolerance 0.3 Da, 13C = 2, fragment mass tolerance 0.6 Da, number of missed cleavages: two, instrument type: ESI-TRAP, fixed modifications: Carbamidomethylation (Cys), variable modifications: Oxidation (Met).

Table 2.8: Antibodies used for immunofluorescence microscopy

antibody	dilution	supplier	catalogue #
primaries			
r ∝ Caspr2	1:200	Abcam	APR8738
m ∝ IP_3R1	1:100	Santa Cruz	SC-271197
m ∝ Na^+K^+ATPase	1:100	Abcam	ab7671
r ∝ VGLUT1	1:100	Synaptic Systems	135303
secondaries			
g ∝ r alexa 594	1:1000	Invitrogen	A11037
g ∝ r alexa 647	1:1000	Invitrogen	A21245
g ∝ m alexa 488	1:1000	Invitrogen	A11001

Table 2.9: Antibodies used for electron microscopy

antibody	dilution	supplier	catalogue #
primaries			
r ∝ Caspr2	1 in 10	Sigma	C8737
m ∝ IP_3R1	1 in 10	Santa Cruz	SC-271197
secondaries			
g ∝ r 15nm gold	1 in 50	Agar Scientific	AGR14003
g ∝ m 5nm gold	1 in 50	Agar Scientific	AGR14008

Table 2.10: Antibodies used for Western blotting

antibody	dilution	supplier	catalogue #
primaries			
r ∝ Caspr2	1:1000	Sigma	C8737
m ∝ Kv1.1	1:1000	Neuromab	73-105
m ∝ Actin	1:500	Abcam	ab3280
m ∝ PSD-95	1:1000	Synaptic Systems	124011
r ∝ Syntaxin	1:1000	Synaptic Systems	110302
r ∝ Munc18	1:1000	Abcam	ab3451
m ∝ penta-His	1:500	Qiagen	34660
m ∝ IP_3R1	1:1000	Neuromab	75-035
m ∝ CNTN1	1:1000	Cambridge Bioscience	13843-1-AP
r ∝ Erk	1:1000	Cell Signalling	9102
r ∝ PErk	1:1000	Cell Signalling	9101
r ∝ PDI	1:1000	Abcam	ab31811
secondaries			
s ∝ m HRP	1:10000	GE Healthcare	NA931V
d ∝ r HRP	1:10000	GE Healthcare	NA934V

Table 2.11: Antibodies used for immunoprecipitations

antibody	supplier	catalogue #
r ∝ Caspr2	Sigma	C8737
g ∝ IP_3R1	Santa Cruz	SC-6093

3 Caspr2 affects Purkinje cell dendritic morphology

3.1 Introduction

Cntnap2$^{-/-}$ mice exhibit cerebellar-specific behavioural abnormalities: eye-blink conditioning, which depends specifically on cerebellar learning, is impaired in these animals[77]. In addition, autoantibodies directed against Caspr2 have been found in sera taken from patients with cerebellar ataxia[15]. Together, these data suggest that Caspr2 has a role in the cerebellum. However, how Caspr2 functions in the cerebellum, at the cellular and molecular levels, is unknown. The overall aim of this thesis was therefore to first describe the function of Caspr2 in the cerebellum, at the cellular level, and then to uncover the molecular substrate for this role.

Further information about the spatial expression pattern of Caspr2 was needed before a cellular function assay could be designed. The aim of the work described in this chapter was therefore two-fold: to describe the cellular and sub-cellular localisation of Caspr2 in detail and to then understand its cellular function, with the expression data informing the design of the functional experiments.

Preliminary information about Caspr2 expression in the cerebellum

The Caspr2 protein was first detected in the brain in 2000[110]. Analysis of individual brain regions revealed Caspr2 expression in several areas, including the cerebellum[110]. Unpublished work, done in the Becker lab, has shown that the shape of the temporal expression pattern of Caspr2 in the cerebellum matches that observed in the studies of expression in whole brain. However, the initial expression of Caspr2 appears to occur much later in the cerebellum (between P5 and P8) than it does in whole brain (E15) (Figure 1.9 and [110]).

In the study in which Caspr2 was initially reported, cerebellar sections were immunostained using an $\propto$ Caspr2 antibody in order to assess the distribution of Caspr2. The resulting strong staining of the white matter indicated expression in Purkinje cell axons[110]. A more recent study then reported that *Cntnap2* is expressed in the cerebellar white matter by P7[56]. This is consistent with the delayed onset of Caspr2 expression, relative to the rest of the brain, observed by the Becker lab (Figure 1.9) and the initial data suggesting Caspr2 is found in the cerebellar white matter[110]. Myelination begins in the cerebellum at P6[47]. As Caspr2 has been detected in the white matter of the cerebellum at P7[56], but has not been observed in the cerebellum prior to P6, it seems likely that Caspr2 is first expressed in the cerebellum in the white matter. However, other immunostaining studies suggest that Caspr2 is also found elsewhere in the cerebellum. One study reports expression in the molecular layer[15], whilst another finds evidence that Caspr2 localises to the granule cell, Purkinje cell and molecular layers of the adult murine cerebellum[67]. Of note, at the beginning of this project no study had yet properly assessed the spatial distribution of Caspr2 in the cerebellum during development.

When present in the rat optic nerve Caspr2 localises to the JXP[110]. Regularly spaced pairs of Caspr2-positive sections along the axons of the cerebellar white mat-

ter, indicative of a JXP localisation have also been observed[110]. Most research to date has focused on the role of Caspr2 at this location, where it scaffolds Shaker-type K^+ channels[112].

The localisation of Caspr2 to the JXP is consistent with Caspr2 being expressed in the cerebellum only after the onset of myelination, as JXP structures require myelinating glia.

Caspr2 controls multiple cellular structures during development

Caspr2 has distinct effects on cellular structures, depending on the cellular context. In myelinated neurons, Caspr2 is required for the timely myelination of axons: *Cntnap2*$^{-/-}$ mice have reduced neocortex grey matter myelination at P21, and show a concomitant decrease in the density of the myelinated fibres of the superficial neocortex. As would be expected, this decreases the propagation speed of action potentials transmitted along these axons. These deficits are no longer detectable at P56[129].

In non-myelinated neurons, Caspr2 appears to regulate neurite morphology. siRNA knockdown of *Cntnap2* in cultured hippocampal pyramidal neurons reduced dendritic arbourisation. Synapse numbers were also counted in the same study and were found to be reduced by the knockdown procedure[5]. Subsequent *in vivo* imaging work suggested that Caspr2 is required for the stabilisation of newly formed spines in the superficial neocortex[53], providing a possible explanation for the reduction in synapse numbers observed by Anderson et al[5].

In summary, Caspr2 is expressed in the cerebellum during cerebellar development. In other brain areas, Caspr2 has been shown to regulate cellular structures during development. As a result, the effect of Caspr2 on cellular morphology in the developing cerebellum was investigated.

3.2 Caspr2 expression in the developing cerebellum

The spatial distribution of Caspr2 in the P14 cerebellum was assessed. Caspr2 has been relatively well studied in myelinated neurons, but little is known about its function in non-myelinated neurites. Caspr2 has previously been found in the dendrites of cortical neurons, in Purkinje cell somata and in the cerebellar molecular layer[67; 110], suggesting it may be expressed in the neurites of the molecular layer and in particular in Purkinje cell dendrites. The development of the molecular layer circuitry, including synaptogenesis involving Purkinje cell dendrites and Purkinje cell dendritic arbourisation, is ongoing at P14. This, together with the severe developmental phenotype that results from Caspr2 dysfunction[140] and that therefore suggests Caspr2 has an important role in development, led to the selection of the P14 time point.

Initially, immunohistochemistry was employed to determine the cerebellar cell types that express Caspr2. Cryo-sections were cut from snap-frozen, P14 murine cerebella and then immunostained using antibodies that target Caspr2 and the Ca^{2+} channel IP_3R1. Antibodies directed against IP_3R1 were included because IP_3R1 immunostaining patterns can be used as a reference to guide the interpretation of other immunostaining patterns: IP_3R1 is highly expressed throughout Purkinje cells and so IP_3R1 immunostaining patterns allow the identification of each of the different layers of the cerebellum (see Figure 1.3 for a description of cerebellar cytoarchitecture).In the *Cntnap2*$^{+/+}$ cerebellum, strong, fibrous Caspr2 staining was observed both in the white matter, which is mostly comprised of Purkinje cell axons, and in the deep molecular layer, where parallel fibres (granule cell axons) and climbing fibres synapse on to Purkinje cell dendrites (Figure 3.1).

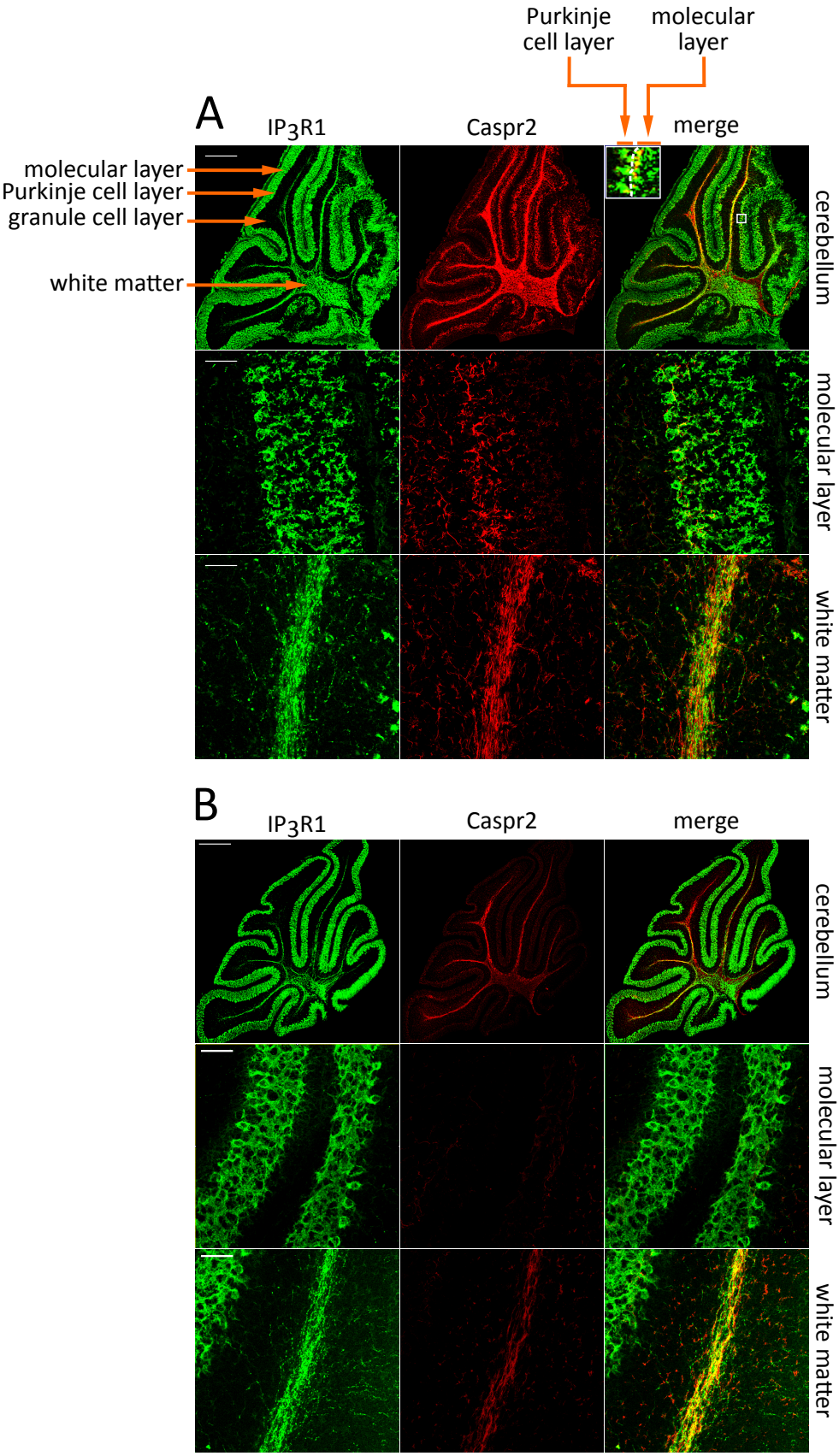


Figure 3.1: continued on the next page

Figure 3.1: Caspr2 expression in the developing cerebellum: immunohistochemistry. Representative images of sections cut from P14 murine cerebella and simultaneously immunostained with antibodies against Caspr2 (red) and IP_3R1 (green). **A)** Wild-type (*Cntnap2*$^{+/+}$) cerebellum. Caspr2 is mostly expressed in the deep molecular layer and the white matter of the developing cerebellum. Inset (framed in white) is 4X zoomed, white dashed line demarcates the boundary between the Purkinje cell and molecular layers. **B)** Knockout (*Cntnap2*$^{-/-}$) cerebellum. Scale bar for whole cerebellum images, 500µm, scale bar for molecular layer and white matter images, 50µm. N = 5 WT, 5 KO, n = 4 sections minimum per animal.

Caspr2 signal was also found in the granule cell layer and in the superficial molecular layer, although it was weaker and much sparser than elsewhere. The Caspr2 staining in the superficial molecular layer also appeared punctate, rather than fibrous. This gross staining pattern suggests Caspr2 is expressed in Purkinje cells and possibly, also in climbing fibres and parallel fibres.

Unexpectedly, Caspr2 staining was also observed in *Cntnap2*$^{-/-}$ cerebella, where it was mostly confined to the white matter (Figure 3.1). Although dimmer than the signal from *Cntnap2*$^{+/+}$ cerebella, the spatial distribution of Caspr2 signal in the white matter of *Cntnap2*$^{-/-}$ cerebella bore a striking resemblance to that seen in the white matter of *Cntnap2*$^{+/+}$ cerebella.

Next, biochemical fractionation was used to investigate the sub-cellular localisation of Caspr2. No neurites in the molecular layer are myelinated. It was therefore not possible that the Caspr2 observed in the deep molecular layer could be localised to the JXP region. Instead, as the molecular layer contains many synaptic sites, it was suspected that Caspr2 might also localise to synapses in the cerebellum. To test this, cerebellar synaptosomes were prepared from P14 murine cerebella and then lysed. Caspr2 levels in the resulting lysate were analysed by Western blotting. The specific enrichment of the synaptic protein $K_v1.2$ (but not actin) shows that the fractionation protocol employed did purify synaptic proteins as intended. Caspr2 was found to be greatly enriched in the synaptic fraction (Figure 3.2A). This suggests that Caspr2 is expressed at synapses in the developing cerebellum.

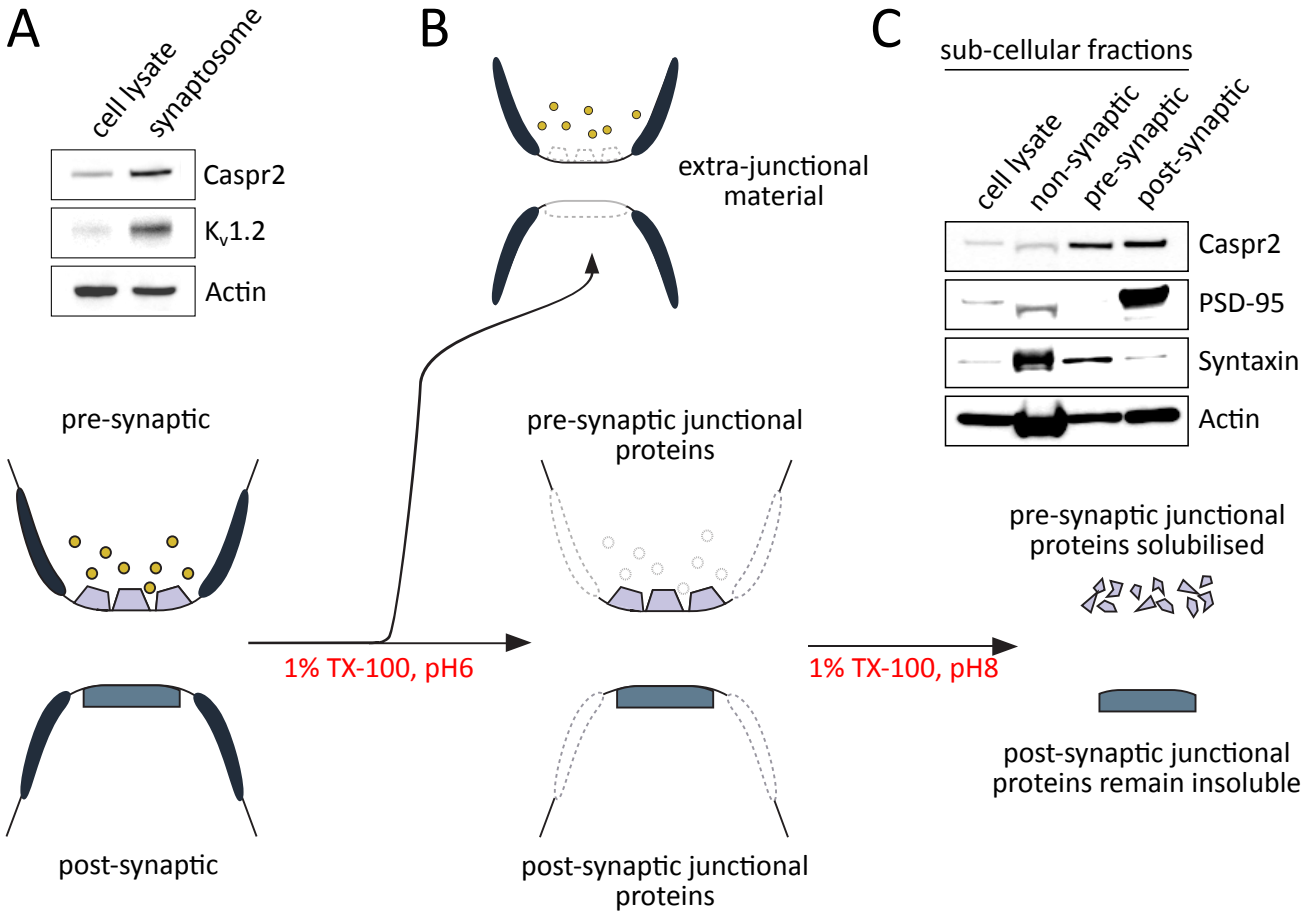


Figure 3.2: Caspr2 expression in the developing cerebellum: biochemical fractionation. **A)** Caspr2 is enriched at synapses in the developing cerebellum. Synaptosomes were isolated from P14 cerebella and then lysed. The resulting lysate was subject to Western blotting. K_V1.2 is known to be enriched at synapses. N = 5 independently processed animals. **B)** Illustration, adapted from [108], of the sub-synaptic fractionation workflow. Sequential incubations with Triton X-100, at increasing pH, separates pre-synaptic and post-synaptic junctional proteins, Tx, Triton X. **C)** Caspr2 is present at both pre- and post-synaptic specialisations. Western blot analysis of P14 cerebella subjected to the protocol outlined in B). Syntaxin is a marker of pre-synaptic specialisations, whilst PSD-95 demarcates post-synaptic specialisations. N = 3 independently processed fractionations (2 animals per fractionation).

Together with the gross Caspr2 spatial expression patterns determined by immunohistochemistry (Figure 3.1), this data suggests that Caspr2 is present at Purkinje cell axon terminals and / or at synapses involving Purkinje cell dendrites in the molecular layer. If Caspr2 is expressed at Purkinje cell-granule cell or Purkinje cell-climbing

fibre synapses, it could be localised at pre-synaptic specialisations (i.e. in granule cells or climbing fibres) or at post-synaptic specialisations (i.e. in Purkinje cells). To identify the sub-synaptic compartment in which Caspr2 is present a sub-synaptic fractionation procedure, adapted from[108] (Figure 3.2B), was used to isolate pre- and post-synaptic specialisations from P14 murine cerebella. Western blot analysis of the resulting fractions revealed that PSD-95, a post-synaptic marker, was confined to the post-synaptic fraction (Figure 3.2C). Syntaxin, a marker of pre-synaptic specialisations, was greatly enriched in the pre-synaptic fraction, relative to the post-synaptic fraction (Figure 3.2C). A small amount of Syntaxin was also detected in the post-synaptic fraction (Figure 3.2C). This is to be expected, as this protein is also expressed in spines (albeit at lower levels than in pre-synaptic terminals), where it is necessary for the trafficking of receptors to the synaptolemma[20]. This distribution of marker proteins indicates that the sub-synaptic fractionation procedure was successful.

Caspr2 was found to co-purify equally with pre- and post-synaptic markers (Figure 3.2C), suggesting it is equally expressed at pre- and post-synaptic specialiations. The enrichment of Caspr2 in the pre-synaptic fraction meant that it was not possible to conclude whether Caspr2 is expressed exclusively in Purkinje cells using this data - the combination of the staining pattern observed in Figure 3.1 and this pre-synaptic enrichment means that Caspr2 could be present in parallel and / or climbing fibres. However, the presence of Caspr2 at post-synaptic specialisations, together with the fact that Caspr2 was found to localise to the deep molecular layer (Figure 3.1), does suggest that Caspr2 is present in the spines of Purkinje cell dendrites.

Neurexin superfamily proteins are typically integral to the cell membrane, with a single, large domain exposed to the extracellular milieu[155]. Caspr2 is known to be a transmembrane protein[103], but it was unclear whether Caspr2 is expressed at the

cell surface or in intracellular vesicles, in the developing cerebellum. To determine if Caspr2 is integral to the cell surface membrane a cell-surface biotinylation assay was performed. Organotypic slices, cut from P9 cerebella, were treated for 30mins with a compound comprised of biotin and a reactive linker, which forms covalent bonds with exposed Lysine residues. This treatment results in the biotinylation of protein domains exposed to the extracellular milieu. These biotinylated proteins can then be purified via affinity chromatography to give extracellular and intracellular protein fractions. The extracellular fraction consists of the (biotinylated) proteins pulled down by the Streptavidin-coated beads, whilst the intracellular fraction consists of the proteins remaining in the supernatant after the lysate has been incubated with the beads i.e. those proteins that have not been biotinylated.

The biotinylated slices were then lysed and analysed by Western blotting. Caspr2 was detected in the extracellular fraction, along with $K_v1.2$, which is known to be an integral cell membrane protein. Actin was not detected in this fraction, indicating that the fractionation procedure excludes intracellular proteins from the extracellular fraction. Caspr2 and $K_v1.2$ were, however, found in the intracellular fraction despite it being knwon that $K_v1.2$ is expressed at the cell surface. This is to be expected for two reasons. First, the biotinylation of extracellular domains is not 100% effective and two, there will always be moieties of cell surface proteins found intracellularly, either being trafficked from the endoplasmic reticulum (ER) after synthesis or in recycling pools. Caspr2, $K_v1.2$ and actin were not detected in the extracellular fraction when the biotinylation step was skipped, suggesting that proteins found in the extracellular fraction were isolated as a result of the biotin-streptavidin interaction. Thus, these data show that Caspr2 is an integral cell membrane protein in the cerebellum (Figure 3.3). Together with the localisation data presented in Figures 3.1 and 3.2, these findings are consistent with Caspr2 being an integral membrane pro-

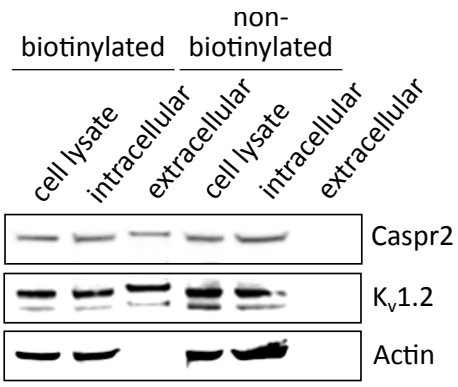


Figure 3.3: Caspr2 is an integral cell membrane protein. Slices were cut from P9 cerebella. Proteins exposed to the extracellular environment were then biotinylated, before the slices were homogenised and lysed. Streptavidin-coated beads were used to isolate biotinylated proteins, which were then assessed by Western blotting. $K_V1.2$ is known to be an integral cell membrane protein. N = 2 independently processed animals.

tein in the synaptolemma of Purkinje cell dendritic spines and possibly also in the syanptolemma of parallel or climbing fibre terminals. This places the ECD of Caspr2 into the synaptic cleft at Purkinje cell synapses in the molecular layer. In addition, as Caspr2 may also be expressed in the synaptolemma of Purkinje cell axon terminals, the Caspr2 ECD might also have a role in the synaptic cleft at Purkinje cell-deep cerebellar nuclei synapses.

3.3 Cloning, expression and purification of recombinant Caspr2 ECD

The function of the ECD of Caspr2, at synapses and in non-myelinated neurites generally, is unknown. Interestingly, *Cntnap2*$^{-/-}$ mice still express the shorter of the two Caspr2 isoforms and are therefore effectively only missing the putative ECD of Caspr2. The effective absence of this domain is enough to cause a cerebellar-specific behavioural phenotype ([77] and Figure 1.6) suggesting that the ECD has an import-

ant functional role in the cerebellum. Thus, in an effort to understand the function of Caspr2 in the molecular layer (which does not contain myelinated axons), it was decided that future efforts would be focused on characterising the role of this particular domain in cerebellar development.

To do this, it was first necessary to produce recombinant Caspr2 ECD. A truncated version of the murine *Cntnap2* cDNA, which encodes only the extracellular domain of Caspr2 (residues 28-1262), was inserted into the pHL-Avitag3 vector[7] (Figure 3.4) using PCR cloning. This vector was chosen because it is very high copy, allows expression in mammalian cells and consistently gives high expression levels. In addition, this vector also provides a secretion signal, a His-tag for use with IMAC during purification and a biotin ligase recognition site. Biotinylation was not necessary for the initial cellular assay, but was going to be necessary for an additional experiment that was also being planned.

The biotinylation of proteins *in vitro* is expensive and inefficient and so it was attempted *in vivo* instead. To do this, a BirA expression construct was included alongside the Caspr2 ECD expression construct. The BirA construct encodes a biotin ligase enzyme, which catalyses biotinylation. The culture medium was also supplemented with biotin, which is readily endocytosed by HEK293FT cells.

To assess the feasibility of using *in vivo* biotinylation, HEK293FT cells were transfected with varying amounts of BirA DNA, alongside a set amount of Caspr2 ECD expression construct. Transfected cells were cultured for 48 hours to allow time for expression to occur. As a result of the secretion signal provided by the pHL-Avitag3 vector, the recombinant ECD Caspr2 produced was secreted into the culture medium. IMAC was used to purify recombinant protein from the conditioned media and an excess of streptavidin HRP was added. Western blotting of the resulting complexes revealed *in vivo* biotinylation to be up to 100% effective (Figure 3.5). Based

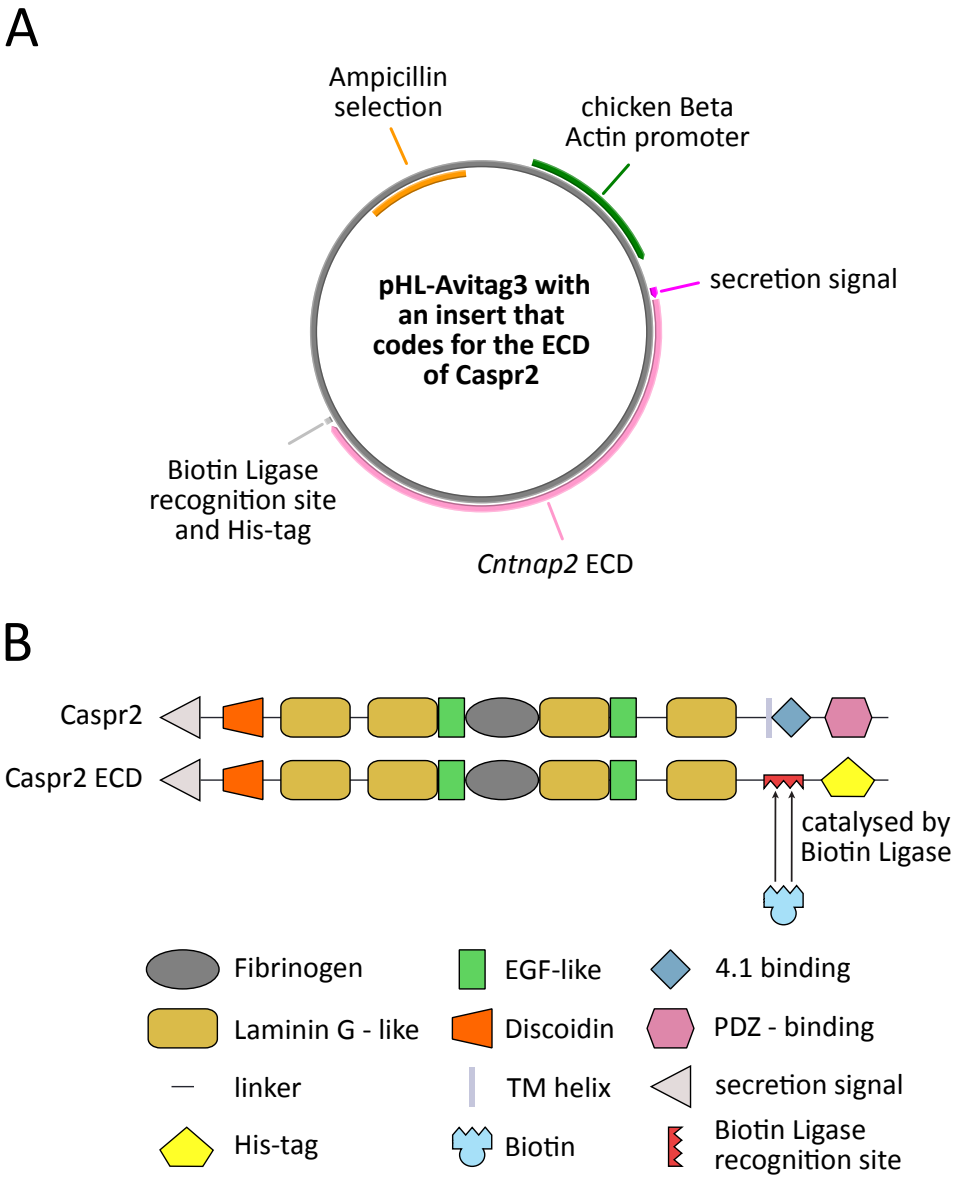


Figure 3.4: The Caspr2 ECD expression construct. Plasmid map of the pHL-Avitag3 expression vector, with a truncated version of the *Cntnap2* cDNA (that codes for the ECD of Caspr2) inserted.

on this success, it was decided that the biotinylation of recombinant Caspr2 ECD would be carried out *in vivo*. HEK293FT cells, cultured in 12L roller bottles, were co-transfected with the Caspr2 ECD in pHL-Avitag3 construct and the BirA expression construct (10% of total DNA). Biotin was again also added to the cell culture medium.

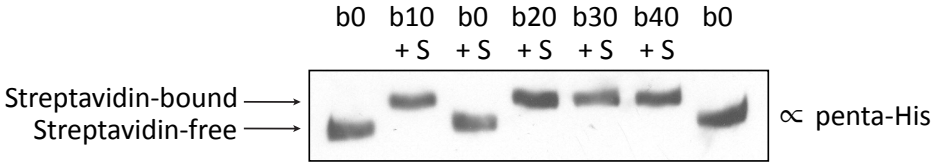


Figure 3.5: Recombinant Caspr2 ECD can be biotinylated *in vivo*. HEK293FT cells were co-transfected with the construct described in Figure 3.4 and varying amounts of a BirA construct. An excess of Streptavidin was added after IMAC purification to assess the effectiveness of the *in vivo* biotinylation reaction. b(x), amount of BirA DNA used to co-transfect (% of total DNA), +S, excess of Streptavidin added.

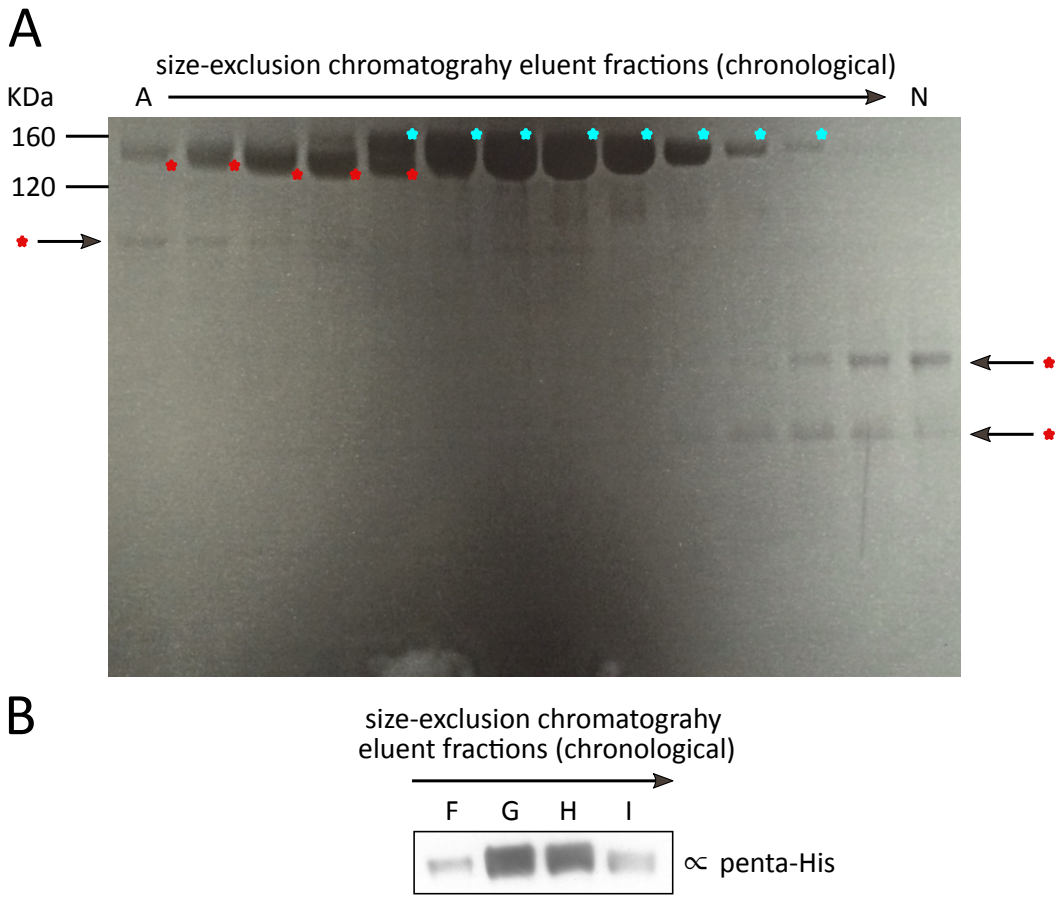


Figure 3.6: Large-scale purification of recombinant Caspr2 ECD. A) The expression construct detailed in Figure 3.4 was used to transfect HEK293FT cells. 96 hours post-transfection, conditioned cell media was purified using IMAC and size exclusion chromatography. The purified protein was run on an sodium dodecyl sulfate-polyacrylamide gel and stained using a Coomassie dye. The obtained protein was highly pure and of a similar molecular weight to that expected for the ECD of Caspr2. **B)** Western blotting of eluent fractions F to I with an antibody directed against penta-His peptide tags confirmed that the purified protein was recombinant Caspr2 ECD. Light blue star, recombinant Caspr2 ECD, red star, contaminant/degradation product.

HEK293FT cell culture and size exclusion chromatography were performed by Maria Carrasquero-Ordaz (Seiradake lab, University of Oxford).

Many protocols for preparing recombinant proteins involve some form of de-glycosylation. This eases purification and ensures a consistent glycosylation state, which is essential for crystallography and other structural techniques. In this case, endogenous Caspr2 glycosylation was preserved in order to avoid interfering with Caspr2 function. Transfected cells were cultured for a slightly longer time (96 hours) than for small-scale preps (48 hours) to ensure as much protein was produced as possible. Recombinant Caspr2 ECD was then purified from the conditioned medium using a combination of two affinity chromatography procedures: IMAC, using a nickel column, followed by size exclusion chromatography. The second purification step was included in the purification procedure for the large-scale batch only because of the need for increased purity. Coomassie staining revealed the protein isolated during the purification procedure was highly pure and of the expected size for recombinant Caspr2 ECD (Figure 3.6A). Western blot analysis of the purified protein confirmed that the purified protein was indeed recombinant Caspr2 ECD (Figure 3.6B).

3.4 Caspr2 affects Purkinje cell dendritic morphology

Next, the functional effect of the purified Caspr2 ECD on Purkinje cell development was investigated. Caspr2 appears to be expressed largely in Purkinje cells and possibly, parallel fibres (Figure 3.1). Given that parallel fibres and climbing fibres synapse on to Purkinje cells and that Neurexins typically participate in trans-synaptic interactions, it is conceivable that any Caspr2 expressed in granule cells or climbing fibres affects Purkinje cells. Both the Caspr2 expressed in parallel fibres or climbing fibres and the Caspr2 expressed in Purkinje cells could therefore function by affecting Purkinje cells. Importantly, in both cases this function could be mediated by the ECD of Caspr2. Consequently, the effect of Caspr2 on Purkinje cells in particular

was examined. As Caspr2 is known to control the dendritic morphology of cultured hippocampal neurons[5], the hypothesis that Caspr2 controls Purkinje cell neurite morphology was investigated first.

To do this, organotypic cerebellar slice cultures were prepared from *Cntnap2*$^{+/+}$ and *Cntnap2*$^{-/-}$ P9 mice and cultured for 7 days. The slices were dosed repeatedly, at regular intervals, with either recombinant Caspr2 ECD or a vehicle treatment (10mM Tris pH 8, 200mM NaCl). The Caspr2 ECD dose used (20µg/mL) was selected based on the dose used in similar experiments elsewhere in the literature[152]. After 8 days of culture, methanol was used to fix the slices by dehydration. The fixed slices were then subjected to immunostaining using an antibody directed against the Purkinje cell marker IP_3R1.

It is common for some Purkinje cells to become separated from the main Purkinje cell layer during these experiments. As the neurites of Purkinje cells that are retained in the main Purkinje cell layer are obscured by the neurites of neighbouring Purkinje cells, only those Purkinje cells that were clearly separate from the Purkinje cell layer, with unobscured neurites, were analysed.

Mature Purkinje cells usually have a single primary dendrite, but immature cells often display multiple primary dendrites, before these are pruned away later in development[23]. In some cases, a second primary dendritic branch is retained by the mature cell[23]. Many of the Purkinje cells analysed were observed to have multiple primary dendrites, consistent with these cells being immature. Interestingly, Purkinje cells taken from *Cntnap2*$^{-/-}$ mice were less likely to display multiple primary dendrites than those taken from *Cntnap2*$^{+/+}$ littermates (Figure 3.7A). This phenotype was rescued by the addition of recombinant Caspr2 ECD (Figure 3.7B). Together, these findings suggest a role for Caspr2 in regulating Purkinje cell dendritic development.

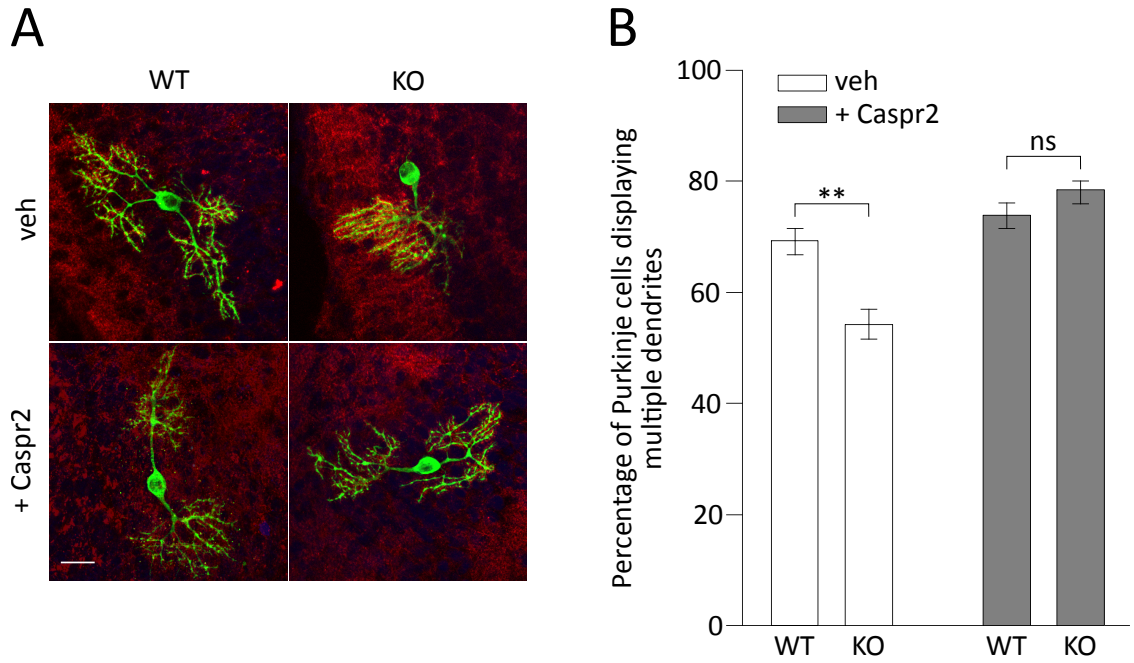


Figure 3.7: Caspr2 affects Purkinje cell dendritic morphology. **A)** Representative images of Purkinje cells, cultured as part of organotypic cerebellar slices, immunostained for IP_3R1 (green) and VGLUT1 (red). Slices were cultured for a week and dosed with either recombinant ECD Caspr2 or a vehicle treatment (10mM Tris pH 8, 200mM NaCl), before being fixed and immunostained. veh, vehicle, scale bar = 25µm. **B)** Quantification of pooled data: addition of recombinant Caspr2 ECD ablates the difference in the number of Purkinje cells with multiple primary dendrites between *Cntnap2*$^{+/+}$ and *Cntnap2*$^{-/-}$ Purkinje cells. The number of Purkinje cells with multiple primary dendrites is presented as a percentage of the total number of Purkinje cells present. Error bars represent 95% confidence intervals. N = 6 WT, 5 KO. A regular two-way ANOVA (genotype$*$treatment) revealed a significant main effect of treatment ($F [1, 18] = 14.13$, $p < 0.0001$), a non-significant main effect of genotype ($F [1, 18] = 4.003$, $p > 0.05$) and a significant interaction between factors ($F [1, 18] = 30.91$, $p < 0.005$). $**$ = $p < 0.01$, ns = not significant, Sidak's multiple comparisons post-hoc test. WT, wild-type (*Cntnap2*$^{+/+}$) mice, KO, knockout (*Cntnap2*$^{-/-}$) mice.

3.5 Discussion

Evidence from the literature, and from previous work done by the Becker lab, suggests that Caspr2 affects cerebellar-specific behaviours. However, nothing was known about the cellular and molecular bases for this. The overall aim of the programme of work presented in this chapter was therefore to uncover the function of Caspr2 in the cerebellum, at the cellular level.

The work presented confirms that Caspr2 is expressed in the developing cerebellum. Most Caspr2 in the developing cerebellum was observed to be highly expressed in the deep molecular layer and the white matter. At a sub-cellular level, Caspr2 was detected at synapses, at both pre- and post-synaptic specialisations.

Using a cell-surface biotinylation assay it also was shown that Caspr2 is an integral cell membrane protein. Informed by these results, the ECD of Caspr2 was selected for further investigation and recombinant Caspr2 ECD was subsequently cloned, expressed and purified.

This recombinant protein was then used in a cellular assay to show that Caspr2 regulates Purkinje cell dendritic morphology during development.

Caspr2 is present at synapses in the molecular layer

Immunostaining of sections, cut from P14 cerebella, revealed that Caspr2 is localised to the deep molecular layer and the white matter in the developing cerebellum, suggesting that Caspr2 is expressed in Purkinje cells and possibly also in other neurites of the molecular layer. In addition, Caspr2 was detected in the granule cell layer, although it appeared much more sparsely distributed here than elsewhere. These data are consistent with previous studies that have reported Caspr2 expression in the white matter [56], the granule cell layer[67] and the molecular layer[15; 67; 122]. In addition, Purkinje cells appear to be positive for Caspr2 in representative images of immunostained cerebella presented in two separate papers[67; 122].

However, most of cerebella studied in these previous reports were taken from adult mice. Only two studies to date have examined the localisation of Caspr2 in the developing cerebellum[15; 56]. Interestingly, in one of these studies, Caspr2 immunostaining was found to be concentrated in the deep molecular layer[15], consistent with the Caspr2 immunostaining pattern observed here. Thus, the spatial distribu-

tion of Caspr2 observed here is consistent with previous work.

Western blot analysis showed that Caspr2 co-purifies with synaptic markers when the developing cerebellum is biochemically fractionated. Together with the immunohistochemistry data presented above, these data suggest that Caspr2 localises to synapses in the molecular layer and / or Purkinje cell axon terminals.

To define the expression of Caspr2 at synapses in greater detail, biochemical fractionation was employed to first isolate the synaptic junction fraction (the proteins that are involved in interactions in the synaptic cleft) and then to split it into pre- and post-synaptic specialisations. The sub-synaptic localisation of Caspr2 was then assessed, for the first time, by Western blot. Caspr2 was found in both pre- and post-synaptic specialisations. It was therefore still unclear if Caspr2 localised to Purkinje cell axon and / or parallel and climbing fibre terminals. However, the presence of Caspr2 at post-synaptic specialisations suggested that Caspr2 must be expressed in Purkinje cell dendritic spines at synapses in the molecular layer, as this was the only post-synaptic site at which Caspr2 could be present given its apparent expression in the white matter and in the deep molecular layer. It should be noted however, that this logic only holds if the spatial expression of Caspr2 is genuinely restricted to these areas. It is possible that the white matter staining observed obscured Caspr2 signal localised to cells of the deep cerebellar nuclei. If this were the case, then it would not be possible to conclude that Caspr2 is expressed at Purkinje cell dendritic spines.

Given that Caspr2 immunostaining was observed to cover all of the molecular layer in adult mouse cerebella[67; 122], it may be that the temporal expression of Caspr2 in parallel and climbing fibres is matched to the formation of Purkinje cell synapses in the molecular layer. These synapses form on a smooth temporal gradient, along the deep-superficial axis, as Purkinje cells extend their developing dendritic trees up

in to the emerging molecular layer.

The presence of Caspr2 in pre- and post-synaptic specialisation fractions, as well as the fact that it is known to be integral to the plasma membrane in other systems, suggests that Caspr2 is also integral to the plasma membrane in cerebellar neurons. A surface protein biotinylation assay was used to assess this hypothesis and Caspr2 was found to have a domain exposed to the extracellular milieu. Given the presence of a secretion signal at the N-terminus of the protein, and the lack of one at the C-terminus, it is very likely that Caspr2 is a type 1a transmembrane protein in the cerebellum. This could be tested by a simple immunohistochemistry experiment, where the permeabilisation step is removed from the usual immunostaining protocol (an antibody that recognises an intracellular Caspr2 epitope is available). Given that Caspr2 is expressed at synapses involving Purkinje cell dendrites, the fact that it is an integral cell membrane protein means that its ECD is expressed in the synaptic cleft of these synapses. As a result, it is possible that direct communication between Purkinje cells and granule cells / climbing fibres is mediated by Caspr2.

Caspr2 regulates Purkinje cell dendritic development

The ECD of Caspr2 was found to be expressed in the synaptic cleft at Purkinje cell-granule synapses, during the period of cerebellar development when Purkinje cell dendritic arbourisation occurs. Dendritic arbourisation is known to be regulated by glutamtergic synaptic input[31] and so the effect of Caspr2 on Purkinje cell dendritic arbourisation was assessed.

To do this, organotypic slices were cut from *Cntnap2*$^{-/-}$ and *Cntnap2*$^{+/+}$ animals and then dosed with recombinant Caspr2 ECD over a 7 day period. Subsequent analysis of Purkinje cell dendritic morphology revealed that the ECD of Caspr2 is necessary for the correct temporal development of the Purkinje cell dendritic arbour. This is

the first description of the function of the ECD of Caspr2 in non-myelinated neurites.

This effect suggests Caspr2 modulates the development of Purkinje cell dendritic morphology, however given the bell-shaped distribution of Purkinje cell primary dendrite number throughout development[23], it is not possible to conclude whether Caspr2 is inhibiting or accelerating Purkinje cell development. Either way, disrupting the rate of Purkinje cell development is likely to have a significant impact on brain function for many reasons. For example, the cerebellum acts to integrate sensory information, which is required for the experience dependent entraining of other brain areas. All cerebellar output is conducted through Purkinje cells and so disrupting the development of these cells would subsequently disrupt the entraining of connected cortical regions.

Interestingly, Caspr2 is known to be required for the stabilisation of new dendritic spines in adult mice[53]. It may be that Caspr2, acting at synapses, similarly stabilises Purkinje cell dendritic spines during development and that this stabilisation is required for synaptotrophic dendritic growth[30; 31].

What might be the molecular basis for the effect the Caspr2 ECD has on Purkinje cell dendritic outgrowth? Caspr2 is expressed in the synaptolemma of Purkinje cell dendritic spines and possibly also in the synaptolemma of apposed granule cell axon terminals. It is therefore capable of transducing information from the synaptic cleft to the Purkinje cell spine cytoplasm.

By participating in trans-synaptic interactions that define synaptic sites, as well as intracellular interactions, Caspr2 may localise the intracellular machinery required to stabilise dendritic spines to synaptic sites. Consistent with this idea, Caspr2 interacts with CASK[136], a protein known to regulate synaptic Ca^{2+} channels[93] and *in trans* with Contactin-2[123]. Although the Caspr2-Contactin-2 interaction is not

known to occur at synapses specifically, both proteins are expressed at synapses in the rat brain[11]. The Caspr2-CASK interaction is mediated by the PDZ-binding domain of Caspr2, which is intracellular[136]. Alternatively, Caspr2 may act in a cell-autonomous fashion, but still be required for the clustering of proteins at synaptic sites needed to stabilise dendritic spines.

In either case, because recombinant Caspr2 ECD alone rescued the dendritic morphology defect observed in *Cntnap2*$^{-/-}$ mice, it is likely that some other transmembrane molecule, integral to the synaptolemma of Purkinje cell dendritic spines, is responsible for transducing signals from the Caspr2 ECD to the Purkinje cell cytoplasm.

Given that Caspr2 localises to synapses involving Purkinje cell dendrites, regulates Purkinje cell morphology and affects hippocampal neuron synapse numbers[5], it would be worthwhile to investigate the possibility that Caspr2 also regulates the number of synapses formed in the molecular layer. Synapsin immunostaining of sectioned cerebella taken from *Cntnap2*$^{+/+}$ and *Cntnap2*$^{-/-}$ mice would allow an assessment of this. In addition, it would be interesting to investigate whether Caspr2 is required for the maintenance of dendritic arbour morphology in adulthood, as well as affecting this during development.

Conclusions

In summary, Caspr2 is expressed in the developing cerebellum and appears to be confined to the white matter, as well as to the synaptolemma at synapses involving Purkinje cell dendrites. It may also localise to the synaptolemma of Purkinje cell axon terminals. The ECD of Caspr2, which is present in the synaptic cleft at synapses involving Purkinje cells in the molecular layer, acts to regulate the development of Purkinje cell dendritic morphology. Additional work, presented in the next

two chapters, was required to understand the molecular mechanism underlying this phenomenon.

4 Identification of synaptic Caspr2-interacting proteins

4.1 Introduction

Having discovered that the ECD of Caspr2 appears to control Purkinje cell dendritic morphology, the next step was to understand the molecular basis for this effect. Caspr2 is part of the Neurexin superfamily of proteins. Neurexins are often thought of as scaffolding proteins[98], functioning by localising different moieties to various specific cellular compartments and thus providing the modularity on which cellular biochemistry depends. The best way to understand the function of these proteins is, of course, by defining the other proteins that they interact with.
The aim of the work described in this chapter was therefore to describe the cognate binding partners of the ECD of Caspr2 in the developing cerebellum, in the hope that this information would help explain how and why Caspr2 affects the development of Purkinje cell dendrite morphology.

Known Caspr2 ECD interaction partners

Although several studies have addressed the role of the ECD of Caspr2, few proteins

that interact with this domain have been identified to date. The first such binding partner uncovered was Contactin-2, which interacts with Caspr2 at the JXP[112; 148]. Contactin-2 is a cell adhesion molecule, which, interestingly, was already known to regulate granule cell neurite outgrowth (Buttiglione et al., 1998). The Contactin-2-Caspr2 interaction is one of a set of interactions required for the correct localisation of Shaker-type K^+ channels at the JXP[112; 148]. Contactin-2, expressed in myelinating oligodendrocytes, interacts *in trans* with Caspr2, expressed in axons[123]. The Contactin-2 immunoglobin domains also bind Shaker-type channels, thus mediating the indirect interaction between them and Caspr2[151]. Although Contactin-2 is also expressed in axons, only the *in trans* interaction is required for Shaker-type channel localisation at the JXP[123].

It has also been proposed that Contactin-1, another member of the Contactin family of cell adhesion proteins, interacts with the ECD of Caspr2[119]. However, *in vivo* evidence for this interaction is currently lacking. Much like Contactin-2, Contactin-1 also mediates neurite outgrowth in granule neurons[27], however the functional consequences of a potential Caspr2-Contactin-1 interaction remain unknown. Of note though, Contactin-1 has been shown to be required for the cell surface localization of Caspr. Mirroring the behaviour of Caspr2 and Contactin-2, these two proteins also form a complex during the myelination process[42; 116]. Thus, given the similarity between Caspr1 and Caspr2 (59.6%), it may be that Contactin-1 and Caspr2 communicate to affect myelination.

Aside from Contactin-1 and Contactin-2, no other proteins have been observed to interact with the ECD of Caspr2.

Known synaptic Caspr2 interaction partners

Thus far, no proteins have been definitively demonstrated to interact with Caspr2 at

synapses. There is limited, circumstantial evidence that the protein Carboxypeptidase E does so, but that is all. Carboxypeptidase E was found both to bind to the intra-cellular domain (ICD) of Caspr2 and to localise to synapses in the rat cortex[102]. However, Caspr2 was not found in the synaptic fraction in this study. Carboxypeptidase E has two known functions: it acts as an exopeptidase enzyme when solubilised [48] and also sorts molecules into the regulated secretory pathway when membrane-bound[36]. This latter function is relevant to the Caspr2-carboxypeptidase E interaction, as it appears to result in the trafficking of Caspr2 to the plasma membrane[102]. As such, if this interaction does occur at synapses, then it may well be essential for the expression of Caspr2 at the synaptolemma.
In summary, very few proteins are known to interact with the ECD of Caspr2 and almost nothing is known about the synaptic interactors of Caspr2. Both of the Caspr2 ECD-interactors reported thus far in the literature are involved in myelination. Even if these proteins also communicate with Caspr2 in non-myelinated neurons, the functional effect of these interactions are likely different to what has been described so far. Thus, the functional interactome of the ECD of Caspr2, when Caspr2 is expressed in non-myelinated neurites, is completely unknown.

4.2 Pull-down experiments identify IP_3R1 as a potential synaptic binding partner of Caspr2 in the cerebellum

The extracellular region of Caspr2 alone is sufficient to affect Purkinje cell dendritic morphology (Figure 3.7) and so efforts were focused on finding interactors for this domain. Caspr2 is likely integral to the synaptolemma (Figures 3.2A and 3.3) and so the ECD of Caspr2 is probably found in the synaptic cleft. Based on this, the search

for Caspr2 ECD binding partners was restricted to synapses in the cerebellum.

A pull-down assay (Figure 4.1A) was used to isolate synaptic Caspr2 ECD interactors. Cerebellar synaptosomes were prepared from P14 *Cntnap2*$^{+/+}$ mice and used as a protein source. Recombinant, biotinylated Caspr2 ECD, produced on a small scale, was coupled to Streptavidin-coated beads and used as bait. Details of protocol adaptations for the small scale and the general approach to recombinant Caspr2 ECD production are given in sections 2.4. and 3.3 respectively. To control for false positives due to aspecific interactions with the beadome, a second set of Streptavidin-coated beads were coated with the contaminant proteins that co-purify with recombinant Caspr2 ECD.

Mass spectrometry (LC-MS/MS) analysis of the pull-down experiment identified the ion channel IP_3R1 as a putative Caspr2 binding partner. Thirty-five separate peptide spectra were matched with IP_3R1 in the test condition, compared to none in the control condition. The total coverage of the primary sequence of IP_3R1 was 17.5%, with twenty-eight distinct sequences contributing to this. Seven of these twenty-eight distinct sequences were significant, where significant was defined as $p<0.05$ and p was the probability that a peptide spectra and fragment sequence could be matched by chance. See appendix B for full details of all of the proteins detected. To confirm this, eluents were ran on a sodium dodecyl sulfate-polyacrylamide gel and subject to immunoblotting. IP_3R1 was indeed found to be specifically enriched when Caspr2 ECD was used to pull-down proteins from cerebellar synaptosomes (Figure 4.1B).

IP_3R1 is a six-transmembrane, calcium-selective ion channel, gated by the ligand inositol 3,4,5-trisphosphate (IP_3)[44]. Previous work on IP_3R1 has largely focused on its classical role at the ER, where activation of IP_3R1 by IP_3 leads to calcium efflux into the cytoplasm (Figure 4.1C)[44; 90]. However, IP_3R1 is also known to localise to the post-synaptic density of Purkinje cells[90].

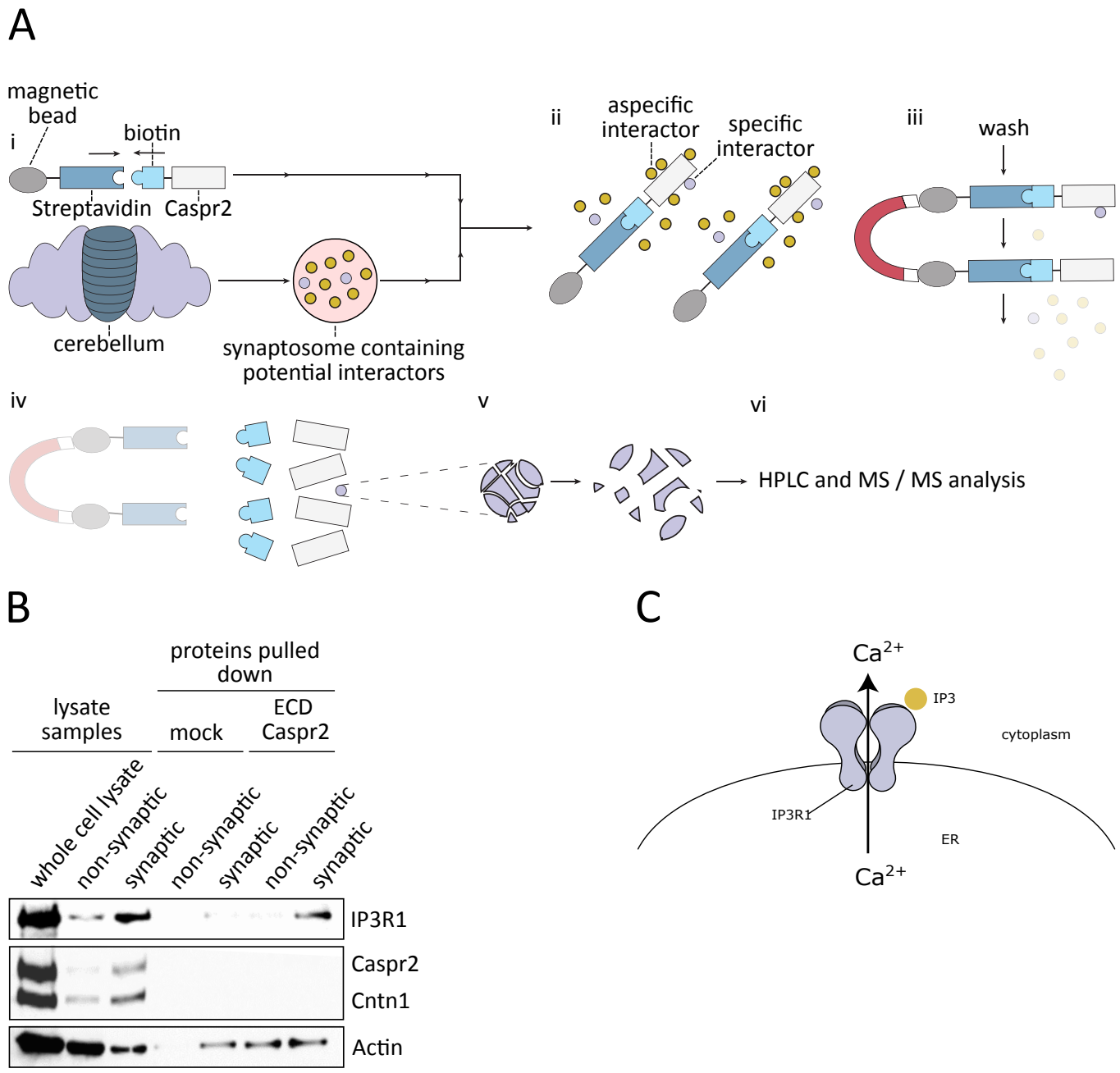


Figure 4.1: Pull-down experiments identify IP_3R1 as a potential synaptic binding partner of Caspr2 in the cerebellum. **A)** Schematic illustration of the pull-down experiment protocol. i, assembly of bait protein complex and preparation of cerebellar synaptosomes, ii, synaptic proteins bind to the bait protein, iii, washing removes aspecific interactors, iv, elution, v, trypsinisation of cognate interactors, vi, analysis of protein fragments. **B)** Western blot of samples sent for MS / MS analysis, showing that synaptic IP_3R1 interacts with Caspr2 ECD in the developing cerebellum. The protocol outlined in A) was used to identify Caspr2 interaction partners in the developing cerebellum. N = 1 pull-down assay only. IP_3R1 was specifically pulled down from a synaptic fraction prepared from P14 murine cerebella, when purified Caspr2 ECD was used as bait. **C)** Illustration of IP_3R1, showing its canonical role in the ER membrane.

4.3 Validation of the Caspr2-IP_3R1 interaction

Pull-down studies are inherently susceptible to type I errors and so a series of further experiments were performed in order to validate the Caspr2-IP_3R1 interaction. The co-IP method is similar to the pull-down method, save that all proteins are present at endogenous levels. This reduces total Caspr2 interactions, making co-IPs a more conservative approach than pull-downs. Consequently, they are useful for validating initial hits from pull-down studies (the reduced power of co-IPs means they are unsuitable for initial screening studies). Co-IPs were therefore duly performed to assess whether Caspr2 and IP_3R1 are *bona fide* interactors *in vitro*. Cerebellar synaptosomes were again prepared from P14 *Cntnap2*$^{+/+}$ mice. After lysis, the resulting solution of synaptic proteins was incubated with antibodies directed against either Caspr2 or IP_3R1. Immunoglobin G-coated Dynabeads were then used as a stationary medium to purify the antibodies, and any antibody-bound proteins, by affinity-chromatography. IP_3R1 was co-immunoprecipitated when Caspr2 was immunoprecipitated from cerebellar synaptosomes (Figure 4.2A). *Vice versa*, Caspr2 was co-immunoprecipitated when IP_3R1 was immunoprecipitated from cerebellar synaptosomes (Figure 4.2A), suggesting that the two proteins do physically interact *in vitro*.

To address the possibility that the apparent Caspr2-IP_3R1 interaction was specific to cerebellar lysates, further co-IP experiments were performed using a heterologous system. HEK293FT cells were co-transfected with full-length IP_3R1 and full-length Caspr2 expression constructs, cultured for 48 hours and then lysed. IP_3R1 was co-immunoprecipitated from the resulting cell lysate when Caspr2 was immunoprecipitated, indicating that the Caspr2-IP_3R1 interaction is not specific to *in vitro* systems derived from the cerebellum (Figure 4.2B).

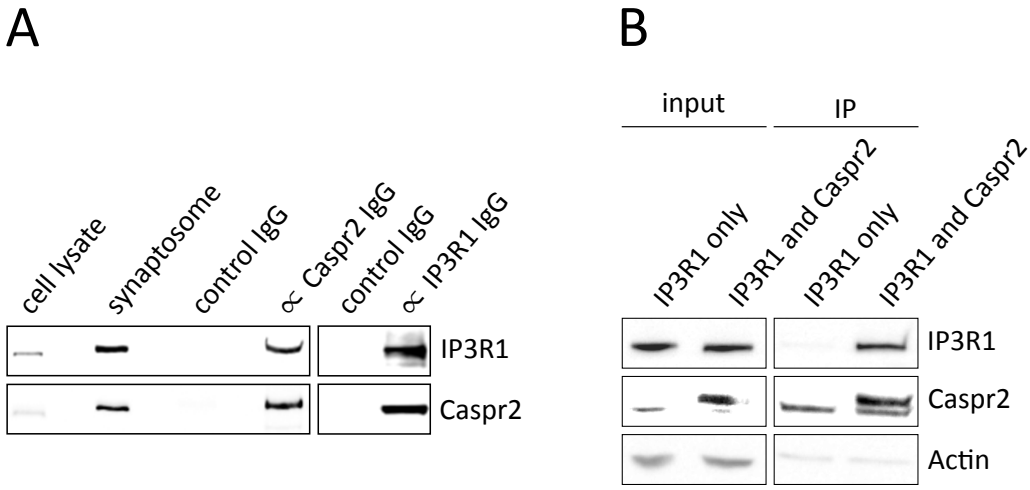


Figure 4.2: Caspr2 and IP_3R1 interact *in vitro*. **A)** IP_3R1 co-immunoprecipitates with Caspr2, and *vice versa*, from murine cerebellar lysates. Caspr2 and IP_3R1 were immunoprecipitated from cerebellar synaptosomes. Co-immunoprecipitated proteins were analysed by Western blot. N = 3 independently processed pairs of immunoprecipitations (2 cerebella per pair of immunoprecipitations). **B)** IP_3R1 co-immunoprecipitates with Caspr2, from HEK293FT cell lysates. An ∝ Caspr2 immunoglobin was used to immunoprecipitate proteins from lysates prepared using HEK293FT cells that were over-expressing either Caspr2 and IP_3R1 or IP_3R1 only. Co-immunoprecipitated proteins were assessed by Western blotting. IP, immunprecipitated. N = 3 independently processed pairs of transfections.

The co-IP experiment described in sub-figure B) was performed by Imogen Prickett (Becker lab, University of Oxford).

Pull-down and co-IP studies indicate the potential interaction of two proteins, but provide no spatial information. As a result, it is possible to observe interactions *in vitro* that are biologically irrelevant because the two proteins involved are localised in distinct cellular compartments. It was therefore important to assess whether IP_3R1 and Caspr2 localise proximal to each other in the cerebellum. To do this, saggital cryo-sections were cut from P14 cerebella and then immunostained using antibodies that target IP_3R1 and Caspr2. As before, strong Caspr2 staining was observed in the the white matter and in the deep molecular layer, whilst IP_3R1 was detected in the white matter, the Purkinje cell layer and throughout the molecular layer (Figures 4.3A and C).

Co-occurrence of Caspr2 and IP_3R1 was assessed using Mander's co-efficients of

co-occurrence. This metric does not assume a linear relationship between channel intensities, unlike co-localisation. Instead, each of two channels is assigned a separate Mander's co-efficient, with the Mander's co-efficient value for each channel defined as the percentage of total intensity for that one channel (across the whole image) present in voxels judged to be positive for the other channel. Mander's co-efficient values above 0.8 are widely accepted as indicative of co-occurence.

For a voxel to judged as positive for signal from a particular channel, the intensity value for that channel must be greater than a certain threshold. This was set using the Coste's auto-thresholding approach, which sets a pair of channel intensity thresholds so that the two channels have a Pearson's correlation coefficient (r) of zero for all voxels where either of the channels are below this threshold. An r value of zero indicates random noise and/or aspecific background and so by defining the threshold for judging a voxel to be positive for signal for a particular channel as $r>0$, noise and background are effectively excluded. This leaves only the voxels that contain at least some "genuine" signal for each channel. Mander's co-efficients were considered the most suitable metric for many reasons. Most importantly, IP_3R1 is known to have many binding partners[113] and so it was not reasonable to expect that the signal for both proteins would have a linear relationship across space. In addition, the oligomeric state in which Caspr2 and IP_3R1 interact was unknown, which also precludes assumptions of linearity. Finally, a co-occurrence metric was required in place of a co-localisation measure, because confocal microscopy does not have enough resolving power to accurately determine co-localisation. Co-occurrence was assessed in both regions of the cerebellum where both Caspr2 and IP_3R1 were observed to be expressed, the deep molecular layer and the white matter (Figures 4.3A and C). Caspr2 and IP_3R1 were found to co-occur in the deep molecular layer, where the Mander's co-efficient value for the Caspr2 channel was 0.856 (Figure 4.3B).

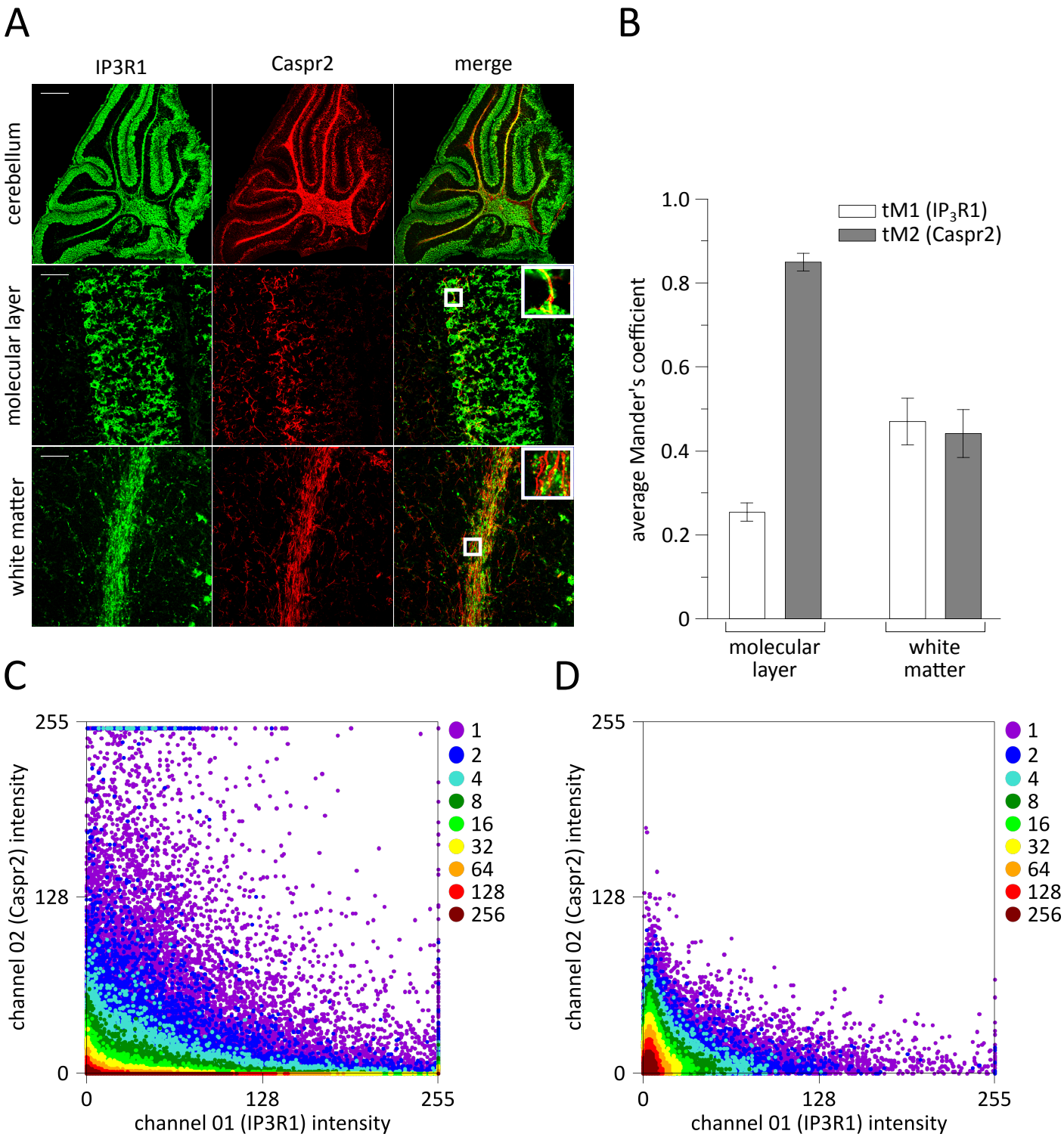


Figure 4.3: Caspr2 and IP_3R1 co-occur in the deep molecular layer of the developing cerebellum. **A)** Representative images of sections cut from WT, P14 murine cerebella and immunostained with antibodies against Caspr2 (red) and IP_3R1 (green). Scale bar for whole cerebellum images = 500µm, scale bar for white matter and molecular layer images = 50µm, insets (framed in white) are 4X zoomed. **B)** Plot of average Mander's coefficients for molecular layer and white matter images. For molecular layer images, average tM1 (IP_3R1) = 0.250, average tM2 (Caspr2) = 0.856. For white matter images, average tM1 (IP_3R1) = 0.461, average tM2 (Caspr2) = 0.472. N = 3 animals, n = 4 sections per animal for analyses of both molecular layer and white matter images. Error bars represent mean ± SEM. **C)** Scatterplot of the example merged molecular layer image from A). The total number of individual voxels with each possible combination of channel intensity values is displayed. **D)** Scatterplot of the example merged white matter image from A).

However, the two proteins did not co-occur in the white matter, where the Mander's co-efficient value for the Caspr2 channel was 0.472 (Figure 4.3B). Thus, Caspr2 and IP_3R1 appear to be localised in close enough proximity for a physical interaction between the two to be possible in the deep molecular layer only.

To further investigate whether IP_3R1 and Caspr2 are in close proximity at synapses in the molecular layer, it was necessary to assess co-localisation. For this, electron microscopy was employed (this technique provides the necessary resolution). P14 murine cerebella were embedded in LR Gold resin and then sectioned using an ultramicrotome. The sections were immunostained with primary, and then gold bead-coupled secondary, antibodies before being imaged. Tissue preservation was compromised in order to ensure antibody penetration and so it was not possible to definitively determine small sub-cellular features in our images. As a result, it was not possible to conclude whether or not Caspr2 and IP_3R1 were localised to synapses. It was also consequently difficult to determine some larger features. For example, the identity of the cell to which the nucleus observed in Figure 4.4 belongs was unclear (although given the position of the cell soma at the deep edge of the molecular layer, it is most likely either a Basket or a Purkinje cell). The identities of the multiple cellular processes observed, including the one shaded yellow in Figure 4.4A, were also ambiguous. Each of these is either a glial process or one of the many types of neurites found in the deep molecular layer.

However, Caspr2 was repeatedly found to be co-localised with IP_3R1 at, or in close proximity to, membranes in the molecular layer (Figure 4.4). These imaging data strongly suggest that the two proteins are localised close enough together that a physical interaction between the two, in the cerebellum, is possible.

Taken together, these validation experiments are consistent with Caspr2 and IP_3R1 interacting in the deep molecular layer of the cerebellum.

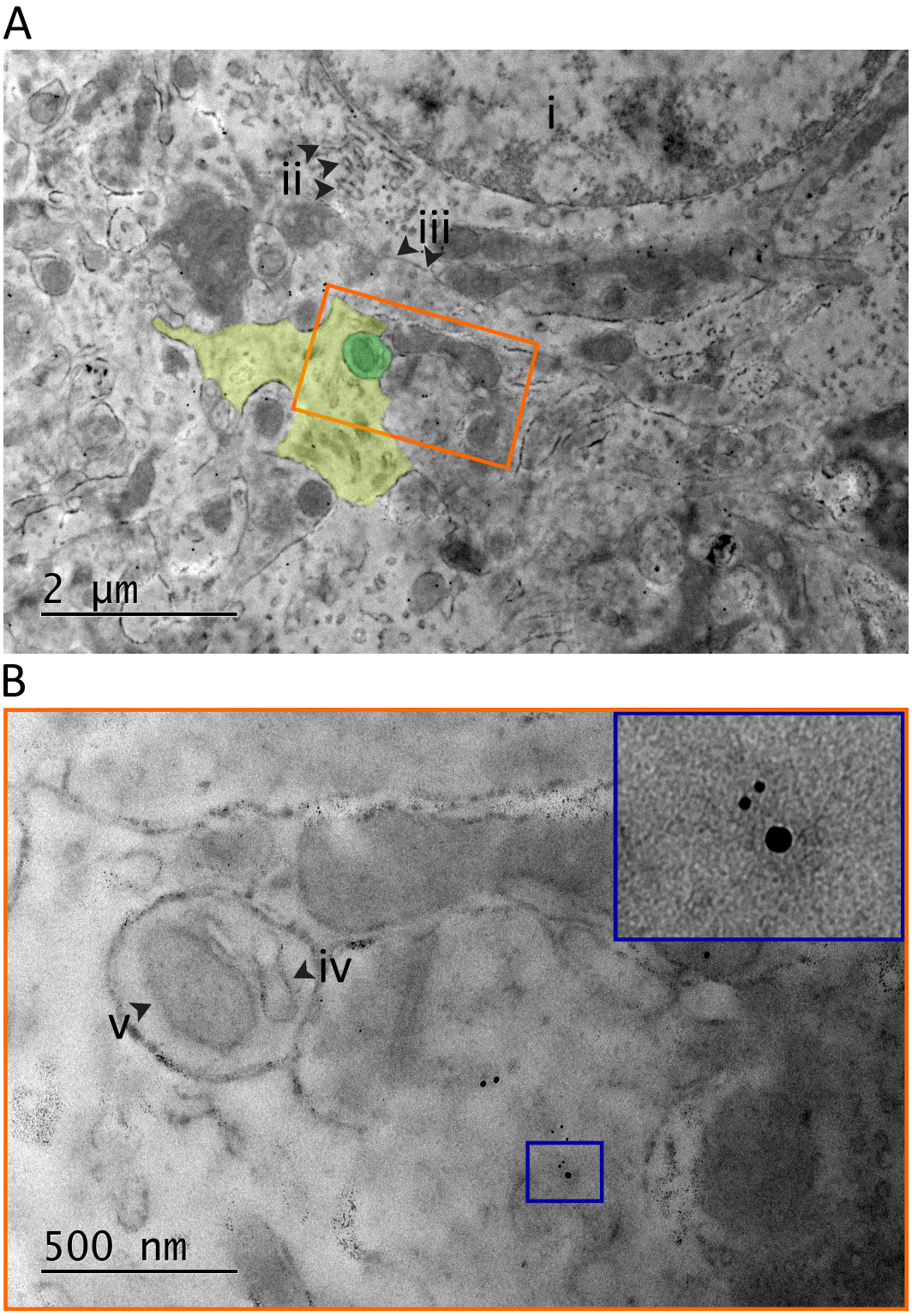


Figure 4.4: Caspr2 and IP_3R1 co-localise in the developing cerebellum. A) Example low magnification electron micrograph of the molecular layer of the murine cerebellum. The orange region is further magnified in B. i, euchromatic nucleus, ii, rough endoplasmic reticulum, iii, cell soma plasma membrane, green shading, parallel fibre, yellow shading, cellular process. **B)** High magnification image of orange region outlined in A), showing co-localisation of gold-bead labelled Caspr2 and IP_3R1 at membranes in the molecular layer of the cerebellum. Blue-rimmed inset is a 4X zoomed image of the region indicated. N = 4 animals, iv, smooth endoplasmic reticulum, v, mitochondrion, larger circle, Caspr2, smaller circle, IP_3R1.

Sectioning was performed by Lynne Cox (Christian lab, University of Oxford) and image collection was performed by Helen Christian (Christian lab, University of Oxford).

4.4 Identification of key binding domains

Having determined that Caspr2 and IP_3R1 interact in the cerebellum, the next step was to characterise the Caspr2-IP_3R1 interaction at the molecular level. There was insufficient information to design a molecular functional assay immediately and so efforts were instead focused on describing the structural basis for Caspr2-IP_3R1 communication. The functions of the various domains of IP_3R1 are well defined, with the IP_3R1 CTD effecting tetramerisation[52], the transmembrane region containing the pore[115] and the large NTD being comprised of Ca^{2+}[45] and IP_3[168] binding sequences. Thus, it was hoped that by understanding the mechanics of the Caspr2-IP_3R1 interaction, its molecular function would be become clear.

To determine which domains mediate Caspr2-IP_3R1 communication, the co-IP experiments used for validation of the interaction were repeated, but with truncated constructs used in place of full length protein. Several Caspr2 deletion constructs, which were kindly provided by Eric Lancaster[103], were assessed first. Although recombinant ECD Caspr2 was used as bait in the initial pull-down experiments, full length Caspr2 was still present in the cerebellar lysates used as a source of potential interactors. Full length Caspr2 was also used in the interaction-validation co-IP experiments. It was therefore possible that either or both of the transmembrane region and the intracellular domain of Caspr2 were necessary intermediates for the Caspr2 ECD-IP_3R1 interaction.

Deletion constructs that included the intracellular and transmembrane domains of Caspr2, but excluded parts of the extracellular domain, were therefore used initially (Figure 4.5A). This approach permitted an assessment of the role of the ECD of Caspr2 in the Caspr2-IP_3R1 interaction, whilst ensuring results were not confounded due to the potential disruption of the roles of the other Caspr2 domains.

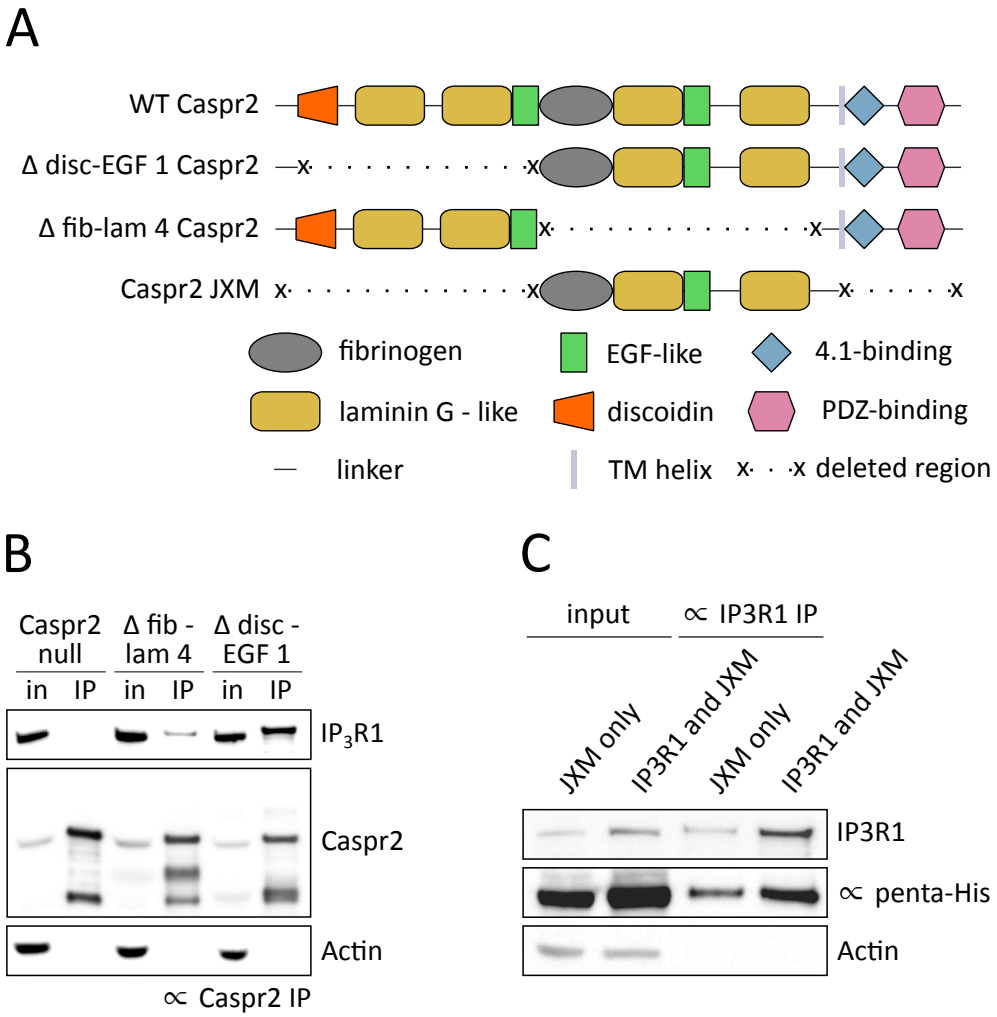


Figure 4.5: Key Caspr2 domains mediate the Caspr2-IP$_3$R1 interaction. Deletion constructs were used to identify the key Caspr2 domains that mediate the Caspr2-IP$_3$R1 interaction. For all experiments, lysates were prepared using HEK293FT cells that were over-expressing the indicated constructs. An appropriate immunoglobin was then used to immunoprecipitate proteins from the prepared lysates. Co-immunoprecipitated proteins were assessed by Western blotting. **A)** Illustration of the Caspr2 deletion constructs used. JXM, juxta-membrane region. **B)** Caspr2 JXM is necessary for the Caspr2-IP$_3$R1 interaction. **C)** Caspr2 JXM is sufficient for the Caspr2-IP$_3$R1 interaction. N = 2 seperately processed sets of independent transfections for both B) and C), in, input, IP, immunoprecipitated.

The co-IP experiment described in sub-figure B) was performed by Imogen Prickett (Becker lab, University of Oxford).

Western blot analysis of these co-IP experiments revealed that the C-terminal region of the extracellular domain of Caspr2 is necessary for the Caspr2-IP$_3$R1 interaction (Figure 4.5B). We termed this C-terminal region the JXM region. To test if the JXM

region was sufficient to mediate communication between Caspr2 and IP_3R1, a construct encoding only the JXM domain was generated (Figure 4.5A). A further co-IP experiment using this construct demonstrated that the JXM domain was indeed sufficient to mediate the Caspr2-IP_3R1 interaction (Figure 4.5C). Taken together, these data suggest that the Caspr2 JXM region mediates the Caspr2-IP_3R1 interaction.

Next, the IP_3R1 domains critical for the Caspr2-IP_3R1 interaction were assessed. Caspr2 and IP_3R1 are both integral membrane proteins. Part of the extracellular domain of Caspr2 (the JXM domain) was found to be both necessary and sufficient for Caspr2-IP_3R1 communication. If the interaction between Caspr2 and IP_3R1 occurs directly, the IP_3R1 domain responsible for mediating the interaction must also be soluble and non-cytoplasmic. However, the vast majority of the IP_3R1 protein resides in the cytoplasm. There are just three loop regions that are both non-cytoplasmic and soluble[43]. Of these, the third luminal loop (third lumenal loop (LL3)) is the only one comprised of more than 21 amino acids and so represents the only IP_3R1 domain likely to interact with Caspr2. A ΔLL3 IP_3R1 construct was generated (Figure 4.6A) and used in place of full length IP_3R1 in a co-IP experiment. Western blot analysis of co-immunoprecipitated proteins revealed that deletion of the IP_3R1 LL3 domain dramatically reduced the amount of IP_3R1 that is co-immunoprecipitated when Caspr2 is immunoprecipitated, relative to when full length IP_3R1 is used (Figure 4.6B). Thus, the IP_3R1 LL3 domain appears to be necessary for Caspr2 and IP_3R1 to communicate.

The next step was to investigate whether the LL3 region is sufficient to mediate the interaction. However, the LL3 domain proved difficult to express in isolation. Fusing the LL3 region to either a HA tag or to GFP did not lead to detectable levels of LL3 expression (data not shown). Moreover, attemtpting to secrete the LL3 domain without a tag was also unsuccessful (data not shown). Expression of LL3 was even-

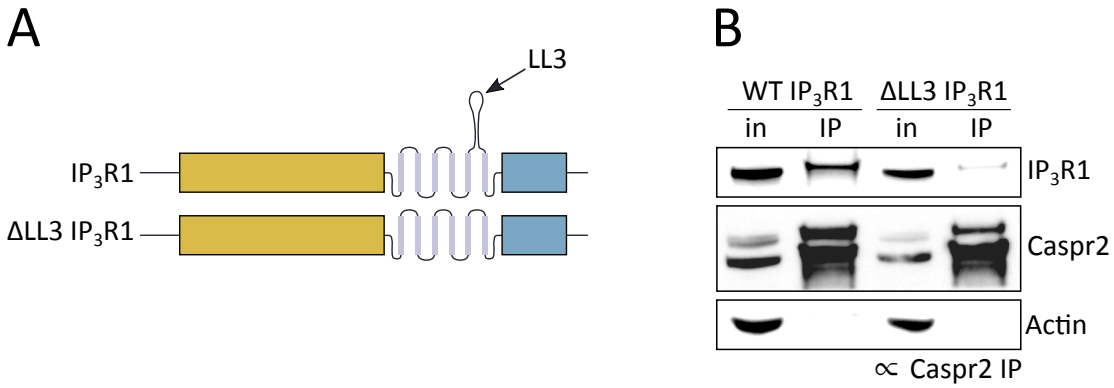


Figure 4.6: The IP_3R1 LL3 domain mediates the Caspr2-IP_3R1 interaction. Deletion constructs were used to identify the key IP_3R1 domains that mediate the Caspr2-IP_3R1 interaction, as described in Figure 4.5. **A)** Illustration of the ΔLL3 IP_3R1 deletion construct used. **B)** The IP_3R1 LL3 region is necessary for the Caspr2-IP_3R1 interaction. N = 2 seperately processed sets of independent transfections. Grey, transmembrane helices, gold, N-terminal domain, blue, C-terminal domain, in, input, IP, immunoprecipitated.

tually achieved via a combination of fusion (with human FC protein) and secretion (data not shown). However, high levels of aspecific binding to this protein were observed in trial assays (data not shown) and so these experiments were halted.

Taken all together, these data reveal that the Caspr2 JXM region and the IP_3R1 LL3 region are critical binding domains that mediate the Caspr2-IP_3R1 interaction.

4.5 Examining the possibility that Caspr2 interacts directly with IP_3R1

Next, the possibility that Caspr2 and IP_3R1 interact directly was tested. To do this,purified Caspr2 and IP_3R1 protein was required. Purified, recombinant Caspr2 ECD was already available (Figure 3.6) and so it was only necessary to purify IP_3R1 at this stage.

Affinity chromatography was used to purify IP_3R1 from rat cerebella, which are a good source of IP_3R1 protein due to the high level of IP_3R1 expression in the cerebel-

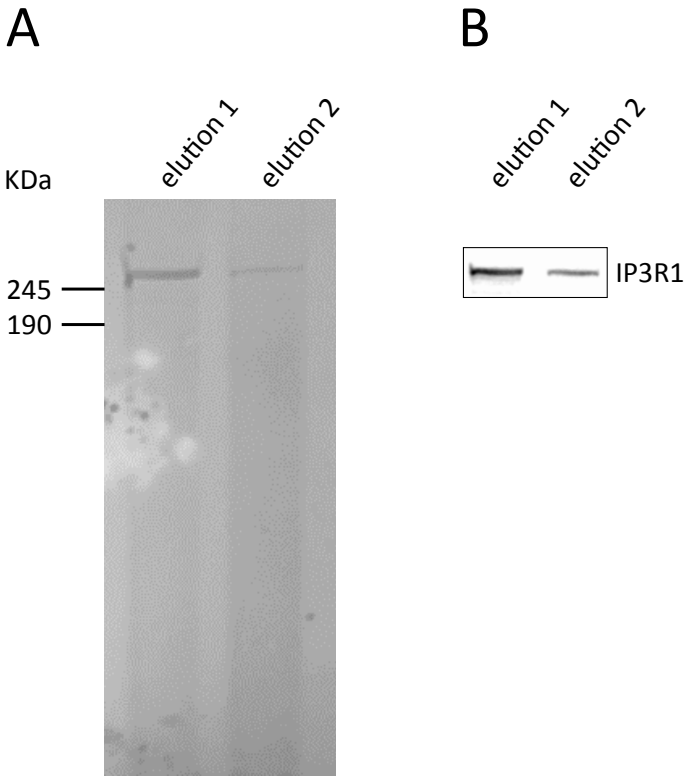


Figure 4.7: IP_3R1 can be purified from rat cerebella. A) Affinity chromatography was used to purify IP_3R1 from microsomes derived from rat cerebella. The purified protein was run on a sodium dodecyl sulfate-polyacrylamide gel and stained using a Coomassie dye. The obtained protein was highly pure and of a similar molecular weight to that expected for full-length IP_3R1 **B)** Western blot analysis of the purified protein confirmed that it was IP_3R1.

lum. IP_3R1 mostly localises to the ER and so, as an initial purification step, microsomes were prepared from pooled rat cerebella. IP_3R1 was then immunoprecipitated from these microsomes in the presence of CHAPS detergent, before being washed with various buffers and then eluted using an excess of immunogenic peptide. A centrifugal spin filter was used both as a final purification step and to concentrate the IP_3R1 protein. Coomassie staining revealed that the protein isolated during the purification procedure was highly pure and of the expected size for full length IP_3R1 (Figure 4.7A). Western blot analysis of the purified protein confirmed that this protein was indeed IP_3R1 (Figure 4.7B).

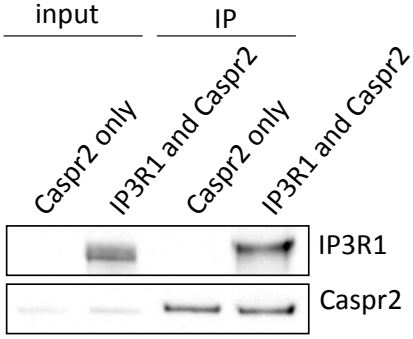


Figure 4.8: Co-IP of recombinant IP_3R1 and Caspr2. Co-immunoprecipitating purified, recombinant Caspr2 ECD and purified IP_3R1, to assess whether or not the Caspr2-IP_3R1 interaction is direct, gave an ambiguous result. Solutions containing Caspr2 ECD only or IP_3R1 and Caspr2 ECD were prepared. An $\propto$ IP_3R1 immunoglobin was then used to immunoprecipitate proteins from solution. Western blotting was used to identify precipitated proteins. N = 7 optimisation attempts, IP, immunoprecipitated.

Due to the low yields obtained using this purification method, it was not possible to use biophysical approaches such as surface plasmon resonance to assess direct binding. A "direct" co-IP was performed instead. Purified, recombinant Caspr2 ECD was combined with purified IP_3R1 in HOS buffer (see Chapter 2) and the IP_3R1 was then immunoprecipitated. The amount of Caspr2 ECD that was co-immunoprecipitated was assessed by Western blotting. Prior to the experiment being run, careful optimisation to ensure an optimal ratio of IP_3R1, antibody and stationary phase was carried out. This was intended to reduce aspecific binding to a minimal level. Despite this, equal amounts of Caspr2 ECD were co-immunoprecipitated in the presence and absence of IP_3R1 (Figure 4.8), suggesting that Caspr2 binds with fairly high affinity to either the $\propto$ IP_3R1 antibody or the immunoglobin G-coated beads used to precipitate the antibody. With this aspecific binding masking any potential Caspr2-IP_3R1 interaction, it was impossible to conclude anything from this experiment.

4.6 IP_3R1 and Caspr2 can interact in the synaptic cleft

Based on the findings presented so far, a hypothesis as to how Caspr2 might interact with IP_3R1 in the cerebellum was constructed. Caspr2 is likely integral to the synaptolemma at both pre- and post-synaptic specialisations in the cerebellum (Figures 3.2A and 3.3) and appears to affect Purkinje cell dendritic morphology (Figure 3.7). It interacts with IP_3R1 (Figure 4.1), in the deep molecular layer (Figures 4.3A and B) via key Caspr2 domains localised in the synaptic cleft (Figures 3.2A, 3.3 and 4.5). Evidence from the literature suggests IP_3R1 is found in many cell types in the cerebellum, but it is especially abundant in Purkinje cells[90]. Further, immunogold labelling coupled with electron microscopy has been used to show that IP_3R1 localises to the post-synaptic density of these cells [90]. Taken together, these results are consistent with Caspr2 and IP_3R1 interacting in the synaptic cleft at parallel fibre-Purkinje cell synapses and / or at climbing fibre-Purkinje cell synapses (Figure 4.9A).

Synaptic junction fractions contain only those proteins that are in direct contact with the synaptic web. Therefore, if IP_3R1 and Caspr2 do interact in the synaptic cleft then it should be possible to detect the Caspr2-IP_3R1 interaction in synaptic junction fractions prepared from cerebellar tissue. A prerequisite for this is that IP_3R1 must be present in these fractions. Western blots previously prepared to examine Caspr2 localisation (Figure 3.3C) were therefore re-examined to determine IP_3R1 expression at pre- and post-synaptic specialisations. IP_3R1 was found to be present at post-synaptic specialisations (Figure 4.9B), consistent with previous reports[90]. Unexpectedly however, IP_3R1 was also found to localise to pre-synaptic specialisations (Figure 4.9B).

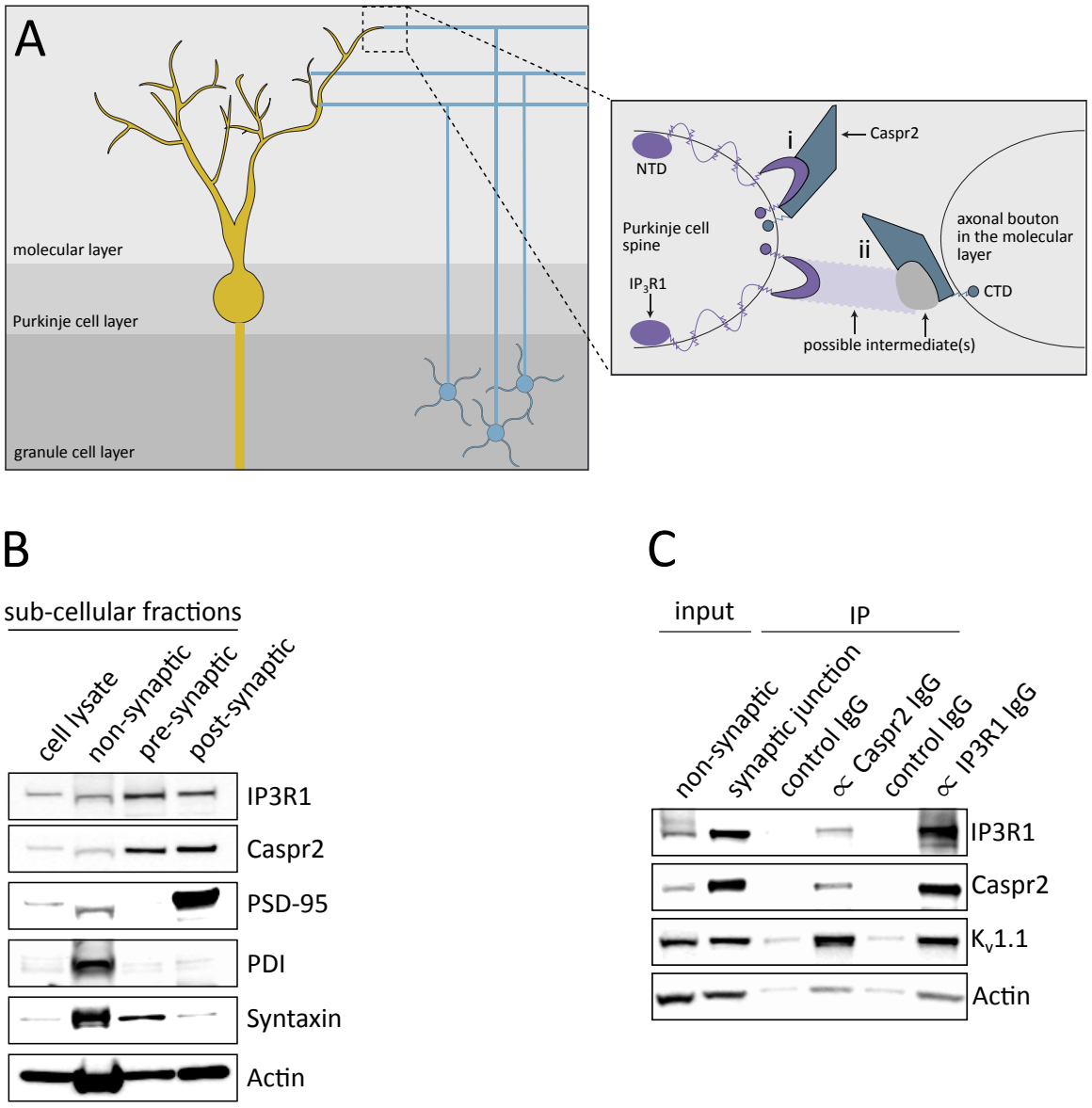


Figure 4.9: IP_3R1 and Caspr2 can interact in the synaptic cleft. A) Illustration highlighting two (of many) potential modes of Caspr2-IP_3R1 binding. i, direct, *in cis* interaction, ii, indirect, *in trans* interaction. Note that these potential modes of interaction are not exhaustive. Other combinations of direct/indirect and *in cis*/*in trans* are possible. Purkinje cell, gold, granule cell, light blue, IP_3R1, purple, Caspr2, turquoise. **B)** Caspr2 and IP_3R1 are both present at pre- and post-synaptic specialisations in the developing cerebellum. PDI demarcates the ER.. Additional Western blot analysis of the samples initially assessed in Figure 3.3C. **C)** Caspr2 and IP_3R1 can interact in the synaptic junction fraction. Synaptic junction fractions were prepared by following the protocol described in Figure 3.3B minus the final Triton X-100 extraction at pH8. Caspr2 and IP_3R1 were separately immunoprecipitated from prepared junctional fractions. Co-immunoprecipitated proteins were then analysed by Western blot. N = 2 seperately processed independent sub-synaptic fractionations for both B) and C), CTD, C-terminal domain, NTD, N-terminal domain, IP, immunoprecipitated.

The presence of IP_3R1 at both pre- and post-synaptic specialisations is consistent with the hypothesis that the Caspr2-IP_3R1 interaction occurs in the synaptic cleft. To test if Caspr2 and IP_3R1 do interact in the synaptic cleft Caspr2 and IP_3R1 were immunoprecipitated from synaptic junction fractions. Co-immunoprecipitated proteins were then assessed by Western blotting. Caspr2 was found to co-immunoprecipitate with IP_3R1 and *vice versa*, IP_3R1 was found to co-immunoprecipitate with Caspr2, showing that Caspr2 and IP_3R1 can interact at synaptic junctions in the cerebellum (Figure 4.9C). Of note, very little of the ER marker PDI was detected in either of the pre- or post-synaptic specialisation fractions in Figure 4.9B. This suggests that the synaptic junction fraction used for the co-IP experiment did not contain much material of ER origin and that the Caspr2-IP_3R1 interaction observed was not associated with the ER. $K_V1.1$, a protein known to interact with the intracellular domain of Caspr2 [110], was also co-immunoprecipitated both when Caspr2 was immunoprecipitated and when IP_3R1 was immunoprecipitated (Figure 4.9C). See Chapter 6 for further discussion of this.

4.7 Discussion

Data presented in the previous chapter suggested that Caspr2 regulates Purkinje cell dendritic morphology during development. However, the molecular mechanism underlying this effect was not clear. Caspr2 has previously been described as a scaffolding protein[112; 148] and data presented in chapter 3 demonstrated that Caspr2 is expressed at synapses. The collective aim of the experiments presented in this chapter was therefore to identify the synaptic binding partners of Caspr2 in the cerebellum. It was hoped that this information would provide molecular clues as to functional effect of Caspr2 in the developing cerebellum.

IP_3R1 was found to interact with the ECD of Caspr2, indicating that Caspr2 may scaffold synaptic ion channels in the developing cerebellum. Validation experiments revealed that the two proteins interact in the deep molecular layer. Key binding domains critical for the interaction were also identified. The localisation of these key domains implied that the Caspr2-IP_3R1 interaction may occur in the synaptic cleft and this was indeed shown to be the case.

IP_3R1 was successfully purified from rat cerebella using affinity chromatography. However, attempts to use this purified protein, to assess whether the Caspr2-IP_3R1 interaction is direct, produced ambiguous results.

IP_3R1 interacts with Caspr2, at synapses in the cerebellum

A pull-down experiment, using recombinant Caspr2 ECD as bait, was employed to identify putative synaptic Caspr2 interactors. Synaptosomes produced using P14 cerebella were used as a bait pool, as Purkinje cell dendritic development is ongoing at this time point. Unexpectedly, IP_3R1 was identified as a putative Caspr2 interactor. This, then, represents the first description of the Caspr2 ECD protein interactome, when Caspr2 is expressed in non-myelinated neurites.

IP_3R1 is a six-transmembrane, Ca^{2+}-selective ion channel, gated by the ligand IP_3[44], and so it appears that Caspr2 may be important in modulating Ca^{2+} currents in the developing cerebellum: an important function given the widespread consequences of Ca^{2+}signalling. Interestingly, IP_3R1 Ca^{2+}signalling is known to control the morphology of Purkinje cell dendrites[144], consistent with Caspr2 affecting Purkinje cell dendritic morphology by acting via IP_3R1.

The IPR31 LL3 domain was found to be necessary for the Caspr2-IP_3R1 interaction. This IP_3R1 domain contains the pore-forming region[115] and so by interacting with the IP_3R1 LL3 domain, Caspr2 (or some intermediate) is positioned close enough to

the pore to affect the pore environment. Depending on the physio-chemical properties of the exact residues in close proximity to the pore, Caspr2 may therefore either act as an inhibitor or an agonist of IP_3R1 Ca^{2+} currents.

It has previously been proposed that the cell adhesion protein Contactin-1 interacts with the ECD of Caspr2[119]. However, Contactin-1 was not enriched in any of the pull-down eluents, suggesting it does not interact with the Caspr2 ECD in the conditions used.

Caspr2 and IP_3R1 interact at synapses involving Purkinje cells, in the molecular layer

Information about the spatial distribution of proteins is lost when different sub-cellular compartments are combined during the preparation of lysates for pull-down assays. This can result in false positives. Proteins that are *bona fide* interactors in a lysate may actually be sequestered in different sub-cellular compartments and thus not interact *in vivo*. Immunohistochemistry and confocal microscopy were therefore used to determine the potential co-occurrence of Caspr2 and IP_3R1 in the developing cerebellum. IP_3R1 and Caspr2 were found to co-occur in the deep molecular layer only. Following this result, immunogold staining combined with electron microscopy was used to assess the spatial relationship between Caspr2 and IP_3R1 at higher resolution. Using this technique, IP_3R1 and Caspr2 were found to co-localise at membranous structures in the molecular layer.

IP_3R1 is known to be highly expressed in Purkinje cells[71]. The IP_3R1 immunofluorescent staining pattern observed here is consistent with Purkinje cell morphology and thus is in line with previous reports from the literature. As in chapter 3, Caspr2 was found in neurite-like structures in the deep molecular layer, which are likely to be either Purkinje cell dendrites, granule cell axons or climbing fibres. Inter-

estingly, these Caspr2-positive, neurite-like structures were observed to occasionally wrap around the edge of the somata of cells in, or very close to, the Purkinje cell layer. Similar Caspr2 immunofluorescence staining patterns have been observed before [49; 122]. These Caspr2-positive, neurite-like structures co-occurred with IP_3R1-positive, Purkinje cell proximal dendrites, suggesting that Caspr2 and IP_3R1 are localised close enough in space to interact, in the deep molecular layer. This notion is supported by the observation that gold bead-labelled IP_3R1 and Caspr2 molecules were found adjacent to each other in electron micrographs of the molecular layer.

Most of the IP_3R1 moieties in a given cell are found in the ER membrane, however IP_3R1 is also known to localise to the post-synaptic density of Purkinje cells[90]. Data reported in the previous chapter showed that Caspr2 also localises to the post-synaptic density of these cells, and possibly to granule cell pre-synaptic terminals as well. Interestingly, the expression of the long isoform of *Cntnap2* peaks (Figure 1.9) around the time of Purkinje cell-granule cell synaptogenesis[3], suggesting that *Cntnap2* expression may be specifically upregulated to ensure an adequate supply Caspr2 to these synapses. Taken all together, then, these data are consistent with Caspr2 and IP_3R1 interacting at synapses involving Purkinje cell dendrites.

In further support of this hypothesis, the dysfunction of Caspr2 induces a phenotype that mimics the that that arises due to the dysfunction of IP_3R1. Staggerer mice harbour a genomic deletion affecting the nuclear receptor RORα[92], which causes a staggering gait, mild tremor and hypotonia. This ataxic phenotype is indicative of cerebellar dysfunction[132]. Consistent with this, *Staggerer* mice cannot accumulate IP_3R1 in Purkinje cells[90; 132]. *Cntnap2*$^{-/-}$ mice do not express the longer Caspr2 isoform[112], but do express the shorter Caspr2 isoform[29] (also see Figure 1.7 for the domain architectures of the two Caspr2 isoforms). In effect, then, these mice do not express the extracellular domain of Caspr2 that is found in the synaptic cleft. The

absence of this domain is sufficient to induce gait and balance deficits in *Cntnap2*$^{-/-}$ mice (Figure 1.6), which are similar to (although less severe than) that observed in *Staggerer* mice.

Purkinje cell-specific *ITPR1*$^{-/-}$ mice and *Cntnap2*$^{-/-}$ mice also both exhibit eyeblink conditioning deficits, a cerebellar-specific phenotype[77; 144]. In addition, both Caspr2 and IP_3R1 appear to be crucial for the correct development of Purkinje cell dendrite morphology (Figure 3.7 and [59]) Notably, IP_3R1 expressed specifically in Purkinje cells is required for correct Purkinje cell dendritic morphology[144].

Together, these data from the literature are consistent with Caspr2 and IP_3R1 acting at the same point in pathways that impact Purkinje cell development and that might consequently affect cerebellar-specific behaviours. Thus, the hypothesis that Caspr2 and IP_3R1 interact at granule cell-Purkinje cell synapses is consistent with what is already known about the two proteins.

Given that the absence of IP_3R1 in Purkinje cells induces a similar Purkinje cell dendrite morphology phenotype to that observed in Figure 3.7, it is possible that Caspr2 acts via IP_3R1 to contol the morphology of these structures during development.

The data presented here strongly support the notion that Caspr2 and IP_3R1 interact at granule cell-Purkinje cell and / or climbing fibre-Purkinje cell synapses. However, this has not been definitively tested. To do this, a proximity ligation assay could be combined with immunostaining for markers of Purkinje cells (e.g. Calbindin), granule cells (e.g. VGLUT1) and climbing fibres (e.g. VGLUT2). Proximity ligation assays rely on the proximity-dependant ligation of oligonucleotide probes linked to secondary antibodies and provide a spatial description of a user-defined protein-protein interaction (the Caspr2-IP_3R1 interaction, in this case).

Caspr2 and IP_3R1 interact in the synaptic cleft

To further validate the interaction between Caspr2 and IP_3R1, and to gain insight into its structural basis, the identity of the key domains that mediate the interaction was investigated. The co-IP experiments originally used to confirm that IP_3R1 and Caspr2 physically interact were repeated, but with selected deletion constructs used in place of full length proteins. The Caspr2 JXM and IP_3R1 LL3 domains were both found to be necessary for the Caspr2-IP_3R1 interaction to take place. In addition, the Caspr2 JXM region was also found to be sufficient. Because the domains critical for Caspr2-IP_3R1 communication were both found to be extracellular regions, and because the interaction takes place at synapses, the possibility that Caspr2 and IP_3R1 interact in the synaptic cleft was examined. Co-IP experiments revealed that Caspr2 and IP_3R1 interact in the synaptic junction fraction (which contains only those proteins integral to the synaptolemma or found in the synaptic cleft). Taken together, these data show that Caspr2 and IP_3R1 do indeed interact in the synaptic cleft.

In order to interact with IP_3R1 in the synaptic cleft, which is only 20nm across, Caspr2 must be able to physically fit inside it. The physical dimensions of solubilised Caspr2 ECD have previously been analysed by others, who used small angle x-ray scattering (SAXS) to do so. When the results of this analysis were reported, the authors suggested that Caspr2 adopts a part extended, part compact structure[119]. However, details of the dimensions of the structure were not given. Examination of the deposited data (small angle scattering biological data bank accession code: SASDBR2), revealed that the compact part of the ECD has suggested dimensions of 50nm$*$145nm$*$100nm, whilst the extended part has suggested dimensions of 50nm$*$145nm$*$30nm. Thus, even if the compact part of the structure were to become extended, perhaps due to an interaction with another protein, the extended part of the Caspr2 extracellular domain is still too large to be present inside in the

synaptic cleft (length in each axis is $>$ 20nm). However, SAXS data represents an ensemble of structures and so given that the length of the extended region in the z-axis is not much larger than the required 20nm, it may be that most of the individual conformations of this region are in fact thin enough to fit inside the synaptic cleft.

When IP_3R1 is present in the cell membrane, the IP_3R1 protein has three separate loop domains exposed to the extracellular milieu. Of these, only the third is of any significant length. This particular loop is part of the pore forming domain[115]. Given the lack of other candidate extracellular domains, it is likely that the IP_3R1 LL3 domain alone facilitates the Caspr2-LL3 interaction. Although, it is possible that it does so in conjunction with another, intracellular IP_3R1 domain.

Other proteins, such as ERp44, have previously been reported to interact with the IP_3R1 LL3 domain. ERp44 is a memner of the thioredoxin family of proteins. It resides in the ER lumen and interacts with IP_3R1 to regulate IP_3R1 Ca^{2+} currents in a $[Ca^{2+}]_{ER}$-dependent manner. When $[Ca^{2+}]_{ER}$ drops, ERp44 interacts with the IP_3R1 LL3 domain and consequently inhibits IP_3R1 Ca^{2+}currents[58]. Thus, it is possible that Caspr2 also modulates IP_3R1 Ca^{2+}currents.

Examining the possibility that the Caspr2-IP_3R1 interaction is direct

An attempt was also made to determine if the Caspr2-IP_3R1 interaction is direct or not. However, low yields of IP_3R1 protein limited the range of experiments possible. A "direct co-IP" assay was attempted, but the result was ambiguous due to high background binding. Thus, in future, the IP_3R1 purification protocol should be optimised to increase the yield of protein sufficiently to make biophysical assays, such as size-exclusion chromatography-multi angle light scattering or surface plasmon resonance, feasible.

Even if Caspr2-IP_3R1 communication is not found to be direct, there is a preced-

ent for Neurexin-superfamily proteins interacting indirectly with ion channels in the synaptic cleft, at Purkinje cell-granule cell synapses. Cbln1, a small, soluble protein which is secreted into the Purkine cell-granule cell synaptic cleft by granule cells, was found to interact both with Neurexin1β and with GluRδ2[152]. GluRδ2, a glutamate receptor, is expressed almost exclusively by Purkinje cells[89], whilst Neurexin1β is found in the synaptolemma of granule cell axon terminals. Cbln1 was found to be necessary for Neurexin1β-GluRδ2 interactions, indicating that Cbln1 acts to physically link these two proteins. A similar mechanism may well underlie Caspr2-IP_3R1 communication.

Conclusions

In summary, Caspr2 interacts with IP_3R1 in the deep molecular layer of the cerebellum, via domains expressed in the synaptic cleft at Purkinje cell-granule cell synapses. Given that IP_3R1 is already known to control Purkinje cell dendritic morphology, it is possible that Caspr2 acts via IP_3R1 to exert its influence on these structures. In addition, that the IP_3R1 LL3 domain is involved in the Caspr2-IP_3R1 interaction implies that Caspr2 may modulate IP_3R1 calcium currents. These two hypothesis are addressed in the following chapter.

5 Functional consequences of the Caspr2-IP_3R1 interaction

5.1 Introduction

After discovering that IP_3R1 is a cognate binding partner of Caspr2 (Chapter 4), the next step was to examine the functional consequences of the Caspr2-IP_3R1 interaction.

Given that Caspr2 had been observed to regulate Purkinje cell dendritic morphology (Figure 3.7), the effect of the interaction on cellular morphology was examined. The effect of Caspr2 on the localisation of IP_3R1 was also assessed, as Caspr2 is known to act as a scaffold[112]. Finally, HEK293FT cells were used to examine the possibility that Caspr2-IP_3R1 communication might alter cytoplasmic Ca^{2+} levels.

Caspr2 in myelinated neurons

Caspr2 was originally found at the JXP, the region adjacent to the paranode in myelinated fibres[110]. Many studies have since examined the role of Caspr2 at this location. Of these, there are several that have focused on the ECD of Caspr2 in particular, the Caspr2 region that is both necessary and sufficient for the Caspr2-IP_3R1

interaction. Thus far, the ECD of Caspr2 has been found to contribute to the scaffolding of Shaker-type K^+ channels at the JXP. Both Caspr2 and Contactin-2 were found to be essential for the correct scaffolding of $K_v1.1$ and $K_v1.2$ at the JXP in the sciatic nerve and in the spinal cord[111; 112; 148], indicating that a complex of the two proteins is necessary for the correct localisation of these important channels.
More recently, it has been shown that Contactin-2 is also required for the correct localisation of Caspr2 and K_V channels in the white matter of the brain, including in the cerebellum[122]. As a likely consequence of this, the absence of Caspr2 disrupts saltatory conductance through myelinated cortical axons[129].

Caspr2 in non-myelinated neurons

The function of full length Caspr2 at non-myelinated locations is the subject of a few recent studies. Caspr2 was first found at synapses in 2008, in the rat brain[11]. Shortly afterwards Nrx-IV, an orthologue of Caspr2, was found to regulate synaptic morphology in *drosophila melagonaster*. Caspr2 over-expression increased the density of active zones and the branching of synaptic terminals, which led to an increase in the number of synaptic boutons[173]. Experiments using cultured murine hippocampal neurons have shown that Caspr2 also affects dendritic arbourisation, with the knockdown of Caspr2 leading to impaired dendritic outgrowth and reduced arbourisation[5]. At the physiological level, inhibitory neuron firing patterns in the somatosensory cortex are asynchronous in *Cntnap2*$^{-/-}$ mice[105; 130].
Caspr2 therefore appears to be important for controlling molecular composition and neuronal structures in neurons, although its function may differ depending on whether the neuron is myelinated. Although the function of the Caspr2 ECD in myelinated neurons has been investigated, how this domain functions elsewhere is unknown. The molecular layer, where Caspr2-IP_3R1 communication likely occurs

(Figure 4.3), is not myelinated and so the role of the Caspr2 ECD in this particular interaction is likely different to what has been described before.

The known functions of IP_3R1

IP_3R1 is a Ca^{2+}-selective ion channel and is gated by the ligand IP_3 [44], which is generated when phosphatidyl inositol-4,5-bisphosphate is cleaved by phospholipase C (producing IP_3 and diacylglycerol).

The vast majority of IP_3R1 is localised in the ER membrane, whilst a few moieties are found at the cell surface[90]. Phospholipase C is involved in a multitude of signalling pathways and so the large population of IP_3R1 in the ER membrane acts as a major Ca^{2+} signalling hub. As such, the IP_3R1 protein influences many different pathways and processes, including several that are neuron-specific. Synaptic plasticity[66], the decoding of action potentials[33] and the regulation of neurite morphology[144] are all controlled by IP_3R1 .

Unsurprisingly, given that it acts as a major signalling hub, IP_3R1 dysfunction in the cerebellum leads to significant behavioural phenotypes. Spinocerebellar ataxias types 15 and 29 are caused by mutations in the *Itpr1* gene[61; 84] and *ITPR1*$^{-/-}$ mice display aberrant cerebellar learning [144]. However, very little is known about the function of IP_3R1 at the plasma membrane, where the Caspr2-IP_3R1 interaction likely occurs.

5.2 Caspr2 inhibits IP_3R1-induced morphology changes

Having found that Caspr2 controls Purkinje cell dendritic development (Figure 3.7) and that Caspr2 and IP_3R1 interact in the developing cerebellum, it was hypothesised that the Caspr2-IP_3R1 interaction might mediate Caspr2-induced Purkinje

cell morphology changes. Ideally, we would have repeated the dendrite morphology experiment described in chapter 3 (Figure 3.7) but with slices from *Cntnap2 / Itpr1* double knockout mice included in addition to slices taken from *Cntnap2*$^{-/-}$ and *Cntnap2*$^{+/+}$ mice. Unfortunately, restricting the expression of IP_3R1 in Purkinje cells causes a very severe dendritic morphology phenotype that would mask any potential effect of Caspr2[90; 132]. In place of this, we turned to HEK293FT cells.

To assess how combining Caspr2 and IP_3R1 impacted cellular morphology, cells over-expressing Caspr2 and / or IP_3R1 were cultured for 48 hours and then fixed and immunostained. An antibody directed against Na^+K^+ATPase was used to outline cells that were transfected with empty vector, to make an assessment of morphology possible. For all other conditions, staining with antibodies directed against Caspr2 and IP_3R1 was sufficient to provide information about cellular morphology.

We found that over-expression of IP_3R1 alone leads to HEK293FT cells producing large extensions reminiscent of filopodia (Figure 5.1A). Strong IP_3R1 staining was observed throughout these extensions, consistent with the expected localisation of IP_3R1 in the ER. When Caspr2 was expressed alone, no change in cellular morphology was observed (Figure 5.1A). Caspr2 staining was restricted to the apparent periphery of the cell, consistent with Caspr2 being integral to the plasma membrane. Although the majority of cells over-expressing IP_3R1 alone produced extensions, when Caspr2 was co-expressed alongside IP_3R1, the percentage of cells with extensions was reduced to basal levels equivalent to those observed in mock transfected cells (Figure 5.1B). This suggests that Caspr2 acts to inhibit IP_3R1-induced morphology changes, raising the interesting possibility that the Caspr2-IP_3R1 interaction may underlie the regulation of Purkinje cell morphology by Caspr2. Interestingly, Caspr2 and IP_3R1 appeared to co-occur at the periphery of the cell (Figure 5.1A), consistent with Caspr2 and IP_3R1 communicating at the plasma membrane. To confirm

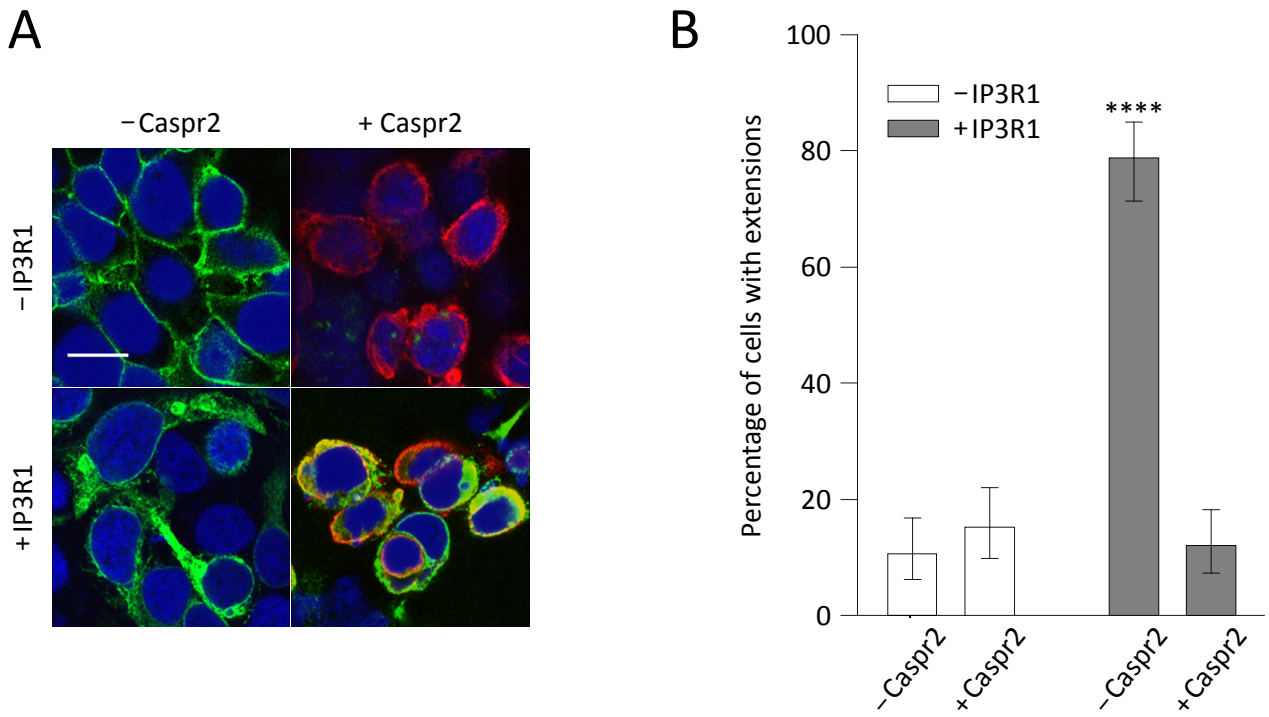


Figure 5.1: Expression of Caspr2 inhibits cellular extensions induced by the expression of IP_3R1. A) Representative images of HEK293FT cells expressing full length Caspr2 and IP_3R1. HEK293FT cells, which were over-expressing the indicated proteins, were cultured for 48 hours and then immunostained with antibodies against Caspr2 (red) and either Na^+K^+ATPase (green, top left image in grids) or IP_3R1 (green, all other images in grid). The number of co-transfected cells with extensions was then counted. **B)** Quantification of pooled data. Scale bar = 25µm, error bars represent 95% confidence intervals, N = 3 independent sets of transfections, n = 50 cells per condition per set of transfections, **** = $p < 0.0001$, chi-squared test with partitioning.

that the inhibition of IP_3R1-induced extensions upon co-expression of Caspr2 was a consequence of the Caspr2-IP_3R1 interaction, we repeated our initial HEK293FT cell morphology experiment (Figure 5.1). However, this time, full length Caspr2 was replaced with the truncated versions of Caspr2 used previously to assess the key binding domains that mediate the Caspr2-IP_3R1 interaction (Figure 4.5A). As the JXM region of Caspr2 was found to be necessary for Caspr2-IP_3R1 interactions, we reasoned that if this interaction is required for the inhibition of IP_3R1-induced extensions then deleting the Caspr2 JXM region would prevent this inhibition.

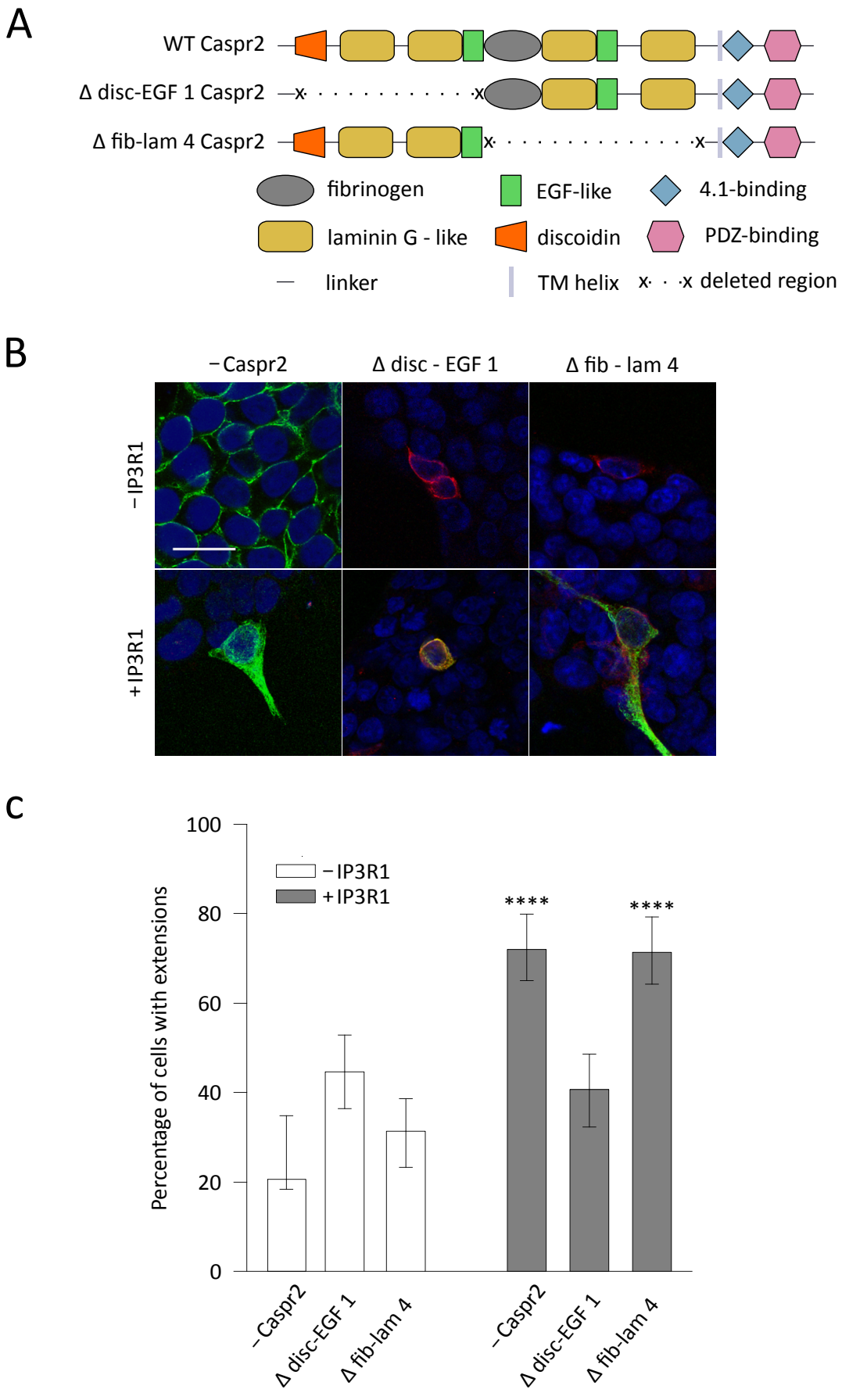


Figure 5.2: continued on next page

Figure 5.2: The Caspr2 JXM domain is required for the inhibition of IP_3R1-induced morphology changes by Caspr2. A) Illustration of Caspr2 deletion constructs used. **B)** Representative images of HEK293FT cells expressing one of two truncated Caspr2 constructs and full length IP_3R1. HEK293FT cells, which were over-expressing the indicated proteins, were cultured for 48 hours and then immunostained with antibodies against Caspr2 (red) and either Na^+K^+ATPase (green, top left image in grids) or IP_3R1 (green, all other images in grid). The number of co-transfected cells with extensions was then counted. **C)** Quantification of pooled data. Scale bar = 25µm, error bars represent 95% confidence intervals, N = 3 independent sets of transfections, n = 50 cells per condition per set of transfections, $****$ = $p < 0.0001$, chi-squared test with partitioning.

The reverse experiment, where the IP_3R1 LL3 region is removed, was not attempted. The LL3 domain is a constituent part of the pore-forming domain and so deleting the LL3 region would render the channel impermeable and thus almost certainly non-functional.

In all cases where proteins were expressed individually, Caspr2 and IP_3R1 staining patterns appeared identical to those observed in Figure 5.1 (Figure 5.2B). Deletion of the JXM domain prevented Caspr2-mediated inhibition of IP_3R1-induced extensions (Figure 5.2C), whereas deletion of the N-terminal section of Caspr2 had no such effect. That the Caspr2 JXM domain is both necessary for Caspr2 and IP_3R1 to interact *in vitro*, and for Caspr2-mediated inhibition of IP_3R1-induced cellular extensions, suggests that the inhibition of IP_3R1-induced extensions upon co-expression of Caspr2 is indeed due to the Caspr2-IP_3R1 interaction. Consistent with this, IP_3R1 does not appear to co-occur with Δ disc-EGF1 Caspr2 (Figure 5.2B), whereas IP_3R1-Caspr2 co-occurrence is maintained when full length Caspr2 is replaced with Δ fiblam4 Caspr2 (Figure 5.2B). However, it is possible that one or both of the Caspr2 deletion constructs used may not be trafficked to the cell surface as full length Caspr2 is. If this is the case, then it may be that the construct-dependent morphology differences observed are in fact a result of a trafficking defect.

5.3 Caspr2 does not affect IP_3R1 localisation

After noting that Caspr2 and IP_3R1 apparently interact to control cellular morphology (Figures 5.1 and 5.2), the next step was to define the molecular basis for this. Caspr2 is part of the Neurexin superfamily of proteins, which are often thought of as scaffolding proteins[98]. Scaffolding proteins function by localising other moieties to specific cellular compartments. Caspr2 is already known to scaffold Shaker-type K^+ channels at the JXP [112] and so, as IP_3R1 is also an ion channel, it was hypothesised that Caspr2 might similarly scaffold IP_3R1. If so, the absence of Caspr2 might disrupt the usual localisation of IP_3R1 . In order to ascertain if this was the case, saggital cryo-sections were cut from the cerebella of *Cntnap2*$^{-/-}$ and *Cntnap2*$^{+/+}$ mice and then immunostained using antibodies directed against IP_3R1 and Caspr2. Consistent with previous observations in *Cntnap2*$^{+/+}$ cerebellum (Figures 3.1 and 4.3), strong IP_3R1 staining was observed in the cell bodies of Purkinje cells, in the white matter and in the molecular layer, in both *Cntnap2*$^{-/-}$ and *Cntnap2*$^{+/+}$ cerebellum (Figure 5.3). Caspr2 then, does not appear to affect the gross localisation of IP_3R1 in the cerebellum. As mentioned in Chapter 3, Caspr2 signal was unexpectedly found in the white matter of the *Cntnap2*$^{-/-}$ cerebellum.

Although no gross changes in IP_3R1 localisation were detected by immunohistochemistry when Caspr2 was removed, it was still possible that changes in IP_3R1 localisation, involving distances below the resolution limit of confocal microscopy, had occurred. Movements over such small distances are often crucial for function. For example, the internalisation of a receptor, which involves a movement of only a few nm, has a dramatic impact on function.

Results from the previous chapter showed that both Caspr2 and IP_3R1 are present at pre- and post-synaptic specialisations and can interact in the synaptic junction

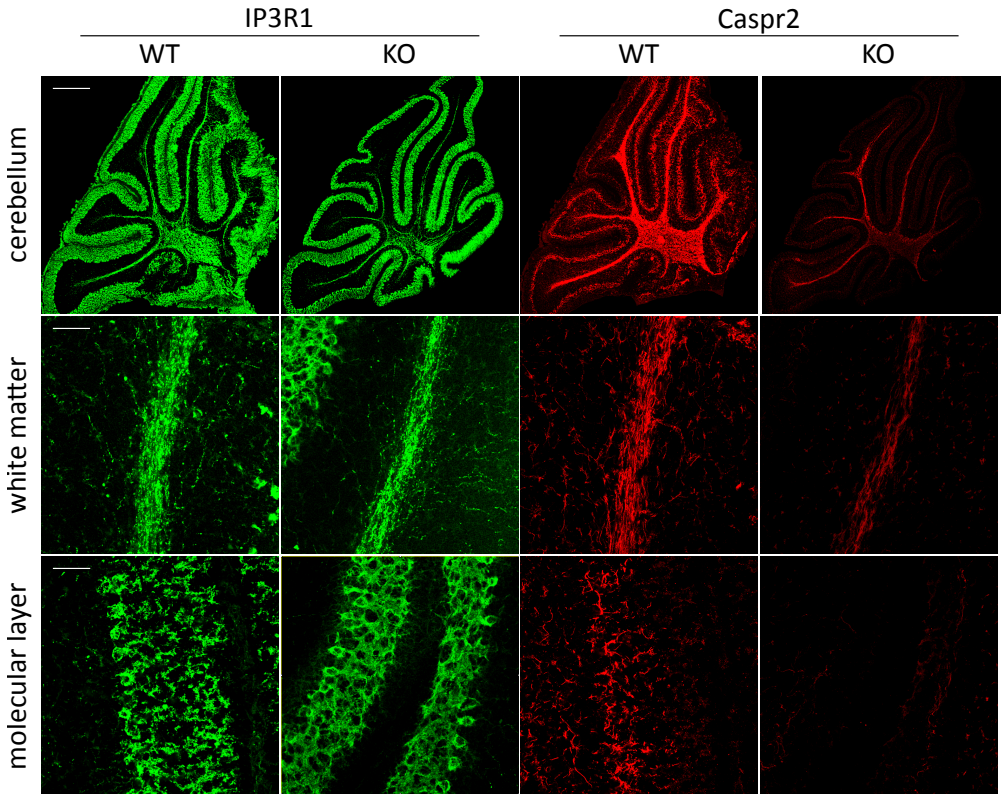


Figure 5.3: The absence of Caspr2 does not affect gross IP_3R1 staining patterns. Representative images of sections cut from *Cntnap2*$^{-/-}$ and *Cntnap2*$^{+/+}$, P14 murine cerebellum and immunostained with antibodies against Caspr2 (red) and IP_3R1 (green). Scale bar for whole cerebellum images = 500m, scale bar for molecular layer and white matter images = 50m. N = 5 WT, 5 KO, n = minimum of 4 sections per animal. WT, wild-type (*Cntnap2*$^{+/+}$) mice, KO, *Cntnap2*$^{-/-}$ mice.

fraction (Figure 4.9). This raised the possibility that Caspr2 scaffolds IP_3R1 at the synaptolemma. If this is the case, the absence of Caspr2 could disrupt the localisation of IP_3R1 at pre- and / or post-synaptic specialisations. Given the size of the synaptolemma, the mislocalisation of IP_3R1 away from the plasma membrane could well involve distances too small to be detected by confocal microscopy.

To investigate if this was the case, pre- and post-synaptic, synaptic junction fractions were prepared from *Cntnap2*$^{-/-}$ and *Cntnap2*$^{+/+}$ mice. The amount of IP_3R1 in these fractions was then analysed by Western blotting. No qualitative difference in IP_3R1 expression was detected (Figure 5.4).

Although the Bradford method was used to try to ensure equal protein loading,

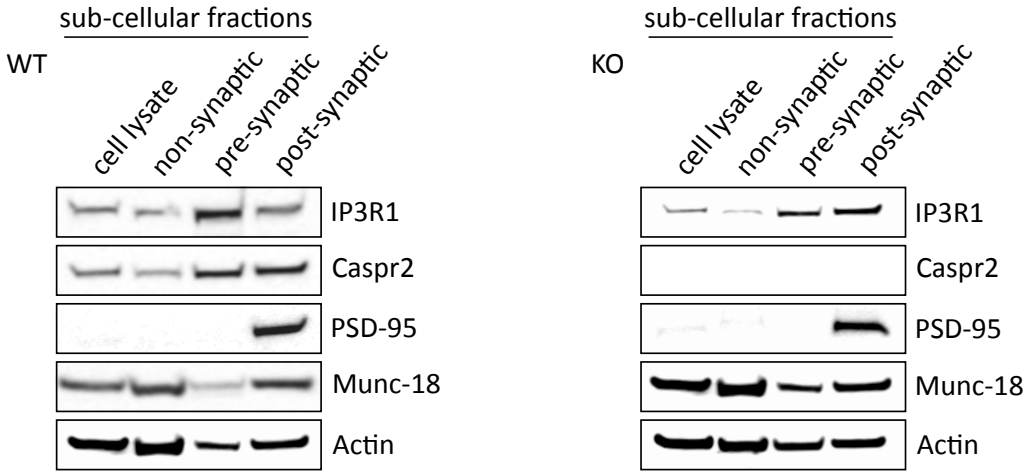


Figure 5.4: The absence of Caspr2 does not perturb the expression of IP_3R1 at synapses. Cerebella from *Cntnap2*$^{+/+}$ and *Cntnap2*$^{-/-}$ mice were subjected to the sub-synaptic fractionation protocol described in Figure 3.2C and the resulting fractions were analysed by Western blotting. Munc18 is a marker of pre-synaptic specialisations, whilst PSD-95 demarcates post-synaptic specialisations. For both genotypes, N = 2 independently processed sub-fractionations (2 whole cerebella per sub-fractionation). WT, wild-type (*Cntnap2*$^{+/+}$) mice, KO, *Cntnap2*$^{-/-}$ mice.

the lack of a reliable loading control protein for these fractions means quantitative comparisons are of questionable worth. That said, there did appear to be a slight decrease in the pre-synaptic IP_3R1:post-synaptic IP_3R1 ratio in the absence of Caspr2 (Figure 5.4). However, Caspr2 is expressed in equal amounts on both sides of the synapse. Consequently, a change in this ratio when Caspr2 is removed is not consistent with a simple model where Caspr2 scaffolds IP_3R1 at both pre- and post-synaptic specialisations. If such a simple model were correct, IP_3R1 expression at both pre- and post-synaptic specialisations would be reduced in the absence of Caspr2.

5.4 Caspr2 regulates Erk phosphorylation

As Caspr2 did not appear to affect the expression of IP_3R1 at synapses, it was hypothesised that the Caspr2-IP_3R1 interaction might regulate IP_3R1 function. The LL3

domain is necessary for the Caspr2-IP_3R1 interaction (Figure 4.7). Other proteins that interact with this domain modulate IP_3R1 Ca^{2+} currents [58] and thus, it was thought that Caspr2 might also regulate IP_3R1 Ca^{2+} currents.

IP_3R1 channels are inward rectifying with respect to the cytoplasm. Thus, if Caspr2 does modulate IP_3R1 Ca^{2+} currents, then cytoplasmic Ca^{2+} levels should be different in the presence and absence of Caspr2. To examine this possibility, the amount of Erk phosphorylation in *Cntnap2*$^{-/-}$ and *Cntnap2*$^{+/+}$ cerebellum was therefore examined. The phosphorylation of Erk was used as a proxy for cytoplasmic Ca^{2+} levels as Erk phosphorylation increases as cytoplasmic Ca^{2+} levels rise. However, it should be noted that Erk phosphorylation is modulated by many different cellular processes and so is not a pure measure of Ca^{2+} concentrations. Cerebella from *Cntnap2*$^{-/-}$ and *Cntnap2*$^{+/+}$ mice were lysed and then analysed by Western blot. Reduced Erk phosphorylation was observed in *Cntnap2*$^{-/-}$ samples, relative to that found in *Cntnap2*$^{+/+}$ samples (Figure 5.5), suggesting that cytoplasmic Ca^{2+} levels are lower in the *Cntnap2*$^{-/-}$ cerebellum than in the cerebella of *Cntnap2*$^{+/+}$ mice. This is consistent with Caspr2 acting as an agonist of IP_3R1 channels. Whilst it is interesting that Caspr2 appears to both interact with a Ca^{2+}-selective ion channel and affect cytoplasmic Ca^{2+} levels in the cerebellum, further work was needed to definitively demonstrate that it modulates IP_3R1 Ca^{2+} currents. HEK293FT cells were used for these additional experiments as these systems are much higher throughput than animal models and multiple variations of a single experiment are often required to dissect a molecular mechanism. HEK293FT cells over-expressing Caspr2 and / or IP_3R1 were cultured for 48 hours and then lysed. Erk phosphorylation, assessed by Western blotting, was again used as a proxy for cytoplasmic Ca^{2+} levels.

Given that Caspr2 appeared to increase cytoplasmic Ca^{2+} levels in the murine cerebellum (Figure 5.5), it was expected that Caspr2 expression in HEK293FT would

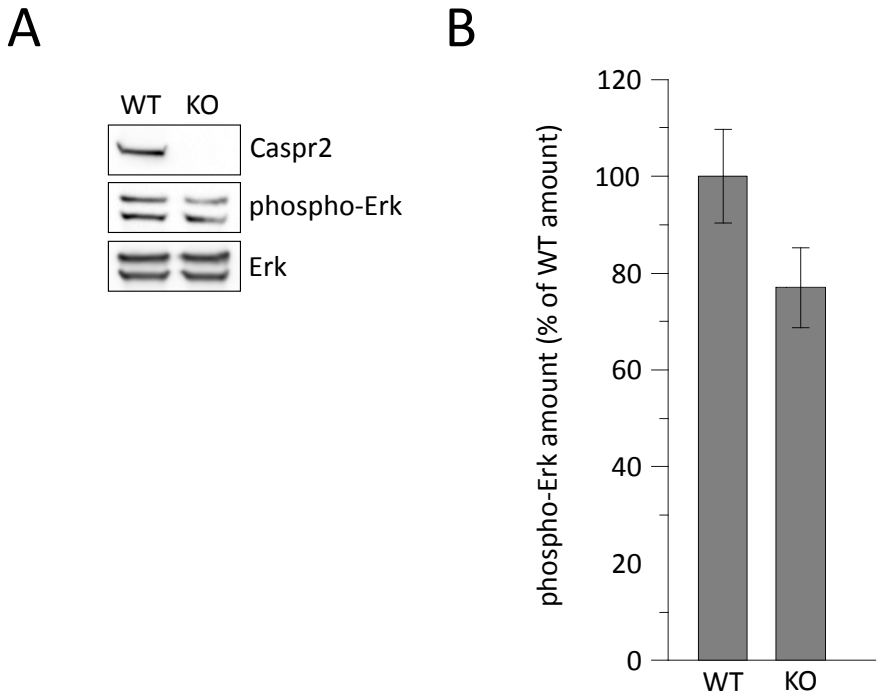


Figure 5.5: Erk phosphorylation is reduced in *Cntnap2*$^{-/-}$ mice. A) Western blot analysis of Erk phosphorylation levels in lysates prepared from *Cntnap2*$^{+/+}$ and *Cntnap2*$^{-/-}$ murine cerebella. **B)** Quantification of pooled data. N = 5 WT, 3 KO. WT, wild-type (*Cntnap2*$^{+/+}$) mice, KO, knockout (*Cntnap2*$^{-/-}$) mice.

cause a similar increase in HEK293FT cells. However, Caspr2 expression in HEK293FT cells had no noticeable effect on Erk phosphorylation (Figure 5.6), indicating that Caspr2 does not act as a simple agonist of IP_3R1 in these cells. Over-expressing IP_3R1 did result in a concomitant rise in Erk phosphorylation (Figure 5.6), suggesting that the assay is capable of detecting changes in cytoplasmic Ca^{2+} that occur as a result of changes to total IP_3R1 signalling.

Thus, the measured effects of Caspr2 on Erk phosporylation in the cerebellum and in HEK293FT cells seemed to be contradictory. However, IP_3R1 in Purkinje cells is known to behave differently from IP_3R1 found elsewhere, raising the possibility that this apparent contradiction occurred because the function of the Caspr2-IP_3R1 interaction varies depending on cellular context. If this is the case and Caspr2 does not act as an agonist of IP_3R1 in HEK293FT cells, it might either act as an antagonist

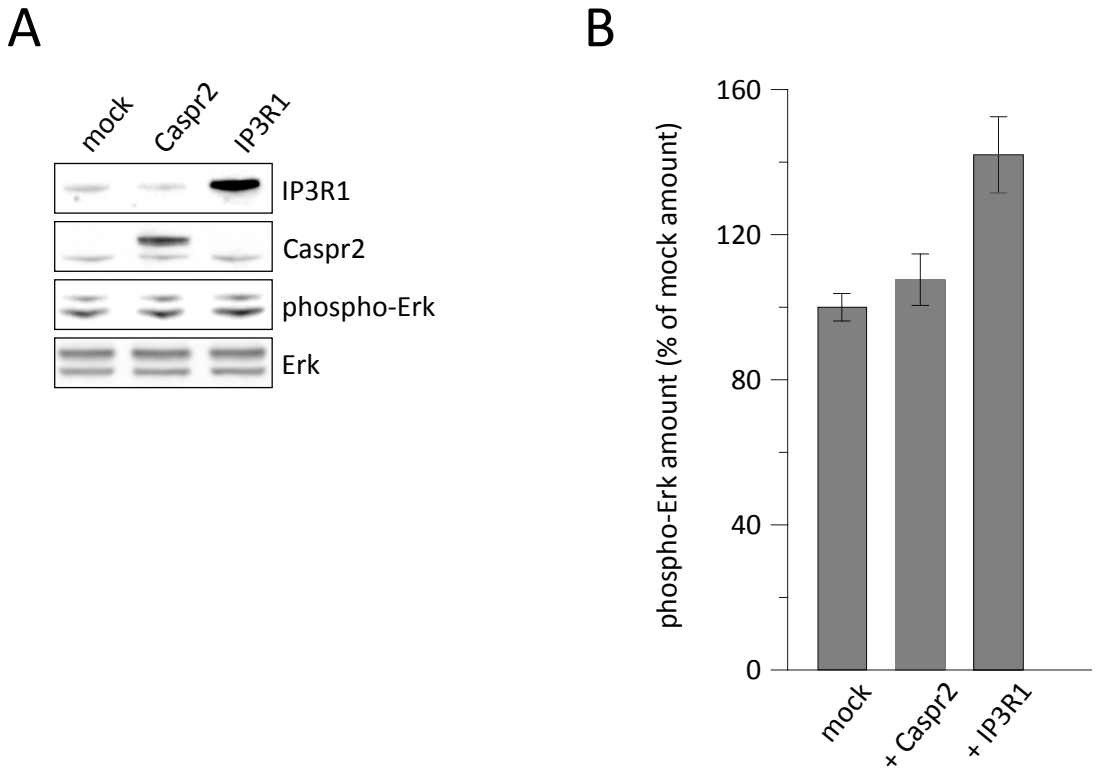


Figure 5.6: Erk phosphorylation is not affected by Caspr2 over-expression in HEK293FT cells. A) Lysates were prepared using HEK293FT cells that were over-expressing the indicated constructs. The level of Erk phosphorylation in these lysates was then assessed by Western blotting. **B)** Quantification of pooled data. N = 6 mock, 3 Caspr2 and 5 IP_3R1 transfections. mock = transfected with empty vector only, in place of Caspr2 and IP_3R1 expression constructs.

of IP_3R1 in HEK293FT cells or have no effect on IP_3R1. To examine this possibility, HEK293FT cells over-expressing Caspr2 and / or IP_3R1 were again cultured for 48 hours. However, instead of then being lysed immediately following culture, they were either dosed with the IP_3R1-agonist CCH or subjected to a vehicle (1XPBS) treatment. PErk levels in the treated cells were then measured as before.

The fold-change in PErk levels induced by CCH, in HEK293FT cells over-expressing IP_3R1, did not vary with Caspr2 expression (Figure 5.7B). Thus, Caspr2 does not act as an antagonist of IP_3R1 in HEK293FT cells. However, it was noticed that post-CCH treatment PErk levels appeared much higher in cells expressing either Caspr2 only, IP_3R1 only or Caspr2 and IP_3R1, than in mock transfected cells (Figure 5.7C). As

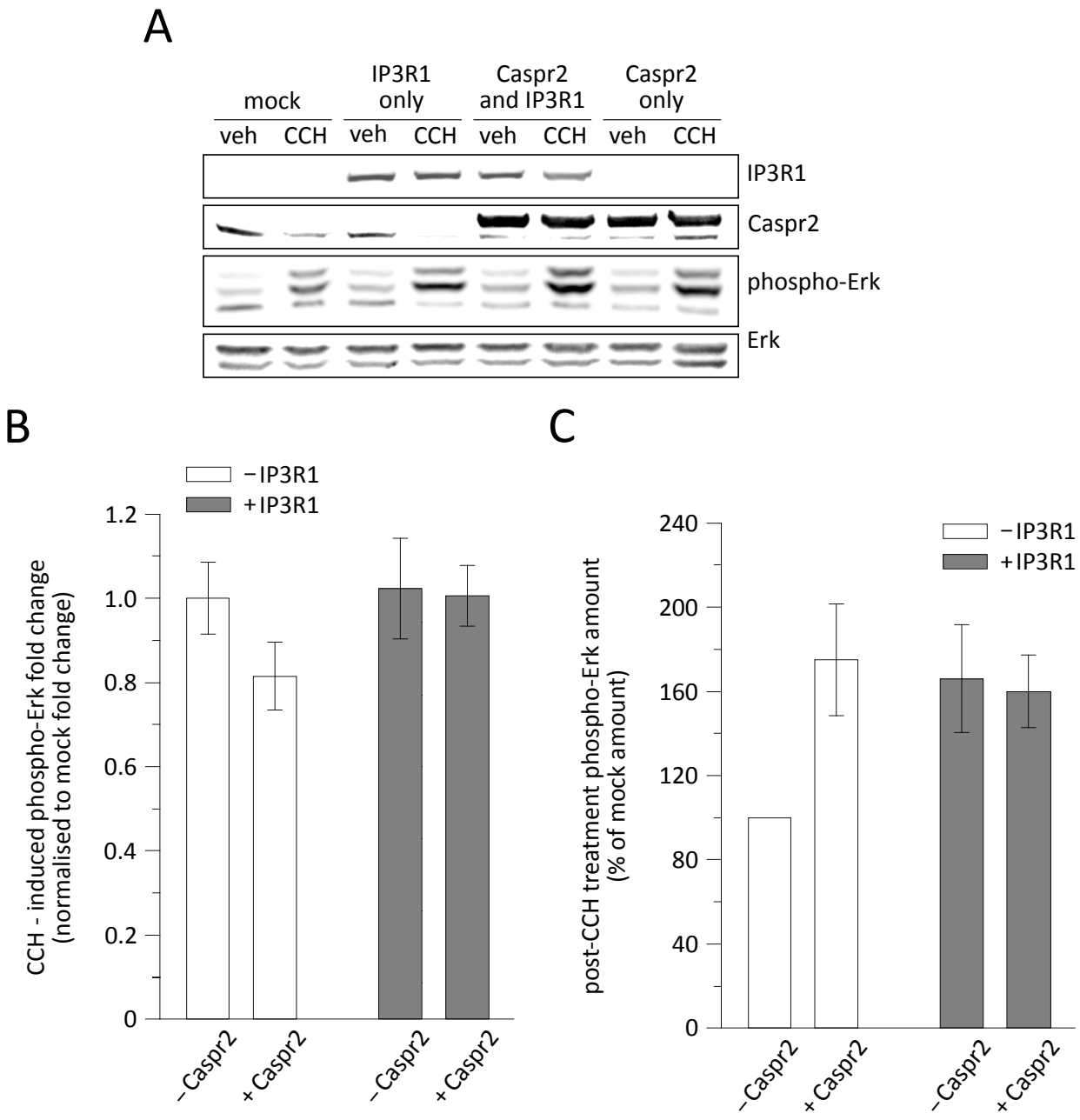


Figure 5.7: Caspr2 boosts post-IP_3R1 agonist treatment Erk phosphorylation, in HEK293FT cells. A) HEK293FT cells, which were over-expressing the indicated constructs, were either dosed with CCH or subjected to a vehicle treatment (1XPBS) and then lysed. The level of Erk phosphorylation in the resulting lysates was assessed by Western blotting. **B)** Quantification of pooled data: Caspr2 does not inhibit IP_3R1 Ca^{2+} currents in HEK293FT cells. N = 4 mock, 3 Caspr2 only, 3 IP_3R1 only and 3 Caspr2 + IP_3R1 transfections. Caspr2 does not affect the relative increase in phospo-Erk levels that occurs when cells over-expressing IP_3R1 are dosed with CCH. **C)** Quantification of pooled data: The presence of Caspr2 increases post-CCH treatment Erk phosphorylation levels, in HEK293FT cells. Over-expression of either Caspr2 or IP_3R1 increases post-CCH treatment PErk levels, relative to post-CCH treatment phospo-Erk levels in cells that were transfected with empty vector. N = 2 Caspr2 only, 2 IP_3R1 only and 2 Caspr2 + IP_3R1 transfections. Mock value is theoretical. mock = transfected with empty vector only, in place of Caspr2 and / or IP_3R1 expression constructs, veh, vehicle, CCH, Carbachol.

CCH is an IP_3R1 agonist, it is not surprising that the cells over-expressing IP_3R1 responded in this way. That cells over-expressing Caspr2 only also responded in this way was unexpected and suggests some synergy between Caspr2 and CCH.

Interestingly, the post-CCH treatment PErk level observed when Caspr2 and IP_3R1 were expressed together was equal to those observed when either Caspr2 or IP_3R1 were expressed alone (Figure 5.7C). If the mechanisms by which IP_3R1 and Caspr2 boost post-CCH Erk phosphorylation are entirely separate, expressing Caspr2 and IP_3R1 together should result in a response greater than that found after expressing either alone. As the responses are equal, it seems likely that the mechanisms underlying the IP_3R1- and Caspr2-mediated increases in post-CCH treatment cytoplasmic Ca^{2+} are interconnected.

Together, these results indicate that Caspr2 acts to increase Erk phosphorylation, consistent with Caspr2 acting to increase cytoplasmic Ca^{2+} levels. It is possible that the Caspr2-IP_3R1 interaction underlies this phenomenon, although the precise nature of how Caspr2 modulates Ca^{2+} levels may vary depending on the cellular context.

5.5 Discussion

Experiments presented in the previous chapter revealed that Caspr2 and IP_3R1 interact at synapses in the cerebellum. However, as it had not been previously documented, the functional consequences of the Caspr2-IP_3R1 interaction were not clear. The aim of the programme of work presented in this chapter was therefore to investigate what these functional consequences might be. Caspr2 was found to control cell morphology via IP_3R1, but was not seen to effect IP_3R1 localisation, suggesting Caspr2 does not solely act in a scaffolding capacity as previously described.

Caspr2 was also found to regulate Erk phosphorylation, a proxy for cytoplasmic Ca^{2+} levels, demonstrating that Caspr2 may well have a significant effect on cellular Ca^{2+} signalling. If so, this would be consistent with Caspr2 modulating IP_3R1 Ca^{2+} currents.

The Caspr2-IP_3R1 interaction and cellular morphology

Caspr2 and IP_3R1 likely interact at Purkinje cell-granule cells synapses, in the molecular layer. They have also now both been shown to regulate Purkinje cell dendritic morphology (Figure 3.7 and [59]). Given this, the influence of the Caspr2-IP_3R1 interaction on cellular morphology was assessed. Caspr2 was found to inhibit IP_3R1-induced extensions in HEK293FT cells, consistent with Caspr2-IP_3R1 communication affecting Purkinje cell dendritic morphology. Given that IP_3R1 is known to be vital for both Purkinje cell dendritic development[59] and for Purkinje cell - granule cell synapse formation[63], this therefore provides a potential molecular mechanism by which Caspr2 may affect Purkinje cell dendritic development in a synaptotrophic manner, as hypothesised in chapter 3.

Interestingly though, Caspr2 appears to have opposing effects in HEK293FT cells (Figure 5.1) and Purkinje cells (Figure 3.7). In HEK293FT cells, expressing Caspr2 reduces the number of IP_3R1- induced extensions observed, whereas dosing Purkinje cells with Caspr2 leads to an increase in the number of primary dendrites seen. This difference may be due to one of many reasons. The over-expression of IP_3R1 in HEKs (relative to the high, but endogenous expression of IP_3R1 in Purkinje cells), the reduced sensitivity of Purkinje cell IP_3R1 [51] and the presence of synaptic spines, that isolate Ca^{2+} signals [100] from the majority of the cytoplasm in Purkinje cells, could all increase the magnitude of any cytoplasmic Ca^{2+} increase downstream of Caspr2 in HEK293FT cells, relative to Purkinje cells. In addition, a full-length Caspr2

construct was used in the HEK293FT cell experiment, whereas only the ECD of Caspr2 was used in the cerebellar slices assay. This means the ICD of Caspr2 was present only in the HEK293FT cell experiment and as such, could have had a confounding functional effect. To exclude this possibility, the HEK293FT extensions experiment should be repeated, but with recombinant Caspr2 ECD used in place of over-expressing the full-length protein.

Another potentially fruitful line of enquiry would be the examination of Purkinje cell-granule cell synaptogenesis in *Cntnap2*$^{-/-}$ mice. The IP_3R1-Caspr2 interaction occurs during Purkinje cell-granule cell synaptogenesis (see Figures 4.1- 4.4 and [3]) and removing either *Cntnap2* [5] or *Itpr1*[59] causes synapse pathologies. Purkinje cell-granule cell synapses are specifically impaired in *ITPR1*$^{-/-}$ mice, and although there is no evidence yet that Caspr2 is necessary for the correct functioning of these synapses, data presented here suggests that it regulates Purkinje cell dendritic morphology (Figure 3.7). Thus, the dysfunction of the Caspr2-IP_3R1 interaction due to the loss of Caspr2 expression may impair granule cell-Purkinje cell synaptogenesis. As described in chapter 3, Synapsin immunostaining of sectioned cerebella taken from *Cntnap2*$^{+/+}$ and *Cntnap2*$^{-/-}$ mice would allow an assessment of this.

Caspr2 function at the molecular level: regulation of cytoplasmic Ca^{2+}

Seeking to understand the molecular basis for the effect of the Caspr2-IP_3R1 interaction on cellular morphology, the possibility that Caspr2 might scaffold IP_3R1 in the same manner that it scaffolds Shaker-type K^+ channels[112] was examined. However, data obtained using immunohistochemistry and biochemical fractionation approaches suggested that Caspr2 is not necessary to determine IP_3R1 localisation. The next step was then to assess whether Caspr2 might modulate IP_3R1 Ca^{2+} currents. Evidence from the literature suggested that proteins interacting with the IP_3R1

LL3 domain would inhibit the passage of Ca^{2+} ions through IP_3R1 [58]. The amount of Erk phosophorylation, a proxy measure of cytoplasmic Ca^{2+} levels, was assessed in *Cntnap2*$^{-/-}$ mice and in HEK293FT cells over-expressing Caspr2 and IP_3R1. In the HEK293FT system, measurements of Erk phosphorylation levels were taken both under basal conditions and after the activation of IP_3R1 receptors with CCH.

Basal Erk phosporylation appeared to be reduced in the *Cntnap2*$^{-/-}$ cerebellum, relative to the *Cntnap2*$^{+/+}$ cerebellum. In addition, when over-expressed in HEK293FT cells, Caspr2 appeared to boost post-CCH treatment Erk phosphorylation levels. These data therefore suggest that rather than inhibiting potential increases in cytoplasmic Ca^{2+} levels, Caspr2 may in fact act to increase cytoplasmic Ca^{2+} levels.

The fact that the effect of Caspr2 on Erk phosphorylation was detectable in untreated cerebella, but only detected in HEK293FT cells post-CCH treatment, suggests that Caspr2 function may be influenced by cellular context. However, this discrepancy may also be due to a difference in the average magnitude of Ca^{2+} signalling in the two systems. For example, HEK293FT cells do not facilitate synaptic transmission and so, on average, there might be less Ca^{2+} signalling in these cells than in the cells of the cerebellum. The magnitude of Erk phosphorylation in organotypic cerebellar slices treated with CCH could be measured to determine if this is the case. It should also be noted that although Caspr2 appeared to act to increase cytoplasmic Ca^{2+} levels, these changes may in fact have been the result of compensatory mechanisms and Caspr2 may actually act to reduce cytoplasmic Ca^{2+} levels. To address this, the HEK293FT cell cytoplasmic Ca^{2+} levels experiment (Figures 5.6 and 5.7) could be repeated, but with a sarcoplasmic/endoplasmic reticulum Ca^{2+}-ATPase pump inhibitor such as Thapsigargin added first to prevent re-filling of the ER. Recombinant Caspr2 ECD could also be added for various intervals in place of over-expressing full-length Caspr2.

Despite the exact effect of Caspr2 on Ca^{2+} currents not being clear, the regulation of Ca^{2+} levels represents a novel role for this protein, as it was previously only known to regulate K^+ signalling[112] (see General discussion for further consideration of this).

The Caspr2-IP_3R1 interaction and cytoplasmic Ca^{2+} levels

The identity of the key domains that mediate Caspr2-IP_3R1 communication are consistent with Caspr2 regulating IP_3R1 Ca^{2+} currents[58]. In addition, the expression of Caspr2 causes changes in Erk phosphorylation levels, which is also consistent with Caspr2 regulating IP_3R1 Ca^{2+} currents. Interestingly, aberrant IP_3R1 Ca^{2+} currents may be common in ASD, having been found in induced pluripotent stem cells derived from individuals with both monogenic and sporadic forms of the condition[126; 127]. Thus, it is likely that IP_3R1 currents are also abnormal in CDFE, further supporting the idea that Caspr2 normally modulates IP_3R1 currents. However, additional experimental work is needed to isolate the specific effect of Caspr2 on IP_3R1 Ca^{2+} currents.

Ca^{2+} imaging of a bilayer system with Caspr2 and IP_3R1 reconstituted into it would provide a definitive test of whether Caspr2 does or does not modulate IP_3R1 currents. It is possible that the Caspr2-mediated changes in Erk phosphorylation observed could result from the scaffolding of other, as yet unidentified Ca^{2+} channels. But, if these changes are indeed due to the modulation of IP_3R1 by Caspr2, this will be the first time Caspr2 has been found to have a non-scaffolding role.

Any such regulation of Purkinje cell IP_3R1 currents by Caspr2 would be expected to have a significant impact on cellular function. The Purkinje cells of *Itpr* mutant mice appear to lack Ca^{2+} spikes altogether[33], suggesting IP_3R1 may be solely responsible for carrying this current. With no redundancy, any disruption of Purkinje

IP_3R1 currents due to dysfunctional Caspr2 would be fully penetrant, hampering Ca^{2+} signalling pathways crucial for a plethora of cellular processes.

Conclusions

In summary, the novel Caspr2-IPR31 interaction first described in the previous chapter appears to regulate cellular morphology. This is consistent with the effect of Caspr2 on Purkinje cell dendritic morphology noted in chapter 3. Interestingly, Caspr2 does not appear to scaffold IP_3R1 in the same way as it scaffolds other proteins [112]. Hence, these data lead us to suggest that Caspr2 must regulate IP_3R1 via a novel molecular mechanism. The direct regulation of IP_3R1 Ca^{2+} conductance by Caspr2 would be consistent with reports of other IP_3R1 LL3 domain interactors[58] and indeed Caspr2 does affect Erk phosphorylation, a proxy for cytoplasmic Ca^{2+} levels. However, further work is required to assess whether Caspr2 controls cytoplasmic Ca^{2+} levels by regulating IP_3R1.

6 General discussion

Under-researched for a long period, recent findings suggesting that the cerebellum has a role in higher order brain functions have rekindled interest in this brain region[142]. However, there is still much to learn about how the cerebellum develops and operates, on the cellular and molecular levels. The dysfunction of the protein Caspr2 causes cerebellar-specific behavioural phenotypes[15; 77], suggesting it has an important role in the cerebellum. Despite this evidence, the cellular and molecular bases for this role remained unclear. The overarching aim of this thesis was therefore to describe the cellular and molecular roles of Caspr2 in the cerebellum. In particular, because of the developmental CDFE phenotype that arises due to the homozygous deletion of *CNTNAP2*[140], efforts were focused on describing the function of Caspr2 in the developing cerebellum.

To begin to address this, the expression pattern of Caspr2 in the developing cerebellum was examined first of all and Caspr2 was found to localise to Purkinje cell synapses in the molecular layer.

Guided by this information, and other available data, further work focused on the function of the ECD of Caspr2, the Caspr2 domain exposed to the synaptic cleft. This domain was shown to be sufficient to affect Purkinje cell dendritic development. Although it has been previously reported that the dendrites of other neuron types are affected by Caspr2, this effect has not been observed in cerebellar Purkinje cells until

now. In addition, that the ECD of Caspr2, as opposed to full length Caspr2, is sufficient to control dendrite morphology, is also a novel finding.

Proteins that interact with the ECD of Caspr2, when Caspr2 is expressed in non-myelinated neurons, were described for the first time. IP_3R1 was found to be a cognate binding partner of Caspr2 in the synaptic cleft, at granule cell-Purkinje cell synapses in the developing cerebellum, suggesting Caspr2 scaffolds ion channels at synapses as well as at the JXP. Functional assays revealed that the Caspr2-IP_3R1 interaction controls cellular morphology, consistent with Caspr2 regulating Purkinje cell dendritic development via IP_3R1. This, then, represents the first molecular explanation of how Caspr2 might affect dendritic outgrowth generally.

As IP_3R1 is a Ca^{2+}-specific ion channel, one hypothesis was that, as a result of interacting with IP_3R1, Caspr2 might modulate cellular Ca^{2+} signalling. Caspr2 was shown to regulate Erk phosphorylation (a proxy for cytoplasmic Ca^{2+} levels, demonstrating that Caspr2 is likely involved in the regulation of multiple ion species and not just K^+. Interestingly, Caspr2 did not appear to scaffold IP_3R1, suggesting that Caspr2 may act as an allosteric modulator (or similar) of IP_3R1. If this is the case, then this would represent the first description of a non-scaffolding role for the Caspr2 protein.

Together, these results provide the first insights into the cellular and molecular functions of Caspr2 in the developing cerebellum. These data improve our understanding of cerebellar development, but they also provide a potential explanation of how Caspr2 dysfunction leads to the cerebellar-associated phenotypes we observe in the clinic.

6.1 The Caspr2-IP_3R1 interaction

Caspr2 assembles a signalling complex capable of driving morphology change

As well as the Shaker-type K^+ channels mentioned above, the ICD of Caspr2 also interacts with numerous other proteins, including the kinase Protein kinase C (PKC)[16]. PKC phosphorylates a multitude of downstream targets and has thus been implicated in a diverse array of cellular processes ranging from muscle contraction to cell migration[164]. Of note, PKC is also known to affect Purkinje cell dendritic development. Aberrant activation of PKC impairs dendritic outgrowth and reduces the size of the dendritic arbour[94]. Thus, by interacting both with IP_3R1 and PKC, Caspr2 may bring multiple regulators of Purkinje cell dendritic morphology in to close proximity with each other.

Although PKC is a kinase, it also acts as a scaffolding protein and interacts with Phospholipase C (PLC)-γ1, via a single, additional scaffolding protein[83]. PLC-γ1 is one of the isotypes of the PLC family of proteins. Each of the different isotypes of PLC are activated as part of separate signalling pathways, but they all catalyse the hydrolysis of Phosphatidylinositol 4,5-bisphosphate (PIP_2) once activated. This hydrolytic cleavage of PIP_2 generates IP_3, the endogenous agonist of the IP_3R1 channel, and diacylglycerol. Thus, IP_3R1 can be activated in response to a variety of cellular events, with the PLC family of proteins effectively encoding environmental information as IP_3R1 Ca^{2+} currents.

Interestingly, the combination of the diacylglycerol produced by the PLC-mediated hydrolysis of PIP_2, and the increase in cytoplasmic Ca^{2+} that results from IP_3R1 activation, effectuates the activation of PKC. So, by interacting with IP_3R1 and PKC (which in turn binds to PLC) Caspr2 acts to assemble a signalling complex capable of rapidly translating the activation of PLC into both PKC activation and cytoplas-

mic Ca^{2+} waves.

One of the PLC isotypes expressed in Purkinje cells is PLC-γ. PLC proteins of this isotype are activated by members of the Receptor tyrosine kinase (RTK) family[158], a group of receptors known to control cell survival, proliferation and morphology. The RTK Tropomyosin receptor kinase C acts specifically at granule cell-Purkinje cell synapses[72] to increase Purkinje cell dendrite growth and branching, by stimulating PLC-γ1[79]. The fact that Caspr2 may also act at these synapses to regulate Purkinje cell dendritic morphology raises the interesting hypothesis that RTKs and Caspr2 might be involved in some of the same signalling pathways.

Thus, taking all of the above together, it is possible that an RTK-PLC-IP_3R1-PKC signalling complex, assembled by Caspr2 at granule cell-Purkinje cell synapses, contributes to RTK-induced Purkinje cell dendritic growth. Consequently, it may be that the *Cntnap2*$^{-/-}$ Purkinje cell dendritic development phenotype observed (see Chapter 3) arises because Caspr2 is necessary for the propagation of information downstream of RTKs.

To test this, immunoprecipitation experiments could be performed to assess whether these proteins interact as a complex. If so, then to follow up organotypic cerebellar slices could be prepared from *Cntnap2*$^{-/-}$ and *Cntnap2*$^{+/+}$ mice and then dosed with Neurotrophin-3, the endogenous agonist of Tropomyosin receptor kinase C[79]. If a RTK-PLC-IP_3R1-PKC is relevant to Purkinje cell dendritic morphology, then the increase in Purkinje cell dendritic arbourisation that should occur in slices taken from *Cntnap2*$^{+/+}$ mice might be impaired or absent in slices taken from *Cntnap2*$^{-/-}$ mice.

It should also be mentioned that as well as binding to the ICD of Caspr2, PKC phosphorylates Thr1292[16], which is located close to the Caspr2 C-terminus. The consequences of this phosphorylation are not yet understood, but it could possibly affect the binding of K^+ channels to the nearby PDZ-binding domain (residues 1317-

1331). In fact, it may well be that the stimulation of the signalling complex described above leads to the phosphorylation of Thr1292 by activated PKC and that this inhibits the interaction between Caspr2 and $K_v1.1$ and $K_v1.2$. Effectors of dendritic growth downstream of PKC would also be activated. Such a mechanism would simultaneously propagate signals promoting dendritic growth and impair mechanisms that prevent it. This hypothesis could be investigated by repeating the co-IP experiments in Chapter 4 where cerebellar tissue was used as a bait pool and additionally treating lysates with the PKC agonist phorbol 12-myristate 13-acetate. If the phosphorylation of Thr1292 does inhibit Caspr2-K^+ channel interactions, then much less $K_v1.1$ and $K_v1.1$ should be co-immunoprecipitated when Caspr2 is immunoprecipitated from lysates treated with phorbol 12-myristate 13-acetate.

Does Caspr2 integrate multiple ion signalling pathways?

The fact that Caspr2 was found to communicate with different ion channels that have different ion specificities is intriguing. Even more interesting, these two Caspr2-ion channel interactions involve different Caspr2 domains. The intracellular domain of Caspr2 interacts indirectly with Shaker-type K^+ channels[110], whilst data presented in Chapter 4 of this thesis suggests that the extracellular domain of Caspr2 is both necessary and sufficient for Caspr2-IP_3R1 communication.

This raises the possibility that Caspr2 may facilitate the integration of K^+ and Ca^{2+} signalling by binding both Shaker-type K^+ channels and IP_3R1 simultaneously and thus bringing them in to close proximity. Consistent with this hypothesis, $K_v1.1$ was co-immunoprecipitated alongside IP_3R1, when Caspr2 was immunoprecipitated from cerebellar synaptosomes. This does not preclude the possibility that Caspr2 interacts with $K_v1.1$ and IP_3R1 separately at synapses in the cerebellum, but it does demonstrate that the two interactions are not mutually exclusive.

The Contactin-2 protein expressed by oligodendrocytes is necessary for the clustering of Shaker-type K^+ channels by Caspr2[123]. However, oligodendrocyte Contactin-2 cannot be present at synapses as these structures are not myelinated. Contactin-2 is also down-regulated in granule cells before granule cell-Purkinje cell synaptogenesis[139]. Therefore, if Caspr2 does localise both $K_v1.1$ and IP_3R1 together at synapses, then oligodendrocyte Contactin-2 must be dispensable for this particular process. If true, this would mean that the composition of the protein complex required for the localisation of K^+ channels by Caspr2 varies by sub-cellular location. It may even be that, in the context of the Caspr2-$K_v1.1$ interaction, Contactin-2 is effectively replaced by IP_3R1 at Purkinje cell-granule cell synapses.

Shaker-type K^+ channels are outward rectifying and voltage-dependent. As such, they act to repolarise cell membrane potentials and dampen neuronal activity. IP_3R1 channels, on the other hand, are activated downstream of the glutamate receptor mGluR1 and propagate signals from incoming action potentials by releasing Ca^{2+} into the cytoplasm. Interestingly, increases in intracellular calcium reduce the inactivation rate of $K_v1.1$[73]. Thus, if $K_v1.1$ were localised close to IP_3R1 by mutual association with Caspr2, the activation of IP_3R1 in response to an incoming action potential would lead to an increase in the number of active $K_v1.1$ channels. It is therefore possible that by interacting with both IP_3R1 and $K_v1.1$, Caspr2 effectively scaffolds a dynamic, negative feedback loop that regulates the propagation of action potentials through the cerebella circuitry. Activation of machinery that propagates information from incoming action potentials (IP_3R1) would be balanced by reduced inactivation of an ion channel that inhibits the flow of this information ($K_v1.1$).

Patch-clamp electrophyiosology could be used to test this hypothesis. IP_3R1, Caspr2 and $K_v1.1$ could all be over-expressed in *Xenopus laevis* eggs and a photolabile, membrane permeable IP_3 analog added. After patching the extracellular membrane, the

caged IP_3 could be activated whilst K^+ currents are recorded. If Caspr2 does scaffold a feedback loop as suggested, then change in the magnitude of post-IP_3 activation K^+ currents should be greater in the presence of Caspr2.

The structural basis of the Caspr2-IP_3R1 interaction

The IP_3R1 LL3 domain mediates the interaction between Caspr2 and IP_3R1. The IP_3R1 LL3 domain is part of the pore-forming region and, consistent with Caspr2 affecting the IP_3R1 pore, Caspr2 appears to increase cytoplasmic Ca^{2+} levels (see Chapter 5). ERP44 also interacts with IP_3R1 by binding to the IP_3R1 LL3 domain. This binding inhibits IP_3R1 Ca^{2+} currents by reducing the open time of the channel[58]. Thus, if Caspr2 does modulate IP_3R1 Ca^{2+} currents specifically, it appears to have an opposite effect to ERP44 despite interacting with the same IP_3R1 domain.

To understand why two proteins could effect such different outcomes, despite binding to the same IP_3R1 domain, the atomistic structures of both the IP_3R1-ERP44 complex and the IP_3R1-caspr2 complex should be determined. Small variations, in the pore environment can have dramatic consequences for conductance. For example, the presence of one or two extra hydrophobic residues can de-wet the pore region. This prevents the solubilisation of ions as they travel through the pore and so completely inhibits conductance[8]. *Vice versa*, exchange of a hydrophobic residue for a hydrophilic one can facilitate pore wetting and increase conductance. As these changes are on the Angstrom scale, only atomistic descriptions can provide the resolution necessary to explain why Caspr2 and ERP44 can both interact with the IP_3R1 ion pore and yet affect IP_3R1 Ca^{2+} currents in opposing ways.

The structure of IP_3R1 has recently been solved by cryo-electron microscopy[43]. Most of the residues present in the IP_3R1 protein were modelled in this structure,

including all of those that compose the pore region. Thus, it may well be worthwhile to use the protocol employed in this study as a starting point to solve the structures of IP_3R1 in complex with Caspr2 and with ERP44. Failing this, co-crystallisation of key domains that mediate these interactions could be attempted. As the IP_3R1 LL3 domain, the Caspr2 ECD and ERP44 are all soluble, purification and crystallisation of these proteins should be relatively straightforward. Indeed, apo-state Caspr2 ECD crystals have already been produced during this study (data not shown).

The Caspr2-IP_3R1 interaction and cerebellar disease

The dysfunction of Caspr2 results in at least two distinct conditions, Caspr2 autoantibody-associated ataxia and CDFE. Could the Caspr2-IP_3R1 interaction be relevant to either of these diseases?

Interestingly, Spinocerebellar ataxia 15 (SCA15) is caused by mutations in IP_3R1[84] and the phenotype displayed by individuals with this condition is very similar to that displayed by Caspr2 autoantibody-associated ataxia patients. Given that data presented here suggests that Caspr2 affects IP_3R1 function in the wild-type condition, this phenocopy suggests that IP_3R1 dysfunction, induced by aberrant Caspr2 function, may underlie Caspr2 autoantibody-associated ataxia.

Patients with several different autism syndromes have also been found to have an IP_3R signalling defect. The length of time IP_3Rs open for is reduced in induced pluripotent stem cells derived from these individuals[126], leading to decreased Ca^{2+} release in response to other signalling cues. In a clinical screen, this same IP_3R dysfunction was then also detected in induced pluripotent stem cells derived from a heterogeneous group of patients with sporadic ASD[127], suggesting this deficit is common to many autism patients. Again, this phenocopy suggests that impaired IP_3R1 function may be common to both CDFE pathology and the pathologies of

other forms of ASD. However, although IP_3R1 dysfunction in CDFE could potentially represent the very first step in the pathological cascade underlying CDFE, it is quite possible that the IP_3R1 signalling deficits found in the clinical screen of ASD patients could be occurring far downstream of the actual aetiologies in these cases. To determine if this is the case, SCA15 patients could be tested to see if they meet the diagnostic criteria for ASD. Although, as all IP_3R1 moieties in SCA15 are dysfunctional and potentially only those at the cell surface are perturbed in the absence of Caspr2, the results of such a comparison should be treated with caution.

6.2 A clue from the clinic: the multiple, distinct phenotypes caused by Caspr2 dysfunction

Diseases have long been defined by shared phenotypes presented at the clinic. In the past, the assumption of a common, underlying molecular aetiology has helped to guide research at the bench. However, there are now several high profile examples of how similar phenotypes can in fact be caused by molecular events more disparate than imagined. Breast cancer, for example, was initially assumed to be one disease, but it has since been re-categorised as a collection of different conditions that have different molecular aetiologies[134]. Less well known are the cases where the dysfunction of one gene or protein leads to multiple, distinct conditions. Conditions in which the *CNTNAP2* gene is dysfunctional fall into the latter category. Homozygous deletion of *CNTNAP2* causes CDFE, a syndromic form of autism[141], whilst ataxia is associated with auto-antibodies that target Caspr2[15]. In these cases, understanding how each of the different phenotypes arises is vital to ensure not just

that treatments can be found for each condition, but also to avoid a treatment for one condition exacerbating or even inducing another. On one hand, this makes developing treatments more challenging, but on the other, the multiple clinical outcomes observed can together provide an important clue to guide bench research.

The auto-antibodies found in the sera of patients with cerebellar ataxia that target Caspr2 recognise an epitope in the extracellular domain of Caspr2. Thus, it is likely that the ataxic phenotype with which they present results from the impairment of the function of Caspr2 ECD. CDFE patients, however, do not express Caspr2. The CDFE phenotype may therefore result from the dysfunction of any or all of the different Caspr2 domains. Could it be then that the differences in phenotypes between Caspr2 autoantibody-associated ataxia and CDFE are a consequence of the different Caspr2 domains involved in the aetiologies of the two conditions? There are more dysfunctional Caspr2 domains in CDFE than in Caspr2 autoantibody-associated ataxia and the endophenotypes observed in CDFE patients are indeed much more severe than those observed in Caspr2 autoantibody-associated ataxia patients. Thus, the detrimental effects of the dysfunction of different Caspr2 domains appears to be cumulative, which is consistent with the idea that the identity of the domains involved in the aetiology of the two conditions determines the resulting phenotype.

As described above, the ECD of Caspr2 interacts with the Ca^{2+} channel IP_3R1, whilst the Caspr2 ICD scaffolds the K^+ channels $K_v1.1$ and $K_v1.2$. Thus, functional Caspr2 interactions with both K^+ and Ca^{2+} channels are lost in CDFE, whereas it may be that the Caspr2-IP_3R1 interaction is lost in Caspr2 autoantibody-associated ataxia, whilst functional Caspr2-Shaker-type channels interactions are retained. The function of IP_3R1 at the cell surface is not yet known, but it is known that there are very few IP_3R1 moieties present at this location[90]. This suggests that disruption of IP_3R1 at the cell membrane would not directly reduce the amplitude of the cumulative

IP_3R1 Ca^{2+} currents that are vital for synaptic function. The function of the $K_v1.1$ / $K_v1.2$ population that interacts with Caspr2, on the other hand, is known. These channels repolarise the cell membrane and help to maintain the resting potential. Caspr2-IP_3R1 communication also only occurs at Purkinje cell-granule cell synapses, whereas Caspr2-K^+ channel interactions occur in the white matter throughout the nervous system. Thus, the loss of Caspr2-K^+ channel interactions may well have a more detrimental impact than the loss of Caspr2-IP_3R1 interactions. The Caspr2 ECD domain, and thus Caspr2-IP_3R1 interactions, are dysfunctional in both CDFE and Caspr2 autoantibody-associated ataxia. However, the Caspr2 ICD domain, and thus Caspr2-K^+ channel interactions, are likely dysfunctional in the more severe CDFE, but not in Caspr2 autoantibody-associated ataxia. Thus, the differences in the interactomes of the ICD and ECD of Caspr2 could explain why the dysfunction of different combinations of Caspr2 domains results in distinct phenotypes.

Another potential factor that could influence the development of differing endophenotypes after *Cntnap2* dysfunction, is the age of onset of said dysfunction. Caspr2 autoantibody-associated ataxia patients present much later in life than those with CDFE, and so it may be that Caspr2 has differing roles in the developing and adult nervous systems and that this explains the difference between the ataxia and CDFE phenotypes. Interestingly, exposing mice to Caspr2 auto-antibodies *in utero* leads to autistic-like symptoms in later life[32], suggesting that the timing of Caspr2 dysfunction does indeed influence the endophenotypes that develop as a result. As the auto-antibodies used in this study[32] target the ECD of Caspr2, this result also suggests that either the particular Caspr2 domain thought to be dysfunctional does not influence the resulting phenotype to a great extent, or that the auto-antibodies also affect the function of the ICD of Caspr2. The latter may well be the case, as a direct interaction between Contactin-2 and the Caspr2 ECD is necessary for Caspr2

ICD-$K_v1.1$ / $K_v1.2$ communication[148].

Either way, if the age of onset of Caspr2 dysfunction affects the resulting phenotype, then it is possible that the initial stages of the pathological cascades underlying CDFE and Caspr2 autoantibody-associated ataxia are identical, with the downstream consequences of this shared pathology differing depending on developmental stage. Given that IP_3R1 has been associated both with ataxia[84] and autism[126; 127], it may therefore be that that impaired Caspr2-IP_3R1 communication is common to both CDFE and Caspr2 autoantibody-associated ataxia.

6.3 Caspr2 in the PNS: developmental diaschisis and ASD

The idea that aberrant IP_3R1 function in the cerebellum, induced by Caspr2 dysfunction, is linked to ASD is consistent with other reports of IP_3R1 signalling deficits in individuals with ASD. However, it should be noted that the dysfunction of Caspr2 likely disrupts multiple interactions and not just the communication between Caspr2 and IP_3R1.

A compelling explanation for why cerebellar dysfunction leads to autism is that when the cerebellum fails to integrate sensory information and fine tune other responses correctly, secondary brain areas are denied the data necessary for proper experience-dependant entraining. This theory has been termed developmental diaschisis[162]. If this theory is correct, ASD should occur regardless of where the block of information is located. For example, both human infants that experienced severe social deprivation in Romanian orphanages[120] and infant monkeys raised with surrogate mothers[101] later developed ASD or an ASD-like phenotype. In these cases, there

was likely no impairment inherent to the cerebellum. Instead, because these infants were left isolated for so long, the information necessary for correct entraining was not available in their environment. The information block here was external. ASD also arises in other cases, where the cerebellum is dysfunctional and thus the information block can be considered internal. Cerebellar injury around birth increases the likelihood of an individual developing ASD in later by around 30-fold[87].
The dysfunction of Caspr2 in the PNS is known to disrupt sensory information flow to the CNS[34] and so, as CDFE individuals do not express Caspr2 globally, this could also contribute to the pathogenesis of this condition. As there is no IP_3R1 in the PNS, aberrant Caspr2 function here must impair communication between Caspr2 and Caspr2 binding partners other than IP_3R1. It is possible, then, that the effects of multiple disrupted interactions converge to prevent sensory information from being passed to secondary cortical regions. This would be interesting, because although it is accepted that the burden of ASD-associated mutations sums in cases where ASD results from a collection of $<$100% penetrant mutations, fully penetrant mutations are generally assumed to induce a single molecular pathology only.

6.4 A potential distinct function for the second, smaller Caspr2 isoform

In Chapters 3 and 5 (Figures 3.1 and 5.3), the examination of cerebellar sections taken from *Cntnap2*$^{+/+}$ and *Cntnap2*$^{-/-}$ animals and co-immunostained using antibodies directed against Caspr2 and IP_3R1 is described.
When the *Cntnap2*$^{-/-}$ mouse line was first generated it was assumed that these mice

would not express any Caspr2 protein[112]. As such, it was expected that no Caspr2 signal would be detected in tissue taken from *Cntnap2*$^{-/-}$ mice. Unexpectedly however, the white matter of the *Cntnap2*$^{-/-}$ cerebellum was found to be positive for Caspr2 (Figures 3.1 and 5.3). This suggests that a protein, with the epitope recognised by the ∝Caspr2 antibody used for immunostaining, exists in the cerebellum of *Cntnap2*$^{-/-}$ mice.

The mutation used to inhibit the expression of Caspr2 in the *Cntnap2*$^{-/-}$ mouse model is an insertion of the *neomycin* gene into the first exon of the *Cntnap2* gene[112]. This means that any potential alternative start sites downstream of this first exon would be unaffected by the mutation. Recently, evidence that such an alternative start site exists in the *Cntnap2* gene has been reported. In 2015, a smaller isoform of the Caspr2 protein was described[29]. This smaller isoform is an N-terminal truncation, missing the first 1224 amino acids of the extracellular domain of the full length protein. This was followed in 2017 by a report of a second, shorter *Cntnap2* transcript produced using an alternative transcription start site located 3′ of the first (long-isoform) *Cntnap2* exon[171]. This transcript encodes the shorter Caspr2 isoform that was first described in 2015.

Thus, the mutation carried by the *Cntnap2*$^{-/-}$ mouse model does not in fact prevent the expression of all isoforms of Caspr2 - the second, smaller isoform is still expressed[29]. Further, the transmembrane and intracellular domains of this smaller isoform are equivalent to the transmembrane and intracellular domains of the larger isoform. As the ICD of Caspr2 contains the epitope recognised by the ∝ Caspr2 antibodies used in this thesis, it may be that the cerebellar white matter of the *Cntnap2*$^{-/-}$ mouse appears to be Caspr2 positive because of the presence of the second, smaller isoform of Caspr2.

If so, then the spatial distribution of the two isoforms appears to be segregated, with

the longer isoform expressed in cerebellar white matter and in the deep molecular layer and the shorter isoform confined solely to the white matter. This is interesting as the smaller isoform includes the intracellular domains necessary for Caspr2-K^+ channel interactions, but not the full JXM domain necessary for Caspr2 interactions with IP_3R1. Caspr2 is already known to scaffold K^+ channels at the JXP of myelinated axons and data presented in Chapter 4 suggest that Caspr2 and IP_3R1 do not interact in the white matter of the cerebellum. Thus, it may be that the shorter isoform of Caspr2 is specialised to interact with $K_v1.1$ and $K_v1.2$ and not with IP_3R1. This may be because IP_3R1 does not localise to the JXP or because Caspr2-IP_3R1 interactions at the JXP would be detrimental. If the latter, it is possible that expression of the shorter isoform of Caspr2 prevents the excessive accumulation of IP_3R1 at Purkinje axon JXPs that would occur if the long isoform was expressed alone, whilst still facilitating the correct clustering of K^+ channels at this location.

6.5 Conclusions

In summary, the data presented in this thesis reveals that Caspr2 interacts with IP_3R1, at Purkinje cell synapses in the molecular layer of the developing cerebellum, to regulate the development of Purkinje cell dendrites. The molecular mechanism underlying the effect of Caspr2-IP_3R1 communication on cellular morphology may well involve the modulation of IP_3R1 Ca^{2+} currents by Caspr2.

Together, these experiments therefore reveal the cellular and molecular functions of the synaptic domain of Caspr2 in the developing cerebellum, providing information about the role of Caspr2 in cerebellar development. As such, this work contributes to the body of knowledge that details how the cerebellum develops and operates and as a result, also contributes to our broader understanding of CNS function. These data

may also help explain how Caspr2 dysfunction leads to the cerebellum-associated phenotypes seen in patients with ASD and ataxia, thus providing a platform for future studies to examine potential treatments for these disorders.

7 References

[1] Allen G, Courchesne E. Differential effects of developmental cerebellar abnormality on cognitive and motor functions in the cerebellum: an fMRI study of autism. *The American Journal of Psychiatry*, 160(2):262–273, 2003

[2] Allin M, Matsumoto H, Santhouse AM, Nosarti C, AlAsady MH, Stewart AL, Rifkin L, Murray RM. Cognitive and motor function and the size of the cerebellum in adolescents born very pre-term. *Brain*, 124(Pt 1):60–66, 2001

[3] Altman J. Postnatal development of the cerebellar cortex in the rat. II. Phases in the maturation of Purkinje cells and of the molecular layer. *The Journal of Comparative Neurology*, 145(4):399–463, 1972

[4] American Psychiatric Association. *Diagnostic and statistical manual of mental disorders 5th ed*. American Psychiatric Association, 2013

[5] Anderson GR, Galfin T, Xu W, Aoto J, Malenka RC, Südhof TC. Candidate autism gene screen identifies critical role for cell-adhesion molecule CASPR2 in dendritic arborization and spine development. *Proceedings of the National Academy of Sciences of the United States of America*, 109(44):18120, 2012

[6] Ango F, di Cristo G, Higashiyama H, Bennett V, Wu P, Huang ZJ. Ankyrin-based subcellular gradient of neurofascin, an immunoglobulin family protein, directs GABAergic innervation at purkinje axon initial segment. *Cell*, 119(2):257–272, 2004

[7] Aricescu AR, Lu W, Jones EY. A time- and cost-efficient system for high-level protein production in mammalian cells. *Acta Crystallographica, Section D, Biological Crystallography*, 62(Pt 10):1243–50, 2006

[8] Aryal P, Sansom MSP, Tucker SJ. Hydrophobic gating in ion channels. *Journal of Molecular Biology*, 427(1):121–130, 2014

[9] Atlas D. Functional and physical coupling of voltage-sensitive calcium channels with exocytotic proteins: ramifications for the secretion mechanism. *Journal of Neurochemistry*, 77(4):972–985, 2001

[10] Bailey A, Phillips W, Rutter M. Autism: towards an integration of clinical, genetic, neuropsychological, and neurobiological perspectives. *Journal of Child Psychology and Psychiatry*, 37(1):89–126, 1996

[11] Bakkaloglu B, O'Roak BJ, Louvi A, Gupta AR, Abelson JF, Morgan TM, Chawarska K, Klin A, Ercan-Sencicek AG, Stillman AA, Tanriover G, Abrahams BS, Duvall JA, Robbins EM, Geschwind DH, Biederer T, Gunel M, Lifton RP, State MW. Molecular cytogenetic analysis and resequencing of contactin associated protein-like 2 in autism spectrum disorders. *The American Journal of Human Genetics*, 82(1):165–73, 2008

[12] Baudouin SJ, Gaudias J, Gerharz S, Hatstatt L, Zhou K, Punnakkal P, Tanaka KF, Spooren W, Hen R, De Zeeuw CI, Vogt K, Scheiffele P. Shared synaptic pathophysiology in syndromic and nonsyndromic rodent models of autism. *Science*, 338(6103):128–32, 2012

[13] Bauman M, Kemper TL. Histoanatomic observations of the brain in early infantile autism. *Neurology*, 35(6):866–874, 1985

[14] Baumgartner S, Littleton JT, Broadie K, Bhat MA, Harbecke R, Lengyel JA, Chiquet-Ehrismann R, Prokop A, Bellen HJ. A Drosophila neurexin is required for septate junction and blood-nerve barrier formation and function. *Cell*, 87(6):1059–1068, 1996

[15] Becker EBE, Zuliani L, Pettingill R, Lang B, Waters P, Dulneva A, Sobott F, Wardle M, Graus F, Bataller L, Robertson NP, Vincent A. Contactin-associated protein-2 antibodies in non-paraneoplastic cerebellar ataxia. *Journal of Neurology, Neurosurgery, and Psychiatry*, 83(4):437–40, 2012

[16] Bel C, Oguievetskaia K, Pitaval C, Goutebroze L, Faivre-Sarrailh C. Axonal targeting of Caspr2 in hippocampal neurons via selective somatodendritic endocytosis. *Journal of cell science*, 122(Pt 18):3403–3413, 2009

[17] Bhat MA, Izaddoost S, Lu Y, Cho KO, Choi KW, Bellen HJ. Discs Lost, a novel multi-PDZ domain protein, establishes and maintains epithelial polarity. *Cell*, 96(6):833–845, 1999

[18] Bhat MA, Rios JC, Lu Y, Garcia-Fresco GP, Ching W, Martin MS, Li J, Einheber S, Chesler M, Rosenbluth J, Salzer JL, Bellen HJ. Axon-glia interactions and the domain organization of myelinated axons requires neurexin IV/Caspr/Paranodin. *Neuron*, 30(2):369–383, 2001

[19] Biederer T, Südhof TC. Mints as adaptors. Direct binding to neurexins and recruitment of munc18. *Journal of Biological Chemistry*, 275(51):39803–39806, 2000

[20] Bin NR, Ma K, Harada H, Tien CW, Bergin F, Sugita K, Luyben TT, Narimatsu M, Jia Z, Wrana JL, Monnier PP, Zhang L, Okamoto K, Sugita S. Crucial Role of Postsynaptic Syntaxin 4 in Mediating Basal Neurotransmission and Synaptic Plasticity in Hippocampal CA1 Neurons. *Cell Reports*, 2018

[21] Biran V, Verney C, Ferriero DM. Perinatal Cerebellar Injury in Human and Animal Models. *Neurology Research International*, 2012:1, 2012

[22] Bottos A, Rissone A, Bussolino F, Arese M. Neurexins and neuroligins: synapses look out of the nervous system. *Cellular and Molecular Life Sciences*, 68(16):2655–2666, 2011

[23] Boukhtouche F, Janmaat S, Vodjdani G, Gautheron V, Mallet J, Dusart I, Mariani J. Retinoid-related orphan receptor alpha controls the early steps of Purkinje cell dendritic differentiation. *Journal of Neuroscience*, 26(5):1531–1538, 2006

[24] Boyle ME, Berglund EO, Murai KK, Weber L, Peles E, Ranscht B. Contactin orchestrates assembly of the septate-like junctions at the paranode in myelinated peripheral nerve. *Neuron*, 30(2):385–397, 2001

[25] Brossard-Racine M, du Plessis AJ, Limperopoulos C. Developmental Cerebellar Cognitive Affective Syndrome in Ex-preterm Survivors Following Cerebellar Injury. *Cerebellum*, 14(2):151, 2014

[26] Buckner RL. The Cerebellum and Cognitive Function: 25 Years of Insight from Anatomy and Neuroimaging. *Neuron*, 80(3):807, 2013

[27] Buttiglione M, Revest JM, Rougon G, Faivre-Sarrailh C. F3 neuronal adhesion molecule controls outgrowth and fasciculation of cerebellar granule cell neurites: a cell-type-specific effect mediated by the Ig-like domains. *Molecular and Cellular Neuroscience*, 8(1):53–69, 1996

[28] Cathala L, Holderith NB, Nusser Z, DiGregorio DA, Cull-Candy SG. Changes in synaptic structure underlie the developmental speeding of AMPA receptor-mediated EPSCs. *Nature neuroscience*, 8(10):1310–1318, 2005

[29] Chen N, Koopmans F, Gordon A, Paliukhovich I, Klaassen RV, van der Schors RC, Peles E, Verhage M, Smit AB, Li KW. Interaction proteomics of canonical Caspr2 (CNTNAP2) reveals the presence of two Caspr2 isoforms with overlapping interactomes. *Biochimica et Biophysica Acta (BBA) - Proteins and Proteomics*, 1854(7):827, 2015

[30] Chen SX, Tari PK, She K, Haas K. Neurexin-neuroligin cell adhesion complexes contribute to synaptotropic dendritogenesis via growth stabilization mechanisms in vivo. *Neuron*, 67(6):967–983, 2010

[31] Cline H, Haas K. The regulation of dendritic arbor development and plasticity by glutamatergic synaptic input: a review of the synaptotrophic hypothesis. *The Journal of physiology*, 2008

[32] Coutinho E, Menassa DA, Jacobson L, West SJ, Domingos J, Moloney TC, Lang B, Harrison PJ, Bennett DLH, Bannerman D, Vincent A. Persistent microglial activation and synaptic loss with behavioral abnormalities in mouse offspring exposed to CASPR2-antibodies in utero. *Acta Neuropathologica*, 2017

[33] Crepel F, Dupont JL, Gardette R. Selective absence of calcium spikes in Purkinje cells of staggerer mutant mice in cerebellar slices maintained in vitro. *The Journal of Physiology*, 346(1):111–125, 1984

[34] Dawes JM, Weir GA, Middleton SJ, Patel R, Chisholm KI, Pettingill P, Peck LJ, Sheridan J, Shakir A, Jacobson L, Gutierrez-Mecinas M, Galino J, Walcher J, Kühnemund J, Kuehn H, Sanna MD, Lang B, Clark AJ, Themistocleous AC, Iwagaki N, West SJ, Werynska K, Carroll L, Trendafilova T, Menassa DA, et al. Immune or Genetic-Mediated Disruption of CASPR2 Causes Pain Hypersensitivity Due to Enhanced Primary Afferent Excitability. *Neuron*, 97(4):806–822.e10, 2018

[35] Dean C, Dresbach T. Neuroligins and neurexins: linking cell adhesion, synapse formation and cognitive function. *Trends in Neurosciences*, 29(1):21–29, 2005

[36] Dhanvantari S, Loh YP. Lipid raft association of carboxypeptidase E is necessary for its function as a regulated secretory pathway sorting receptor. *Journal of Biological Chemistry*, 275(38):29887–29893, 2000

[37] D'Mello AM, Crocetti D, Mostofsky SH, Stoodley CJ. Cerebellar gray matter and lobular volumes correlate with core autism symptoms. *NeuroImage, Clinical*, 7:631–9, 2015

[38] Doolittle RF, Feng DF, Johnson MS. Computer-based characterization of epidermal growth factor precursor. *Nature*, 307(5951):558–560, 1984

[39] Durand CM, Betancur C, Boeckers TM, Bockmann J, Chaste P, Fauchereau F, Nygren G, Rastam M, Gillberg IC, Anckarsäter H, Sponheim E, Goubran-Botros H, Delorme R, Chabane N, Mouren-Simeoni MC, de Mas P, Bieth E, Rogé B, Héron D, Burglen L, Gillberg C, Leboyer M, Bourgeron T. Mutations in the gene encoding the synaptic scaffolding protein SHANK3 are associated with autism spectrum disorders. *Nature Genetics*, 39(1):25–27, 2006

[40] Ellegood J, Anagnostou E, Babineau BA, Crawley JN, Lin L, Genestine M, DiCicco-Bloom E, Lai JKY, Foster JA, Peñagarikano O, Geschwind DH, Pacey LK, Hampson DR, Laliberté CL, Mills AA, Tam E, Osborne LR, Kouser M, Espinosa-Becerra F, Xuan Z, Powell CM, Raznahan A, Robins DM, Nakai N, Nakatani J, et al. Clustering autism: using neuroanatomical differences in 26 mouse models to gain insight into the heterogeneity. *Molecular psychiatry*, 20(1):118–125, 2014

[41] Englund C, Kowalczyk T, Daza RAM, Dagan A, Lau C, Rose MF, Hevner RF. Unipolar brush cells of the cerebellum are produced in the rhombic lip and migrate through developing white matter. *Journal of Neuroscience*, 26(36):9184–9195, 2006

[42] Faivre-Sarrailh C, Gauthier F, Denisenko-Nehrbass N, Le Bivic A, Rougon G, Girault JA. The glycosylphosphatidyl inositol-anchored adhesion molecule F3/contactin is required for surface transport of paranodin/contactin-associated protein (caspr). *The Journal of Cell Biology*, 149(2):491–502, 2000

[43] Fan G, Baker ML, Wang Z, Baker MR, Sinyagovskiy PA, Chiu W, Ludtke SJ, Serysheva II. Gating machinery of InsP3R channels revealed by electron cryomicroscopy. *Nature*, 527(7578):336–341, 2015

[44] Ferris CD, Huganir RL, Supattapone S, Snyder SH. Purified inositol 1,4,5-trisphosphate receptor mediates calcium flux in reconstituted lipid vesicles. *Nature*, 342(6245):87–89, 1989

[45] Finch EA, Turner TJ, Goldin SM. Calcium as a coagonist of inositol 1,4,5-trisphosphate-induced calcium release. *Science (New York, NY)*, 252(5004):443–446, 1991

[46] Fine EJ, Ionita CC, Lohr L. The history of the development of the cerebellar examination. *Seminars in Neurology*, 22(4):375–384, 2003

[47] Foran DR, Peterson AC. Myelin acquisition in the central nervous system of the mouse revealed by an MBP-Lac Z transgene. *Journal of Neuroscience*, 1992

[48] Fricker LD, Snyder SH. Purification and characterization of enkephalin convertase, an enkephalin-synthesizing carboxypeptidase. *Journal of Biological Chemistry*, 258(18):10950–10955, 1983

[49] Fujita E, Tanabe Y, Momoi MY, Momoi T. Cntnap2 expression in the cerebellum of Foxp2(R552H) mice, with a mutation related to speech-language disorder. *Neuroscience Letters*, 506(2):277–280, 2011

[50] Fujita M. Adaptive filter model of the cerebellum. *Biological Cybernetics*, 45(3):195–206, 1982

[51] Fujiwara A, Hirose K, Yamazawa T, Iino M. Reduced IP3 sensitivity of IP3 receptor in Purkinje neurons. *Neuroreport*, 12(12):2647–2651, 2001

[52] Galvan DL, Mignery GA. Carboxyl-terminal sequences critical for inositol 1,4,5-trisphosphate receptor subunit assembly. *Journal of Biological Chemistry*, 277(50):48248–48260, 2002

[53] Gdalyahu A, Lazaro M, Peñagarikano O, Golshani P, Trachtenberg JT, Geschwind DH. The Autism Related Protein Contactin-Associated Protein-Like 2 (CNTNAP2) Stabilizes New Spines: An In Vivo Mouse Study. *PLOS One*, 10(5):e0125633, 2015

[54] Gilbert PF, Thach WT. Purkinje cell activity during motor learning. *Brain Research*, 128(2):309–328, 1977

[55] Gollan L, Salomon D, Salzer JL, Peles E. Caspr regulates the processing of contactin and inhibits its binding to neurofascin. *The Journal of Cell Biology*, 163(6):1213–1218, 2003

[56] Gordon A, Salomon D, Barak N, Pen Y, Tsoory M, Kimchi T, Peles E. Expression of Cntnap2 (Caspr2) in multiple levels of sensory systems. *Molecular and Cellular Neuroscience*, 70:42, 2015

[57] Hata Y, Butz S, Südhof TC. CASK: a novel dlg/PSD95 homolog with an N-terminal calmodulin-dependent protein kinase domain identified by interaction with neurexins. *Journal of Neuroscience*, 16(8):2488–2494, 1996

[58] Higo T, Hattori M, Nakamura T, Natsume T, Michikawa T, Mikoshiba K. Subtype-Specific and ER Lumenal Environment-Dependent Regulation of Inositol 1,4,5-Trisphosphate Receptor Type 1 by ERp44. *Cell*, 120(1):85–98, 2005

[59] Hisatsune C, Kuroda Y, Akagi T, Torashima T, Hirai H, Hashikawa T, Inoue T, Mikoshiba K. Inositol 1,4,5-trisphosphate receptor type 1 in granule cells, not in Purkinje cells, regulates the dendritic morphology of Purkinje cells through brain-derived neurotrophic factor production. *Journal of Neuroscience*, 26(42):10916–10924, 2006

[60] Holmes G. The Croonian Lectures on the clinical symptoms of cerebellar disease and their interpretation. Lecture II. 1922. *Cerebellum (London, England)*, 6(2), 2007

[61] Huang L, Chardon JW, Carter MT, Friend KL, Dudding TE, Schwartzentruber J, Zou R, Schofield PW, Douglas S, Bulman DE, Boycott KM. Missense mutations in ITPR1 cause autosomal dominant congenital nonprogressive spinocerebellar ataxia. *Orphanet Journal of Rare Diseases*, 7:67, 2012

[62] Huguet G, Ey E, Bourgeron T. The Genetic Landscapes of Autism Spectrum Disorders. *Annual Review of Genomics and Human Genetics*, 14(1):191, 2013

[63] Ichikawa R, Hashimoto K, Miyazaki T, Uchigashima M, Yamasaki M, Aiba A, Kano M, Watanabe M. Territories of heterologous inputs onto Purkinje cell dendrites are segregated by mGluR1-dependent parallel fiber synapse elimination. *Proceedings of the National Academy of Sciences*, 113(8):2282–2287, 2016

[64] Ichise T, Kano M, Hashimoto K, Yanagihara D, Nakao K, Shigemoto R, Katsuki M, Aiba A. mGluR1 in cerebellar Purkinje cells essential for long-term depression, synapse elimination, and motor coordination. *Science (New York, NY)*, 288(5472):1832–1835, 2000

[65] Inda MC, DeFelipe J, Muñoz A. Voltage-gated ion channels in the axon initial segment of human cortical pyramidal cells and their relationship with chandelier cells. *Proceedings of the National Academy of Sciences of the United States of America*, 103(8):2920–2925, 2006

[66] Inoue T, Kato K, Kohda K, Mikoshiba K. Type 1 inositol 1,4,5-trisphosphate receptor is required for induction of long-term depression in cerebellar Purkinje neurons. *Journal of Neuroscience*, 18(14):5366–5373, 1998

[67] Irani SR, Alexander S, Waters P, Kleopa KA, Pettingill P, Zuliani L, Peles E, Buckley C, Lang B, Vincent A. Antibodies to Kv1 potassium channel-complex proteins leucine-rich, glioma inactivated 1 protein and contactin-associated protein-2 in limbic encephalitis, Morvan's syndrome and acquired neuromyotonia. *Brain*, 133(9):2734–48, 2010

[68] Ito M. Neural design of the cerebellar motor control system. *Brain Research*, 40(1):81–84, 1972

[69] Ito M. Control of mental activities by internal models in the cerebellum. *Nature Reviews Neuroscience*, 9(4):304–313, 2008

[70] Jamain S, Quach H, Betancur C, Råstam M, Colineaux C, Gillberg IC, Soderstrom H, Giros B, Leboyer M, Gillberg C, Bourgeron T. Mutations of the X-linked genes encoding neuroligins NLGN3 and NLGN4 are associated with autism. *Nature Genetics*, 34(1):27–29, 2003

[71] Jarius S, Scharf M, Begemann N, Stöcker W, Probst C, Serysheva II, Nagel S, Graus F, Psimaras D, Wildemann B, Komorowski L. Antibodies to the inositol 1,4,5-trisphosphate receptor type 1 (ITPR1) in cerebellar ataxia. *Journal of Neuroinflammation*, 11:206, 2014

[72] Joo W, Hippenmeyer S, Luo L. Neurodevelopment. Dendrite morphogenesis depends on relative levels of NT-3/TrkC signaling. *Science*, 346(6209):626–629, 2014

[73] Jow F, Zhang ZH, Kopsco DC, Carroll KC, Wang K. Functional coupling of intracellular calcium and inactivation of voltage-gated Kv1.1/Kvbeta1.1 A-type K+ channels. *Proceedings of the National Academy of Sciences of the United States of America*, 101(43):15535–15540, 2004

[74] Kandel ER, Schwartz JH, Jessel TM, Kandel ER, Schwartz JH, Jessel TM. *Principles of Neural Science*. McGraw-Hill, 2000

[75] Kapfhammer JP. Cellular and molecular control of dendritic growth and development of cerebellar purkinje cells. *Progress in Histochemistry and Cytochemistry*, 39(3):131–182, 2004

[76] Kim HG, Kishikawa S, Higgins AW, Seong IS, Donovan DJ, Shen Y, Lally E, Weiss LA, Najm J, Kutsche K, Descartes M, Holt L, Braddock S, Troxell R, Kaplan L, Volkmar F, Klin A, Tsatsanis K, Harris DJ, Noens I, Pauls DL, Daly MJ, MacDonald ME, Morton CC, Quade BJ, et al. Disruption of neurexin 1 associated with autism spectrum disorder. *The American Journal of Human Genetics*, 82(1):199–207, 2008

[77] Kloth AD, Badura A, Li A, Cherskov A, Connolly SG, Giovannucci A, Bangash MA, Grasselli G, Peñagarikano O, Piochon C, Tsai PT, Geschwind DH, Hansel C, Sahin M, Takumi T, Worley PF, Wang SS. Cerebellar associative sensory learning defects in five mouse autism models. *eLife*, 4:e06085, 2015

[78] Koekkoek SKE, Yamaguchi K, Milojkovic BA, Dortland BR, Ruigrok TJH, Maex R, De Graaf W, Smit AE, VanderWerf F, Bakker CE, Willemsen R, Ikeda T, Kakizawa S, Onodera K, Nelson DL, Mientjes E, Joosten M, De Schutter E, Oostra BA, Ito M, De Zeeuw CI. Deletion of FMR1 in Purkinje cells enhances parallel fiber LTD, enlarges spines, and attenuates cerebellar eyelid conditioning in Fragile X syndrome. *Neuron*, 47(3):339–352, 2005

[79] Lamballe F, Tapley P, Barbacid M. trkC encodes multiple neurotrophin-3 receptors with distinct biological properties and substrate specificities. *The EMBO Journal*, 12(8):3083–3094, 1993

[80] Lancaster E, Huijbers MGM, Bar V, Boronat A, Wong A, Martinez-Hernandez E, Wilson C, Jacobs D, Lai M, Walker RW, Graus F, Bataller L, Illa I, Markx S, Strauss KA, Peles E, Scherer SS, Dalmau J. Investigations of caspr2, an autoantigen of encephalitis and neuromyotonia. *Annals of Neurology*, 69(2):303–311, 2011

[81] Larsell O. The morphogenesis and adult pattern of the lobules and fissures of the cerebellum of the white rat. *The Journal of Comparative Neurology*, 97(2):281–356, 1952

[82] Larsell O. The cerebellum of the cat and the monkey. *The Journal of Comparative Neurology*, 99(1):135–199, 1953

[83] Lee IH, You JO, Ha KS, Bae DS, Suh PG, Rhee SG, Bae YS. AHNAK-mediated activation of phospholipase C-gamma1 through protein kinase C. *Journal of Biological Chemistry*, 279(25):26645–26653, 2004

[84] van de Leemput J, Chandran J, Knight MA, Holtzclaw LA, Scholz S, Cookson MR, Houlden H, Gwinn-Hardy K, Fung HC, Lin X, Hernandez D, Simon-Sanchez J, Wood NW, Giunti P, Rafferty I, Hardy J, Storey E, Gardner RJM, Forrest SM, Fisher EMC, Russell JT, Cai H, Singleton AB. Deletion at ITPR1 underlies ataxia in mice and spinocerebellar ataxia 15 in humans. *PLOS Genetics*, 3(6):e108, 2007

[85] Leto K, Arancillo M, Becker EB, Buffo A, Chiang C, Ding B, Dobyns WB, Dusart I, Haldipur P, Hatten ME, Hoshino M, Joyner AL, Kano M, Kilpatrick DL, Koibuchi N, Marino S, Martinez S, Millen KJ, Millner TO, Miyata T, Parmigiani E, Schilling K, Sekerková G, Sillitoe RV, Sotelo C, et al. Consensus Paper: Cerebellar Development. *Cerebellum*, 15(6):789–828, 2015

[86] Leto K, Bartolini A, Yanagawa Y, Obata K, Magrassi L, Schilling K, Rossi F. Laminar fate and phenotype specification of cerebellar GABAergic interneurons. *Journal of Neuroscience*, 29(21):7079–7091, 2009

[87] Limperopoulos C, Bassan H, Gauvreau K, Robertson RL, Sullivan NR, Benson CB, Avery L, Stewart J, Soul JS, Ringer SA, Volpe JJ, duPlessis AJ. Does cerebellar injury in premature infants contribute to the high prevalence of long-term cognitive, learning, and behavioral disability in survivors? *Pediatrics*, 120(3):584–593, 2007

[88] Littleton JT, Bhat MA, Bellen HJ. Deciphering the function of neurexins at cellular junctions. *The Journal of Cell Biology*, 137(4):793–796, 1997

[89] Lomeli H, Sprengel R, Laurie DJ, Köhr G, Herb A, Seeburg PH, Wisden W. The rat delta-1 and delta-2 subunits extend the excitatory amino acid receptor family. *FEBS letters*, 315(3):318–322, 1993

[90] Maeda N, Niinobe M, Inoue Y, Mikoshiba K. Developmental expression and intracellular location of P400 protein characteristic of Purkinje cells in the mouse cerebellum. *Developmental Biology*, 133(1):67–76, 1989

[91] Marfatia SM, Leu RA, Branton D, Chishti AH. Identification of the protein 4.1 binding interface on glycophorin C and p55, a homologue of the Drosophila discs-large tumor suppressor protein. *Journal of Biological Chemistry*, 270(2):715–719, 1995

[92] Matysiak-Scholze U, Nehls M. The structural integrity of ROR alpha isoforms is mutated in staggerer mice: cerebellar coexpression of ROR alpha1 and ROR alpha4. *Genomics*, 43(1):78–84, 1997

[93] Maximov A, Südhof TC, Bezprozvanny I. Association of neuronal calcium channels with modular adaptor proteins. *Journal of Biological Chemistry*, 274(35):24453–24456, 1999

[94] Metzger F, Kapfhammer JP. Protein kinase C activity modulates dendritic differentiation of rat Purkinje cells in cerebellar slice cultures. *The European Journal of Neuroscience*, 12(6):1993–2005, 2000

[95] Middleton FA, Strick PL. Anatomical evidence for cerebellar and basal ganglia involvement in higher cognitive function. *Science (New York, NY)*, 266(5184):458–461, 1994

[96] Mignery GA, Newton CL, Archer BT, Südhof TC. Structure and expression of the rat inositol 1,4,5-trisphosphate receptor. *Journal of Biological Chemistry*, 265(21):12679–12685, 1990

[97] Missler M, Südhof TC. Neurexins: three genes and 1001 products. *Trends in Genetics*, 14(1):20–26, 1998

[98] Missler M, Zhang W, Rohlmann A, Kattenstroth G, Hammer RE, Gottmann K, Südhof TC. Alpha-neurexins couple Ca2+ channels to synaptic vesicle exocytosis. *Nature*, 423(6943):939–948, 2003

[99] Moretti P, Levenson JM, Battaglia F, Atkinson R, Teague R, Antalffy B, Armstrong D, Arancio O, Sweatt JD, Zoghbi HY. Learning and memory and synaptic plasticity are impaired in a mouse model of Rett syndrome. *Journal of Neuroscience*, 26(1):319–327, 2006

[100] Noguchi J, Matsuzaki M, Ellis-Davies GCR, Kasai H. Spine-neck geometry determines NMDA receptor-dependent Ca2+ signaling in dendrites. *Neuron*, 46(4):609–622, 2005

[101] Novak MA, Suomi SJ. Abnormal behaviour in nonhuman primates and models of development. In TM Burbacher, GP Sackett, KS Grant (editors), *Primate Models of Children's Health and Developmental Disabilities*, pages 141–160. Academic Press, Boston, 2008

[102] Oiso S, Takeda Y, Futagawa T, Miura T, Kuchiiwa S, Nishida K, Ikeda R, Kariyazono H, Watanabe K, Yamada K. Contactin-associated protein (Caspr) 2 interacts with carboxypeptidase E in the CNS. *Journal of Neurochemistry*, 109(1):158–167, 2009

[103] Olsen AL, Lai Y, Dalmau J, Scherer SS, Lancaster E. Caspr2 autoantibodies target multiple epitopes. *Neurology Neuroimmunology and Neuroinflammation*, 2(4):e127, 2015

[104] Peles E, Nativ M, Lustig M, Grumet M, Schilling J, Martinez R, Plowman GD, Schlessinger J. Identification of a novel contactin-associated transmembrane receptor with multiple domains implicated in protein-protein interactions. *The EMBO Journal*, 16(5):978–988, 1997

[105] Peñagarikano O, Abrahams BS, Herman EI, Winden KD, Gdalyahu A, Dong H, Sonnenblick LI, Gruver R, Almajano J, Bragin A, Golshani P, Trachtenberg JT, Peles E, Geschwind DH. Absence of CNTNAP2 leads to epilepsy, neuronal migration abnormalities, and core autism-related deficits. *Cell*, 147(1):235–46, 2011

[106] Peter S, Ten Brinke MM, Stedehouder J, Reinelt CM, Wu, Zhou H, Zhou K, Boele HJ, Kushner SA, Lee MG, Schmeisser MJ, Boeckers TM, Schonewille M, Hoebeek FE, De Zeeuw CI. Dysfunctional cerebellar Purkinje cells contribute to autism-like behaviour in Shank2-deficient mice. *Nature Communications*, 7:12627, 2016

[107] Petrenko AG, Perin MS, Davletov BA, Ushkaryov YA, Geppert M, Südhof TC. Binding of synaptotagmin to the alpha-latrotoxin receptor implicates both in synaptic vesicle exocytosis. *Nature*, 353(6339):65–68, 1991

[108] Phillips GR, Huang JK, Wang Y, Tanaka H, Shapiro L, Zhang W, Shan WS, Arndt K, Frank M, Gordon RE, Gawinowicz MA, Zhao Y, Colman DR. The presynaptic particle web: ultrastructure, composition, dissolution, and reconstitution. *Neuron*, 32(1):63–77, 2001

[109] Pinatel D, Hivert B, Saint-Martin M, Noraz N, Savvaki M, Karagogeos D, Faivre-Sarrailh C. The Kv1-associated molecules TAG-1 and Caspr2 are selectively targeted to the axon initial segment in hippocampal neurons. *Journal of Cell Science*, 130(13):2209–2220, 2017

[110] Poliak S, Gollan L, Martinez R, Custer A, Einheber S, Salzer JL, Trimmer JS, Shrager P, Peles E. Caspr2, a new member of the neurexin superfamily, is localized at the juxtaparanodes of myelinated axons and associates with K+ channels. *Neuron*, 24(4):1037–1047, 2000

[111] Poliak S, Gollan L, Salomon D, Berglund EO, Ohara R, Ranscht B, Peles E. Localization of Caspr2 in myelinated nerves depends on axon-glia interactions and the generation of barriers along the axon. *Journal of Neuroscience*, 21(19):7568–7575, 2001

[112] Poliak S, Salomon D, Elhanany H, Sabanay H, Kiernan B, Pevny L, Stewart CL, Xu X, Chiu SY, Shrager P, Furley AJW, Peles E. Juxtaparanodal clustering of Shaker-like K+ channels in myelinated axons depends on Caspr2 and TAG-1. *The Journal of Cell Biology*, 162(6):1149–1160, 2003

[113] Prole DL, Taylor CW. Inositol 1,4,5-trisphosphate receptors and their protein partners as signalling hubs. *The Journal of physiology*, 594(11):2849–2866, 2016

[114] Quinn DP, Kolar A, Wigerius M, Gomm-Kolisko RN, Atwi H, Fawcett JP, Krueger SR. Pan-neurexin perturbation results in compromised synapse stability and a reduction in readily releasable synaptic vesicle pool size. *Scientific Reports*, 7:42920, 2017

[115] Ramos-Franco J, Galvan D, Mignery GA, Fill M. Location of the permeation pathway in the recombinant type 1 inositol 1,4,5-trisphosphate receptor. *The Journal of General Physiology*, 114(2):243–250, 1999

[116] Rios JC, Melendez-Vasquez CV, Einheber S, Lustig M, Grumet M, Hemperly J, Peles E, Salzer JL. Contactin-associated protein (Caspr) and contactin form a complex that is targeted to the paranodal junctions during myelination. *Journal of Neuroscience*, 20(22):8354–8364, 2000

[117] Ritvo ER, Freeman BJ, Scheibel AB, Duong T, Robinson H, Guthrie D, Ritvo A. Lower Purkinje cell counts in the cerebella of four autistic subjects: initial findings of the UCLA-NSAC Autopsy Research Report. *The American Journal of Psychiatry*, 143(7):862–866, 1986

[118] Rodenas-Cuadrado P, Pietrafusa N, Francavilla T, La Neve A, Striano P, Vernes SC. Characterisation of CASPR2 deficiency disorder - a syndrome involving autism, epilepsy and language impairment. *BMC Medical Genetics*, 17(1):8, 2016

[119] Rubio-Marrero EN, Vincelli G, Jeffries CM, Shaikh TR, Pakos I, Ranaivoson FM, von Daake S, Demeler B, De Jaco A, Perkins G, Ellisman MH, Trewhella J, Comoletti D. Structural characterization of the extracellular domain of CASPR2 and insights into its association with the novel ligand Contactin1. *Journal of Biological Chemistry*, page jbc.M115.705681, 2015

[120] Rutter M, Andersen-Wood L, Beckett C, Bredenkamp D, Castle J, Groothues C, Kreppner J, Keaveney L, Lord C, O'Connor TG. Quasi-autistic patterns following severe early global privation. English and Romanian Adoptees (ERA) Study Team. *Journal of Child Psychology and Psychiatry, and Allied Disciplines*, 40(4):537–549, 1999

[121] Santos SD, Iuliano O, Ribeiro L, Veran J, Ferreira JS, Rio P, Mulle C, Duarte CB, Carvalho AL. Contactin-associated protein 1 (Caspr1) regulates the traffic and synaptic content of α-amino-3-hydroxy-5-methyl-4-isoxazolepropionic acid (AMPA)-type glutamate receptors. *Journal of Biological Chemistry*, 287(9):6868–6877, 2012

[122] Savvaki M, Panagiotaropoulos T, Stamatakis A, Sargiannidou I, Karatzioula P, Watanabe K, Stylianopoulou F, Karagogeos D, Kleopa KA. Impairment of learning and memory in TAG-1 deficient mice associated with shorter CNS internodes and disrupted juxtaparanodes. *Molecular and Cellular Neuroscience*, 39(3):478–490, 2008

[123] Savvaki M, Theodorakis K, Zoupi L, Stamatakis A, Tivodar S, Kyriacou K, Stylianopoulou F, Karagogeos D. The expression of TAG-1 in glial cells is sufficient for the formation of the juxtaparanodal complex and the phenotypic rescue of tag-1 homozygous mutants in the CNS. *Journal of Neuroscience*, 30(42):13943–13954, 2010

[124] Schmahmann JD. Disorders of the cerebellum: ataxia, dysmetria of thought, and the cerebellar cognitive affective syndrome. *The Journal of Neuropsychiatry and Clinical Neurosciences*, 16(3):367–378, 2004

[125] Schmahmann JD, Sherman JC. The cerebellar cognitive affective syndrome. *Brain*, 121 (Pt 4):561–579, 1998

[126] Schmunk G, Boubion BJ, Smith IF, Parker I, Gargus JJ. Shared functional defect in IPR-mediated calcium signaling in diverse monogenic autism syndromes. *Translational Psychiatry*, 5(9):e643, 2015

[127] Schmunk G, Nguyen RL, Ferguson DL, Kumar K, Parker I, Gargus JJ. High-throughput screen detects calcium signaling dysfunction in typical sporadic autism spectrum disorder. *Scientific Reports*, 7:40740, 2017

[128] Schreiner D, Nguyen TM, Russo G, Heber S, Patrignani A, Ahrné E, Scheiffele P. Targeted combinatorial alternative splicing generates brain region-specific repertoires of neurexins. *Neuron*, 84(2):386–398, 2014

[129] Scott R, Sánchez-Aguilera A, van Elst K, Lim L, Dehorter N, Bae SE, Bartolini G, Peles E, Kas MJH, Bruining H, Marín O. Loss of Cntnap2 Causes Axonal Excitability Deficits, Developmental Delay in Cortical Myelination, and Abnormal Stereotyped Motor Behavior. *Cerebral Cortex*, page Epub ahead of print, 2017

[130] Selimbeyoglu A, Kim CK, Inoue M, Lee SY, Hong ASO, Kauvar I, Ramakrishnan C, Fenno LE, Davidson TJ, Wright M, Deisseroth K. Modulation of prefrontal cortex excitation/inhibition balance rescues social behavior in CNTNAP2-deficient mice. *Science Translational Medicine*,

9(401):eaah6733, 2017

[131] Sheng M. PDZs and receptor/channel clustering: rounding up the latest suspects. *Neuron*, 17(4):575–578, 1996

[132] Sidman RL, Lane PW, Dickie MM. Staggerer, a new mutation in the mouse affecting the cerebellum. *Science*, 137(3530):610–612, 1962

[133] Sillitoe RV, Joyner AL. Morphology, molecular codes, and circuitry produce the three-dimensional complexity of the cerebellum. *Annual Review of Cell and Developmental Biology*, 23(1):549–577, 2007

[134] Sørlie T, Wang Y, Xiao C, Johnsen H, Naume B, Samaha RR, Børresen-Dale AL. Distinct molecular mechanisms underlying clinically relevant subtypes of breast cancer: gene expression analyses across three different platforms. *BMC Genomics*, 7:127, 2006

[135] Sotelo C. Development of "Pinceaux" formations and dendritic translocation of climbing fibers during the acquisition of the balance between glutamatergic and gamma-aminobutyric acidergic inputs in developing Purkinje cells. *The Journal of Comparative Neurology*, 506(2):240–262, 2007

[136] Spiegel I, Salomon D, Erne B, Schaeren-Wiemers N, Peles E. Caspr3 and caspr4, two novel members of the caspr family are expressed in the nervous system and interact with PDZ domains. *Molecular and Cellular Neurosciences*, 20(2):283–297, 2002

[137] Stoodley CJ, D'Mello AM, Ellegood J, Jakkamsetti V, Liu P, Nebel MB, Gibson JM, Kelly E, Meng F, Cano CA, Pascual JM, Mostofsky SH, Lerch JP, Tsai PT. Altered cerebellar connectivity in autism and cerebellar-mediated rescue of autism-related behaviors in mice. *Nature neuroscience*, 20(12):1744–1751, 2017

[138] Stoodley CJ, MacMore JP, Makris N, Sherman JC, Schmahmann JD. Location of lesion determines motor vs. cognitive consequences in patients with cerebellar stroke. *NeuroImage, Clinical*, 12:765–775, 2016

[139] Stottmann RW, Rivas RJ. Distribution of TAG-1 and synaptophysin in the developing cerebellar cortex: relationship to Purkinje cell dendritic development. *The Journal of Comparative Neurology*, 395(1):121–135, 1998

[140] Strauss KA, Puffenberger EG, Huentelman MJ, Gottlieb S, Dobrin SE, Parod JM, Stephan DA, Morton DH. Recessive symptomatic focal epilepsy and mutant contactin-associated protein-like 2. *The New England Journal of Medicine*, 354(13):1370–1377, 2006

[141] Strauss KA, Puffenberger EG, Huentelman MJ, Gottlieb S, Dobrin SE, Parod JM, Stephan DA, Morton DH. Recessive symptomatic focal epilepsy and mutant contactin-associated protein-like 2. *The New England Journal of Medicine*, 354(13):1370–1377, 2006

[142] Strick PL, Dum RP, Fiez JA. Cerebellum and nonmotor function. *Annual Review of Neuroscience*, 32:413–434, 2009

[143] Südhof TC. Synaptic Neurexin Complexes: A Molecular Code for the Logic of Neural Circuits. *Cell*, 171(4):745–769, 2017

[144] Sugawara T, Hisatsune C, Le TD, Hashikawa T, Hirono M, Hattori M, Nagao S, Mikoshiba K. Type 1 inositol trisphosphate receptor regulates cerebellar circuits by maintaining the spine morphology of purkinje cells in adult mice. *Journal of Neuroscience*, 33(30):12186–12196, 2013

[145] Szatmari P, Paterson AD, Zwaigenbaum L, Roberts W, Brian J, Liu XQ, Vincent JB, Skaug JL, Thompson AP, Senman L, Feuk L, Qian C, Bryson SE, Jones MB, Marshall CR, Scherer SW, Vieland VJ, Bartlett C, Vonne Mangin, Goedken R, Segre A, Pericak-Vance MA, Cuccaro ML, Gilbert JR, Wright HH, et al. Mapping autism risk loci using genetic linkage and chromosomal rearrangements. *Nature Genetics*, 39(3):319–328, 2007

[146] Takeuchi K, Gertner MJ, Zhou J, Parada LF, Bennett MVL, Zukin RS. Dysregulation of synaptic plasticity precedes appearance of morphological defects in a Pten conditional knockout mouse model of autism. *Proceedings of the National Academy of Sciences of the United States of America*, 110(12):4738–43, 2013

[147] Tan GC, Doke TF, Ashburner J, Wood NW, Frackowiak RS. Normal variation in fronto-occipital circuitry and cerebellar structure with an autism-associated polymorphism of CNTNAP2. *NeuroImage*, 53(3):1030–42, 2010

[148] Traka M, Goutebroze L, Denisenko N, Bessa M, Nifli A, Havaki S, Iwakura Y, Fukamauchi F, Watanabe K, Soliven B, Girault JA, Karagogeos D. Association of TAG-1 with Caspr2 is essential for the molecular organization of juxtaparanodal regions of myelinated fibers. *The Journal of Cell Biology*, 162(6):1161–1172, 2003

[149] Traut W, Weichenhan D, Himmelbauer H, Winking H. New members of the neurexin superfamily: multiple rodent homologues of the human CASPR5 gene. *Mammalian Genome : Official Journal of the International Mammalian Genome Society*, 17(7):723–731, 2006

[150] Tsai PT, Hull C, Chu Y, Greene-Colozzi E, Sadowski AR, Leech JM, Steinberg J, Crawley JN, Regehr WG, Sahin M. Autistic-like behaviour and cerebellar dysfunction in Purkinje cell Tsc1 mutant mice. *Nature*, 488(7413):647–651, 2012

[151] Tzimourakas A, Giasemi S, Mouratidou M, Karagogeos D. Structure-function analysis of protein complexes involved in the molecular architecture of juxtaparanodal regions of myelinated fibers. *Biotechnology journal*, 2(5):577–583, 2007

[152] Uemura T, Lee SJ, Yasumura M, Takeuchi T, Yoshida T, Ra M, Taguchi R, Sakimura K, Mishina M. Trans-Synaptic Interaction of GluRδ2 and Neurexin through Cbln1 Mediates Synapse Formation in the Cerebellum. *Cell*, 141(6):1068, 2010

[153] Ullrich B, Ushkaryov YA, Südhof TC. Cartography of neurexins: more than 1000 isoforms generated by alternative splicing and expressed in distinct subsets of neurons. *Neuron*, 14(3):497–507, 1995

[154] Ushkaryov YA, Hata Y, Ichtchenko K, Moomaw C, Afendis S, Slaughter CA, Südhof TC. Conserved domain structure of beta-neurexins. Unusual cleaved signal sequences in receptor-like neuronal cell-surface proteins. *Journal of Biological Chemistry*, 269(16):11987–11992, 1994

[155] Ushkaryov YA, Petrenko AG, Geppert M, Südhof TC. Neurexins: synaptic cell surface proteins related to the alpha-latrotoxin receptor and laminin. *Science*, 257(5066):50–56, 1992

[156] Ushkaryov YA, Südhof TC. Neurexin III alpha: extensive alternative splicing generates membrane-bound and soluble forms. *Proceedings of the National Academy of Sciences of the United States of America*, 90(14):6410–6414, 1993

[157] Vaughn JE. Fine structure of synaptogenesis in the vertebrate central nervous system. *Synapse (New York, NY)*, 3(3):255–285, 1989

[158] Vetter ML, Martin-Zanca D, Parada LF, Bishop JM, Kaplan DR. Nerve growth factor rapidly stimulates tyrosine phosphorylation of phospholipase C-gamma 1 by a kinase activity associated with the product of the trk protooncogene. *Proceedings of the National Academy of Sciences of the United States of America*, 88(13):5650–5654, 1991

[159] Viltono L, Patrizi A, Fritschy JM, Sassoè-Pognetto M. Synaptogenesis in the cerebellar cortex: differential regulation of gephyrin and GABAA receptors at somatic and dendritic synapses of Purkinje cells. *The Journal of Comparative Neurology*, 508(4):579–591, 2008

[160] Wagner MJ, Kim TH, Savall J, Schnitzer MJ, Luo L. Cerebellar granule cells encode the expectation of reward. *Nature*, 544(7648):96–100, 2017

[161] Walsh T, McClellan JM, McCarthy SE, Addington AM, Pierce SB, Cooper GM, Nord AS, Kusenda M, Malhotra D, Bhandari A, Stray SM, Rippey CF, Roccanova P, Makarov V, Lakshmi B, Findling RL, Sikich L, Stromberg T, Merriman B, Gogtay N, Butler P, Eckstrand K, Noory L, Gochman P, Long R, et al. Rare structural variants disrupt multiple genes in neurodevelopmental pathways in schizophrenia. *Science*, 320(5875):539–543, 2008

[162] Wang SS, Kloth AD, Badura A. The Cerebellum, Sensitive Periods, and Autism. *Neuron*, 83(3):518–532, 2014

[163] Watanabe M, Kano M. Climbing fiber synapse elimination in cerebellar Purkinje cells. *The European Journal of Neuroscience*, 34(10):1697–1710, 2011

[164] Webb BL, Hirst SJ, Giembycz MA. Protein kinase C isoenzymes: a review of their structure, regulation and role in regulating airways smooth muscle tone and mitogenesis. *British Journal of Pharmacology*, 130(7):1433–1452, 2000

[165] Whittaker DE, Riegman KLH, Kasah S, Mohan C, Yu T, Sala BP, Hebaishi H, Caruso A, Marques AC, Michetti C, Smachetti MES, Shah A, Sabbioni M, Kulhanci O, Tee WW, Reinberg D, Scattoni ML, Volk H, McGonnell I, Wardle FC, Fernandes C, Basson MA. The chromatin remodeling factor CHD7 controls cerebellar development by regulating reelin expression. *Journal of Clinical Investigation*, 127(3):874–887, 2017

[166] Wolpert DM, Kawato M. Multiple paired forward and inverse models for motor control. *Neural Networks*, 11(7-8):1317–1329, 2003

[167] Yan J, Noltner K, Feng J, Li W, Schroer R, Skinner C, Zeng W, Schwartz CE, Sommer SS. Neurexin 1alpha structural variants associated with autism. *Neuroscience Letters*, 438(3):368–370, 2008

[168] Yoshikawa F, Morita M, Monkawa T, Michikawa T, Furuichi T, Mikoshiba K. Mutational analysis of the ligand binding site of the inositol 1,4,5-trisphosphate receptor. *Journal of Biological Chemistry*, 271(30):18277–18284, 1996

[169] Zahir FR, Baross A, Delaney AD, Eydoux P, Fernandes ND, Pugh T, Marra MA, Friedman JM. A patient with vertebral, cognitive and behavioural abnormalities and a de novo deletion of NRXN1alpha. *Journal of Medical Genetics*, 45(4):239–243, 2007

[170] Zhang L, Mabwi HA, Palange NJ, Jia R, Ma J, Bah FB, Sah RK, Li D, Wang D, Bah FBM, Togo J, Jin H, Ban L, Feng X, Zheng Y. Expression Patterns and Potential Biological Roles of Dip2a. *PlOS One*, 10(11):e0143284, 2015

[171] Zhang P, Dimont E, Ha T, Swanson DJ, Hide W, Goldowitz D. Relatively frequent switching of transcription start sites during cerebellar development. *BMC Genomics*, 18(1):461, 2017

[172] Zhao WD, Liu DX, Wei JY, Miao ZW, Zhang K, Su ZK, Zhang XW, Li Q, Fang WG, Qin XX, Shang DS, Li B, Li QC, Cao L, Kim KS, Chen YH. Caspr1 is a host receptor for meningitis-causing Escherichia coli. *Nature Communications*, 9(1):2296, 2018

[173] Zweier C, de Jong EK, Zweier M, Orrico A, Ousager LB, Collins AL, Bijlsma EK, Oortveld MA, Ekici AB, Reis A, Schenck A, Rauch A. CNTNAP2 and NRXN1 Are Mutated in Autosomal-Recessive Pitt-Hopkins-like Mental Retardation and Determine the Level of a Common Synaptic Protein in Drosophila. *The American Journal of Human Genetics*, 85(5):655, 2009

Appendix A: Alignment of Caspr-family primary protein sequences

The primary sequences of the murine Caspr-family proteins are provided below, for reference. Sequences are aligned to provide an estimate of similarity, and thus the likely divergence of function of these proteins over the course of evolution. Note that the murine genome contains three separate paralogues of *Cntnap5*, whereas the human genome contains only one *Cntnap5* gene. Moreover, no studies have thus far confirmed the presence of the Caspr5 protein *in vivo* and so the sequences for these protein provided here are theoretical translations only.

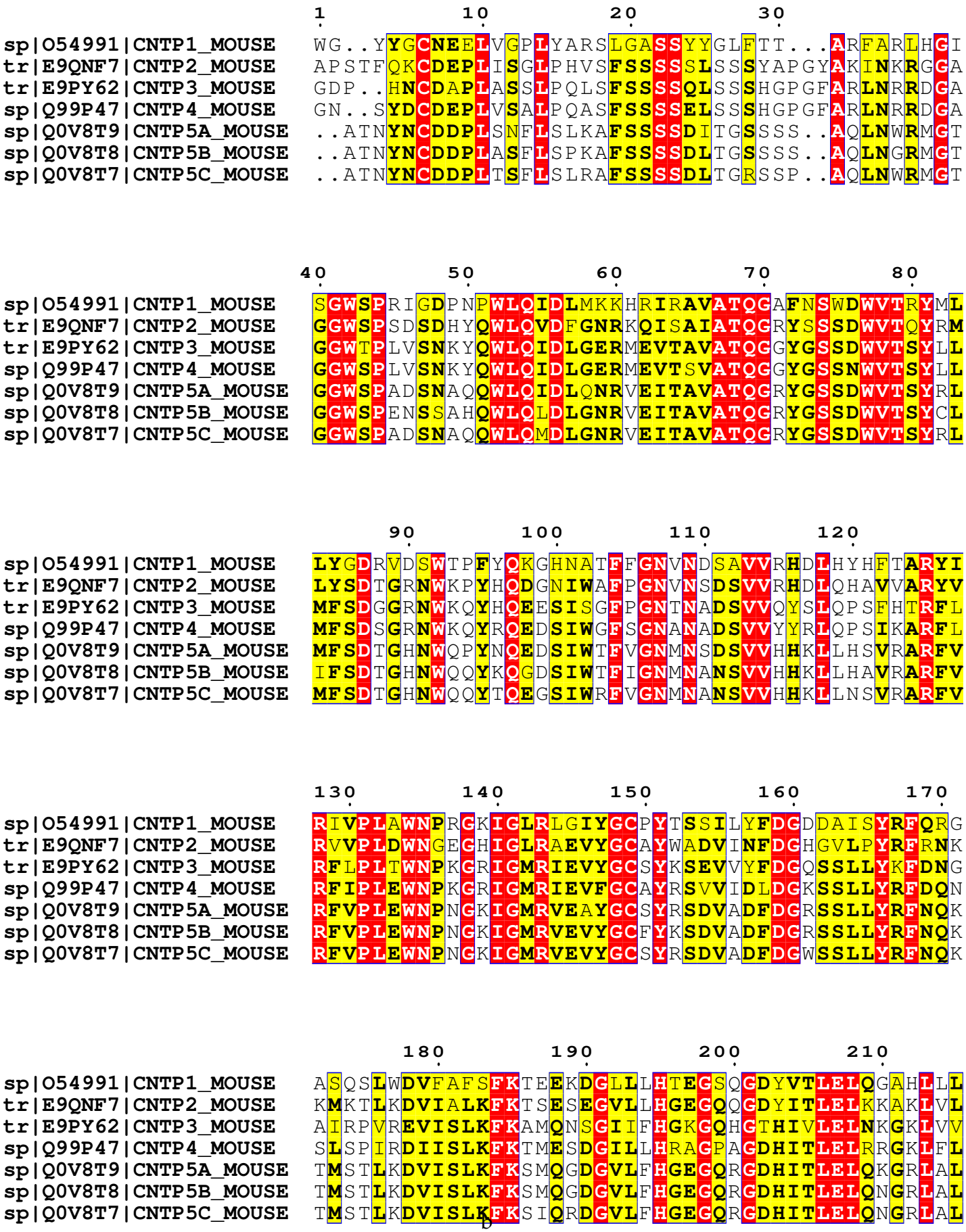
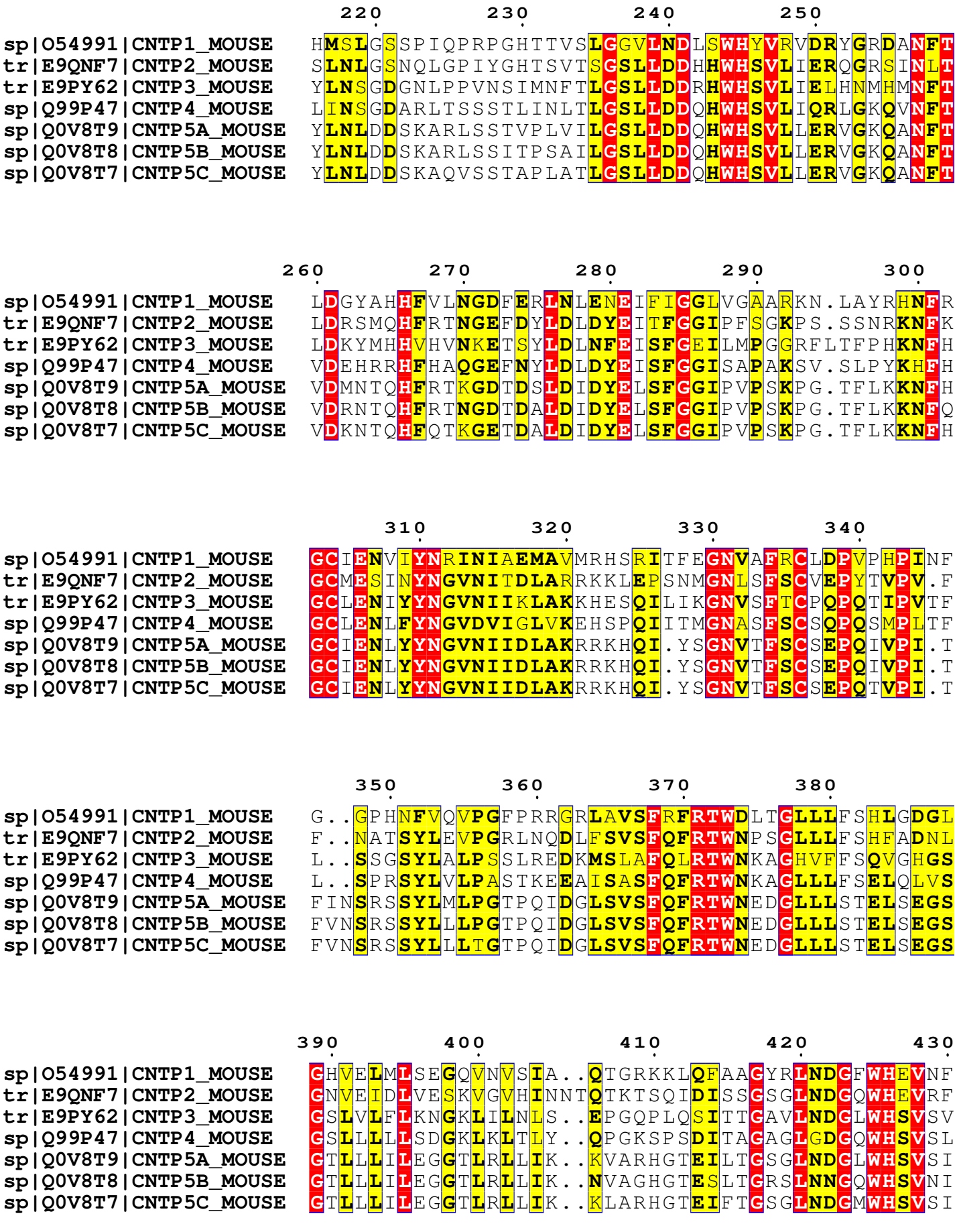
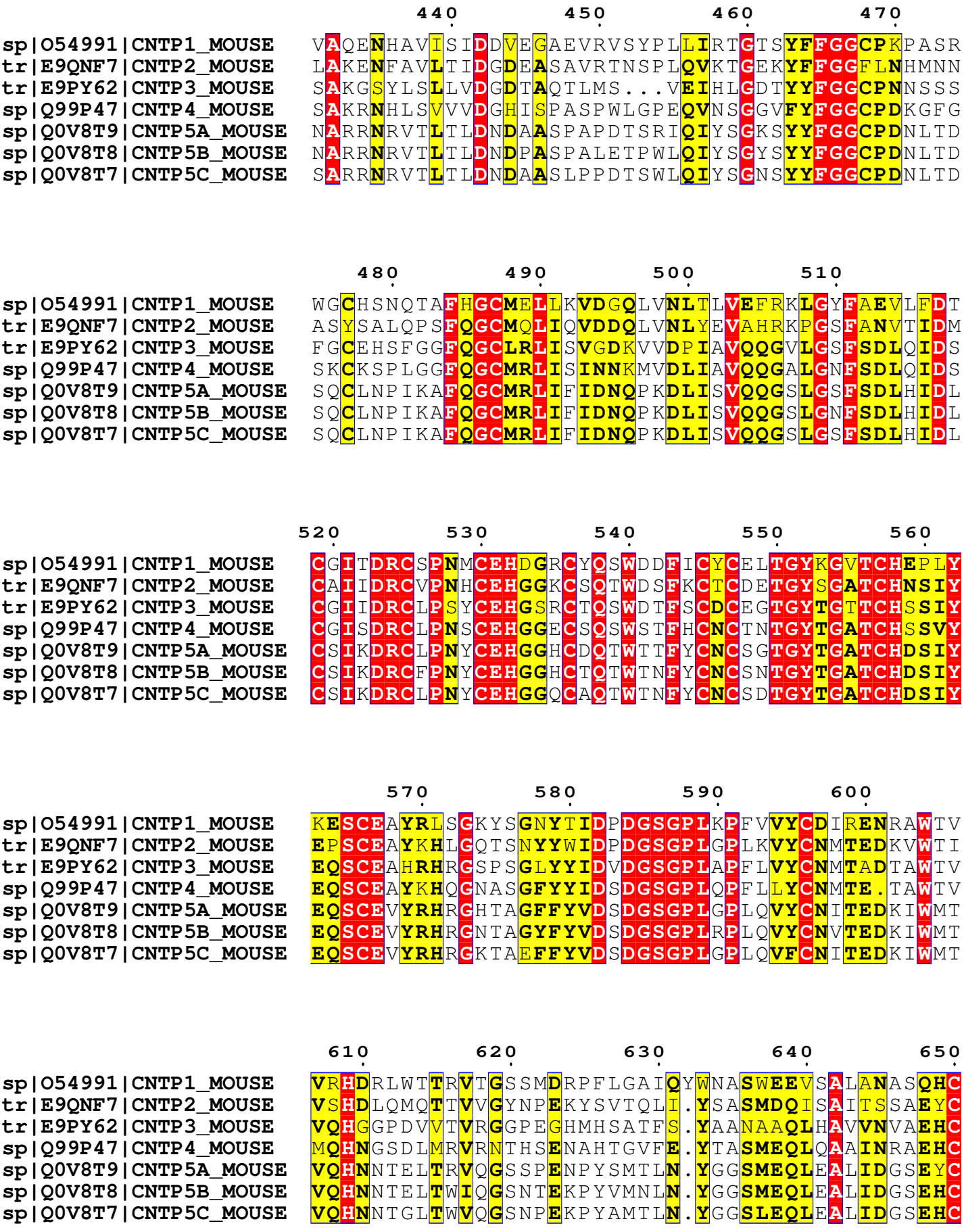
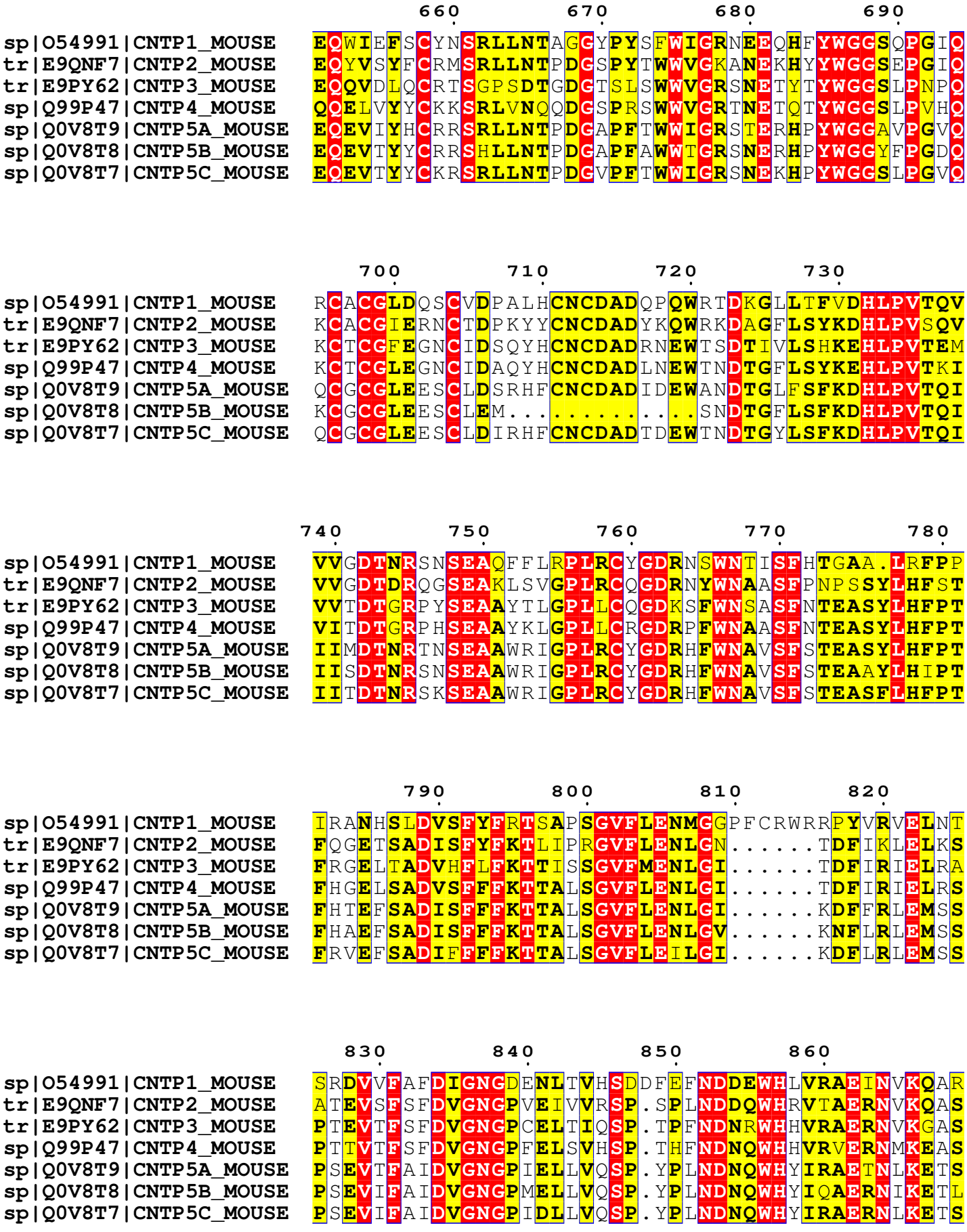
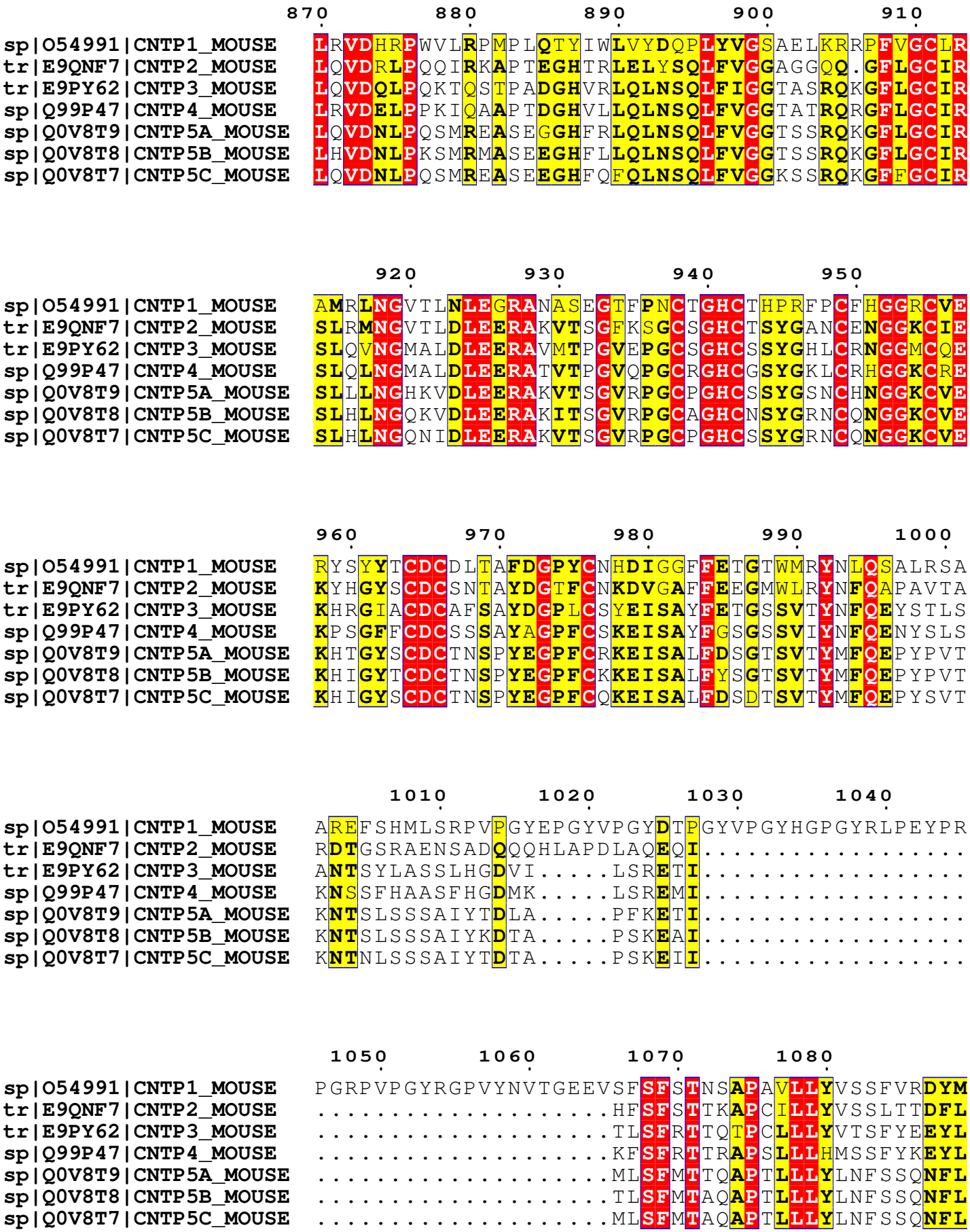


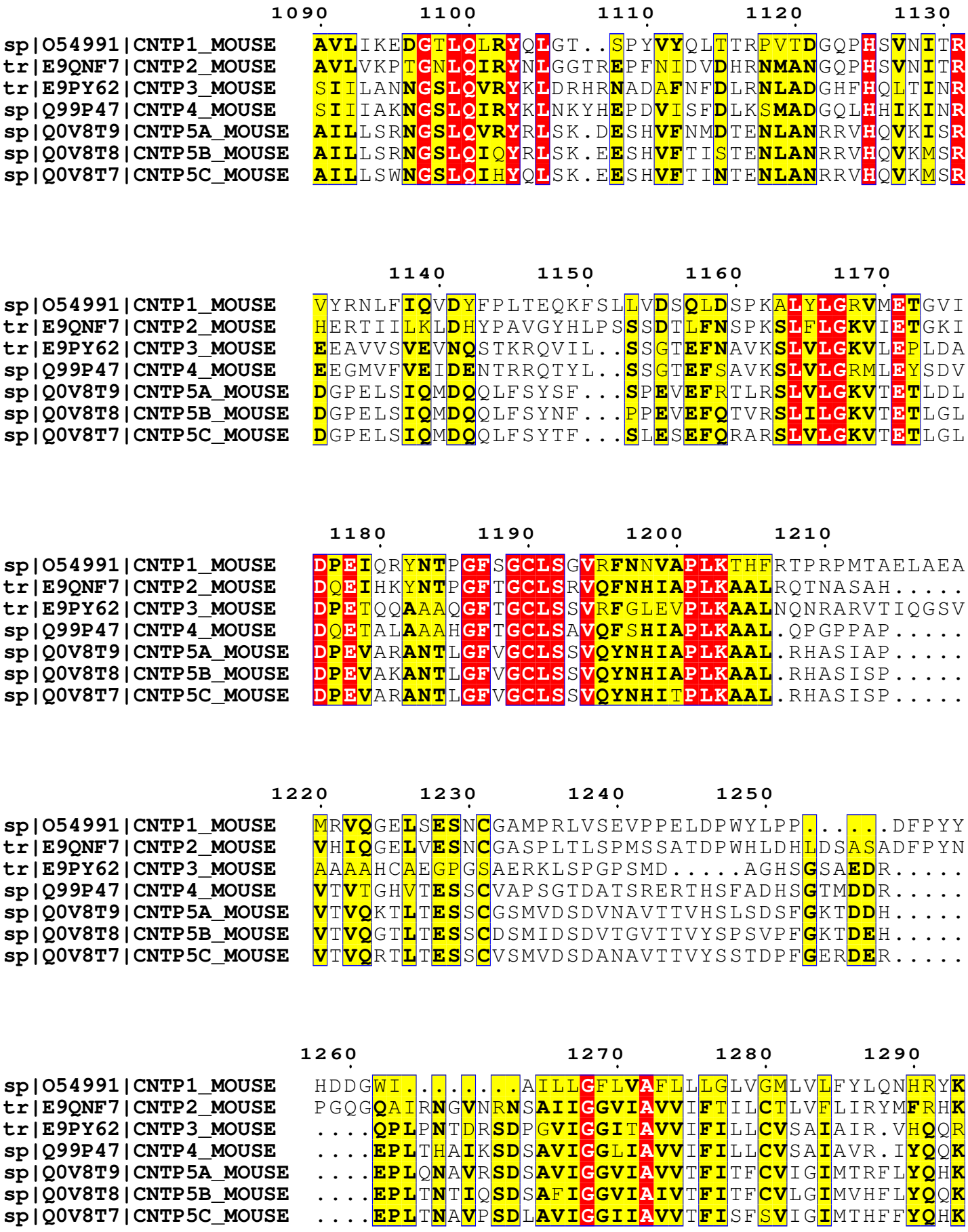
Figure A.1: Continued over the next 6 pages.


220 230 240 250
sp|O54991|CNTP1_MOUSE HMSLGSSPIQPRPGHTTVSLGGVLNDLSWHYVRVDRYGRDANFT
tr|E9QNF7|CNTP2_MOUSE SLNLGSNQLGPIYGHTSVTSGSLLDDHHWHSVLIERQGRSINLT
tr|E9PY62|CNTP3_MOUSE YLNSGDGNLPPVNSIMNFTLGSLLDDRHWHSVLIELHNMHMNFT
sp|Q99P47|CNTP4_MOUSE LINSGDARLTSSSTLINLTLGSLLDDQHWHSVLIQRLGKQVNFT
sp|Q0V8T9|CNTP5A_MOUSE YLNLDDSKARLSSTVPLVILGSLLDDQHWHSVLLERVGKQANFT
sp|Q0V8T8|CNTP5B_MOUSE YLNLDDSKARLSSITPSAILGSLLDDQHWHSVLLERVGKQANFT
sp|Q0V8T7|CNTP5C_MOUSE YLNLDDSKAQVSSTAPLATLGSLLDDQHWHSVLLERVGKQANFT
260 270 280 290 300
sp|O54991|CNTP1_MOUSE LDGYAHHFVLNGDFERLNLENEIFIGGLVGAARKN.LAYRHNFR
tr|E9QNF7|CNTP2_MOUSE LDRSMQHFRTNGEFDYLDLDYEITFGGIPFSGKPS.SSNRKNFK
tr|E9PY62|CNTP3_MOUSE LDKYMHHVHVNKETSYLDLNFEISFGEILMPGGRFLTFPHKNFH
sp|Q99P47|CNTP4_MOUSE VDEHRRHFHAQGEFNYLDLDYEISFGGISAPAKSV.SLPYKHFH
sp|Q0V8T9|CNTP5A_MOUSE VDMNTQHFRTKGDTDSLDIDYELSFGGIPVPSKPG.TFLKKNFH
sp|Q0V8T8|CNTP5B_MOUSE VDRNTQHFRTNGDTDALDIDYELSFGGIPVPSKPG.TFLKKNFQ
sp|Q0V8T7|CNTP5C_MOUSE VDKNTQHFQTKGETDALDIDYELSFGGIPVPSKPG.TFLKKNFH
310 320 330 340
sp|O54991|CNTP1_MOUSE GCIENVIYNRINIAEMAVMRHSRITFEGNVAFRCLDPVPHPINF
tr|E9QNF7|CNTP2_MOUSE GCMESINYNGVNITDLARRKKLEPSNMGNLSFSCVEPYTVPV.F
tr|E9PY62|CNTP3_MOUSE GCLENIYYNGVNIIKLAKKHESQILIKGNVSFTCPQPQTIPVTF
sp|Q99P47|CNTP4_MOUSE GCLENLFYNGVDVIGLVKEHSPQIITMGNASFSCSQPQSMPLTF
sp|Q0V8T9|CNTP5A_MOUSE GCIENLYYNGVNIIDLAKRRKHQI.YSGNVTFSCSEPQIVPI.T
sp|Q0V8T8|CNTP5B_MOUSE GCIENLYYNGVNIIDLAKRRKHQI.YSGNVTFSCSEPQIVPI.T
sp|Q0V8T7|CNTP5C_MOUSE GCIENLYYNGVNIIDLAKRRKHQI.YSGNVTFSCSEPQTVPI.T
350 360 370 380
sp|O54991|CNTP1_MOUSE G..GPHNFVQVPGFPRRGRLAVSFRFRTWDLTGLLLFSHLGDGL
tr|E9QNF7|CNTP2_MOUSE F..NATSYLEVPGRLNQDLFSVSFQFRTWNPSGLLLFSHFADNL
tr|E9PY62|CNTP3_MOUSE L..SSGSYLALPSSLREDKMSLAFQLRTWNKAGHVFFSQVGHGS
sp|Q99P47|CNTP4_MOUSE L..SPRSYLVLPASTKEEAISASFQFRTWNKAGLLLFSELQLVS
sp|Q0V8T9|CNTP5A_MOUSE FINSRSSYLMLPGTPQIDGLSVSFQFRTWNEDGLLLSTELSEGS
sp|Q0V8T8|CNTP5B_MOUSE FVNSRSSYLLLPGTPQIDGLSVSFQFRTWNEDGLLLSTELSEGS
sp|Q0V8T7|CNTP5C_MOUSE FVNSRSSYLLLTGTPQIDGLSVSFQFRTWNEDGLLLSTELSEGS
390 400 410 420 430
sp|O54991|CNTP1_MOUSE GHVELMLSEGQVNVSIA..QTGRKKLQFAAGYRLNDGFWHEVNF
tr|E9QNF7|CNTP2_MOUSE GNVEIDLVESKVGVHINNTQTKTSQIDISSGSGLNDGQWHEVRF
tr|E9PY62|CNTP3_MOUSE GSLVLFLKNGKLILNLS..EPGQPLQSITTGAVLNDGLWHSVSV
sp|Q99P47|CNTP4_MOUSE GSLLLLLSDGKLKLTLY..QPGKSPSDITAGAGLGDGQWHSVSL
sp|Q0V8T9|CNTP5A_MOUSE GTLLLILEGGTLRLLIK..KVARHGTEILTGSGLNDGLWHSVSI
sp|Q0V8T8|CNTP5B_MOUSE GTLLLILEGGTLRLLIK..NVAGHGTESLTGRSLNNGQWHSVNI
sp|Q0V8T7|CNTP5C_MOUSE GTLLLILEGGTLRLLIK..KLARHGTEIFTGSGLNDGMWHSVSI


440 450 460 470
sp|O54991|CNTP1_MOUSE VAQENHAVISIDDVEGAEVRVSYPLLIRTGTSYFFGGCPKPASR
tr|E9QNF7|CNTP2_MOUSE LAKENFAVLTIDGDEASAVRTNSPLQVKTGEKYFFGGFLNHMNN
tr|E9PY62|CNTP3_MOUSE SAKGSYLSLLVDGDTAQTLMS...VEIHLGDTYYFGGCPNNSSS
sp|Q99P47|CNTP4_MOUSE SAKRNHLSVVVDGHISPASPWLGPEQVNSGGVFYFGGCPDKGFG
sp|Q0V8T9|CNTP5A_MOUSE NARRNRVTLTLDNDAASPAPDTSRIQIYSGKSYYFGGCPDNLTD
sp|Q0V8T8|CNTP5B_MOUSE NARRNRVTLTLDNDPASPALETPWLQIYSGYSYYFGGCPDNLTD
sp|Q0V8T7|CNTP5C_MOUSE SARRNRVTLTLDNDAASLPPDTSWLQIYSGNSYYFGGCPDNLTD
480 490 500 510
sp|O54991|CNTP1_MOUSE WGCHSNQTAFHGCMELLKVDGQLVNLTLVEFRKLGYFAEVLFDT
tr|E9QNF7|CNTP2_MOUSE ASYSALQPSFQGCMQLIQVDDQLVNLYEVAHRKPGSFANVTIDM
tr|E9PY62|CNTP3_MOUSE FGCEHSFGGFQGCLRLISVGDKVVDPIAVQQGVLGSFSDLQIDS
sp|Q99P47|CNTP4_MOUSE SKCKSPLGGFQGCMRLISINNKMVDLIAVQQGALGNFSDLQIDS
sp|Q0V8T9|CNTP5A_MOUSE SQCLNPIKAFQGCMRLIFIDNQPKDLISVQQGSLGSFSDLHIDL
sp|Q0V8T8|CNTP5B_MOUSE SQCLNPIKAFQGCMRLIFIDNQPKDLISVQQGSLGNFSDLHIDL
sp|Q0V8T7|CNTP5C_MOUSE SQCLNPIKAFQGCMRLIFIDNQPKDLISVQQGSLGSFSDLHIDL
520 530 540 550 560
sp|O54991|CNTP1_MOUSE CGITDRCSPNMCEHDGRCYQSWDDFICYCELTGYKGVTCHEPLY
tr|E9QNF7|CNTP2_MOUSE CAIIDRCVPNHCEHGGKCSQTWDSFKCTCDETGYSGATCHNSIY
tr|E9PY62|CNTP3_MOUSE CGIIDRCLPSYCEHGSRCTQSWDTFSCDCEGTGYTGTTCHSSIY
sp|Q99P47|CNTP4_MOUSE CGISDRCLPNSCEHGGECSQSWSTFHCNCTNTGYTGATCHSSVY
sp|Q0V8T9|CNTP5A_MOUSE CSIKDRCLPNYCEHGGHCDQTWTTFYCNCSGTGYTGATCHDSIY
sp|Q0V8T8|CNTP5B_MOUSE CSIKDRCFPNYCEHGGHCTQTWTNFYCNCSNTGYTGATCHDSIY
sp|Q0V8T7|CNTP5C_MOUSE CSIKDRCLPNYCEHGGQCAQTWTNFYCNCSDTGYTGATCHDSIY
570 580 590 600
sp|O54991|CNTP1_MOUSE KESCEAYRLSGKYSGNYTIDPDGSGPLKPFVVYCDIRENRAWTV
tr|E9QNF7|CNTP2_MOUSE EPSCEAYKHLGQTSNYYWIDPDGSGPLGPLKVYCNMTEDKVWTI
tr|E9PY62|CNTP3_MOUSE EQSCEAHRHRGSPSGLYYIDVDGSGPLAPFLVYCNMTADTAWTV
sp|Q99P47|CNTP4_MOUSE EQSCEAYKHQGNASGFYYIDSDGSGPLQPFLLYCNMTE.TAWTV
sp|Q0V8T9|CNTP5A_MOUSE EQSCEVYRHRGHTAGFFYVDSDGSGPLGPLQVYCNITEDKIWMT
sp|Q0V8T8|CNTP5B_MOUSE EQSCEVYRHRGNTAGYFYVDSDGSGPLRPLQVYCNVTEDKIWMT
sp|Q0V8T7|CNTP5C_MOUSE EQSCEVYRHRGKTAEFFYVDSDGSGPLGPLQVFCNITEDKIWMT
610 620 630 640 650
sp|O54991|CNTP1_MOUSE VRHDRLWTTRVTGSSMDRPFLGAIQYWNASWEEVSALANASQHC
tr|E9QNF7|CNTP2_MOUSE VSHDLQMQTTVVGYNPEKYSVTQLI.YSASMDQISAITSSAEYC
tr|E9PY62|CNTP3_MOUSE VQHGGPDVVTVRGGPEGHMHSATFS.YAANAAQLHAVVNVAEHC
sp|Q99P47|CNTP4_MOUSE MQHNGSDLMRVRNTHSENAHTGVFE.YTASMEQLQAAINRAEHC
sp|Q0V8T9|CNTP5A_MOUSE VQHNNTELTRVQGSSPENPYSMTLN.YGGSMEQLEALIDGSEYC
sp|Q0V8T8|CNTP5B_MOUSE VQHNNTELTWIQGSNTEKPYVMNLN.YGGSMEQLEALIDGSEHC
sp|Q0V8T7|CNTP5C_MOUSE VQHNNTGLTWVQGSNPEKPYAMTLN.YGGSLEQLEALIDGSEHC


660 670 680 690
sp|O54991|CNTP1_MOUSE EQWIEFSCYNSRLLNTAGGYPYSFWIGRNEEQHFYWGGSQPGIQ
tr|E9QNF7|CNTP2_MOUSE EQYVSYFCRMSRLLNTPDGSPYTWWVGKANEKHYYWGGSEPGIQ
tr|E9PY62|CNTP3_MOUSE EQQVDLQCRTSGPSDTGDGTSLSWWVGRSNETYTYWGGSLPNPQ
sp|Q99P47|CNTP4_MOUSE QQELVYYCKKSRLVNQQDGSPRSWWVGRTNETQTYWGGSLPVHQ
sp|Q0V8T9|CNTP5A_MOUSE EQEVIYHCRRSRLLNTPDGAPFTWWIGRSTERHPYWGGAVPGVQ
sp|Q0V8T8|CNTP5B_MOUSE EQEVTYYCRRSHLLNTPDGAPFAWWTGRSNERHPYWGGYFPGDQ
sp|Q0V8T7|CNTP5C_MOUSE EQEVTYYCKRSRLLNTPDGVPFTWWIGRSNEKHPYWGGSLPGVQ
700 710 720 730
sp|O54991|CNTP1_MOUSE RCACGLDQSCVDPALHCNCDADQPQWRTDKGLLTFVDHLPVTQV
tr|E9QNF7|CNTP2_MOUSE KCACGIERNCTDPKYYCNCDADYKQWRKDAGFLSYKDHLPVSQV
tr|E9PY62|CNTP3_MOUSE KCTCGFEGNCIDSQYHCNCDADRNEWTSDTIVLSHKEHLPVTEM
sp|Q99P47|CNTP4_MOUSE KCTCGLEGNCIDAQYHCNCDADLNEWTNDTGFLSYKEHLPVTKI
sp|Q0V8T9|CNTP5A_MOUSE QCGCGLEESCLDSRHFCNCDADIDEWANDTGLFSFKDHLPVTQI
sp|Q0V8T8|CNTP5B_MOUSE KCGCGLEESCLEM.....SNDTGFLSFKDHLPVTQI
sp|Q0V8T7|CNTP5C_MOUSE QCGCGLEESCLDIRHFCNCDADTDEWTNDTGYLSFKDHLPVTQI
740 750 760 770 780
sp|O54991|CNTP1_MOUSE VVGDTNRSNSEAQFFLRPLRCYGDRNSWNTISFHTGAA.LRFPP
tr|E9QNF7|CNTP2_MOUSE VVGDTDRQGSEAKLSVGPLRCQGDRNYWNAASFPNPSSYLHFST
tr|E9PY62|CNTP3_MOUSE VVTDTGRPYSEAAYTLGPLLCQGDKSFWNSASFNTEASYLHFPT
sp|Q99P47|CNTP4_MOUSE VITDTGRPHSEAAYKLGPLLCRGDRPFWNAASFNTEASYLHFPT
sp|Q0V8T9|CNTP5A_MOUSE IIMDTNRTNSEAAWRIGPLRCYGDRHFWNAVSFSTEASYLHFPT
sp|Q0V8T8|CNTP5B_MOUSE IISDTNRSNSEAAWRIGPLRCYGDRHFWNAVSFSTEAAYLHIPT
sp|Q0V8T7|CNTP5C_MOUSE IITDTNRSKSEAAWRIGPLRCYGDRHFWNAVSFSTEASFLHFPT
790 800 810 820
sp|O54991|CNTP1_MOUSE IRANHSLDVSFYFRTSAPSGVFLENMGGPFCRWRRPYVRVELNT
tr|E9QNF7|CNTP2_MOUSE FQGETSADISFYFKTLIPRGVFLENLGN.....TDFIKLELKS
tr|E9PY62|CNTP3_MOUSE FRGELTADVHFLFKTTISSGVFMENLGI.....TDFIRIELRA
sp|Q99P47|CNTP4_MOUSE FHGELSADVSFFFKTTALSGVFLENLGI.....TDFIRIELRS
sp|Q0V8T9|CNTP5A_MOUSE FHTEFSADISFFFKTTALSGVFLENLGI.....KDFFRLEMSS
sp|Q0V8T8|CNTP5B_MOUSE FHAEFSADISFFFKTTALSGVFLENLGV.....KNFLRLEMSS
sp|Q0V8T7|CNTP5C_MOUSE FRVEFSADIFFFFKTTALSGVFLEILGI.....KDFLRLEMSS
830 840 850 860
sp|O54991|CNTP1_MOUSE SRDVVFAFDIGNGDENLTVHSDDFEFNDDEWHLVRAEINVKQAR
tr|E9QNF7|CNTP2_MOUSE ATEVSFSFDVGNGPVEIVVRSP.SPLNDDQWHRVTAERNVKQAS
tr|E9PY62|CNTP3_MOUSE PTEVTFSFDVGNGPCELTIQSP.TPFNDNRWHHVRAERNVKGAS
sp|Q99P47|CNTP4_MOUSE PTTVTFSFDVGNGPFELSVHSP.THFNDNQWHHVRVERNMKEAS
sp|Q0V8T9|CNTP5A_MOUSE PSEVTFAIDVGNGPIELLVQSP.YPLNDNQWHYIRAETNLKETS
sp|Q0V8T8|CNTP5B_MOUSE PSEVIFAIDVGNGPMELLVQSP.YPLNDNQWHYIQAERNIKETL
sp|Q0V8T7|CNTP5C_MOUSE PSEVIFAIDVGNGPIDLLVQSP.YPLNDNQWHYIRAERNLKETS


870 880 890 900 910
sp|O54991|CNTP1_MOUSE LRVDHRPWVLRPMPLQTYIWLVYDQPLYVGSAELKRRPFVGCLR
tr|E9QNF7|CNTP2_MOUSE LQVDRLPQQIRKAPTEGHTRLELYSQLFVGGAGGQQ.GFLGCIR
tr|E9PY62|CNTP3_MOUSE LQVDQLPQKTQSTPADGHVRLQLNSQLFIGGTASRQKGFLGCIR
sp|Q99P47|CNTP4_MOUSE LRVDELPPKIQAAPTDGHVLLQLNSQLFVGGTATRQRGFLGCIR
sp|Q0V8T9|CNTP5A_MOUSE LQVDNLPQSMREASEGGHFRLQLNSQLFVGGTSSRQKGFLGCIR
sp|Q0V8T8|CNTP5B_MOUSE LHVDNLPKSMRMASEEGHFLLQLNSQLFVGGTSSRQKGFLGCIR
sp|Q0V8T7|CNTP5C_MOUSE LQVDNLPQSMREASEEGHFQFQLNSQLFVGGKSSRQKGFFGCIR
920 930 940 950
sp|O54991|CNTP1_MOUSE AMRLNGVTLNLEGRANASEGTFPNCTGHCTHPRFPCFHGGRCVE
tr|E9QNF7|CNTP2_MOUSE SLRMNGVTLDLEERAKVTSGFKSGCSGHCTSYGANCENGGKCIE
tr|E9PY62|CNTP3_MOUSE SLQVNGMALDLEERAVMTPGVEPGCSGHCSSYGHLCRNGGMCQE
sp|Q99P47|CNTP4_MOUSE SLQLNGMALDLEERATVTPGVQPGCRGHCGSYGKLCRHGGKCRE
sp|Q0V8T9|CNTP5A_MOUSE SLLLNGHKVDLEERAKVTSGVRPGCPGHCSSYGSNCHNGGKCVE
sp|Q0V8T8|CNTP5B_MOUSE SLHLNGQKVDLEERAKITSGVRPGCAGHCNSYGRNCQNGGKCVE
sp|Q0V8T7|CNTP5C_MOUSE SLHLNGQNIDLEERAKVTSGVRPGCPGHCSSYGRNCQNGGKCVE
960 970 980 990 1000
sp|O54991|CNTP1_MOUSE RYSYYTCDCDLTAFDGPYCNHDIGGFFETGTWMRYNLQSALRSA
tr|E9QNF7|CNTP2_MOUSE KYHGYSCDCSNTAYDGTFCNKDVGAFFEEGMWLRYNFQAPAVTA
tr|E9PY62|CNTP3_MOUSE KHRGIACDCAFSAYDGPLCSYEISAYFETGSSVTYNFQEYSTLS
sp|Q99P47|CNTP4_MOUSE KPSGFFCDCSSSAYAGPFCSKEISAYFGSGSSVIYNFQENYSLS
sp|Q0V8T9|CNTP5A_MOUSE KHTGYSCDCTNSPYEGPFCRKEISALFDSGTSVTYMFQEPYPVT
sp|Q0V8T8|CNTP5B_MOUSE KHIGYTCDCTNSPYEGPFCKKEISALFYSGTSVTYMFQEPYPVT
sp|Q0V8T7|CNTP5C_MOUSE KHIGYSCDCTNSPYEGPFCQKEISALFDSDTSVTYMFQEPYSVT
1010 1020 1030 1040
sp|O54991|CNTP1_MOUSE ARFSHMLSRPVPGYEPGYVPGYDTPGYVPGYHGPGYRLPEYPR
tr|E9QNF7|CNTP2_MOUSE RDTGSRAENSADQQQHLAPDLAQEQI.....
tr|E9PY62|CNTP3_MOUSE ANTSYLASSLHGDVI.....LSRETI.....
sp|Q99P47|CNTP4_MOUSE KNSSFHAASFHGDMK.....LSREMI.....
sp|Q0V8T9|CNTP5A_MOUSE KNTSLSSSAIYTDLA.....PFKETI.....
sp|Q0V8T8|CNTP5B_MOUSE KNTSLSSSAIYKDTA.....PSKEAI.....
sp|Q0V8T7|CNTP5C_MOUSE KNTNLSSSAIYTDTA.....PSKEII.....
1050 1060 1070 1080
sp|O54991|CNTP1_MOUSE PGRPVPGYRGPVYNVTGEEVSFSFSTNSAPAVLLYVSSFVRDYM
tr|E9QNF7|CNTP2_MOUSE .....HFSFSTTKAPCILLYVSSLTTDFL
tr|E9PY62|CNTP3_MOUSE .....TLSFRTTQTPCLLLYVTSFYEEYL
sp|Q99P47|CNTP4_MOUSE .....KFSFRTTRAPSLLLHMSSFYKEYL
sp|Q0V8T9|CNTP5A_MOUSE .....MLSFMTTQAPTLLLYLNFSSQNFL
sp|Q0V8T8|CNTP5B_MOUSE .....TLSFMTAQAPTLLLYLNFSSQNFL
sp|Q0V8T7|CNTP5C_MOUSE .....MLSFMTAQAPTLLLYLNFSSQNFL


1090 1100 1110 1120 1130
sp|O54991|CNTP1_MOUSE AVLIKEDGTLQLRYQLGT..SPYVYQLTTRPVTDGQPHSVNITR
tr|E9QNF7|CNTP2_MOUSE AVLVKPTGNLQIRYNLGGTREPFNIDVDHRNMANGQPHSVNITR
tr|E9PY62|CNTP3_MOUSE SIILANNGSLQVRYKLDRHRNADAFNFDLRNLADGHFHQLTINR
sp|Q99P47|CNTP4_MOUSE SIIIAKNGSLQIRYKLNKYHEPDVISFDLKSMADGQLHHIKINR
sp|Q0V8T9|CNTP5A_MOUSE AILLSRNGSLQVRYRLSK.DESHVFNMDTENLANRRVHQVKISR
sp|Q0V8T8|CNTP5B_MOUSE AILLSRNGSLQIQYRLSK.EESHVFTISTENLANRRVHQVKMSR
sp|Q0V8T7|CNTP5C_MOUSE AILLSWNGSLQIHYQLSK.EESHVFTINTENLANRRVHQVKMSR
1140 1150 1160 1170
sp|O54991|CNTP1_MOUSE VYRNLFIQVDYFPLTEQKFSLLVDSQLDSPKALYLGRVMETGVI
tr|E9QNF7|CNTP2_MOUSE HERTIILKLDHYPAVGYHLPSSSDTLFNSPKSLFLGKVIETGKI
tr|E9PY62|CNTP3_MOUSE EEAVVSVEVNQSTKRQVIL..SSGTEFNAVKSLVLGKVLEPLDA
sp|Q99P47|CNTP4_MOUSE EEGMVFVEIDENTRRQTYL..SSGTEFSAVKSLVLGRMLEYSDV
sp|Q0V8T9|CNTP5A_MOUSE DGPELSIQMDQQLFSYSF...SPEVEFRTLRSLVLGKVTETLDL
sp|Q0V8T8|CNTP5B_MOUSE DGPELSIQMDQQLFSYNF...PPEVEFQTVRSLILGKVTETLGL
sp|Q0V8T7|CNTP5C_MOUSE DGPELSIQMDQQLFSYTF...SLESEFQRARSLVLGKVTETLGL
1180 1190 1200 1210
sp|O54991|CNTP1_MOUSE DPEIQRYNTPGFSGCLSGVRFNNVAPLKTHFRTPRPMTAELAEA
tr|E9QNF7|CNTP2_MOUSE DQEIHKYNTPGFTGCLSRVQFNHIAPLKAALRQTNASAH.....
tr|E9PY62|CNTP3_MOUSE DPETQQAAAQGFTGCLSSVRFGLEVPLKAALNQNRARVTIQGSV
sp|Q99P47|CNTP4_MOUSE DQETALAAAHGFTGCLSAVQFSHIAPLKAAL.QPGPPAP.....
sp|Q0V8T9|CNTP5A_MOUSE DPEVARANTLGFVGCLSSVQYNHIAPLKAAL.RHASIAP.....
sp|Q0V8T8|CNTP5B_MOUSE DPEVAKANTLGFVGCLSSVQYNHIAPLKAAL.RHASISP.....
sp|Q0V8T7|CNTP5C_MOUSE DPEVARANTLGFVGCLSSVQYNHITPLKAAL.RHASISP.....
1220 1230 1240 1250
sp|O54991|CNTP1_MOUSE MRVQGELSESNCGAMPRLVSEVPPELDPWYLPP.....DFPYY
tr|E9QNF7|CNTP2_MOUSE VHIQGELVESNCGASPLTLSPMSSATDPWHLDHLDSASADFPYN
tr|E9PY62|CNTP3_MOUSE AAAAHCAEGPGSAERKLSPGPSMD.....AGHSGSAEDR.....
sp|Q99P47|CNTP4_MOUSE VTVTGHVTESSCVAPSGTDATSRERTHSFADHSGTMDDR.....
sp|Q0V8T9|CNTP5A_MOUSE VTVQKTLTESSCGSMVDSDVNAVTTVHSLSDSFGKTDDH.....
sp|Q0V8T8|CNTP5B_MOUSE VTVQGTLTESSCDSMIDSDVTGVTTVYSPSVPFGKTDEH.....
sp|Q0V8T7|CNTP5C_MOUSE VTVQRTLTESSCVSMVDSDANAVTTVYSSTDPFGERDER.....
1260 1270 1280 1290
sp|O54991|CNTP1_MOUSE HDDGWI.....AILLGFLVAFLLLGLVGMLVLFYLQNHRYK
tr|E9QNF7|CNTP2_MOUSE PGQGQAIRNGVNRNSAIIGGVIAVVIFTILCTLVFLIRYMFRHK
tr|E9PY62|CNTP3_MOUSE ....QPLPNTDRSDPGVIGGITAVVIFILLCVSAIAIR.VHQQR
sp|Q99P47|CNTP4_MOUSE ....EPLTHAIKSDSAVIGGLIAVVIFILLCVSAIAVR.IYQQK
sp|Q0V8T9|CNTP5A_MOUSE ....EPLQNAVRSDSAVIGGVIAVVTFITFCVIGIMTRFLYQHK
sp|Q0V8T8|CNTP5B_MOUSE ....EPLTNTIQSDSAFIGGVIAIVTFITFCVLGIMVHFLYQQK
sp|Q0V8T7|CNTP5C_MOUSE ....EPLTNAVPSDLAVIGGIIAVVTFISFSVIGIMTHFFYQHK

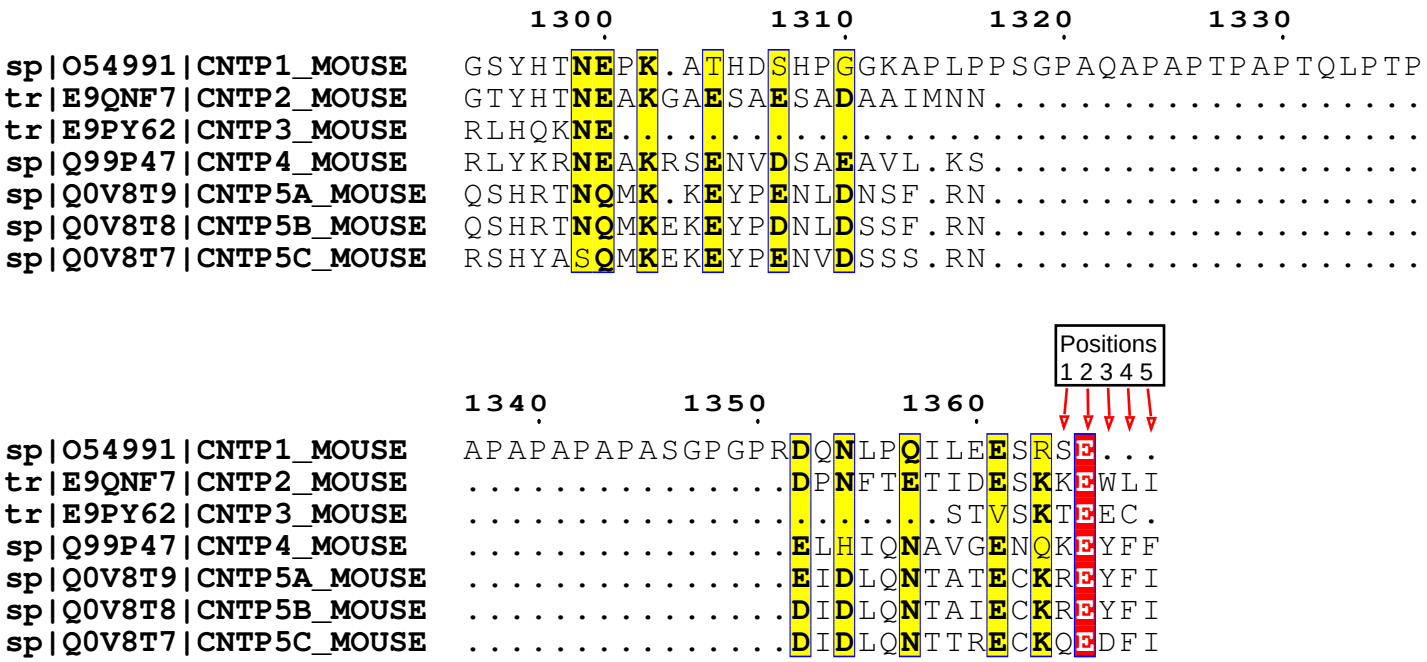


Figure A.1: Alignment of Caspr-family primary protein sequences. All sequences were obtained from Uniprot. The relevant Uniprot accession code for each sequence is provided in the second column from the left. Sequence alignments were calculated using DIALIGN and ESPript was used both to assess similarities between sequences and to generate the final image presented (ESPript global score = 0.7). Regions boxed in blue contain sequences that are either similar or strictly conserved. A yellow background indicates that, on average, residues are similar across all sequences. Within these regions, individual residues that are highly similar to each other are denoted by a bold, black font. Strictly conserved residues are shown in a white font on a red background. C-terminal positions 1-5, which are discussed in the main text in the context of the Caspr-family C-terminal PDZ-binding domain, are indicated with red arrows.

Appendix B: LC-MS/MS data

Details of the protein hits assigned to the *mus musculus* species during LC-MS/MS analysis of the pull-down experiment are presented below. All of the proteins that were detected are listed (in order of Mascot score, largest first). Table B.1 lists the proteins detected in the control condition, whilst Table B.2 lists the proteins detected when recombinant Caspr2 ECD was used as bait. Accession numbers are for the Uniprot database. The false discovery rate was set at 5%, thus individual matches were judged to be significant if $p<0.05$. p was the probability that a peptide spectra and protein fragment could be matched due to random chance. Significant distinct sequences are distinct sequences supported by at least one significant match.

Table B.1: Pull-down experiment LC-MS/MS data: bait = mock

accession #	Mascot score	total matches	total significant matches	total distinct sequences	total significant distinct sequences	coverage (%)	description
P99024	777	39	26	16	13	47.7	Tubulin beta-5 chain
P68372	759	41	21	17	12	46.5	Tubulin beta-4B chain
Q7TMM9	738	40	26	18	12	52.1	Tubulin beta-2A chain
Q9CWF2	723	39	26	18	12	52.1	Tubulin beta-2B chain
Q9D6F9	632	33	18	15	11	38.7	Tubulin beta-4A chain
Q9ERD7	630	34	22	15	11	42.9	Tubulin beta-3 chain
P14873	613	31	8	30	8	17.2	Microtubule-associated protein 1B
P60710	476	34	14	17	9	62.4	Actin, cytoplasmic 1
E9Q1F2	446	29	13	14	8	60.7	Actin, cytoplasmic 1
P68369	440	18	11	12	7	41.7	Tubulin alpha-1A chain
P05213	370	17	10	11	6	38.8	Tubulin alpha-1B chain
P05214	348	13	8	9	6	30.9	Tubulin alpha-3 chain
A0A1D5RLD8	329	13	8	8	5	31.2	Glyceraldehyde-3-phosphate dehydrogenase
Q9QYR6-2	325	23	6	23	6	9.3	Isoform 2 of Microtubule-associated protein 1A
P62631	325	14	9	8	6	22.5	Elongation factor 1-alpha 2
P10126	321	18	9	11	6	37.4	Elongation factor 1-alpha 1
P17182	309	13	6	11	6	34.6	Alpha-enolase
S4R1W1	294	12	7	7	4	32.4	Glyceraldehyde-3-phosphate dehydrogenase
Q922F4	292	22	8	13	5	38.3	Tubulin beta-6 chain
E9Q5F4	291	24	9	12	5	70.2	Actin, cytoplasmic 1 (Fragment)
S4R257	260	9	5	7	4	33.9	Glyceraldehyde-3-phosphate dehydrogenase (Fragment)

Continued on next page

Table B.1: Continued from the previous page

accession #	Mascot score	total matches	total significant matches	total distinct sequences	total significant distinct sequences	coverage (%)	description
Q6PHC1	258	11	5	9	5	35.8	Alpha-enolase
F6RT34	256	11	4	9	4	49.1	Myelin basic protein (Fragment)
D3YUT3	237	7	5	7	5	45.1	40S ribosomal protein S19 (Fragment)
P63268	230	19	8	8	5	19.9	Actin, gamma-enteric smooth muscle
B1ATY1	219	13	6	6	5	38.6	Actin, cytoplasmic 2
P62806	216	6	3	5	3	45.6	Histone H4
G3UZ07	213	20	6	10	4	50.4	Actin, cytoplasmic 2 (Fragment)
P04370	212	8	3	7	3	40	Myelin basic protein
Q8BFZ3	207	17	8	8	4	36.2	Beta-actin-like protein 2
Q9D8N0	196	6	3	5	2	13.3	Elongation factor 1-gamma
Q8QZT1	194	7	4	6	3	27.8	Acetyl-CoA acetyltransferase, mitochondrial
F8WGM8	191	10	5	5	4	45.7	Actin, cytoplasmic 2 (Fragment)
P04104	188	19	9	8	3	15.4	Keratin, type II cytoskeletal 1
P10854	188	10	4	7	3	58.7	Histone H2B type 1-M
A0A1D5RM76	181	10	9	3	2	37.7	Tubulin beta-3 chain
Q921R2	179	6	4	6	4	35	40S ribosomal protein S13
Q9JJZ2	176	7	3	5	3	18.5	Tubulin alpha-8 chain
D3Z5R8	173	7	4	7	4	41.5	40S ribosomal protein S19 (Fragment)
S4R223	164	4	4	4	4	36.1	40S ribosomal protein S19
P68368	163	10	4	7	3	31	Tubulin alpha-4A chain
P62751	163	5	3	5	3	26.9	60S ribosomal protein L23a
E9Q1Z0	161	10	6	4	2	9.5	Keratin 90

Continued on next page

Table B.1: Continued from the previous page

accession #	Mascot score	total matches	total significant matches	total distinct sequences	total significant distinct sequences	coverage (%)	description
A2AQ07	152	17	4	10	1	39	Tubulin beta-1 chain
Q6NXH9	147	8	6	4	2	8.9	Keratin, type II cytoskeletal 73
P25444	146	6	3	6	3	28.7	40S ribosomal protein S2
P62908	143	8	2	8	2	41.6	40S ribosomal protein S3
B0QZL1	142	9	2	7	2	48.9	Alpha-enolase (Fragment)
P16330	140	5	3	5	3	14.3	2,3-cyclic-nucleotide 3-phosphodiesterase
P04370-2	139	4	2	4	2	31.3	Isoform 2 of Myelin basic protein
A0A2R8VHF3	134	6	4	4	2	20.6	Tubulin alpha chain (Fragment)
P01029	134	9	2	9	2	9.1	Complement C4-B
Q8BP67	133	7	2	6	1	29.3	60S ribosomal protein L24
Q5SVI0	132	6	2	6	2	9.8	Calcium/calmodulin-dependent protein kinase type II subunit beta
A0A0U1RQ96	125	10	5	4	2	22.6	Actin, gamma-enteric smooth muscle (Fragment)
A0A0G2JFH2	122	16	1	15	1	16.2	Microtubule-associated protein (Fragment)
P97351	120	4	3	3	3	17	40S ribosomal protein S3a
P14115	117	4	2	4	2	27	60S ribosomal protein L27a
Q9JHU4	117	21	2	20	2	7.5	Cytoplasmic dynein 1 heavy chain 1
P50446	115	10	5	5	1	10.7	Keratin, type II cytoskeletal 6A
E9Q0F0	114	23	2	18	1	25.1	Keratin 78
D3YVC1	111	5	2	5	2	26.8	40S ribosomal protein S2 (Fragment)
P20357	111	15	1	15	1	11.2	Microtubule-associated protein 2
A0A0J9YUE9	108	9	2	8	2	21.9	Dynamin-1

Continued on next page

Table B.1: Continued from the previous page

accession #	Mascot score	total matches	total significant matches	total distinct sequences	total significant distinct sequences	coverage (%)	description
D3YV43	107	8	1	8	1	63.9	40S ribosomal protein S3
Q9Z2T6	106	5	3	3	1	6.9	Keratin, type II cuticular Hb5
Q6ZWX6	106	5	1	5	1	20.3	Eukaryotic translation initiation factor 2 subunit 1
A3KGU7	105	19	1	17	1	9.9	Spectrin alpha chain, non-erythrocytic 1
Q9CXW4	104	2	1	2	1	14.6	60S ribosomal protein L11
A2A513	104	12	4	5	1	16.6	Keratin, type I cytoskeletal 10
P24369	100	4	2	4	2	17.1	Peptidyl-prolyl cis-trans isomerase B
F6U7V1	100	31	1	31	1	13	Ryanodine receptor 2
A0A0N4SV66	100	3	2	3	2	27.8	Histone H2A
P62242	100	4	2	2	2	13.5	40S ribosomal protein S8
P67984	97	3	2	3	2	28.9	60S ribosomal protein L22
P60867	96	8	1	6	1	51.3	40S ribosomal protein S20
A0A2R8VHL8	94	5	1	5	1	32.9	Poly(rC)-binding protein 2 (Fragment)
A0A1L1SQA8	93	4	2	4	2	36.6	40S ribosomal protein S25
P62754	92	4	2	3	1	16.9	40S ribosomal protein S6
D3YZ68	91	8	2	5	2	44.2	Elongation factor 1-alpha 1 (Fragment)
E9PZ43	91	9	2	8	2	14.4	Microtubule-associated protein
P51410	91	3	1	3	1	23.4	60S ribosomal protein L9
P62702	90	5	1	5	1	27	40S ribosomal protein S4, X isoform
P07724	89	5	1	5	1	11.2	Serum albumin

Continued on next page

Table B.1: Continued from the previous page

accession #	Mascot score	total matches	total significant matches	total distinct sequences	total significant distinct sequences	coverage (%)	description
Q6PHZ2-5	88	7	1	7	1	19.9	Isoform 4 of Calcium/calmodulin-dependent protein kinase type II subunit delta
P39054-2	85	8	1	7	1	12.1	Isoform 2 of Dynamin-2
D3YZY0	83	11	3	5	2	20.4	Actin, gamma-enteric smooth muscle (Fragment)
E9Q1G8	81	6	1	6	1	14.4	Septin-7
Q6ZWN5	79	3	1	3	1	22.2	40S ribosomal protein S9
Q9Z1Q9	79	8	2	8	2	12.6	Valine-tRNA ligase
A0A0J9YTY0	79	3	1	3	1	9.6	Septin-11
D3YVU4	77	12	1	11	1	13.3	Lysine-specific demethylase 2B
Q6A078	76	19	1	18	1	11.4	Centrosomal protein of 290 kDa
Q8CGP0	74	4	1	3	1	29.4	Histone H2B type 3-B
D3YUQ9	73	4	1	3	1	24.9	Elongation factor 1-delta (Fragment)
S4R1N6	72	2	2	2	2	18.7	40S ribosomal protein S18
A0A0N4SV63	72	14	1	14	1	11	Dysferlin
Q8VED5	72	6	2	5	1	13	Keratin, type II cytoskeletal 79
P14131	71	2	2	2	2	9.6	40S ribosomal protein S16
Q60605	70	5	1	5	1	80.8	Myosin light polypeptide 6
E9Q606	68	9	2	5	2	57.3	Actin, cytoplasmic 1 (Fragment)
P63038	65	13	1	8	1	25.7	60 kDa heat shock protein, mitochondrial
V9GX06	64	4	3	1	1	6.6	Uncharacterized protein (Fragment)
A0A0A0MQC7	64	5	1	5	1	13.2	Microtubule-associated protein
Q6IFZ6	63	7	3	5	1	11.2	Keratin, type II cytoskeletal 1b

Continued on next page

Table B.1: Continued from the previous page

accession #	Mascot score	total matches	total significant matches	total distinct sequences	total significant distinct sequences	coverage (%)	description
B1ARR7	62	4	1	4	1	38.7	Alpha-enolase (Fragment)
Q9Z0N2	62	6	1	6	1	17.4	Eukaryotic translation initiation factor 2 subunit 3, Y-linked
Q8C0E9	62	7	1	7	1	20.8	PH and SEC7 domain-containing protein 3
A0A286YCW8	61	4	1	4	1	27	Calcium/calmodulin-dependent protein kinase type II subunit gamma (Fragment)
P02104	60	5	2	3	1	32	Hemoglobin subunit epsilon-Y2
A2AVA0	60	10	1	9	1	6.2	Sushi, von Willebrand factor type A, EGF and pentraxin domain-containing protein 1
G3X977	60	7	1	7	1	16.2	Inter-alpha trypsin inhibitor, heavy chain 2
P35979	60	4	1	3	1	21.2	60S ribosomal protein L12
Q91UZ1	59	7	1	7	1	11.3	Phosphoinositide phospholipase C
A0A140T8L3	59	2	1	2	1	8.6	Uncharacterized protein
P61514	57	1	1	1	1	19.6	60S ribosomal protein L37a
P62918	56	3	1	3	1	16.3	60S ribosomal protein L8
P70696	54	4	1	3	1	22	Histone H2B type 1-A
P27661	54	3	1	3	1	30.1	Histone H2AX
Q9R1T4-2	54	7	1	7	1	17.6	Isoform I of Septin-6
P62849-2	53	4	1	4	1	45.4	Isoform 2 of 40S ribosomal protein S24

Continued on next page

Table B.1: Continued from the previous page

accession #	Mascot score	total matches	total significant matches	total distinct sequences	total significant distinct sequences	coverage (%)	description
Q8VEK3-2	53	4	1	4	1	6.8	Isoform 2 of Heterogeneous nuclear ribonucleoprotein U
A0A0A6YWC8	53	2	1	2	1	7.3	Vimentin
A0A0U1RQ71	52	2	1	2	1	43.4	40S ribosomal protein S13
Q6P9N8	51	5	1	5	1	11.4	Trafficking protein, kinesin-binding 2
Q3UYR4	51	7	1	7	1	10.5	Espin-like protein
G3UZR1	50	2	1	1	1	28.8	Tubulin beta-5 chain (Fragment)
D3Z536	50	2	1	2	1	7.5	Uncharacterized protein
D3YTY6	49	2	1	2	1	9.9	Uncharacterized protein
G3UY93	49	7	1	7	1	10.8	Valine-tRNA ligase (Fragment)
P15864	49	2	1	2	1	9.4	Histone H1.2
Q6ZWZ7	48	4	1	4	1	30.4	60S ribosomal protein L17
A0A1B0GRR3	47	4	1	4	1	40	40S ribosomal protein S11
F6ZQN5	46	4	1	4	1	63.7	Coiled-coil domain-containing 24 (Fragment)
Q9D5N8	44	5	1	5	1	13.3	Spermidine/spermine N(1)-acetyltransferase-like protein 1
Q6ZWQ9	43	3	1	3	1	39.5	MCG5400
P43274	41	3	1	3	1	11.4	Histone H1.4
P62264	41	1	1	1	1	11.3	40S ribosomal protein S14
V9GXA7	40	2	1	2	1	19	Uncharacterized protein
A0A0R4J0J7	40	7	1	6	1	21.3	MAM domain-containing protein 2
B0R0C1	39	7	1	7	1	15.5	Myelin transcription factor 1
C0HKC8	39	6	1	6	1	18.5	Sperm motility kinase 3A
E9Q2D1	31	5	1	3	1	55.6	Actin, cytoplasmic 1 (Fragment)

Table B.2: Pull-down experiment LC-MS/MS data: bait = Caspr2 ECD

accession #	Mascot score	total matches	total significant matches	total distinct sequences	total significant distinct sequences	coverage (%)	description
P14873	967	42	18	36	14	25.4	Microtubule-associated protein 1B
Q9CWF2	714	47	29	19	13	56.6	Tubulin beta-2B chain
P99024	709	46	25	19	12	57.4	Tubulin beta-5 chain
P68372	665	42	17	18	10	55.7	Tubulin beta-4B chain
Q9CPW0	598	31	14	20	10	18.7	Contactin-associated protein-like 2
P11881-2	585	35	9	28	7	17.5	Isoform 2 of Inositol 1,4,5-trisphosphate receptor type 1
Q9D6F9	554	39	14	17	9	51.6	Tubulin beta-4A chain
Q9ERD7	552	42	20	16	9	43.6	Tubulin beta-3 chain
P63260	452	28	9	16	8	52.5	Actin, cytoplasmic 2
Q9JHU4	426	39	3	39	3	13.4	Cytoplasmic dynein 1 heavy chain 1
P05213	423	25	13	12	7	36.6	Tubulin alpha-1B chain
E9Q5F4	340	17	6	11	6	50.6	Actin, cytoplasmic 1 (Fragment)
P68134	339	20	7	12	6	37.7	Actin, alpha skeletal muscle
A2ARP8	337	24	6	20	6	9	Microtubule-associated protein 1A
E9Q1F2	331	19	7	10	6	50.8	Actin, cytoplasmic 1
Q922F4	329	28	8	13	4	37.4	Tubulin beta-6 chain
P05214	325	17	8	10	6	28.4	Tubulin alpha-3 chain
G3UZ07	260	15	5	9	5	43.3	Actin, cytoplasmic 2 (Fragment)
P04370-10	254	10	4	8	4	39.3	Isoform 10 of Myelin basic protein
A0A0G2JDN7	241	12	5	12	5	18.2	Microtubule-associated protein
P17182	238	12	3	12	3	44.7	Alpha-enolase
Q8BFZ3	234	13	4	9	4	37	Beta-actin-like protein 2
A0A0G2JFH2	216	17	4	16	4	13	Microtubule-associated protein (Fragment)

Continued on next page

Table B.2: Continued from the previous page

accession #	Mascot score	total matches	total significant matches	total distinct sequences	total significant distinct sequences	coverage (%)	description
F7A0B0	209	12	3	10	3	39.3	Myelin basic protein (Fragment)
A0A2R8VHF3	208	15	7	6	3	29.6	Tubulin alpha chain (Fragment)
P20357	208	16	3	16	3	14.7	Microtubule-associated protein 2
Q3UH59	208	18	3	18	3	14.4	Myosin-10
P01029	207	16	4	13	3	10.1	Complement C4-B
D3YUT3	199	5	4	5	4	34.6	40S ribosomal protein S19 (Fragment)
Q8QZT1	195	6	3	6	3	24.1	Acetyl-CoA acetyltransferase, mitochondrial
A0A1D5RLD8	188	9	5	6	4	25.8	Glyceraldehyde-3-phosphate dehydrogenase
P10126	185	12	1	10	1	32	Elongation factor 1-alpha 1
Q6PHC1	183	9	2	9	2	39.9	Alpha-enolase
P62806	183	7	3	6	3	46.6	Histone H4
Q6PIC6	180	12	2	11	2	18.1	Na^+/K^+-transporting ATPase subunit alpha-3
Q6ZWY9	178	4	2	4	2	29.4	Histone H2B type 1-C/E/G
G3UYG0	171	13	3	8	3	65.2	Actin, cytoplasmic 2
O55143	162	11	3	8	2	13.9	Sarcoplasmic/endoplasmic reticulum calcium ATPase 2
B1ATY1	159	14	4	6	3	48.4	Actin, cytoplasmic 2
A0A0A0MQA5	158	12	4	7	3	25.4	Tubulin alpha chain (Fragment)
G3UZR1	148	6	3	3	2	68.2	Tubulin beta-5 chain (Fragment)
A0A1D5RM76	145	16	11	4	2	41	Tubulin beta-3 chain

Continued on next page

Table B.2: Continued from the previous page

accession #	Mascot score	total matches	total significant matches	total distinct sequences	total significant distinct sequences	coverage (%)	description
D3YZY0	145	9	3	6	3	24.4	Actin, gamma-enteric smooth muscle (Fragment)
S4R257	143	8	4	5	3	26.4	Glyceraldehyde-3-phosphate dehydrogenase (Fragment)
A0A0G2JDY5	142	4	3	4	3	15	Microtubule-associated protein (Fragment)
S4R2F3	137	20	1	19	1	8.1	Ankyrin-2
Q8BP67	133	6	4	3	2	17.8	60S ribosomal protein L24
P04370-2	132	4	2	3	2	9.2	Isoform 2 of Myelin basic protein
Q8CGP0	126	5	1	5	1	52.4	Histone H2B type 3-B
Q64523	126	4	3	3	2	27.9	Histone H2A type 2-C
Q68FG2	124	17	1	17	1	12.8	Spectrin beta chain
D3YUG3	121	5	3	5	3	26.3	40S ribosomal protein S19 (Fragment)
P50446	120	8	3	6	1	14.5	Keratin, type II cytoskeletal 6A
A2AQ07	119	8	2	6	1	24.8	Tubulin beta-1 chain
P46460	117	8	1	7	1	9.9	Vesicle-fusing ATPase
G3X977	116	8	1	6	1	11.4	Inter-alpha trypsin inhibitor, heavy chain 2
A0A1D5RM20	115	7	2	5	2	26.5	Actin, alpha skeletal muscle (Fragment)
P39053-4	114	11	1	10	1	17.1	Isoform 4 of Dynamin-1
A0A0U1RQ96	112	4	2	3	2	16.4	Actin, gamma-enteric smooth muscle (Fragment)
O88935-1	111	7	3	7	3	22.8	Isoform Ib of Synapsin-1

Continued on next page

Table B.2: Continued from the previous page

accession #	Mascot score	total matches	total significant matches	total distinct sequences	total significant distinct sequences	coverage (%)	description
P62830	109	4	1	4	1	23.6	60S ribosomal protein L23
P04104	109	5	1	4	1	6	Keratin, type II cytoskeletal 1
F8WGM8	106	7	3	3	2	33.3	Actin, cytoplasmic 2 (Fragment)
Q9JJZ2	106	8	2	4	2	13.6	Tubulin alpha-8 chain
A0A140T8T4	106	6	3	5	2	35.4	Uncharacterized protein
S4R223	105	2	2	2	2	36.1	40S ribosomal protein S19
P62852	104	6	1	6	1	39.2	40S ribosomal protein S25
P62751	103	5	2	3	2	20.5	60S ribosomal protein L23a
Q9Z329-3	101	14	1	13	1	7.4	Isoform 3 of Inositol 1,4,5-trisphosphate receptor type 2
A0A0U1RNJ1	98	14	1	14	1	11.8	Fatty acid synthase
Q9CXW4	98	3	1	3	1	26.4	60S ribosomal protein L11
A0A0N4SWH7	97	7	1	6	1	29.1	Inositol 1,4,5-trisphosphate receptor type 1 (Fragment)
P35979	95	3	1	3	1	24.2	60S ribosomal protein L12
O55131	90	9	1	7	1	21.6	Septin-7
P63038	90	12	1	10	1	27.1	60 kDa heat shock protein, mitochondrial
P70696	88	4	1	4	1	27.6	Histone H2B type 1-A
Q3UGX2	88	13	1	13	1	8.5	Spectrin beta chain
P62264	88	5	2	4	2	23.2	40S ribosomal protein S14
P61514	86	2	1	2	1	37	60S ribosomal protein L37a
P97351	86	6	1	6	1	35.2	40S ribosomal protein S3a
Q3UHR0	85	15	1	15	1	9.6	BAH and coiled-coil domain-containing protein 1

Continued on next page

Table B.2: Continued from the previous page

accession #	Mascot score	total matches	total significant matches	total distinct sequences	total significant distinct sequences	coverage (%)	description
Q91VB8	84	7	1	4	1	48.6	Alpha globin 1
P14115	82	3	2	3	2	14.9	60S ribosomal protein L27a
P02104	82	3	2	3	2	29.9	Hemoglobin subunit epsilon-Y2
A0A2R8VHF9	80	14	1	14	1	9	Myosin-11
A0A140LJB1	79	2	2	1	1	9.2	Contactin-associated protein-like 2 (Fragment)
P70670	79	12	1	11	1	7.9	Nascent polypeptide-associated complex subunit alpha, muscle-specific form
E9Q4Z2	76	14	1	13	1	8.6	Acetyl-CoA carboxylase 2
P67984	75	1	1	1	1	10.2	60S ribosomal protein L22
Q8VDN2	73	5	1	5	1	6.5	Na^+/K^+-transporting ATPase subunit alpha-1
Q9R1T4-2	73	5	1	4	1	8.9	Isoform I of Septin-6
Q9JMH9-2	71	11	1	11	1	12.4	Isoform 2 of Unconventional myosin-XVIIIa
Q6A078	67	23	1	22	1	13.5	Centrosomal protein of 290 kDa
F6SVV1	67	3	1	2	1	19.8	40S ribosomal protein S7
Q91VC3	65	7	1	6	1	18	Eukaryotic initiation factor 4A-III
E9Q0F0	64	13	1	11	1	16.2	Keratin 78
E9Q1Z0	64	8	3	5	1	11.3	Keratin 90
A0A286YEB7	63	3	1	2	1	28	40S ribosomal protein S24
P07724	63	5	1	5	1	10.4	Serum albumin
G3UZK9	62	5	1	5	1	15.5	Microtubule-associated protein 2 (Fragment)

Continued on next page

Table B.2: Continued from the previous page

accession #	Mascot score	total matches	total significant matches	total distinct sequences	total significant distinct sequences	coverage (%)	description
Q9CR49	60	3	1	3	1	29.9	Globin b1
P24369	60	3	1	3	1	19.9	Peptidyl-prolyl cis-trans isomerase B
B1ARR7	59	4	1	4	1	53.8	Alpha-enolase (Fragment)
P17426-2	58	8	1	6	1	11.8	Isoform B of AP-2 complex subunit alpha-1
Q6IFZ6	58	4	2	3	1	9.3	Keratin, type II cytoskeletal 1b
Q3UZG4	58	4	1	4	1	21.9	Aminoacyl tRNA synthase complex-interacting multifunctional protein 1
A0A0A6YW72	58	11	1	11	1	8.9	Dachsous cadherin-related 2
Q61753	58	5	1	5	1	19.3	D-3-phosphoglycerate dehydrogenase
D3YXK2	57	14	1	10	1	14.9	Scaffold attachment factor B1
V9GX06	55	4	1	4	1	49.7	Uncharacterized protein (Fragment)
P62242	55	2	1	2	1	12.5	40S ribosomal protein S8
A0A1D5RLA1	54	4	1	3	1	22.5	Inositol 1,4,5-trisphosphate receptor type 1 (Fragment)
P43277	54	5	1	5	1	19.9	Histone H1.3
P63276	54	3	1	2	1	20	40S ribosomal protein S17
P0C0S6	53	2	1	2	1	21.9	Histone H2A.Z
A0A140T8L3	53	2	1	2	1	8.6	Uncharacterized protein
Q3TLQ0	52	5	1	5	1	16.7	Microtubule-associated protein
Q8BPU7	52	8	1	8	1	19.9	Engulfment and cell motility protein 1
B1ARA5	51	2	1	2	1	9.1	60S ribosomal protein L26

Continued on next page

Table B.2: Continued from the previous page

accession #	Mascot score	total matches	total significant matches	total distinct sequences	total significant distinct sequences	coverage (%)	description
Q8BND5-2	51	5	1	4	1	8.5	Isoform 2 of Sulfhydryl oxidase 1
E9Q2D1	49	4	1	2	1	20.4	Actin, cytoplasmic 1 (Fragment)
A0A0G2JDU1	46	3	1	3	1	42.2	Microtubule-associated protein (Fragment)
Q6P9K8-3	46	6	1	6	1	7.3	Isoform 3 of Caskin-1
Q7TPH6	46	13	1	13	1	5.1	E3 ubiquitin-protein ligase MYCBP2
P62918	45	2	1	2	1	13.2	60S ribosomal protein L8
B1AQF4	44	2	1	2	1	19	Dual-specificity protein phosphatase 3
A2A513	43	6	1	4	1	11.9	Keratin, type I cytoskeletal 10
F6UQQ9	42	4	1	2	1	14.3	Uncharacterized protein
Q8VDP3-2	41	4	1	4	1	6.5	Isoform 2 of [F-actin]-monooxygenase MICAL1
D3YWH9	41	1	1	1	1	6.6	40S ribosomal protein S9
A0A0R4J1E2	41	4	1	4	1	11.7	Elongation factor 1-delta
P18760	41	1	1	1	1	8.4	Cofilin-1
Q08879	41	4	1	4	1	6.1	Fibulin-1
A2A547	40	4	1	4	1	25.8	Ribosomal protein L19
D3Z6F5	39	5	1	4	1	14.1	ATP synthase subunit alpha
P02088	29	2	1	2	1	23.1	Hemoglobin subunit beta-1